Electro-spinning and Characterisation of Neat Lignin Fibres

By Rohit Jordi Jassi

UNIVERSITY OF BIRMINGHAM

A thesis submitted to the

University of Birmingham

For the degree of

DOCTOR OF PHILOSOPHY

School of Metallurgy and Materials

College of Engineering and Physical Sciences

University of Birmingham

May 2025

Abstract

Lignin is a complex and abundant biopolymer, which is often fractionated, functionalised, and/or blended with synthetic or natural polymers to facilitate its processing into fibres via wet, melt, or electro-spinning methods. These traditional processes are typically complicated and involve multiple steps, limiting the scalability and economic feasibility of lignin fibre production. This study explores a novel approach to electro-spin neat BioChoice softwood Kraft lignin using a single-solvent, dimethyl sulfoxide (DMSO), aiming to simplify the process and enhance fibre uniformity.

Previous attempts to electro-spin lignin using DMSO alone, resulted mainly in electro-spraying rather than continuous fibre formation, underscoring the need to optimise solution properties and spinning conditions. In this study, thermal treatment was used to modify the lignin solution characteristics, enabling the successful electro-spinning of neat lignin in DMSO without the need for additives or co-polymers. Therefore, this work investigated whether refluxing lignin in DMSO at specified temperatures could produce a solution with suitable molecular properties, such as increased molecular weight and chain entanglement for effective fibre formation.

To test this hypothesis, neat lignin in DMSO was refluxed at temperatures of 80, 100, 120, 140, and 160 °C under a nitrogen atmosphere. The solutions and corresponding electro-spun fibres were then characterised using nuclear magnetic resonance (NMR), Fourier-transform infrared spectroscopy (FTIR), electrical conductivity, and viscosity measurements to determine their suitability for electro-spinning. Electro-spinning was conducted at 55 °C using a custom-designed rig, followed by drying the fibres at 100 °C for 4 hours in a vacuum oven to remove residual solvent.

The electro-spun fibres were analysed using differential scanning calorimetry (DSC), thermogravimetric analysis (TGA), and image analysis to assess their thermal properties, stability, and morphology respectively. The results indicated that unfused fibres with circular cross-sections were obtained when the lignin was refluxed at 120, 140, and 160 °C, supporting the research hypothesis that elevated reflux temperatures prior to electro-spinning increased the molecular weight and provide adequate chain entanglement for fibre formation. This hypothesis is supported by the gel permeation chromatography (GPC) analysis, which demonstrated that vacuum drying lignin at elevated temperatures resulted in increased molecular weight and polydispersity. This trend is attributed to thermal-induced reactions, which enhance molecular

chain entanglement. These changes improve the rheological properties of lignin solutions, facilitating more stable electro-spinning and successful fibre formation. The resulting electro-spun lignin fibres were successfully thermostabilised and carbonised, yielding continuous carbon fibre mats suitable for further structural and morphological analysis.

This study demonstrates a novel and simplified method for electro-spinning neat lignin using a single-solvent system, potentially revolutionising the production of lignin-based fibres by reducing the need for extensive chemical modifications and co-polymer blending. The findings highlight the efficacy of DMSO in facilitating high-quality lignin fibre formation, aligning with green chemistry principles and paving the way for more sustainable and cost-effective lignin utilisation.

Acknowledgments

First and foremost, I would like to express my sincere gratitude to Professor Gerard Fernando for his invaluable supervision, guidance, and unwavering support throughout the course of my PhD. His insightful feedback, patient mentorship, and meetings were instrumental in shaping my research design, experimental work, and analytical approach. His commitment and encouragement have been key to the successful completion of this thesis.

I am also thankful to my co-supervisor, Dr. Zoe Schnepp, for their advice and continued support during my studies. My sincere thanks go to Frank Biddlestone, Cecile Le Duff and Mark Jeeves for training me to use the equipment in the laboratory.

I would like to sincerely thank Austin Tomlinson for his support throughout my PhD, particularly for his help with formatting the thesis throughout, and offering thoughtful advice and encouragement along the way.

I would like to thank my colleagues Siheng Shao and Elira He for their invaluable support and guidance throughout my PhD, particularly for their assistance in conducting laboratory work and performing experiments. I would also like to thank my colleagues Inam Khan, Bongkot Hararak, James Willberry, Yuting Liu, Elif Dede, Maximilian Hlatky and Madhav Ramesh, for their constant encouragement and support throughout my PhD. Thanks, are also due to the staff at the School of Metallurgy and Materials, University of Birmingham, for their assistance and support throughout my time at the university.

Finally, I would like to extend my heartfelt thanks to my family and friends, especially my parents and brother, for their unwavering love and emotional support. Their belief in me has been a constant source of strength and encouragement throughout my thesis.

Contents

List of Figures

List of Tables

List of Abbreviations

Polyacrylonitrile - PAN

Dimethyl sulfoxide - DMSO

Dimethylformamide - DMF

Glass transition temperature - T_g

Weight average molecular weight - Mw

Polydispersity index - PDI

Near-Field Electro-spinning - NFES

Poly(ethylene oxide) - PEO

Scanning electron microscopy - SEM

Gel permeation chromatography - GPC

Differential scanning calorimetry - DSC

Thermogravimetric analysis - TGA

Derivative thermogravimetry - DTG

Fourier transform infrared spectroscopy - FTIR

Nuclear magnetic resonance - NMR

Proton Nuclear magnetic resonance - ^{1}H NMR

Carbon Nuclear magnetic resonance - ^{13}C NMR

Heteronuclear Single Quantum Coherence - HSQC

X-ray diffraction - XRD

Liquid chromatography-mass spectrometry - LC-MS

Gas chromatography-mass spectrometry - GC-MS

High-performance liquid chromatography - HPLC

1. Introduction

1.1. Introduction and motivation

Lignin, a complex and plentiful organic compound present in the cell walls of plants, serves a vital function in imparting structural strength and durability against deterioration (1). Lignin has attracted considerable attention in materials science and engineering due to its abundant availability and wide range of possible applications. Usually, lignin is separated into different parts, modified to have certain functions, and mixed with either synthetic or natural polymers to make it easier to turn into fibres using processes like wet, melt, or electro-spinning (2).

This study especially examines the electro-spinning of neat BioChoice softwood Kraft lignin using a single-solvent system, namely dimethyl sulfoxide (DMSO). DMSO, is a type of solvent that is non-toxic, polar and aprotic. It is well-known for its capacity to dissolve a broad spectrum of organic and inorganic substances. This characteristic makes it highly desirable as a solvent in the processing of lignin (3). The prior endeavours to electro-spin lignin with other solvents or cosolvents primarily led to electro-spraying, where the solution forms droplets instead of uninterrupted fibres. This problem highlights the need of optimising the characteristics of the solution and the conditions under which it is spun to achieve the desired fibre morphology.

Electro-spinning is an adaptable method used to create nanofibres from a wide range of materials, such as polymers (4), composites (5) and biomaterials (6). The process entails the application of a high voltage to a solution or molten polymer, resulting in the creation of fine fibres through a jet that solidifies as the solvent evaporates or cools respectively (7). The technique provides substantial manipulation of fibre diameter, porosity, and surface area, rendering it appropriate for utilisation in filtration, biomedical devices, and advanced composites (8). The difficulty in electro-spinning lignin arises from its inclination to undergo cross-linking and generate high-molecular-weight fractions, especially when exposed to temperatures over 140 °C (9).

A significant motivation behind this study is the production of uniform lignin fibres from a single-solvent system without any chemical modification or copolymer blending (10). Using unaltered lignin streamlines the procedure and circumvents the possible ecological and financial expenses linked to the use of supplementary chemicals. Utilising a solitary solvent solution such as DMSO can result in a simpler, more economical, and easily expandable approach for manufacturing lignin fibres. Not only does it simplify the fibre production process, making it

more cost-effective and scalable, but DMSO is also considered less toxic compared to many other common lignin solvents, such as formaldehyde-based solutions or phenolic solvents (11,12). Furthermore, the unique aspect of electro-spinning lignin with DMSO alone is novel in its capacity to enable the creation of fibres without the necessity of intricate chemical alterations or the incorporation of additional polymers. This technique adheres to the principles of green chemistry by diminishing the dependence on numerous solvents and additives.

In order to address the difficulties of using a single-solvent system, a study was conducted on the electro-spinning of 100% (w/v) lignin in DMSO. Prior to this, the solution was subjected to refluxing at different temperatures (80, 100, 120, 140, and 160 °C) under a nitrogen atmosphere. The objective was to get partial cross-linking and the most suitable molecular weight to ensure efficient chain entanglement, which is crucial for the formation of uninterrupted fibres. The solutions were analysed using nuclear magnetic resonance (NMR), Fourier-transform infrared spectroscopy (FTIR), conductivity, and viscosity measurements. Following this, electro-spinning was conducted at a temperature of 55 °C using a custom-built apparatus, and the resulting fibres were dried at 100 °C in a vacuum furnace to eliminate any remaining solvent or moisture that remained.

The electro-spun fibres were characterised using differential scanning calorimetry (DSC), thermogravimetric analysis (TGA), and image analysis to assess their thermal characteristics, stability, and shape. The findings revealed that when lignin was subjected to reflux at temperatures of 120, 140, and 160 °C, it resulted in the production of unfused fibres with circular cross-sections. The results generated in the current study suggest that subjecting lignin to reflux at these temperatures causes partial cross-linking, which is essential for achieving the desired molecular weight and chain entanglement required for successful electro-spinning of lignin-DMSO uniform fibres.

Using a solution for electro-spinning is more effective than heat treatment of solid lignin powder for producing uniform fibres due to several key factors. Firstly, solutions allow control over viscosity, which is critical for stable jet formation and consistent fibre diameter during electro-spinning. Dissolving lignin in a solvent facilitates molecular-level mixing prior to fibre formation, which can promote uniformity in the resulting fibres (13,14). Additionally, processing lignin from a solution can reduce thermal degradation compared to high-temperature melt processing, helping to preserve its chemical structure and mechanical properties (15). Electro-

spinning from a solution enables fine-tuning of fibre properties through adjustable parameters such as concentration, solvent type, and applied voltage (16). Although parameters like voltage can also be varied in melt electro-spinning, solution-based methods generally offer a broader range of processing conditions and operate at lower temperatures, which can be advantageous when working with heat-sensitive materials like lignin (17,18). Moreover, using solvents provides flexibility for incorporating additives or modifiers, making solution electro-spinning a versatile and controlled approach for producing uniform nanofibres (19,20).

This thesis presents a streamlined technique for electro-spinning neat lignin utilising a single-solvent system, which has the potential to facilitate the development of more environmentally friendly and effective manufacturing processes for lignin-based fibres. The results not only add to the current understanding of lignin processing but also emphasise the potential of DMSO as a single-solvent for producing high-quality lignin fibres without requiring chemical alterations.

1.2. Research hypothesis

The research hypotheses in the current thesis are that:

(i) As-received lignin can be electro-spun without fractionation or blending with other polymers.

(ii) Controlled heat treatment of as-received lignin in DMSO can be used to increase its viscosity and molecular weight distribution and thus enable electro-spinning.

(iii) Conventional analytical techniques can be used to characterise and demonstrate that structural changes take place when as-received lignin is subjected to controlled heat treatment in DMSO.

1.3. Aims and objectives

(i) To characterise as-received lignin using conventional thermal, rheological, electrical and spectral techniques.

The characterisation techniques that will be used include differential scanning calorimetry (DSC), thermogravimetric analysis (TGA), electrical conductivity, parallel-plate rheometry, X-ray diffraction (XRD), elemental analysis, gel permeation chromatography (GPC), Fourier transform infrared spectroscopy (FTIR) and nuclear magnetic resonance spectroscopy (NMR). The morphology of fibres will be characterised using scanning electron microscopy (SEM) and image analysis.

(ii) To study the effect of specified methods of heat-treating lignin with a view to increasing its polymer concentration in solution.

Dried lignin will be dissolved in DMSO at a range of concentrations and temperatures to identify the optimum solution characteristics for electro-spinning. The characterisation techniques mentioned above will be used to characterise the solutions.

(iii) To identify the optimum electro-spinning parameters for producing nano-fibres.

The electro-spinning parameters such as the applied voltage, temperature, humidity and solution viscosity optimised to enable the electro-spinning of neat lignin.

(iv) To oxidise and carbonise the electro-spun neat lignin fibres.

The electro-spun neat lignin fibres will be oxidised and carbonised in a tube furnace to produce carbonised fibres.

1.4. Structure of thesis

Chapter 1: Introduction

Chapter 1 provides an overview of the context and rationale for the study, emphasising the significance of lignin and its uses. The study begins by stating the research hypothesis, which is then followed by a thorough discussion of the study's aims and objectives.

Chapter 2: Literature Review

Chapter 2 presents a thorough examination of the literature pertaining to the topic, with a specific emphasis on the composition, extraction, characterisation, solubility, and electro-spinning of lignin. The section commences by examining the chemical makeup of lignin and its variability, which is contingent upon the source of biomass. The chapter subsequently examines different techniques employed for extracting lignin in both industrial and laboratory environments, such as Kraft, soda, organosolv, steam explosion, and ionic liquids extraction. An in-depth analysis was conducted to examine the effects of these extraction procedures on the structure and physicochemical characteristics of lignin. The chapter also discusses the characterisation techniques employed for the analysis of lignin, including FTIR, NMR (encompassing proton, carbon and HSQC techniques), GPC and elemental analysis. Additionally, this section examines the solubility of lignin in various solvents, with a specific emphasis on DMSO. It then provides a summary of electro-spinning methods and their use in

relation to lignin. The chapter ends with a conclusion of the literature covered and how they relate to the work done in this thesis project.

Chapter 3: Experimental Methodology

Chapter 3 provides comprehensive details of the experimental procedures utilised in this thesis investigation. The Softwood Kraft lignin (BioChoice) underwent a drying regime in a vacuum oven at a temperature of 80 °C in order to eliminate any moisture present before it was used. The solvents chosen for this experiment were anhydrous DMSO and deuterated DMSO. Special precautions were taken to ensure that moisture did not contaminate the solvents. The characterisation techniques employed were DSC for thermal analysis, TGA to determine degradation temperatures, and FTIR to examine chemical bonding. Elemental analysis yielded information about the composition of lignin, whereas NMR revealed specific structural characteristics. The rheological parameters were assessed using a parallel-plate rheometer, while electrical conductivity studies were also conducted on the lignin solutions. GPC was conducted to determine the molecular weight and polydispersity of lignin samples. This chapter also outlines the procedure for preparing lignin/DMSO solutions and provides details about the experimental conditions used to evaluate the impact of heat treatment temperatures on lignin characteristics. These approaches were crucial for examining the appropriateness of lignin for electro-spinning and its subsequent applications.

Chapter 4: Results and Discussion

Chapter 4 examines the different methods used to analyse electro-spun lignin samples and discuss their significance. SEM and Image Analysis provide a detailed examination of the physical characteristics of electro-spun lignin/DMSO fibres. A range of analytical techniques were employed, including FTIR to examine chemical bonding and functional groups, NMR spectroscopy for detailed structural analysis, elemental analysis to determine elemental composition, GPC for molecular weight and DSC for thermal analysis. The chapter also discusses viscosity and conductivity measurements to understand the rheological properties of the lignin/DMSO solutions and their impact on fibre formation. The findings from these characterisation techniques are used to assess the structural integrity, thermal stability, and overall quality of the electro-spun lignin fibres. These investigations jointly enhance comprehension of lignin's behaviour and possible applications in fibre manufacturing.

Chapter 5: Conclusion

Chapter 5 of the thesis provides a concise summary of the conclusions derived from the research findings. This chapter emphasises the key accomplishments and contributions, including the successful electro-spinning of lignin/DMSO blends and the comprehensive characterisation of the resulting fibres.

Chapter 6: Recommendations for future work

Chapter 6 addresses the constraints of the existing study and provides suggestions for future endeavours, proposing avenues to build upon the findings and go into unexplored areas of inquiry.

2. Literature review

2.1. Lignocellulosic biomass

Lignocellulosic biomass is the most abundant, natural renewable source on earth, with an estimated annual production of 181.5 billion tons globally, with only 8.2 billion tons utilised in industrial applications (21). Lignocellulosic biomass refers to the cell wall material composed of multiple different layers, which are separated from neighbouring cells by the intercellular middle lamella (22,23), as illustrated in Figure 1.

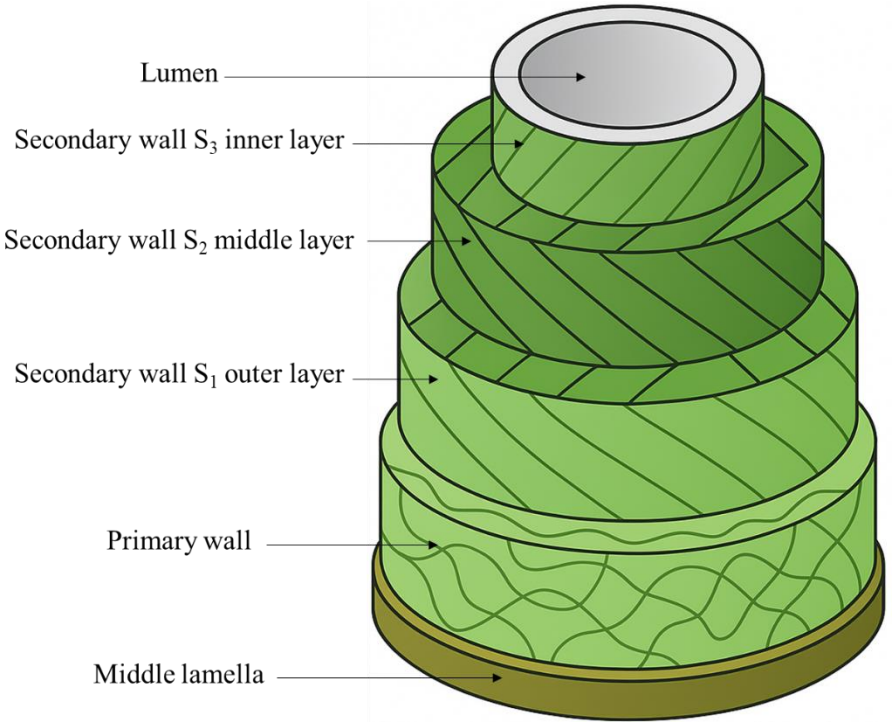

Figure 1. Structure of the cell wall in wood, adapted from Rytioja et al., (23).

Lignocellulosic biomass is primarily composed of three structural components: cellulose, hemicellulose, and lignin (24). Cellulose is a linear polysaccharide made of glucose molecules and provides structural support to plant cell walls. Hemicellulose, a more complex and branched polysaccharide, consists of various sugar monomers and binds with cellulose fibres, adding strength and flexibility. Lignin, is a complex organic polymer, that fills the spaces between cellulose and hemicellulose, providing rigidity and resistance to microbial deterioration (25,26). Together, these components form a robust and durable material, making lignocellulosic biomass a promising feedstock for biofuel production and other bioproducts (24,27,28). Lignin content varies among plant species due to growth conditions and location, which can influence biomass processing and thus the lignin content can differ (29).

The contents of these components in biomass vary depending on the biomass type; although typically; cellulose, hemicellulose, and lignin encompass 40-60, 20-40, and 10-25 weight percentage of biomass materials respectively, with the rest of the biomass being composed of smaller quantities of ash and extractives (22,24,27,28).

As shown in Figure 2, cellulose is embedded in a dense matrix of hemicellulose and lignin known as the lignocellulosic matrix, creating a protective sheath around the cellulose (24,25,30). The majority of lignin in biomass is found in the middle lamella and the secondary cell wall of biomass species (31–33).

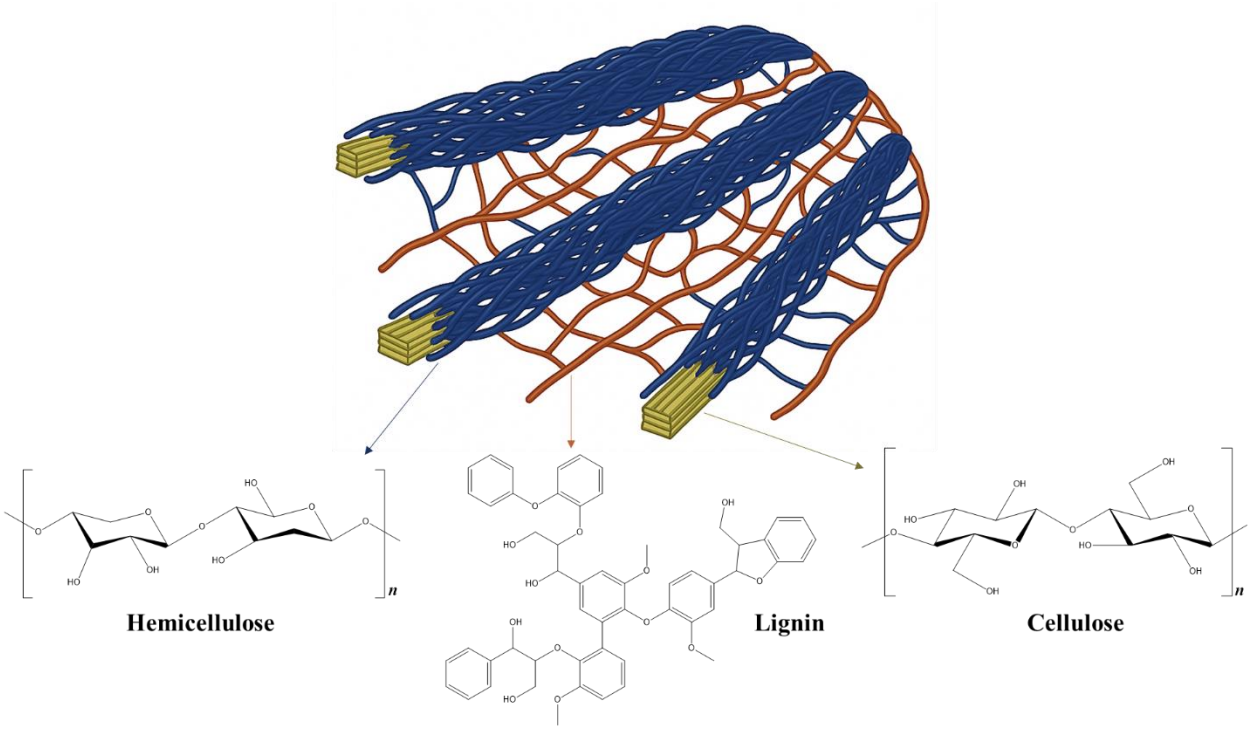

Figure 2. Schematic of the lignocellulosic matrix, with repeating units of hemicellulose, lignin and cellulose, adapted from Liu et al., (30).

Lignin is an aromatic biopolymer found in terrestrial plants. After cellulose, lignin is the second most abundant polymer in nature. Different plant species contain varying levels of lignin, and its chemical composition and molecular weight can differ depending on the parent plant (24–26,31,34,35).

2.1.1. Lignin composition in biomass

Lignin in biomass varies based on the type of wood. Softwood trees (coniferous species like pine, spruce, and fir) contain "softwood lignin," which is rich in guaiacyl (G) units derived from coniferyl alcohol. In contrast, hardwood trees (deciduous species like oak, maple, and birch)

have "hardwood lignin," which contains a mixture of guaiacyl (G) and syringyl (S) units, derived from coniferyl and sinapyl alcohol, respectively (24,36).

The system used to identify and categorise the many kinds of lignin found in plant cell walls is known as lignin nomenclature. The lignin nomenclature scheme, which is based on the relative quantity of the three primary monomers found in lignin; syringyl (S), guaiacyl (G), and p-hydroxyphenyl (H), is the most popular systems used to name and categorise lignin (37,38).

Lignin monomers, also known as monolignols, are the basic building blocks that polymerise to form lignin. These monolignols include syringyl (S), derived from sinapyl alcohol; guaiacyl (G), derived from coniferyl alcohol; and p-hydroxyphenyl (H), derived from p-coumaryl alcohol, which are illustrated in Figure 3 (37,38).

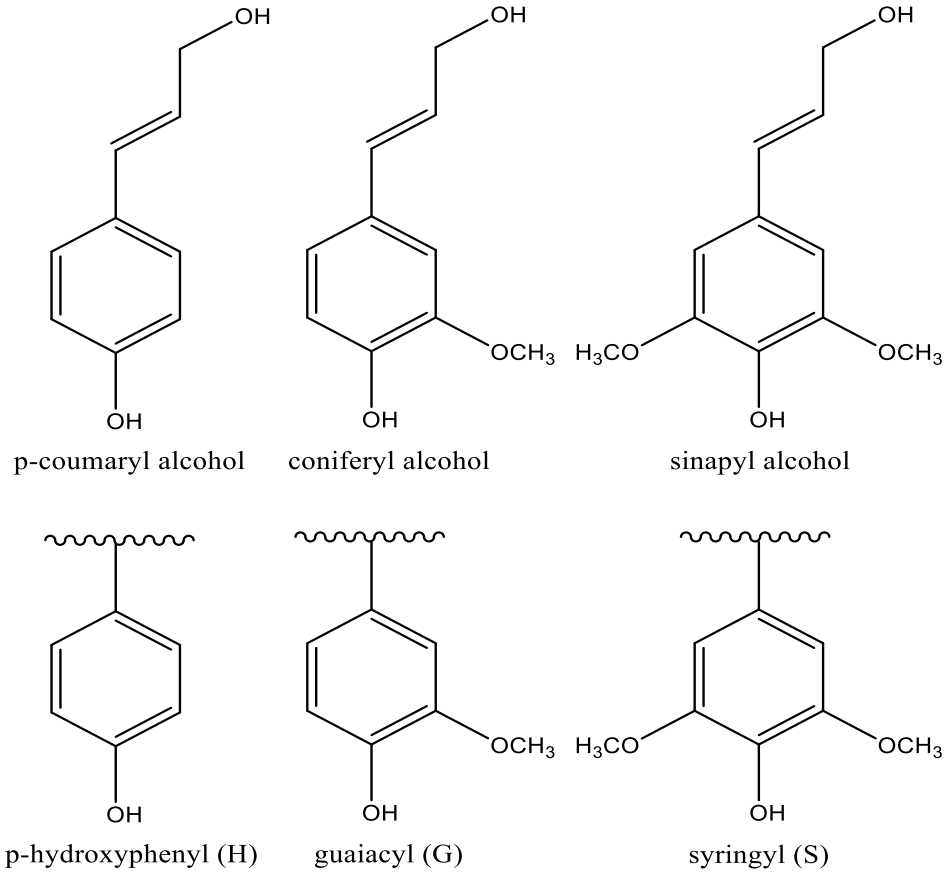

Figure 3. Illustration of primary monomers associated with the structure of lignin, including H,G & S units (22,31,32).

Syringyl units have two methoxy groups attached to their aromatic ring, making them less prone to cross-linking and contributing to the solubility and flexibility of the lignin polymer. Guaiacyl units have one methoxy group on their aromatic ring, are more common in softwoods, and

contribute to the rigidity and stability of the lignin structure due to their propensity for cross-linking, whilst p-hydroxyphenyl units, have no methoxy groups on their aromatic ring and are found less frequently in plant species than guaiacyl and syringyl units (32,39).

The softwood species of lignins are formed from the guaiacyl unit (G) only; whilst hardwood lignins are formed from both guaiacyl and syringyl (G & S) units, as illustrated in Figure 3 (22,32).

The S:G monomer ratio is used to categorise lignin, whereas the H monomer is often less abundant and has less of an impact on the lignin's overall characteristics (36,40,41). The labelling convention for the lignin monomers for the G unit in particular is shown in Figure 4.

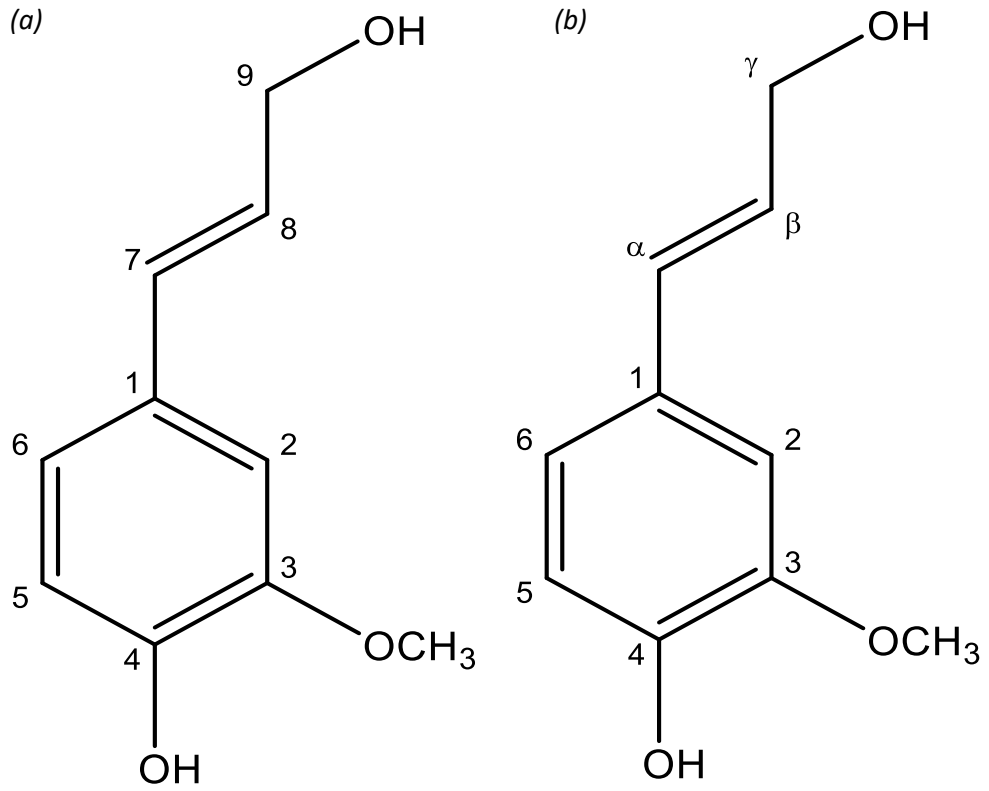

Figure 4. Labelling convention for monolignols (Guaiacyl G-Unit). (a) IUPAC nomenclature (b) wood chemistry terminology (22,31,32).

Guaiacyl (G) unit content is high (>95%) in softwood lignin while syringyl (S) unit content is low (<5%) (42). As a result, the lignin structure in softwoods becomes extremely rigid and dense, providing strength and resistance to degradation (43). Additionally, the low molecular weight of softwood lignin makes it simpler to degrade in commercial operations like the Kraft process (see Section 2.2) (31,37,44).

A higher S unit content in hardwood lignin (45-75%) contributes to its more flexible and open structure (42). Hardwood lignin contains higher amounts of syringyl (S) units, making it more flexible and less condensed compared to softwood lignin, which has a higher content of guaiacyl (G) units and is more condensed and inflexible (31,34).

A schematic representation of the lignins found in softwood and hardwood, is shown in Figure 5, derived from NMR & GPC analysis by Lancefield *et al*., (39,45–48).

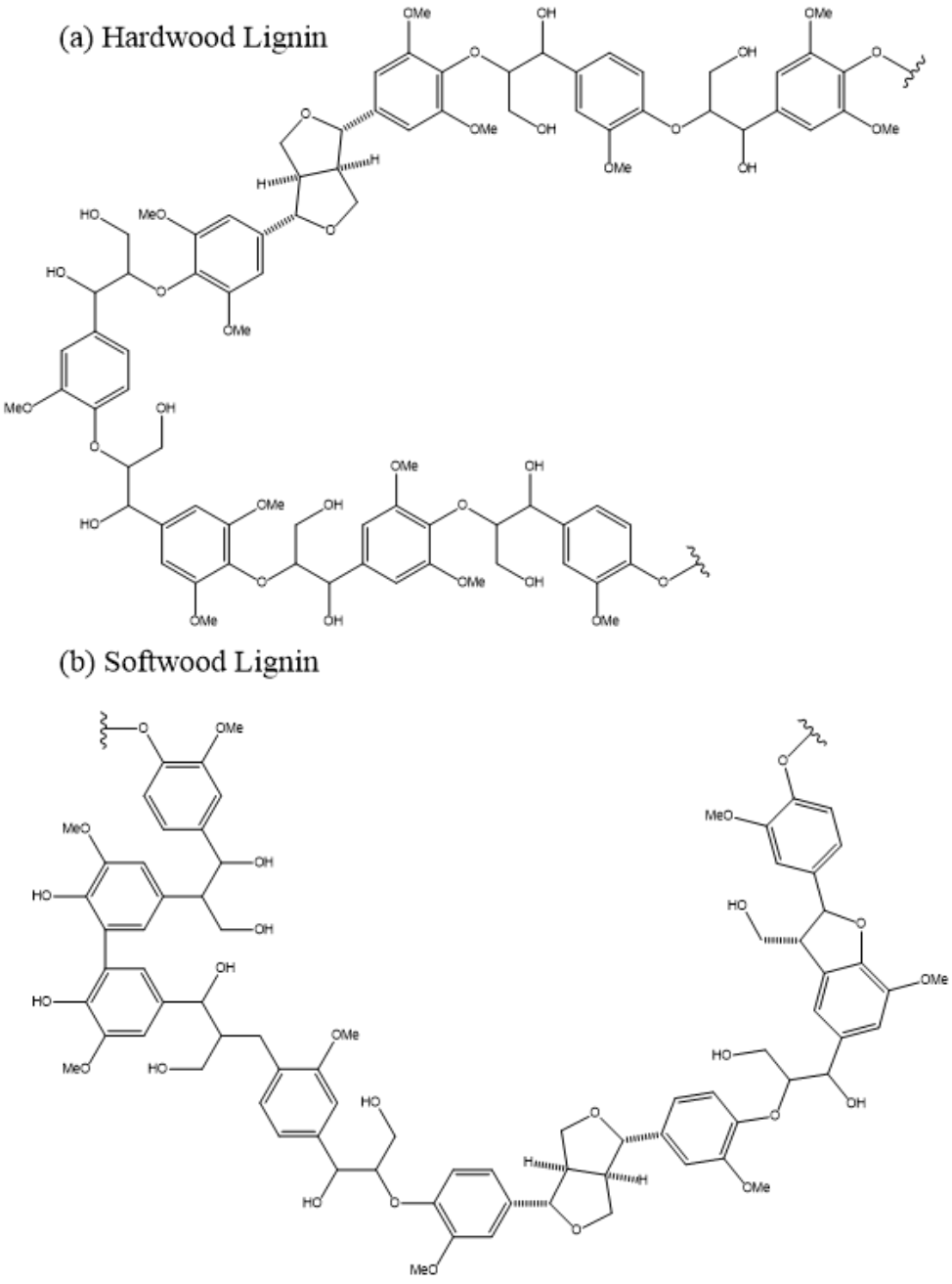

Figure 5. Structural segment representation of hardwood (a) and softwood (b) lignins, adapted from Lancefield et al., (39).

To comprehend the chemistry underlying lignin's structure, it is important to consider the wide variation in reactivity of its linkages or functional groups. The most frequently seen links in the lignin structure are the α and β-O-4 ether linkages, aliphatic, and phenolic OH-groups, which are related to the phenylpropane skeleton, as illustrated in Figure 6 (45,49,50).

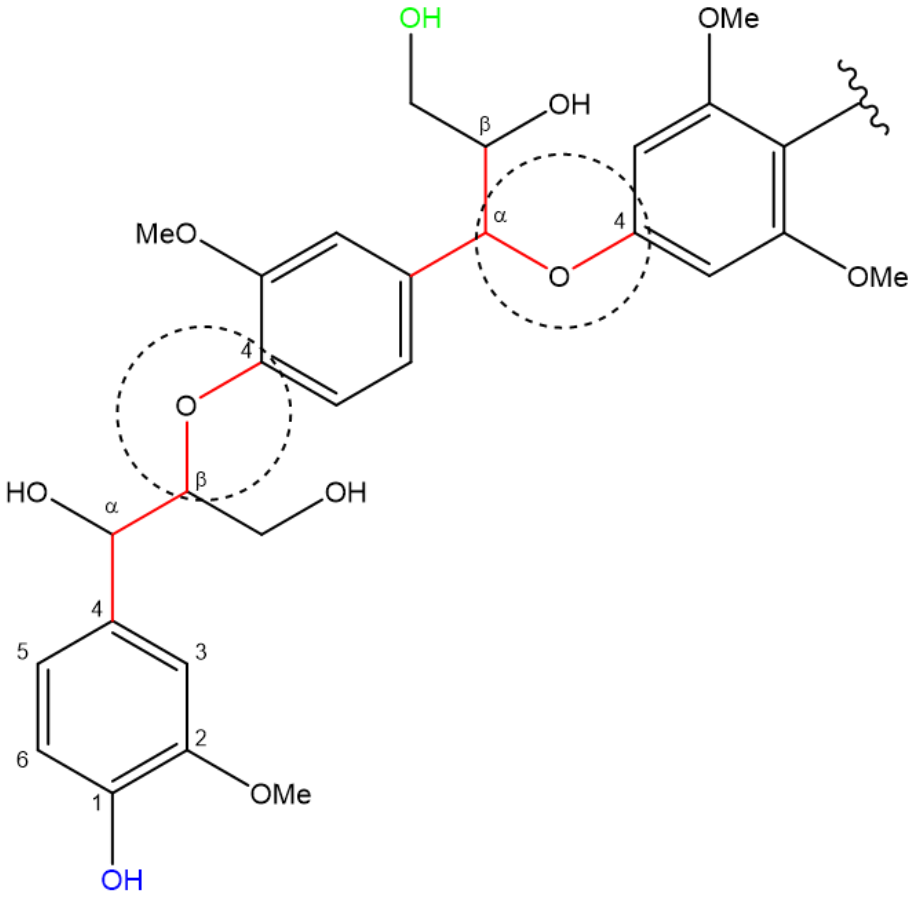

Figure 6. The α-O-4 (right circle), β-O-4 (left circle), aliphatic (green), and phenolic (blue) OH-groups are the most reactive bond types in the structure of lignin (45,49,50).

The phenolic α-O-4 links in lignin are the common reactive sites, whilst the phenolic β-O-4 couplings in alkaline solutions are much less reactive, as reported by Evstigneev *et al*., (51). In alkaline conditions, the β-O-4 linkages are relatively stable and less prone to cleavage compared to α-O-4 linkages, which are more susceptible to reactions such as hydrolysis and oxidation (49,51,52). As suggested by Li *et al*., (53), the cleavage of α-O-4 and β-O-4 links or condensation reactions into monomeric lignin fragments can take place in an acidic solution. These fragments can then undergo further reactions with other molecules, such as aldehydes, as illustrated in Figure 7 (49,53).

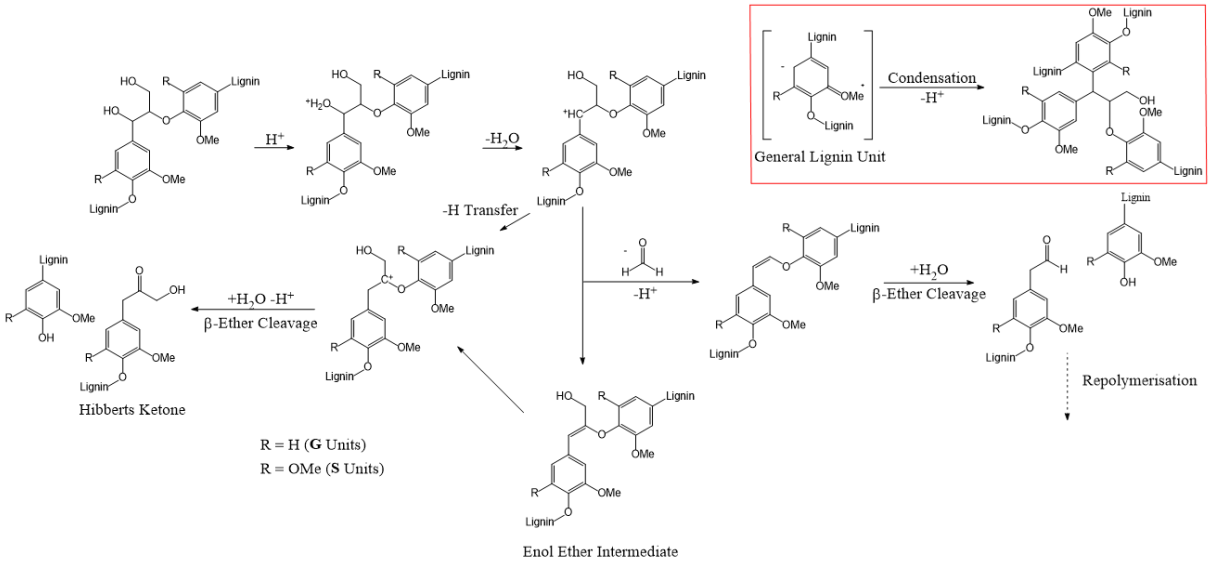

Figure 7. Mechanism of lignin condensation routes, adapted from Li et al., (53).

The β-O-4 ether bond, is the most common bond between lignin monomers (54). This primary linkage is both the main obstacle of lignin investigations that aim to cleave the β-O-4 bond for the isolation and decomposition of lignin (54–56). Additional common linkages seen in lignin including the β-O-4 linkage are the 4-O-5, α-O-4, β-5, β-1 and 5-5 bonds, which form a 3-D irregular and amorphous structure, these linkages are shown in Figure 8 (57,58).

As reported by Zemek *et al*., (59), native wood lignin is comprised of 11 phenolic monomeric fragments, with ferulic and coumaric acids serving as the main phenolics in native lignin. The three monomeric aromatic alcohols; coumaryl, coniferyl, and sinapyl alcohols are polymerised to form lignin (60,61). The amounts of these alcohols vary amongst plant species, which explains variation in lignin concentrations. For instance, according to Jung and Fahey *et al*., (60), lignin from hardwoods includes 400 g/kg of sinapyl alcohols, 40 g/kg of p-coumaryl, and 560 g/kg of coniferyl. In contrast, lignin from softwoods contains 60 g/kg of sinapyl, 140 g/kg of p-coumaryl, and 800 g/kg of coniferyl. Because of its strong ether and carbon–carbon bonds (seen in Figure 8), lignin is difficult to breaking down (60,62).

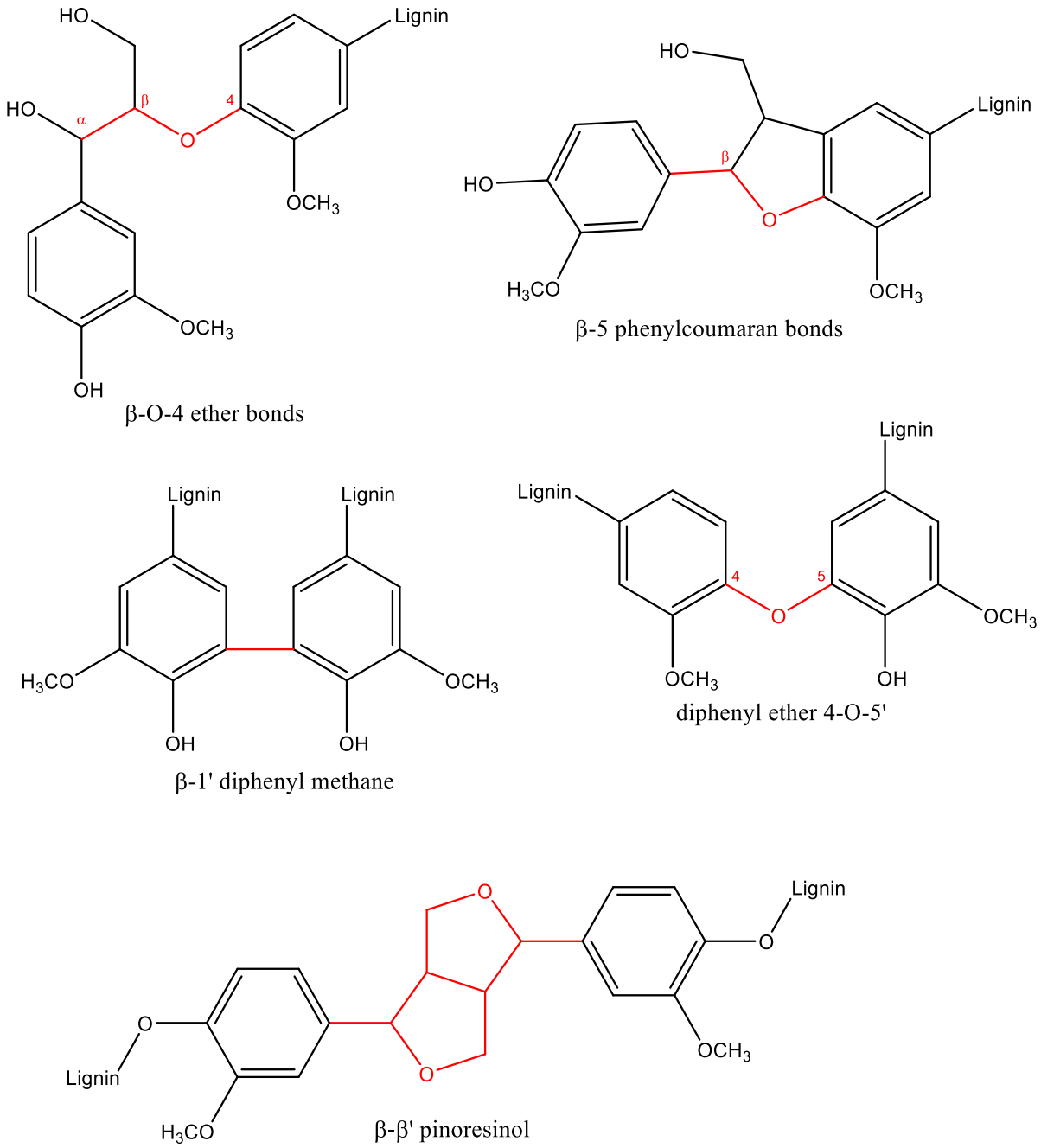

Figure 8. The interunitary chemical linkages typically found in lignin (278,283).

2.1.2. Lignin interaction with moisture

Lignin and other plant-derived polymers interact with moisture, which affects their processing and properties. Water in lignocellulosic materials like wood and lignin exists mainly in two forms: free water and bound water (63). Free water fills the cavities (cell lumina) and is easier to remove during drying. Bound water, in contrast, is absorbed within the cell walls, see Figure 1, and forms strong hydrogen bonds with the chemical components such as cellulose,

hemicellulose, lignin, and pectin (64,65). Removing bound water requires more energy and can lead to structural changes (66,67).

The fibre saturation point marks the stage when all available sites within the cell wall are occupied by bound water, and any additional water is present as free water. In freshly cut ("green") wood, the moisture content is particularly high, sometimes exceeding the dry weight of the material. Moisture content can also vary between hardwood and softwood plants species. The hydrophilic nature of lignocellulosic fibres comes mainly from their chemical composition and structure (68). Cellulose and hemicellulose contain hydroxyl groups that readily form hydrogen bonds with water, facilitating moisture absorption, see Figure 2. Hemicelluloses, abundant in the amorphous regions of the cell wall, significantly contribute to water uptake. Studies have shown that removing hemicellulose and lignin reduces the capacity of fibres to absorb moisture, confirming their role in water retention (66,67,69–71).

Water diffusion occurs primarily in the amorphous regions, where molecules have more freedom to interact with water. In cellulose, for example, bound water mostly attaches to hydroxyl groups in the amorphous phase, while the crystalline regions absorb little moisture. Similarly, hemicellulose and pectin, particularly in the middle lamella, contribute to moisture uptake due to their polar groups (72,73).

When considering electro-spun fibres, the structure of the fibres further promotes water absorption. Their porous architecture and large surface area create pathways and storage spaces for water. This moisture can lead to swelling, dimensional changes, and reduced mechanical properties, which are important considerations when using lignin-based materials in applications such as composites, electro-spun fibres, or environments with fluctuating humidity (74,75). Overall, understanding how moisture interacts with lignin and related polymers is essential for optimising drying processes and improving material stability.

2.2. Lignin extraction

The established methods that are used to extract lignin from plants include Organosolv, soda-aqueous treatment, Kraft pulping (76,77), hydrolysis (25,78), alkali treatment (28,79), steam explosion (80,81), ammonia fibre expansion (80,82), deep eutectic solvents (80,83), and using ionic liquids (24,28,79,84–88). A summary of lignin isolation methods is illustrated in Table 1.

The utilisation of the soda process is widely employed to extract lignin (89). The soda process involves the use of sodium hydroxide (NaOH) in pressurised reactors at temperatures ranging from 140 to 170 °C, which causes the breaking of α-aryl ether bonds in the phenolic units of lignin, as mechanistically demonstrated in Figure 9 (90,91).

Table 1. Summary of selected methods for separating lignin from biomass.

Type of Lignin	Separation Method	References
Kraft lignin	Precipitation (pH change)	(92–94)
	Ultrafiltration	(94–97)
Soda lignin	Precipitation (pH change)	(98–100)
	Ultrafiltration	(101,102)
Soda-aqueous Lignin	Extraction (NaOH)	(85,103)
Lignosuphonates lignin	Ultrafiltration	(104,105)
Hydrolysis lignin	Filtration	(106,107)
	Extraction (NaOH)	(86,108,109)
Organosolv lignin	Dissolved air flotation	(110,111)
	Precipitation (addition of non-solvent)	(112–114)
Ionic liquid lignin	Precipitation (addition of non-solvent)	(86,115,116)

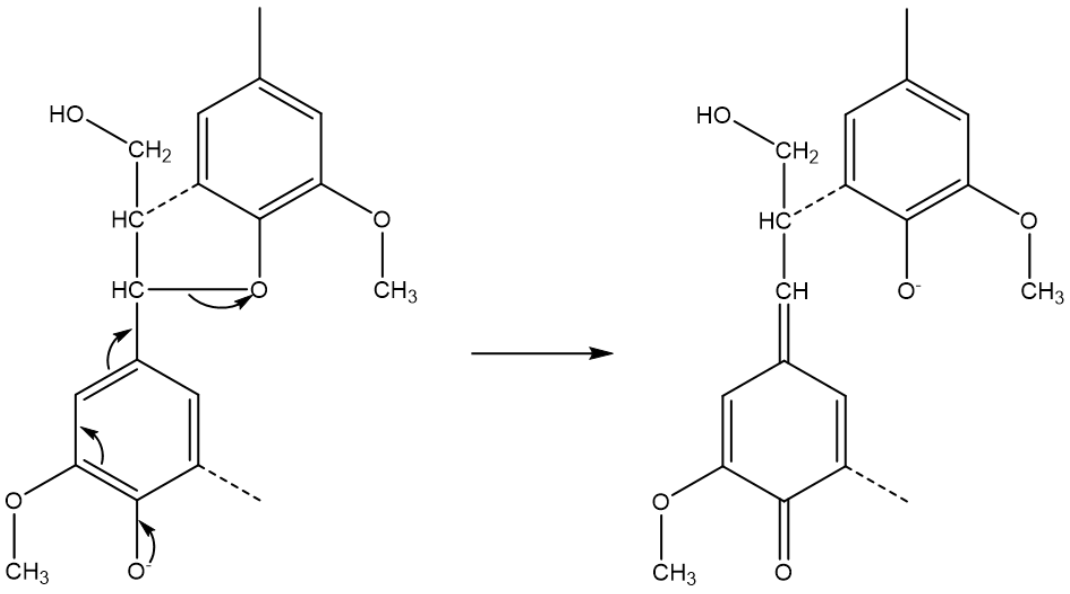

Figure 9. Alkaline cleavage of a-aryl ether bonds in phenolic arylpropane units. The dotted lines indicate possible linkages to adjacent lignin units (91).

Chemical treatments are commonly used to extract lignin from lignocellulosic biomass, although these treatments can result in the presence of residual chemicals in the final lignin product. An example of a widely used technique for extracting lignin is the Kraft process, which involves the use of sodium hydroxide and sodium sulphide to degrade lignocellulosic materials (92–94).

The presence of residual sodium and sulphur molecules from the Kraft process can persist in the lignin structure, causing changes to its chemical and physical characteristics (117).
The application of acidic treatments, such as those employed in the Sulfite pulping process, can result in the presence of residual sulphur dioxide and other sulphurous compounds, which have the potential to alter the properties of lignin (118). Residual sulphur compounds from Sulfite pulping can boost the adhesive capabilities of lignin in adhesives. This is because they increase the availability of reactive sites for bonding, as reported by Mansouri *et al.,* (119).
Lignin can undergo numerous chemical modifications due to the presence of residual acids and bases. Under acidic circumstances, the β-O-4 connections in lignin (see Figure 8), which are the most prevalent type of linkage, are frequently broken. This leads to the formation of smaller fragments with lower molecular weights (120). On the other hand, alkaline circumstances can enhance the process of lignin condensation, resulting in an elevation in both the molecular weight and cross-linking density (121). These modifications can impact the solubility of lignin, making it more difficult to handle for applications that need precise molecular weight distributions and availability of functional groups (122).
Residual acidic groups in coatings can enhance the hydrophilicity of lignin, making it more compatible with water-based systems (123). However, this can also decrease its resistance to moisture and biodegradation, as reported by Doherty *et al.,* (101). The molecular weight and structure of lignin are crucial factors in the synthesis of carbon fibre. Residual bases can enhance cross-linking, resulting in the production of high-strength carbon fibres (124). Nevertheless, an excessive amount of cross-linking can result in the lignin being brittle and challenging to transform into fibres, as reported by Kadla *et al.,* (125). Additionally, Kai *et al.,* found that lignin obtained through an alkaline pulping technique exhibited enhanced efficacy as a phenol replacement, in comparison to lignin obtained using acidic procedures (126).

2.2.1. Solvent lignin interactions

Lignin's capability to form distinct intermolecular interactions with the hydroxyl, carbonyl, and aliphatic groups in its structure is correlated with its particular solvent solubility (127).

Ponnuchamy *et al*., (128), investigated the single-step fractionation of industrial hardwood Kraft lignin utilising ethanol, acetone, diethyl ether, and hexane, four organic solvents with varying polarity.

Density functional theory (DFT) is a quantum-mechanical simulation method that may be used to predict atomic and molecular-level properties (58). The density functional theory done by Ponnuchamy *et al*., (128), revealed that ethanol had the highest contact energy with lignin, followed by acetone, diethyl ether, and hexane. The DFT results for hydrogen bonds and noncovalent interactions showed that γ-OH is the primary interaction site in the lignin model, with ethanol's high polarity enabling stronger solvation. The chosen lignin model (see Figure 10) consists of three main linkages, namely β-O-4, α-O-4, and 5-5′, which together account for around 10% of softwood lignins (129).

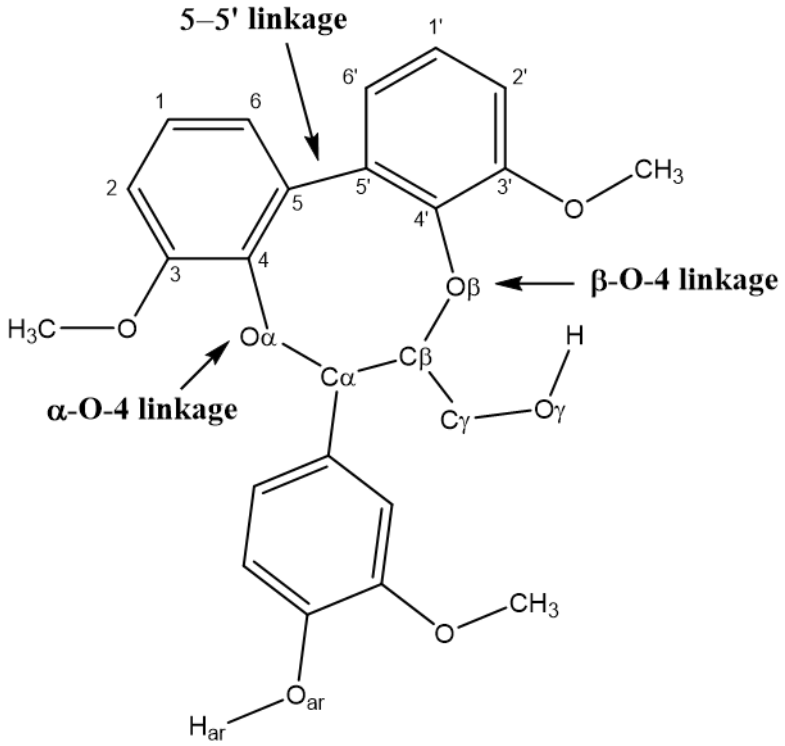

Figure 10. Structure of lignin model compound used in the study by Ponnuchamy et al. (128).

The interaction energy (ΔE) of the various lignin model configurations was defined as the disparity in energy between the most stable configuration and the equivalent isolated geometries. Hexane, the least polar solvent, showed the lowest interaction energy (45.01 kJ/mol), while ethanol showed the highest (55.53 kJ/mol), with acetone ranking second at approximately 7.5 kJ/mol lower than ethanol (128,129).

Ethanol also formed the shortest hydrogen bond (2.22 Å) with lignin, involving the

electronegative oxygen in ethanol and a hydrogen on the aromatic ring. Among all solvents, ethanol produced the strongest hydrogen bonds, followed by acetone, diethyl ether, and hexane (128,130,131).

Higher polarity solvents (ethanol and acetone) achieved greater solubility yields (70–80%) for hardwood Kraft lignin than moderate or low polarity solvents, confirming ethanol as the most efficient solvent for fractionation and supporting previous experimental findings (129,132).

Lignin's processability can be enhanced by fractionation and purification, which remove contaminants and change the molecular weight and polydispersity. Lignin fractionation allows the conversion of heterogeneous, low-quality lignins into more uniform, high-value lignin products by reducing contaminants and internal variation in their chemical and structural features. To achieve this, cost-effective technologies that produce lignin fractions with specific properties such as low polydispersity, low ash content, or varying phenolic content are required. Additionally, lignin's processability can be improved through chemical modifications like acetylation, etherification, and graft copolymerization (133,134).

2.2.2. Lignin cross-linking

Cross-linking significantly influences the mechanical and thermal properties of polymers and is widely employed to modify polymer performance. Cross-linking is generally linked to the polymerisation of monomers containing multiple functional groups or the establishment of chemical or physical links between polymer chains (135). Using a cross-linker with numerous functional groups during the polymerisation process is known as in situ cross-linking (136). Cross-linking that occurs after the initial polymerisation process is finished is referred to as post-crosslinking. The post-crosslinking process frequently involves reactions that are brought on by chemicals and elevated temperatures (137,138).

Cross-linking alters polymer structure by reducing chain mobility, increasing network density, and raising the glass transition temperature (T_g). As density increases, polymers become more rigid, less viscous, and insoluble due to strong covalent bonds linking the chains. Extensive cross-linking can transform a thermoplastic into a thermoset (135,139). Initially, cross-linking alters the arrangement of molecules in a specific area, leading to a reduction in the mobility of polymer chains, enhancing network density and thus increasing the glass transition temperature of lignin when cross-linked. As the level of cross-linking density increases, polymers often exhibit increased rigidity and reduced viscosity. Cross-linking leads to insolubility due to the

formation of strong covalent bonds that interconnect the polymer chains. An increased concentration of cross-linking alters the characteristics of the material, transforming it from a thermoplastic to a thermoset (135,140).

Lignin's irregular 3D aromatic structure and poor solubility in common organic solvents such as alcohols, halogenated solvents, acetone, and water (138). Consequently, utilising unprocessed natural lignin as a primary source for advanced functional polymers is challenging without undergoing chemical treatment.
Cross-linked lignin-based polymers have been synthesised using dialdehydes (138), diacids (141), and diisocyanates (142), which connect lignin chains through reactive functional groups that serve to connect polymer chains. However, dense cross-linking combined with high aromaticity often results in brittle materials (138,143).

Controlling cross-linking density is therefore essential to achieve desired properties. Flexible polyols such as polybutadiene glycol (144), polycaprolactones (145), and poly(ethylene glycol) (146) can be used as comonomers to act as spacers, increasing the distance between cross-link sites and improving flexibility and processability (147,148). An alternative method for inactivating hydroxyl groups on lignin involves employing capping agents to obstruct excessive reaction sites of lignin. A capping agent is a functional molecule that can obstruct the reaction sites by chemically reacting with surplus hydroxyl groups on lignin (149,150). Kim *et al*., (138), devised a highly effective approach for controlling softwood Kraft lignin cross-linking utilising acetic acid as a capping agent.

Martins de Paula *et al*., (151), employed lignin to cross-link and strengthen the collagen in dentin. In plant cell walls, ferulic acid can esterify arabinoxylans, linking polysaccharides to lignin and influencing wall extensibility and digestibility (152–154). Ferulates act as connectors between lignin and polysaccharides. At elevated temperatures, alkaline hydrolysis liberated the ferulates that were connected by ether bonds, thereby verifying their involvement in the process of cross-linking. Ferulates participated in radical coupling processes with individual units of lignin, resulting in their incorporation into the overall structure of lignin (155–157). Ferulates acted as nucleation sites for lignification by forming covalent bonds with lignin monomers, as illustrated in Figure 11.

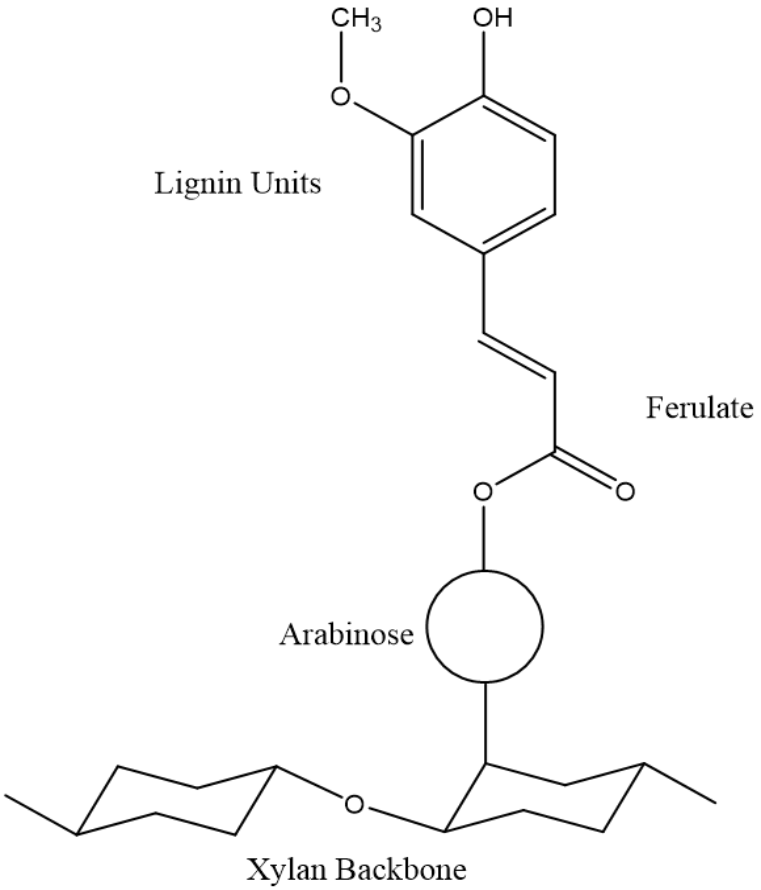

Figure 11. The schematic diagram illustrates the process of ferulate radical coupling to lignin, resulting in the connection of both coniferyl and sinapyl alcohol residues to accessible ferulates (152).

Mainka *et al.,* characterised the cross-linking reactions that occur during lignin heat treatment, following black liquor washing and drying to remove impurities (158). Black liquor washing is a process in the Kraft pulping industry that removes dissolved wood components, including lignin, from black liquor, a byproduct of cellulose extraction. This process is essential for purifying cellulose fibres, recovering chemicals for reuse, and isolating lignin for potential applications (159,160).

The cross-linking of the lignin macromolecules is shown in Figure 12. The primary reaction responsible for cross-linking, was the stabilisation process (9).

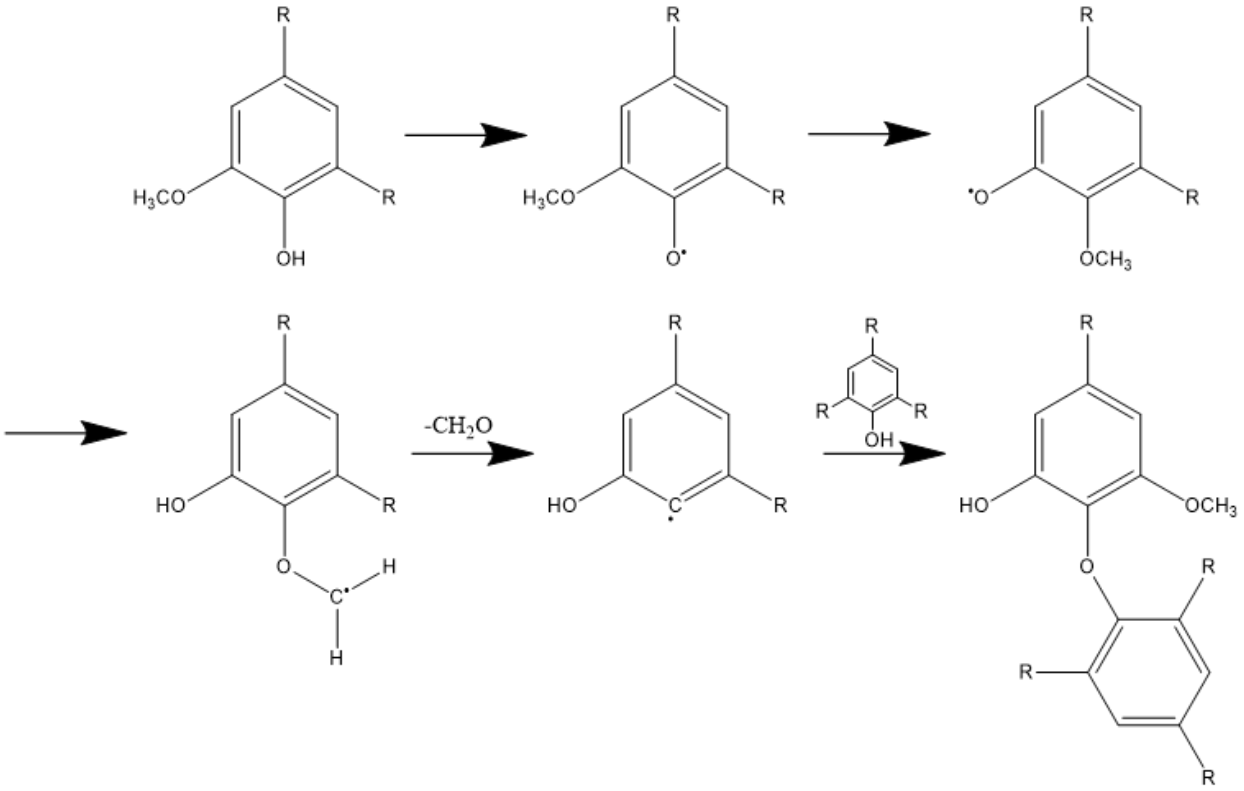

Figure 12. Formation of cross-linkages in lignin macromolecules from free radical polymerisation, adapted from Mainka et al., (158).

2.3. Solubility of lignin in organic solvents

The solubility of lignin in organic solvents is crucial for the successful production of electro-spun lignin fibres. In this thesis, using DMSO as a single-solvent system facilitates the dissolution of lignin, allowing for a homogeneous and stable solution. This solubility is essential for achieving the desired viscosity and electro-spinnability of the lignin solution, which directly impacts the fibre morphology and quality. Adequate dissolution ensures that lignin chains are well-dispersed and aligned during electro-spinning, leading to uniform fibre formation and improved mechanical properties of the resulting nanofibres. Polymer dissolution enables phenomena such as solvent diffusion and chain disentanglement (161).

Lignin is an aromatic polymer that has strong hydrogen bonds and ester linkages with cellulose and hemicellulose to provide binding throughout the lignocellulosic biomass (as seen in Figure 2). For cellulose, increased hydrogen bonding typically reduces solubility. For lignin, the relationship is less straightforward due to its structural complexity and variability in hydrogen bonding. The solubility of lignin is influenced by a range of factors including its molecular structure, molecular weight, hydrophilic moieties and the solvent used. (162–168). Acetylation, in which hydrogen atoms are replaced with acetyl groups ($CH_3C{=}O$), can enhance lignin's

solubility in organic solvents. Acetylated lignins have been used in applications such as carbon fibres, microspheres, thermoplastic composites, and polyurethanes (169–173).

When a polymer encounters a solvent that is thermodynamically compatible, the process of dissolving the polymer often consists of chain disentanglement and diffusion of the solvent. The solubility parameter (δ) theory, which is a valuable prognosis for non-polar and slightly polar polymers, can explain a polymer's solubility in organic solvents (161,167,174).

The contribution of functional and atomic groups can also be used to calculate the solubility parameter of lignin. Cohesive energy (E) and molar volume (V_m) are calculated by accounting for the contributions of atomic and functional groups within each phenylpropanoid unit, see Figure 3. The Hildebrand solubility parameters depend on non-polar interactions when hydrogen bonds are absent. Therefore, any lignin-solvent interactions also consider hydrogen bonding interactions based on the Hansen theory (161,167,174).

Hansen developed the solubility parameters using a theory based on different types of molecular interactions, including dispersive forces, dipole–dipole interactions, and hydrogen bonding (167,175). A significant molecular interaction is hydrogen bonding, which is substantially stronger than dipole-dipole interactions even though it is much weaker than covalent bonds (175–177). Hansen's theory is used to evaluate the hydrogen bonding ability of organic solvents in dissolving lignin, as hydrogen bonding is a key interaction between the hydroxyl groups of lignin and solvents capable of hydrogen bonding (167,168,178).

The capacity to dissolve the lignin should rise when the solvent's and lignin's solubility parameters are the similar, according to the Hildebrand theory, as discussed later in the following section (see Section 2.3.1). As a result, one of the most effective solvents for lignin dissolution is anticipated to be DMSO, solubility parameter 26.69 $MPA^{1/2}$, which has a solubility parameter similar to that of lignin (24.30-25.49 $(MPA)^{1/2}$) (179). Pyridine exhibits a solubility parameter of 10.69 $(MPA)^{1/2}$. It has a lower solubility parameter than lignin and can be used as an alternative solvent for lignin. This is explained by the high solubility of lignin in pyridine and the acid-base interaction between pyridine and the phenolic groups in lignin (167,168,180). Generalised reactions involving pyridine and lignin interactions are shown in Figure 13 (143).

Sameni *et al*., (167), investigated the solubility of lignin and acetylated lignin in a variety of organic solvents, including DMSO, pyridine, ethyl acetate, chloroform, THF, dichloromethane,

acetone and ethanol. The acetylated lignin samples were entirely soluble in all the listed solvents, whereas native lignin only showed solubility in pyridine and DMSO (181,182).

Ni and Hu *et al*., (183), reported that ALCELL lignin (δ = 28.0 $MPA^{1/2}$) showed maximum solubility in ethanol–water mixtures at ~70% ethanol, with solubility decreasing beyond this point. Lignin was most soluble when the solvent's δ-value was similar to that of the lignin, and when the hydrogen bonding capability of solutions with various ethanol concentrations was comparable (183,184). Shukry *et al*., (168), found Acetosolv lignins (δ = 20.45-25.97 $MPA^{1/2}$) soluble in pyridine, dioxane, and DMSO, with solubility improving with longer pulping times and higher acetic acid concentrations.

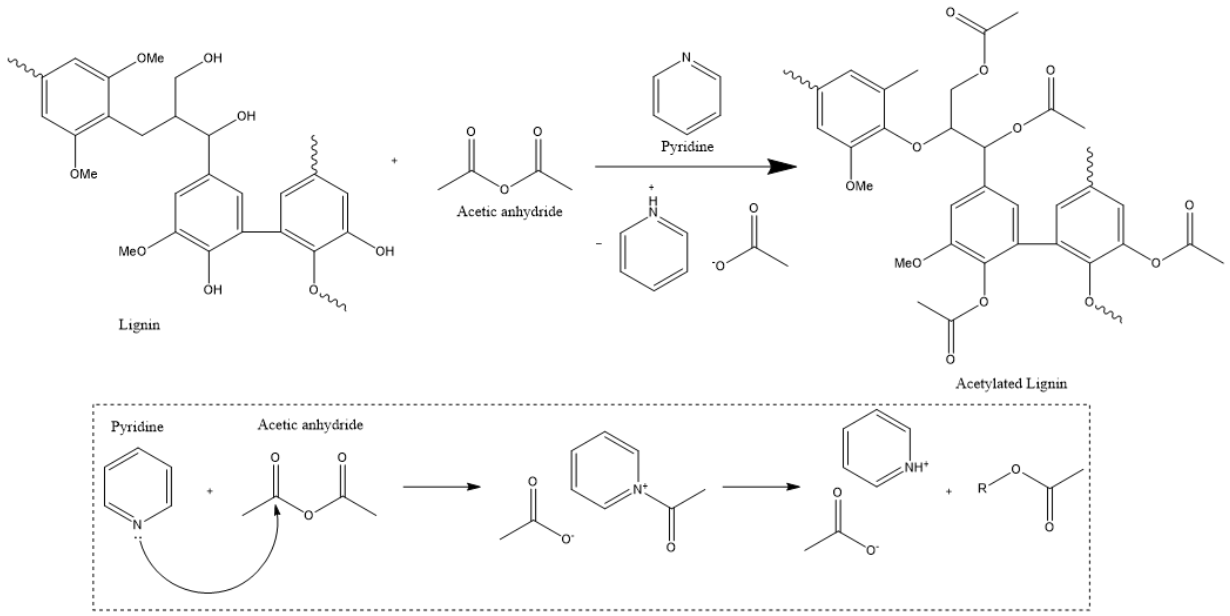

Figure 13. Acetylation of lignin using pyridine and acetic anhydride, adapted from Buono et al., (143).

Schuerch *et al*., (185), reported that ideal lignin solvents had δ-values near 11, and solubility improved with higher hydrogen bonding capability. Despite having a lower hydrogen bonding parameter value than dioxane and DMSO, pyridine acts atypically because it is capable of dissolving lignin. The unexpected solubility of lignin in pyridine may be the result of an acid-base interaction between pyridine and the phenolic groups in lignin, see Figure 13 (186).

Quesada-Medina *et al*., (174), found that hydrolysed lignin from almond shells (δ = 29.86 $MPA^{1/2}$) dissolved more readily in solvents whose δ-values matched that of the lignin. Wang *et al*., (187), observed that lignin solubility in 1,4-butanediol/water peaked at 80% butanediol (14.6 g/L), with δ-values decreasing from 45.63 to 22.68 $MPA^{1/2}$ (182,188).

Lignin dissolution is usually a difficult initial step that is necessary for many applications and production processes. However, a large range of solvents for lignin have already been discovered; of these, deep eutectic solvents, ionic liquids, and organic solvents are particularly important (11). Melro *et al*., (11), found that the most widely used and commercialised source of lignin is lignosulfonates, primarily because of its broad pH water solubility and typically high molecular weights (1000-400,000 g/mol) (122). The solubility of Kraft lignin on the other hand, is adverse in a variety of solvents (ethanol, methanol, dichloromethane). Whilst γ-valerolactone (GVL) based binary systems emerged as a popular organic solvent because of its high solubility in lignin. Pyridinium formate, on the other hand, performed on par with the ionic liquids, dissolving up to 700 g/kg of lignin (162,189–191). While a deep eutectic based solvent system consisting of propionic acid:urea (2:1) at 40 °C, lignin solubility reaches 746 g/kg (11,192). Kraft lignin dissolves more readily at high and low pH due to changes in ionisation: at high pH, deprotonation increases electrostatic repulsion; at low pH, protonation can enhance dissolution (193,194).

Highly efficient solvent systems for dissolving different forms of lignin were established by Xue *et al*., (189). They used binary solvent systems, which comprised of GVL and one co-solvent such as water, ionic liquids, DMSO, or dimethylformamide (DMF), structures illustrated in Figure 14. GVL/water was the most effective solvent system. At 39 °C, the solubility of lignin may still be as high as 38.1 g/100 g when 50% of the material was water. The low viscosity and hydrogen bond interaction between lignin and GVL/water solvent solutions are responsible for the improved performance (189,195).

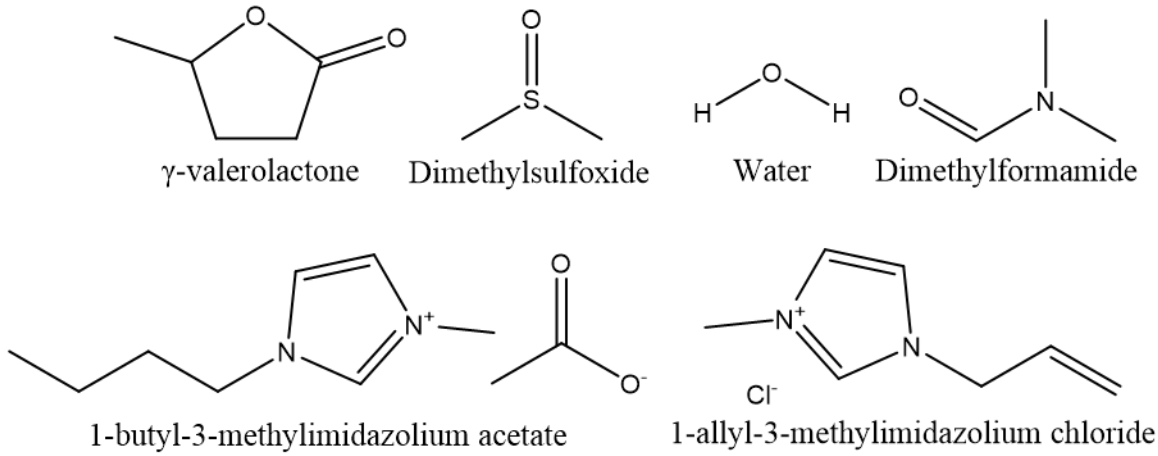

Figure 14. Lignin solvent systems structures; GVL, DMSO, DMF, [Bmim]OAc, and [Amim]Cl by Xue et al. (189).

The solubility of Kraft lignin in DMSO at 90 °C was reported to be greater than 20% (w/v) by Sun *et al*., (196) which is in line with the Xue *et al*., (189) findings about the solubility of Kraft lignin at 70 °C (around 17 g/100 g solvent). As reported by Swatloski *et al*., pyridinium-based solvents show reduced lignin solubility with increasing water content, becoming negligible above 50% (v/v). High water levels compete for hydrogen bonding sites on the solvent anion, reducing its ability to interact with lignin (162,197).

2.3.1. Hildebrand solubility parameter

The Hildebrand solubility parameter (δ-value) hypothesis can be used to describe how the concentration of organic solvent affects the solubility of the lignin, particularly in non-polar or polar systems. It is especially useful in the interactions between polymers and solvents since it can accurately predict how solvents will cause polymers to swell and become soluble. The solubility of a polymer in a solvent will increase in accordance with this hypothesis, when the solvent's hydrogen-bonding capacity rises to an appropriate δ-value and the polymer's solubility parameters are closer together (174,182).

A network polymer like lignin must have its monomers disrupted to be dissolved, this is because hydrogen bonding plays a significant role as a molecular interaction between the hydroxyl groups of lignins and the organic solvents that have the capacity to create hydrogen bonds with lignin (167). When the structure of the polymer's repeating unit is known, one technique for calculating the δ-value of the polymer is based on the contribution of atomic and functional groups (198). The repeating unit in lignin is referred to as the phenylpropane unit (see Figure 9).

In accordance with Hildebrand's theory, the cohesive energy density (E/Vm) equals the cohesive energy density (cal/cm^3), and the solubility of a polymer in a solvent can be calculated as the square root of the cohesive energy density (175,182).

$$E = \sum \Delta e_i \quad (1)$$

$$V = \sum \Delta v_i \quad (2)$$

Where the Δe_i and Δv_i are the additive atomic and functional group contributions for the energy of vaporization (E) and molar volume (V) (182,199).
The δ-value is then calculated by the following equation:

$$\delta = \left(\frac{E}{V}\right)^{\frac{1}{2}} \quad (3)$$

The solubility parameter (δ) according to the Hildebrand theory and the hydrogen bonding parameter (δ_h) based on the Hansen theory for solvents typically used to dissolve lignin are provided in Table 2. Organic solvents like ethanol or methanol have a significantly greater hydrogen bonding parameter compared to other organic solvents, thanks to their capacity to form hydrogen bonds (168). The solubility of lignin in the solvent decreases when there is a larger discrepancy between the two solubility parameters. Thus, the solubility of lignin may be accurately predicted using the solubility parameter theory (167,178).

While Hildebrand solubility parameters were used for initial comparison, it is recognised that they are best suited for non-polar or slightly polar systems. Given the polar nature of DMSO and lignin, with hydrogen bonding and dipole–dipole interactions, the Hansen solubility parameter approach would be more appropriate for accurately describing their interactions (167,178).

Table 2. Solubility Parameter (δ– from Hildebrand Theory) and Hydrogen Bonding Parameter (δ_h– from Hansen Theory) of Organic Solvents and Water (167).

Solvent	**δ (MPA$^{1/2}$)**	**δ_h (MPA$^{1/2}$)**
Diethyl Ether	15.55	5.93
Ethyl Acetate	18.61	7.36
Chloroform	18.82	7.77
Tetrahydrofuran (THF)	19.43	7.77
Acetone (ACE)	20.05	9.00
Dichloromethane (DCM)	20.45	6.95
Benzene	20.45	9.00
Toluene	21.07	6.55
Dimethyl sulfoxide (DMSO)	26.39	12.27
Ethanol	26.39	10.64
Methanol	29.66	22.30
Water	48.07	42.14

2.3.2. Lignin complexation with DMSO

DMSO is widely used as a solvent in electro-spinning due to its strong solvating power and ability to dissolve a variety of polymers, including lignin (200–202). Its effectiveness stems from its capacity to disrupt lignin's intermolecular interactions and solvate polar functional groups,

such as hydroxyl (-OH) and methoxy (-OCH_3) groups (see Figure 3), enabling the dissolution of lignin (203,204).

The interaction between DMSO and lignin is primarily governed by hydrogen bonding and dipole–dipole interactions. The oxygen and sulphur atoms in DMSO can form hydrogen bonds with lignin's polar groups, while oxygen lone pairs also interact with aromatic rings and other electron-rich regions, as shown in Figure 15 (205,206). HSQC NMR spectra provide evidence of associated elimination reactions, such as the detection of an αC–H cross-peak at δC/δH 137/7.26 ppm corresponding to an enol ether product (207).

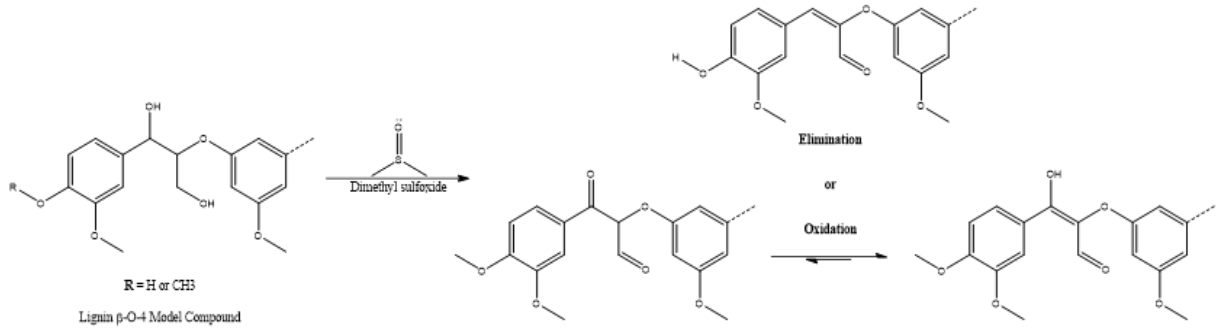

Figure 15. Oxidation and elimination reaction scheme of lignin β-O-4 model compounds via dimethyl sulfoxide (207).

The ability of DMSO to interact with lignin and dissolve it depends on several factors, including the molecular weight and structure of lignin, the concentration of lignin in the solution, and the temperature. Higher lignin concentrations and elevated temperatures generally enhance the solubility of lignin in DMSO (202).

Lower molecular weight lignin has greater solubility in DMSO than higher molecular weight lignin. For example, lignin with a molecular weight ranging from 1,000 to 3,000 g/mol is often more soluble than lignin with molecular weights exceeding 10,000 g/mol (208,209).

The level of lignin in the DMSO solution is another critical component. While increasing the concentration of lignin in DMSO initially enhances its solubility, there is a saturation point beyond which no more lignin can dissolve. Proper optimisation of lignin concentration is essential to achieve a homogenous solution without reaching the saturation point where additional lignin would no longer dissolve effectively and thus be unable to electro-spin the resulting lignin/DMSO solution as it is too viscous/not dissolved efficiently. For analytical purposes, such as NMR, concentrations between 5–20% (w/v) are typical, with 10% (w/v) often found to give complete dissolution (12,206,210,211).

Temperature plays a critical role, with solubility increasing substantially above 60 °C due to viscosity reduction and enhanced molecular motion. Optimal dissolution generally occurs at

100–120 °C, although exceeding 120 °C can cause degradation of both lignin and DMSO, reducing solubility and altering lignin's functional properties (212). Understanding the interaction between DMSO and lignin is crucial for the electro-spinning of lignin-based materials. It helps in determining the appropriate solvent system and optimising the processing parameters to achieve successful electro-spinning of lignin.

2.4. Electro-spinning

Electro-spinning is a method of creating fibres by using electrostatic charge to elongate polymer jets into thin filaments with diameters ranging from tens of nanometres to a few micrometres (13). There are two primary methods, solution electro-spinning and melt electro-spinning, with the choice depending on the polymer state and the desired application. In solution electro-spinning, a polymer is dissolved in a suitable solvent to form a viscous solution, which is subjected to an electric field that draws it into fine fibres as the solvent evaporates. This method is commonly used for thermoplastic polymers soluble in specific solvents, suitable for applications such as filtration, tissue engineering, and drug delivery (213,214). In contrast, melt electro-spinning involves heating the polymer above its melting point and extruding the molten polymer through a spinneret under an electric field. This avoids solvent residues, offering advantages for biomedical implants and other solvent-sensitive applications (215,216). Thus, the selection of method is influenced by the polymer's solubility, thermal properties, and intended fibre application.

The electro-spinning process starts with a polymer solution in a syringe connected to a metal needle, exposed to a strong electrostatic field between the charged nozzle and grounded collector. As voltage increases, charge accumulation, repulsion among polymer chains, and attraction to the collector deform the polymer droplet into a Taylor cone. Once the electrostatic force exceeds surface tension, the solution is expelled as a fine jet. During flight, the jet is stretched and thinned before being randomly deposited on the collector as a non-woven mat. Initially the jet travels straight from the Taylor cone, but then exhibits a characteristic "whipping action" due to electrodynamic instabilities (19,20). These fibres are then randomly deposited onto the collector, forming a non-woven mat or web. This technique allows precise control over fibre diameter and morphology (35,217,218).

Electro-spinning produces continuous fibres with diameters ranging from the micrometre (μm) to nanometre (nm) scale (219). Effective spinning requires the polymer solution to have sufficient

conductivity, and the applied voltage to overcome surface tension forces (220–222). Although applicable to many soluble polymers, some require solution or property modification for successful spinning.

The electro-spinning setup typically includes a syringe fitted with a fine needle (inner diameter 0.1-1 mm) connected to a high-voltage power supply. A grounded conductive collector (or rotating drum) is positioned 10-25 cm from the nozzle (4,223–226). Depending on the configuration, the needle can be positioned vertically or parallel to the collector surface, see Figure 16 (4). As the feeding pump dispenses the solution, a droplet forms at the needle tip. Under increasing electrostatic field strength, this droplet elongates into a Taylor cone (219). When the electrostatic force surpasses surface tension, a charged jet emerges and accelerates toward the collector. During flight, the solvent evaporates, allowing polymer chains to connect and solidify into fibres (218,227). The flight time, influenced by the distance between spinneret and collector, determines whether fibres have sufficient time to form; insufficient distance can result in irregularities or bead defects (224,225).

A key phenomenon during electro-spinning is bending/whipping instability, where the jet undergoes erratic spiralling motion. This instability, driven by electrostatic repulsion, fluid dynamics, and environmental conditions, strongly influences fibre diameter, uniformity, and orientation (227). The degree of "free" charge, influenced by solvent dielectric constant and solution conductivity, also contributes. Higher conductivity generally increases whipping, producing more random fibre orientation; a critical surface charge density is required for this behaviour (218,227). Optimising solvent choice and process parameters help reduce excessive whipping and improve fibre consistency.

Solvent selection is critical, as it influences minimum polymer concentration for spinnability, solution conductivity, fibre morphology, and environmental impact. Many commonly used solvents, such as chloroform, trifluoroethanol, and DMF; are hazardous, creating challenges in safety, disposal, and regulatory compliance (180,228,229). Increasingly, greener alternatives such as water, ethanol, methanol, acetic acid, acetone, and DMSO are being adopted to maintain fibre quality while improving process safety and sustainability (219,228,230).

Near-field electro-spinning (NFES) is a specialised variant in which the spinneret–collector distance is reduced to a few millimetres, creating a stronger local electric field and enabling precise control over fibre diameter and placement (231,232). NFES can be used with both

solutions and melts, reduces solvent consumption, and is suited to high-resolution applications such as nanotechnology, tissue engineering, and sensing (233).

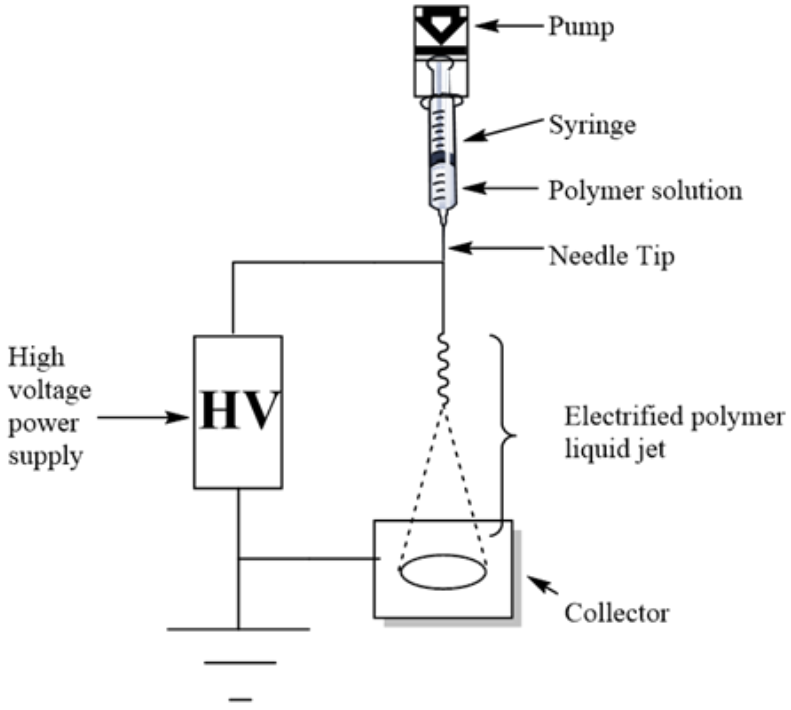

Figure 16. Schematic illustration of a typical electro-spinning setup (4).

2.4.1. Chain entanglement

In electro-spinning, chain entanglement plays a critical role in the formation of continuous and stable fibres. Chain entanglement refers to the physical intertwining of polymer chains, which leads to the formation of a network-like structure. This entanglement occurs as a result of an increased molecular weight and flexibility of the polymer chains (176,234,235).

During the electro-spinning process, a polymer solution or melt is subjected to an electric field, causing the polymer to experience stretching and elongation. The elongation forces the polymer chains to align and entangle with each other, forming a network of interconnected chains. This entanglement provides mechanical strength and integrity to the resulting electro-spun fibres (88,219).

The level of chain entanglement is influenced by several factors, with molecular weight being a key parameter. Higher molecular weights result in longer polymer chains, increasing the probability of chain entanglement. High molecular weight in lignin context typically refers to lignin with a weight-average molecular weight (M_w) above 10,000 g/mol. For example, electro-spinning solutions of lignin blended with high molecular weight poly(ethylene oxide) (PEO) have shown improved spinnability and fibre formation due to better chain entanglement (236).

Consequently, polymers with higher molecular weights generally exhibit better electro-spinnability and produce more consistent and uniform fibres with improved mechanical properties (237).

Additionally, the concentration and viscosity of the polymer solution, as well as the processing conditions such as applied voltage and distance between the spinneret and collector, can also impact chain entanglement (238).

The polymer solution's concentration and viscosity are critical parameters that affect chain entanglement in the process of electro-spinning. Greater concentrations of polymers result in elevated solution viscosity, which strengthens chain entanglement by facilitating the creation of a network-like structure among the polymer chains. Conversely, solutions that have a polymer concentration that is too low do does not have enough interlocking chains, which leads to the creation of beads instead of fibres (239). On the other hand, solutions with very high polymer concentrations might be challenging to electro-spin properly because they become too viscous and thus cannot be spun. Therefore, chain entanglement is fundamental for the production of fibres that are continuous and stable

The chain entanglement is substantially influenced by processing parameters, such as the applied voltage and the distance between the spinneret and the collector. The supplied voltage generates the electric field required to surpass the surface tension of the polymer solution at the tip of the spinneret. Increased voltages can amplify the elongation of the polymer jet, resulting in enhanced alignment and tangling of the polymer chains. Excessively high voltages can lead to destabilisation of the jet, resulting in flaws in the fibres (236,239).

In the context of fibre alignment, chain entanglement also influences the degree to which polymer chains can orient along the direction of the applied electric field. Highly entangled systems resist chain mobility during elongational flow, potentially reducing the extent of molecular alignment within the fibre (240). On the other hand, moderate entanglement levels can balance fibre continuity and chain mobility, enabling improved chain orientation, especially when assisted by collector geometries that impose directional deposition, such as parallel electrodes or the Vee-shaped collector (241,242). Enhanced molecular alignment within fibres has been correlated with improved mechanical properties, orientation and uniformity, all of which are desirable in high-performance polymeric materials (243). Therefore, controlling the degree of chain entanglement through polymer concentration, molecular weight, and solvent interactions is crucial for tuning fibre alignment and the resulting functional properties.

The entanglement of polymer chains in electro-spinning is fundamental for the formation of uniform fibres with desirable properties. It provides structural stability, prevents fibre breakage, and enables the retention of the fibrous structure during subsequent processing or applications. Therefore, understanding and controlling chain entanglement are vital for optimising electro-spinning processes and achieving the desired fibre morphology and performance (3,237,244). Attaining adequate chain entanglement requires optimising the concentration and viscosity of the polymer solution, as well as carefully managing the applied voltage and the distance between the spinneret and the collector.

2.4.2. Bead formation

Bead formation is a common feature observed in electro-spun fibres and is influenced by solution properties, processing parameters, and environmental conditions. Solution properties play a central role. Low viscosity or insufficient polymer concentration reduces chain entanglement, leading to spherical bead formation instead of continuous fibres (245). High surface tension similarly favours droplet formation, while rapid solvent evaporation, driven by solvent volatility, can cause jet instability and bead defects (245,246).

The voltage supplied during electro-spinning has an impact on the creation of the Taylor cone and the stability of the jet. Inadequate voltage can result in the creation of beads because it fails to sufficiently extend the jet (13). The flow rate of the polymer solution is another valuable element influencing bead formation. If the flow rate is high, it can result in the formation of beads if the jet does not have the time to elongate and become thinner before the solvent evaporates (247). The spacing between the needle and the collector also affects the creation of beads. Inadequate stretching of the jet can result in the formation of beads across a small distance (248).

Environmental conditions also have an impact on bead formation. Elevated humidity levels can impede the evaporation of solvents, resulting in the production of beaded droplets on fibre mats (240). The temperature of the solution has an impact on solution viscosity and surface tension, which in turn can affect the formation of beads (249).

Beading can also arise from Rayleigh instability, where insufficient viscosity or concentration prevents jet stability, allowing capillary forces to break the jet into droplets (19,250,251). Minimising bead formation requires optimising polymer concentration, viscosity, surface tension, applied voltage, flow rate, needle–collector distance, and ambient conditions to maintain a stable, continuous jet and produce uniform electro-spun fibres.

2.4.3. Electro-spinning of lignin

Lignin is a promising polymer for electro-spinning due to its high aromatic content, which imparts thermal stability and structural integrity to the resulting fibres (252,253). This property makes lignin-based fibres suitable for applications requiring resistance to thermal degradation. Lignin contains many functional groups, including hydroxyl (-OH), methoxy (-OCH_3), carbonyl (C=O), and carboxyl (-COOH) groups, which contribute to its favourable characteristics for electro-spinning (see Figure 8). The presence of these functional groups enhances the ability of lignin to dissolve in different solvents, which is essential for creating spinning solutions with the desired viscosity and conductivity for electro-spinning (254). Hydroxyl groups facilitate hydrogen bonding, which stabilises the electro-spinning jet and results in the production of homogeneous fibres with reduced defects, such as beads (243). In addition, the presence of different functional groups in lignin offers possibilities for chemically altering its structure, which can be used to customise the properties of the fibres to match specific application needs, this includes increasing hydrophilicity or improving conductivity (255). These functional groups also facilitate cross-linking processes, which improve the resilience and chemical stability of the fibres.

Lignin is readily accessible, mostly as a byproduct of the pulp and paper industry, which makes it a cost-effective choice for electro-spinning applications on a wide scale. Furthermore, the biodegradability of fibres derived from lignin guarantees that they can be safely dissolved at the conclusion of their lifespan, hence minimising their environmental footprint (256,257).

Successful electro-spinning of lignin requires dissolving it in an appropriate solvent system to achieve a solution with suitable viscosity and conductivity. Solvent choice, lignin molecular weight, and processing parameters, such as applied voltage, flow rate, and needle–collector distance, directly affect fibre morphology. While bead formation can occur, optimising electro-spinning conditions can minimise defects (41,257). Common lignin solvents include DMF, DMAc, acetone, acetic acid, and ionic liquids (258). Moreover, the sustainable and biodegradable nature of lignin makes it a highly attractive option for the production of eco-friendly nanofibres. This broadens its range of possible uses, extending from environmental cleanup to biomedical devices (257,258).

Mikeš *et al.,* (259), evaluated multiple solvent systems (DMF, DMAc, methanol) based on the Hansen solubility theory and then evaluated their solubility and electro-spinnability capabilities

for softwood Kraft lignin. Only DMF and DMAc produced spinnable solutions at high lignin concentrations (1–12 Pa·s viscosity), although beaded mats were obtained.

Parot *et al*., (258), successfully electro-spun neat softwood organosolv lignin in DMF at 57 % (w/v) without bead formation, producing fibres 400–1600 nm in diameter (Tg = 120 °C). Optimal parameters included 30 kV applied voltage, 0.4 mL/h flow rate, 20 cm working distance, and 35–45 % humidity. Previous members of the University of Birmingham research group (Bongkot Hararak & Inam Khan) produced neat softwood Kraft lignin fibres without polymer blending, using acetone-fractionated lignin dissolved in an acetone/DMSO binary solvent (2:1 v/v). This yielded fibres with either random or aligned orientation (260).

Despite these advances, challenges remain in improving lignin solubility, stabilising spinning solutions, and controlling fibre morphology. Further understanding of lignin–solvent process interactions will be key to advancing neat lignin electro-spinning.

2.5. Heat treatment of lignin fibres

Electro-spun lignin fibres are produced as precursors for carbon fibre production. Precursor fibres require thermal treatment; by thermostabilisation, carbonisation and graphitisation; to form graphitic carbon structures. Generally, lignin fibres are oxidatively thermostabilised at specified rates prior to carbonisation (35,261).

2.5.1. Thermostabilisation

During thermostabilisation, thermal oxidation occurs by which precursor lignin fibres are heated slowly between 200 °C and 300 °C in air, converting fusible fibre into rigid fibre. The main purpose of this step is to induce cross-linking of lignin macromolecules and therefore prepare a stabilised structure incapable of fibre softening or fusion during carbonisation at higher temperatures (35,261–263). Throughout thermostabilisation, extensive mass loss of volatiles (via H_2O, CO_2, and CO) is commonly seen at higher temperatures or extensive stabilisation times (261,262).

Thermostabilisation needs to be kept at slow enough heating rate to allow cleavage of C-C linkages and to maintain the glass transition temperature (T_g), at which the polymer goes from an amorphous rigid state to a more flexible state. Harsher treatment conditions (longer durations, slower heating rates and higher temperatures) favour oxygen introduction in the macromolecule and will increase the T_g, but can lead to extensive degradation, resulting in undesired fused fibres (35,261).

Previous members of the University of Birmingham research group (Bongkot Hararak & Inam Khan), reported that nitrogen-stabilised fibres were prone to fusion, whereas air-stabilised fibres maintained integrity and exhibited increased oxygen content due to the formation of carbonyl and carboxyl groups (204,260). Air-stabilised fibres degraded gradually over a broader temperature range (250–900 °C) compared with nitrogen-stabilised fibres.

2.5.2. Carbonisation

In carbonisation, stabilised fibres are heated to 800–1400 °C in nitrogen or argon to remove non-carbon elements and promote the formation of aromatic, sp^2-bonded carbon structures (35,262,263). Lignin's high carbon content (~60 %) favours graphitic development, although its structural heterogeneity limits tensile strength due to reduced molecular orientation (261,264). During carbonisation of lignin fibres, dehydration, decarboxylation, demethoxylation, cross-linking and aromatisation reactions take place. Whilst most of the non-carbon elements are released, as listed in Table 3 (264,265).

Table 3. Relative atomic composition of stabilised softwood Kraft lignin fibres, carbonised at different temperatures, as reported by Kleinhans et al., (265).

Temperature (°C)	Carbon (atom %)	Oxygen (atom %)	Sulphur (atom %)
20	74.8	24.8	0.4
300	76.0	23.6	0.4
500	84.3	15.3	0.4
1000	90.7	9.0	0.3
1200	90.8	8.9	0.3

2.5.3. Graphitisation

The graphitisation of lignin-based carbon fibres involves a transformation that occurs following thermostabilisation and carbonisation. During thermostabilisation, lignin fibres are subjected to elevated temperatures in an oxygen-rich environment, leading to cross-linking and stabilisation of the fibre structure. In the subsequent carbonisation phase, the stabilised fibres are heated in an inert atmosphere to very high temperatures, typically above 1000 °C. As the carbon atoms reorganise into graphitic structures, the material undergoes graphitisation, where the carbon atoms arrange into a crystalline, planar lattice resembling graphite. This transformation significantly increases the electrical conductivity, mechanical strength, and thermal stability of

the resulting carbon fibres, making them suitable for advanced applications in electronics, energy storage, and composite materials. The graphitisation of lignin carbon fibres occurs when fibres are heated above 1600 °C, up to 3000 °C (35,266).

At graphitisation temperatures, turbostratic carbon (disordered graphite) repairs its defects, as graphitic structures are built, although usually resulting in carbon fibres with poor mechanical performance. Amplified carbonisation rates introduce defects in carbon fibres, which is unwanted when achieving high strength carbon fibres (266).

2.5.4. Lignin pyrolysis

Pyrolysis is a thermochemical decomposition process that occurs in the absence of oxygen at elevated temperatures, typically ranging from 300 °C to 800 °C. During pyrolysis, organic materials, such as biomass or polymers, are broken down into smaller molecules, resulting in the formation of solid (char), liquid (bio-oil or tar), and gaseous products (syngas) (267,268).

Figure 17, displays the lignin fragmentation pyrolysis pathways mechanistically, displaying the production of char, with by-products of gaseous products (water, methane, carbon monoxide and carbon dioxide) and other phenols (33,267). Figure 17 illustrates the structural composition of native lignin and highlights the primary interunit linkages that are susceptible to thermal cleavage.

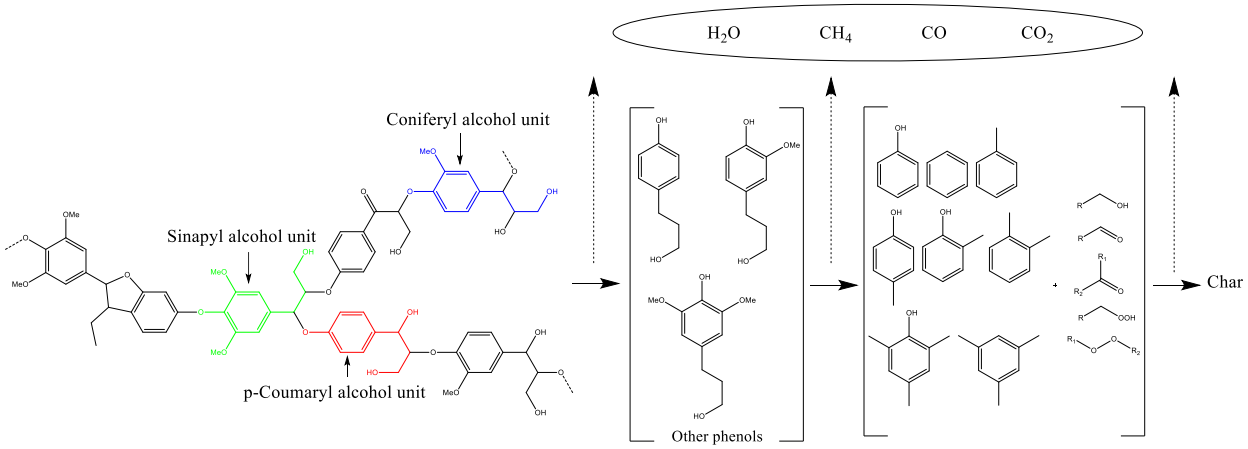

Figure 17. Mechanisms of native lignin pyrolysis and fragmentation pathways (33,267).

Following the cleavage of aryl ether linkages, such as β-O-4, the lignin chain depolymerises into free radical fragments with increased mobility. Further cracking of these intermediates produces vapour products, or cross-linking and repolymerisation produces solid char. The rigid cavities created by the cross-linking of the viscous matrix trap mobile intermediates. This mechanism

prevents volatiles from being released while encouraging the secondary reactions of mobile species that are confined in the holes (269,270).

This process is often used for converting biomass into biofuels, producing activated carbon, or recycling waste materials. While pyrolysis is a broad process aimed at thermochemical decomposition of organic materials into solid, liquid, and gas products at high temperatures, carbonisation is a specific type of pyrolysis focused on maximising the production of carbon-rich char. Thermostabilisation, on the other hand, is a pre-treatment process that enhances the thermal stability of materials at lower temperatures to prepare them for further processing (267,271,272).

For the development of a lignocellulosic biorefinery to produce carbon fibres, polymer additives, green aromatics, or biofuels, an understanding of lignin softening, cross-linking and pyrolysis is crucial. The viscoelastic behaviour of lignin as a function of temperature is such that upon heating, lignin undergoes softening, through glass transition overlapped with depolymerisation, and is followed by the solidification of the softened material, “char”, by cross-linking reactions (160,273).

When lignin is heated above 300 °C in an inert atmosphere, it can undergo the process of pyrolysis, which involves the breakdown of the polymer into smaller molecular fragments. During pyrolysis, lignin molecules are subjected to high temperatures in the absence of oxygen, leading to the formation of a variety of intermediate products, such as phenols, aldehydes, and ketones (271,274,275).

As a result of this process, the lignin molecule undergoes extensive cross-linking, resulting in the formation of a complex, three-dimensional network of interconnected structures. The degree of cross-linking that occurs during pyrolysis can also be controlled by adjusting the temperature and other process parameters, allowing production of lignin-based materials with tailored properties (33,267). However, it is important to note that the process of lignin pyrolysis and cross-linking can also lead to the production of harmful pollutants, such as polycyclic aromatic hydrocarbons (PAHs), which can have negative impacts on human health and the environment. As a function of temperature, condensed aromatic carbons increased while protonated and oxygenated aromatic carbons decreased, as reported by Shrestha *et al.*, when investigating lignin softening and pyrolysis (273). They also emphasise the slow deterioration of methoxyl and side chain carbons.

Sharma *et al.*, reported via SEM analysis of lignin char produced at 250 °C, which showed the lignin particles soften and fuse into a mass of matrix and vesicles. The vesicles form when volatile gases within the softened lignin matrix are released, and they keep their enlarged shape even after cooling (276). They found that the softening of lignin is due to glass phase transition overlapped with the scission of covalent bonds, giving more low molecular weight mobile lignin species (160,273). From around 150 °C, the neat lignin creates a soft material, and from 200 °C on, it begins to form a more rigid material. Mobile liquid-like intermediates become stuck in the stiff char at temperatures between 210 and 330 °C, generating cavities (270).

The pyrolysis mechanism of lignin, as proposed by Yang *et al*., is shown in Figure 18 (277). Lignin undergoes a multi-step thermal decomposition process, consisting of moisture evaporation (< 200 °C), primary decomposition (250–500 °C), and carbonisation (> 500 °C). During pyrolysis, the highly crosslinked polymeric structure of lignin, comprising p-hydroxyphenyl, guaiacyl, and syringyl units interconnected via C–C and C–O bonds, undergoes bond cleavage, leading to the formation of monomeric and oligomeric phenols, as well as aromatic hydrocarbons (269,270). As pyrolysis progresses, side-chain functional groups such as carboxyl, carbonyl, and methoxy detach from the aromatic rings, resulting in the release of small gas molecules including CO_2 and CH_4. Finally, direct carbonisation forms stable biochar (160,273).

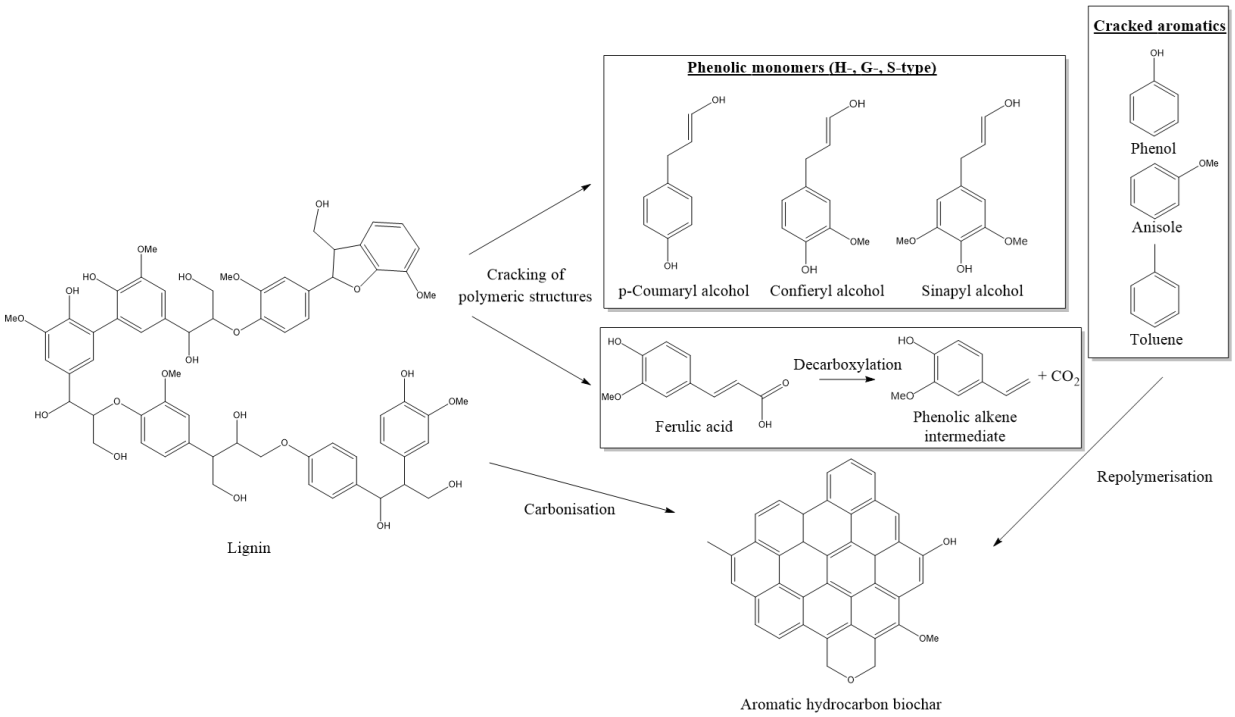

Figure 18. Proposed mechanism of lignin pyrolysis, adapted from Yang et al.*,* (277).

The pyrolysis pathway of lignin begins with the amorphous lignin chains starting to move around at temperatures around 150 °C, indicating the onset of physical changes in its structure due to thermal activation. As the temperature increases to approximately 170 °C, weak interactions between the lignin molecules lead to chain slippage, allowing the chains to slide past each other more freely as thermal energy overcomes the intermolecular forces holding them together. This phenomenon corresponds to the swelling and softening of the lignin matrix, as the material transitions from a rigid state to a more flexible and pliable form, which serves as a precursor to further degradation and transformation during pyrolysis. Overall, these temperature ranges illustrate the significant physical changes that occur in lignin as it is subjected to heat. (269,270). While Figure 17 emphasises the origin and chemical structure of the native lignin and its initial degradation products, Figure 18 describes the thermal degradation pathways and end products, offering a more process-oriented perspective. Together, the figures provide a comprehensive overview of lignin pyrolysis, from structural precursors to reaction mechanisms and final products.

2.6. Manufacturing carbon fibres from lignin and PAN

Carbon fibres are known for their strength and lightweight properties, which make them valuable in various industries including the automotive, aerospace, sporting goods, and wind turbine. The majority of carbon fibres used in commercial and industrial settings come from petroleum-based precursors like polyacrylonitrile (PAN) and mesophase pitch, both of which are costly and account for a sizable portion of the overall costs associated with developing and processing a carbon fibre (278,279).

PAN has traditionally been the primary component of commercial carbon fibres; however, the price of standard grade PAN, which is currently around $10 per kg, poses a significant barrier to carbon fibre applications, as reported by Imarc in 2024 (280,281). When considering the cost for manufacturing carbon fibres, the production of the precursor (often PAN) accounts for more than 50% of the total cost. The carbonisation process accounts for 23% of the residual cost, with the remaining cost proportion going to the size and spooling procedures (158,278,282). Lignin is an alternate precursor with the greatest potential for replacing petroleum-based precursors. Lignin is a key research topic because of its potential abundance, high carbon content, renewable nature, and inexpensive cost. On the other hand, lignin does not meet the conventionally accepted commercial standards for a carbon fibre polymer precursor, which include linear and flexible structure, high degree of symmetry, large molecular mass, high degree of crystallinity, and high

degree of orientation (278,283).

Furthermore, lignin is unique in the fact that it has a high carbon content (~60%) and contains aromatic monomers (monolignols), see Figure 4. This aromaticity makes it conceivable to utilise lignin to produce carbon fibres because of the high carbon content, presenting a chance to increase carbon efficiency and production costs of carbon fibre on an industry-wide basis (278,279).

Lignin is a commonly available and economical carbon fibre precursor since it is a natural waste by-product of the paper industry and bio refineries (158,278,279). Thus, lignin offers a great deal of potential as a raw material for making new natural-based carbon fibres, providing savings in cost, whilst producing a carbon fibre from renewable resources (158,279,282). Lignin, as a promising precursor for fibre production, can be effectively transformed into nanofibres through electro-spinning, a technique that harnesses its unique chemical properties and structural characteristics to create high-performance materials for various applications.

Mainka *et al.,* reported the major reactions that occur during heat treatment of lignin pellets to carbon fibres (158). Following the treatment, the quantities of hydroxyl groups in both pellets and lignin fibre dropped, as reported in ^{31}P NMR spectroscopy. This was related to the growing cross-linked connections between the lignin macromolecules. The oxidised fibre sample exhibited a low solubility. Whilst a single signal at about 165 ppm was detected for the carbonised lignin fibre, via ^{13}C NMR spectroscopy, which is attributed to the presence of anhydride and ester groups. All other signals vanished; a possible explanation hypothesised for this occurrence would be the thorough interconnection of the lignin monomers (9).

The elementary analysis determined that the hardwood lignin that was employed had a carbon level of approximately 60%. The carbon content of the pellets was somewhat higher (67%). The fibre that had undergone oxidation exhibited the maximum amount of oxygen (41%), which served as evidence of the successful cross-linking of the lignin monomers. The carbonised fibre exhibited the maximum carbon content, measuring at 97%. Therefore, the carbonisation process was executed successfully (9,158). A comprehensive summary of papers that have used lignin to produce carbon fibres is shown in Table 4.

Table 4. Summary of papers that have used lignin in the production of carbon fibres.

Title	Authors	Journal/Book	Year	Key Findings	Limitations	Reference
Lignin-based Carbon Fibers for Composite Applications	Kadla, J.F. *et al.*	*Carbon*	2002	This study demonstrated that lignin could be spun into carbon fibres with potential use in composites.	Focused primarily on carbonised fibres; limited discussion of neat lignin fibre morphology/properties prior to carbonisation.	(125)
Lignin-based Carbon Fibers: Effect of Synthetic Polymer Blending on Fiber Properties	Kubo, S. & Kadla, J.F.	*Journal of Polymers and the Environment*	2005	Examined the production of lignin-based carbon fibres and how polymer blending can affect fibre properties, including molecular weight and chemical composition.	Used lignin synthetic polymer blends rather than neat lignin fibres, making direct comparison to neat lignin systems limited.	(284)
Lignin-based carbon fibres: Oxidative thermostabilization of Kraft lignin	Braun, J. L., Holtman, K. M., & Kadla, J. F.	*Advanced Functional Materials*	2005	Focused on the heat treatment of lignin fibres used as precursors for carbon fibres.	Emphasis on stabilisation/carbonisation; minimal detail on spinning process or as-spun neat lignin fibre properties.	(9)
Recent advances in low-cost carbon fibre manufacture from lignin	Baker, D.A. & Rials, T.G.	*Journal of Applied Polymer Science*	2013	Comprehensive review of different lignin sources for producing carbon fibres, focusing on production methods and material properties.	Broad review covering blends, modified lignins, and carbonised fibres; lacks targeted information on neat lignin fibre spinning and pre-carbonisation characterisation.	(285)
A new method for stabilizing softwood Kraft lignin fibres for carbon fiber production	Norberg, I. *et al.*	*Journal of Applied Polymer Science*	2013	Investigated the use of Kraft lignin in carbon fibre production, highlighting	Focuses on post-spinning stabilisation and carbonisation; does not characterise neat lignin	(286)

				stabilisation and carbonisation techniques.	fibres before thermal treatment in detail.	
Lignin as an alternative precursor for sustainable carbon fibres	Mainka, H. *et al.*	*Journal of Materials Research*	2015	Provided a detailed analysis of the potential of lignin from different biomass sources as a precursor for carbon fibres.	Includes multiple lignin sources and blends; less emphasis on neat lignin fibre spinning performance without additives.	(282)
Lignin-based carbon fibres: Formation, modification and potential applications	Wang, S. *et al.*	*Green Energy & Environment*	2022	Comprehensive overview on the formation of lignin fibres and nanofibres. Future development of lignin-based carbon fibres.	Review covers modified lignin, blends, and nanofibres; neat lignin fibres discussed only briefly and often in the context of post-treatment.	(18)

The conversion of lignin into carbon fibres involves a multi-step process that includes fibre formation, thermal stabilisation, and carbonisation. As illustrated in Figure 19, electro-spun lignin fibres undergo thermal stabilisation, during which oxidation reactions occur, rendering the fibres infusible and capable of withstanding subsequent high-temperature treatment without melting. This step is critical to ensure the structural integrity of the fibres during pyrolysis. In the carbonisation stage, the stabilised fibres are heated in an inert atmosphere (typically nitrogen), resulting in the release of volatile compounds such as hydrocarbons, carbon monoxide, carbon dioxide, and water (287,288).

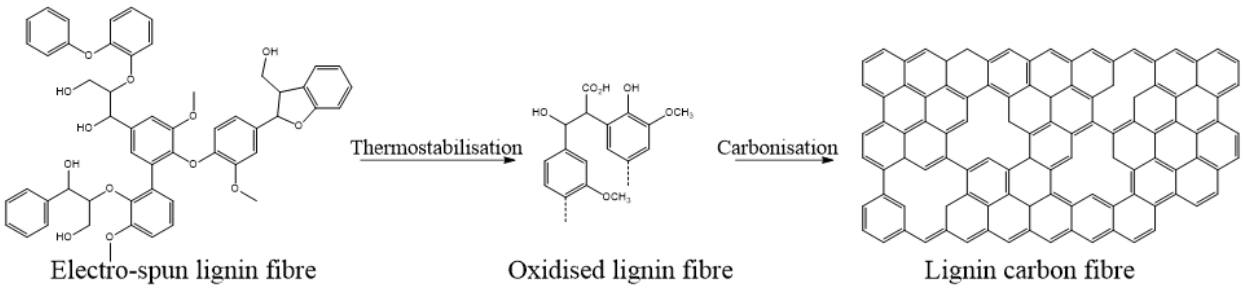

Figure 19. Schematic representation of the conversion process from lignin to carbon fibre, adapted from Raguaskas et al., (287).

What remains is a carbon-rich material with morphology influenced by the precursor lignin's structure and the processing conditions. However, lignin-derived carbon fibres, especially those obtained from industrial Kraft lignin, often exhibit limited mechanical performance due to porosity and low graphitic alignment.

PAN-based carbon fibre precursors account for roughly 90-96% of carbon fibres produced (35). When lignin and PAN are compared as carbon fibre precursors, lignin is more affordable, by over 50% cheaper than PAN (282,289). This economic advantage, combined with its renewable nature, makes lignin a highly attractive raw material for sustainable carbon fibre production (278). However, beyond cost, the structural characteristics of each precursor influence their suitability for carbon fibre formation. PAN possesses a linear nitrile-containing structure, which readily undergoes cyclisation during stabilisation to form ladder-like conjugated structures, as shown in Figure 20 (288).

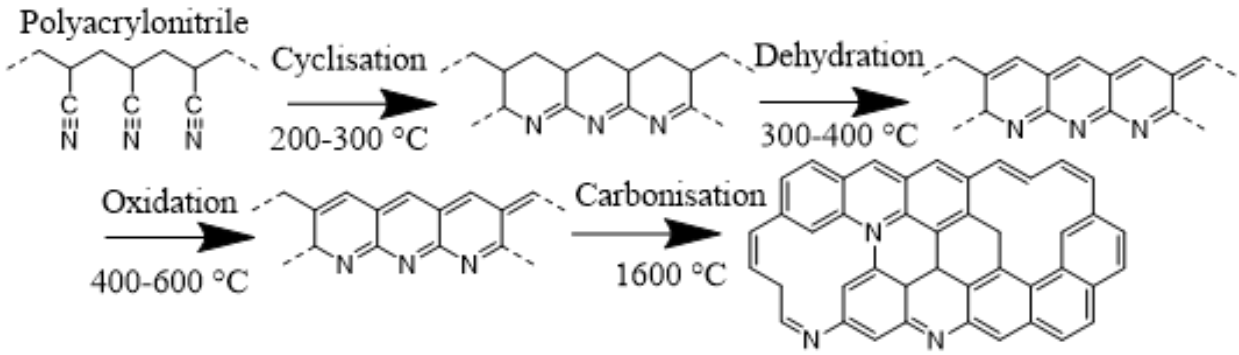

Figure 20. Model reaction pathway from PAN to carbon phase, adapted from Frank et al., (288).

The thermal stabilisation pathway of PAN involves a series of key structural transformations that prepare the polymer for carbon fibre production. The cyclisation is accompanied by dehydrogenation and oxidation reactions, which increase the aromatic character of the polymer and render it infusible. The resulting stabilised PAN structure is rigid and thermally stable, allowing it to withstand the high temperatures of subsequent carbonisation. This facilitates the development of a turbostratic carbon phase during carbonisation, contributing to PAN's success as a high-performance carbon fibre precursor (290–292).

In contrast, lignin is an amorphous, highly branched aromatic polymer with a complex and variable structure depending on its source and extraction method. This structural heterogeneity poses challenges for consistent fibre formation and the development of graphitic order. However, lignin's aromatic framework, see Figure 3, enables it to undergo deoxygenation, crosslinking, and ring fusion reactions under high-temperature treatment (211,293). These thermal processes

can lead to partial structural reorganisation and the formation of turbostratic carbon, characterised by disordered, misaligned graphene layers, see Figure 19. Unlike PAN, which forms aligned ladder-like structures during stabilisation that facilitate graphitic stacking, lignin lacks the molecular regularity needed for such transformation (287,294).

Although lignin is a sustainable and low-cost precursor with high carbon content, its structural heterogeneity limits graphitic alignment and fibre performance, whereas PAN's linear, cyclisable structure consistently produces high-strength carbon fibres despite its higher cost (see Table 5).

Table 5. Comparison of lignin and PAN as carbon fibre precursors (282,287,289,294)

Carbon fibre precursor	**Lignin**	**PAN**
Availability	Waste by-product, abundant, renewable	Petroleum-based, synthetic
Cost	Cheap (≥50% less than PAN)	Expensive (~$10/kg)
Structure	Amorphous, branched, heterogeneous, source-dependent	Linear, nitrile polymer, uniform
Stabilisation	Oxidation → crosslinking; irregular, porosity issues	Cyclisation and dehydrogenation → ladder-like rigid structure
Carbonisation	Deoxygenation, ring fusion → turbostratic, misaligned graphene	Well-aligned turbostratic carbon
Carbon yield	High (~60% inherent C, up to 97% after carbonisation in studies)	High, predictable
Performance	Poor graphitic alignment, lower mechanical strength	Industry-standard high-performance fibres
Sustainability	Renewable, eco-friendly	Non-renewable petrochemical source

2.7. Characterisation of lignin

Structural characterisation is essential for understanding lignin's native architecture, its chemical reactivity, and structural changes following processes such as electro-spinning and heat treatment. It is also crucial for comparing lignin obtained from different industrial and

pretreatment methods. Analytical approaches can be broadly categorised as destructive or non-destructive.

The destructive techniques encompass acidolysis (295), hydrogenolysis (296), alkaline nitrobenzene oxidation (297), copper oxidation (298), permanganate oxidation (299), ozonation (300), thioacidolysis (301), and derivatisation, that is followed by reductive cleavage (1,302). These methods are particularly valuable for determining structural metrics such as the S/G ratios of lignin. However, the majority of these approaches primarily concentrate on the targeted cleavage of ether β-O-4 bonds (see Figure 6), resulting in only a portion of the lignin fragments being suitable for structural study. This is because lignin often consists of both β-O-4 and carbon-carbon (C-C) bonds. Harsh isolation conditions can also degrade native lignin by breaking β–O–4 bonds and promoting new C–C linkages (296).

Non-destructive techniques encompass spectroscopic and microscopic methods that preserve lignin's overall structure, such as UV microscopy, FTIR, Raman spectroscopy, and NMR. Among these, advanced NMR approaches, including 2D HSQC and ^{31}P NMR, are particularly effective for detailed structural elucidation of isolated lignin fractions (29). Complementary analyses such as; FTIR (303), ^{1}H, ^{13}C, ^{31}P, and 2D HSQC NMR (264,304–306), GPC (168), HPLC (86), SEM (307), and thermal analysis (TGA and DSC) (27,292,308), are routinely employed to evaluate lignin's chemical composition, molar mass distribution, morphology, and thermal behaviour (80).

2.7.1. Fourier transform infrared spectroscopy (FTIR)

FTIR spectroscopy is widely used for characterising lignin by detecting the absorption of infrared light at specific wavenumbers corresponding to molecular vibrations. Each molecule absorbs distinct wavelengths of light, resulting in distinctive vibrations that function as a "fingerprint" for that material (309–311). The technique produces a spectrum of absorbance versus wavenumber, typically in the mid-infrared region (4000–400 cm^{-1}), enabling identification of functional groups, monitoring of chemical changes, and comparative analysis of structural differences between samples (309,312).

FTIR is a dependable method employed to ascertain alterations in the functional groups of lignin compounds (313). FTIR provides a quantitative description of the presence of carbonyl groups (C=O), aromatic structures, and substitution patterns in the benzene ring (314,315).

The absorption bands between 3420–3405 cm^{-1} are typically attributed to aromatic and aliphatic OH groups, while the peak typically seen between 2960 and 2925 cm^{-1} corresponds to the

vibrations of CH_3 and CH_2 groups (80). The FTIR spectra of various biomass samples, including oil palm fronds, oil palm empty fruit bunch (316), kenaf, aspen wood (317), sugar cane bagasse (318), wheat straw, pine straw (25), alfa grass (319), and flax fibre (320), exhibited functionality of absorption bands in the region of 1800–400 cm^{-1} (308). These absorption bands indicate the presence of the H, G and S units (shown in Figure 3), in the structure of lignin (24). As reported in the literature, the detection of a peak at 1160 cm^{-1} suggests the presence of characteristic HGS units in the structure of lignin (318,321). In addition, absorbance peaks at 1272, 1219, and 1033 cm^{-1} indicates the existence of G units in biomass samples (319). Similarly, the absorbance peak at 1324 and 1125 cm^{-1} indicates the presence of S units in the lignin structure. The presence of phenolic hydroxyl groups is reported at 1365 cm^{-1} and carbonyl groups at 1705–1715 cm^{-1}. Whilst, the occurrence of signals at 1460 cm^{-1} is associated with the asymmetric deformation of C-H bonds in methyl, methylene, and methoxyl groups (80,322). Another signal which can be observed at 1030 cm^{-1} indicates the existence of aliphatic OH and ether in lignin samples (318,322). The absorption band that can be found at 1738–1709 cm^{-1} represents the stretching of the C=O bond in unconjugated ketones, carbonyls, and ester groups. Meanwhile, the band at 1606–1607 cm^{-1} corresponds to the stretching of C=C bonds in benzene rings (313,323).

Akbari *et al.,* (324), analysed electro-spun softwood Kraft lignin fibre mats using FTIR spectroscopy, collated in Table 6. They reported the peaks seen at 1429–1509 cm^{-1} and 1601 cm^{-1} corresponding to the presence of C–C aromatic rings (325). The alcohol peaks of the lignins exhibited distinct bands at 1260–1270 cm^{-1} and 1330–1375 cm^{-1}, which corresponded to the guaiacyl and syringyl components, respectively. Furthermore, the presence of the carbonyl group was observed within the range of 1700–1715 cm^{-1} (326). The most prominent band in lignin is the O–H band, which occurred at 1300–1400 cm^{-1} and is attributed to the existence of alcoholic and phenolic structures in lignin. Moreover, the C=C bonds in the aromatic rings of lignin was seen at a wavenumber of 1595 cm^{-1}. A further peak seen at 1655 and 1705 cm^{-1} provides further evidence of the hydroxyl groups of lignin (327).

Table 6. Main chemical elements in lignin samples and their range of evolution, detected using FTIR by Akbari et al (324).

Wavenumber (cm^{-1})	Functional Group	Vibration	Compounds	References
974–1058	C–O	Stretching	R–OH	(325,328)
1000–1300	C–O	Stretching		(326,329)
1093–1188	C–C	Skeleton		(328)
1310–1365	$C–CH_3$	Bending	Alkyls	(326,328)
1300–1400	O–H	Bending		(330,331)
1513	C=C–OH	Stretching		(326)
1613	C=C	Stretching	Aromatics	(326)
1645–1750	O–H	Bending	H_2O	(328)
2020–2220	C–O	Stretching	CO	(328)
2210–2390	C=O	Stretching	CO_2	(326,328)
2750–2990	$C–H_2$	Asymmetric Stretching		(328,329)
2904–2979	C–H	Stretching		(325)
2990–3010	C–H	Stretching		(325,329)
3020–3190	C–H	Stretching	CH_4	(325,330)
3500–3600	O–H	Stretching		(325,329)
3823–3870	O–H	Stretching		(325,328)

2.7.2. Nuclear magnetic resonance spectroscopy characterisation of lignin (^{1}H, ^{13}C, and 2D ^{13}C-^{1}H 2D heteronuclear single quantum coherence (HSQC) NMR)

NMR spectroscopy provides detailed quantitative and qualitative information on lignin structure, functional groups, and interunit linkages without the need for calibration. It detects the interaction between radiofrequency radiation and NMR-active nuclei (e.g., ^{1}H, ^{13}C, ^{31}P), producing spectra in which chemical shifts reflect the nuclei's molecular environment (332–334). Only nuclei with non-zero spin ($I \neq 0$) are observable, and higher magnetic fields improve resolution and sensitivity. These are referred to as NMR-active nuclei, such as ^{1}H, ^{2}H, ^{13}C, and ^{15}N. NMR-active nuclei act as magnets, able to align with external magnetic fields, a

phenomenon known as magnetisation (335–337).
Some NMR-active nuclei can assume two distinct orientations when they align with an external magnetic field. One orientation aligns with the lowest energy state of the nucleus, parallel to the external magnetic field, while the other aligns with the greatest energy state of the nucleus, antiparallel to the external magnetic field. The energy level differential (ΔE) is influenced by the magnetic field, impacting the sensitivity of the approach (336–338). Magnetic resonance occurs when nuclei are exposed to radiofrequency irradiation. This results in transitions between energy levels, whereby alterations in the alignment of atomic nuclei spin occur.
Although less sensitive than fluorescence or ultraviolet methods, NMR offers the unique advantage of resolving structural detail at low energy levels and under near-ambient conditions. (339–341). Sample sizes required are typically in the milligram range (10–100 mg), needed to produce high-quality NMR spectra (342,343).

For lignin, both destructive and non-destructive analytical techniques are used, but NMR is among the most powerful non-destructive approaches. Despite the benefits, conventional ^{1}H and ^{13}C NMR can suffer from signal overlap, whereas 2D correlation techniques such as HSQC greatly improve resolution (304). Recent developments in quantitative 2D HSQC pulse sequences have enabled accurate determination of polymerisation degree and branching (344,345).

2.7.2.1. NMR Spectroscopy of Lignin

^{1}H NMR and ^{13}C NMR spectroscopy are two of the most dependable and thorough physical and chemical approaches for characterising lignins. The interpretation of lignins' ^{1}H and ^{13}C NMR spectra still presents several challenges. One such issue is signal assignment, which arises from the strong overlap of signals for ^{1}H and ^{13}C nuclei in lignin found in comparable but distinct chemical environments (346).

The qualitative and quantitative knowledge of lignin structure has been greatly assisted by ^{13}C NMR, primarily because of its high resolution and chemical shift dispersion (347). There are two kinds of NMR spectra, high and low resolution (338). The horizontal scale is labelled in both instances in terms of chemical shift and rises from right to left with a slight peak at zero (if depicted) due to tetramethylsilane (TMS), which is used as a standard. Because it cannot discern between the distinct peaks, a low-resolution spectrum appears simpler in the various peak groupings. Some of the peaks in a high-resolution spectrum are divided into signal groups, as

opposed to a cluster of peaks. Modern correlative approaches in two and three dimensions are now effective instruments for finding structural units (194,342,348,349).

2D NMR is a typical technique in which more than one NMR peak is displayed in a spectrum. Lignin chemistry assignments have more thoroughly assigned using 3D NMR. Spectrometers capable of creating stronger magnetic fields (1000 MHz > 60 MHz), can greatly improve sensitivity and spectrum dispersion (194,342).

2.7.2.2. Proton NMR of Lignin

Prior to 1968, in Ludwig's; "Lignins: Occurrence, Formation, Structure and Reactions", lignin model compounds, synthesised, isolated, and degraded lignins and subsequent derivatives were reviewed thoroughly. The 1964 research by Ludwig, Nist, and McCarthy as well as the 1968 review by Lenz served as the foundation for a large portion of the work that was reported (194,343,350).

Lundquist *et al*., (351), have employed proton NMR with magnetic field strengths of up to 500 MHz to carry out comprehensive and methodical investigations on several types of lignins, including Kraft, milled and acetylated lignins (347). Approximately 7% of isolated lignins were found to have formyl groups. The primary causes were coniferaldehyde and vanillin end-groups, illustrated in Figure 21 (352). The study involved the analysis of lignins extracted from birch and spruce, using spectra obtained from model compounds. The lignins were purified to minimise the presence of carbohydrates (306,347,351).

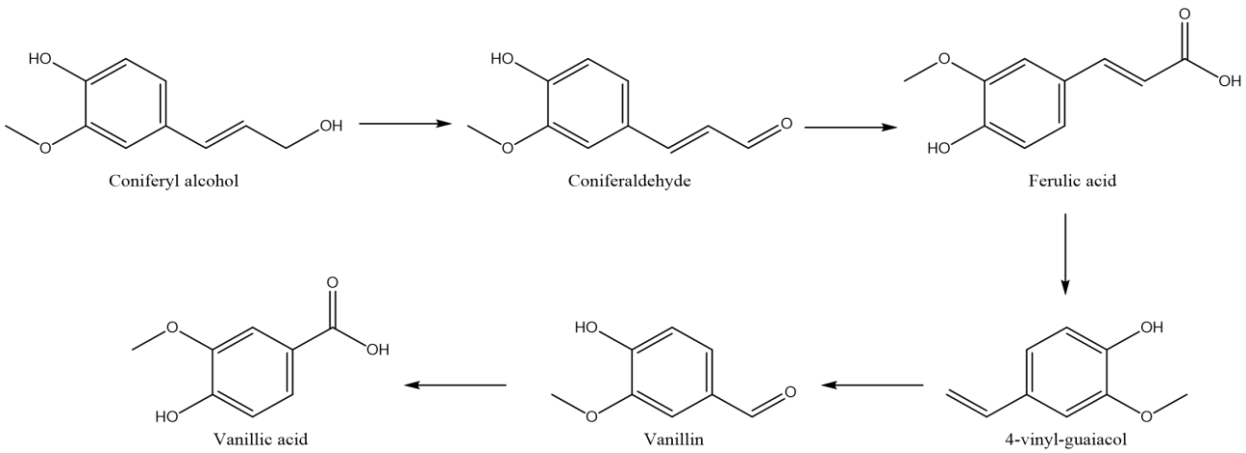

Figure 21. Production of vanillin through lignin thermal degradation (352).

Pylypchuk *et al*., (206,353), characterised Kraft lignin fractions of spruce and eucalyptus using ^{1}H liquid-state NMR spectroscopy. Methoxy groups from the syringyl and guaiacyl units of

lignin were the major groups identified. Furthermore, the presence of aliphatic moieties was indicated, mainly via the lignin side chains (351,354).

The solvent DMSO-d_6 is preferred for ^{1}H NMR due to its low proton exchange, which sharpens hydroxyl resonances (8.1–9.3 ppm) and enables accurate quantification (12,206,342). Aldehyde protons (9.3–10.3 ppm) and acetate methyl protons from acetylated derivatives are also well resolved in DMSO-d_6 (306,342).

The ^{1}H NMR spectroscopy demonstrates the partitioning of hydrogen (proton) signals into several structural areas. The aromatic proton in S and G units of the lignin structure exhibits a signal intensity peak within the range of 6.2 to 8.0 ppm, as reported by Lundquist *et al.*, (351,355). The highest intensity signals of OH in β-O-4 structures are usually observed between 4.0 and 6.0 ppm. The signal peak seen at 5.31 ppm corresponds to H in β-5′ structures (see Figure 8) (351,355). The presence of a methoxy group related to the proportion of G:S units are typically indicated by a sharp signal at 3.1-4.2 ppm (308). Peaks corresponding to acetyl groups are observed in the 1.7-2.4 ppm region, while aliphatic moieties, which are side chains of the lignin structure, are attributed to the 0.8-1.5 ppm region (356).

By examining numerous model compounds in ^{1}H NMR, it was possible to attribute the chemical shift of phenolic OH with certainty. In the lignins characterised by Zeng *et al*., (357), the total concentration of phenolic OH was 5.0 units per 100 Ar. The phenolic H, G, and S units were given to the saturated phenolic OH area (9.4–8.0 ppm). The total aliphatic OH content was also estimated by the sum of α-OH in β-O-4 structures (see Figure 6). As a result of variations in the S/G ratio, the results indicated that wheat straw had roughly 110–116 methoxyl groups per 100 Ar. A cell wall with a greater S/G ratio, such as hardwood (160 units for 100 Ar), results in higher methoxyl groups because every S unit has two functional groups of them (12,357–360).

2.7.2.3. Carbon NMR spectroscopy of Lignin

^{13}C NMR is a powerful but time-consuming method for quantifying lignin structure, with major contributions from Nimz *et al*., (38), who catalogued 40 chemical shift assignments for milled wood lignins from diverse species. Aromatic carbons generally appear at 104–160 ppm, while the aliphatic side-chain region lies between 50–90 ppm (38,342,343,351). ^{13}C NMR spectroscopy is often employed to quantify the carbon signals associated with various hydroxyl groups in lignin.

Hardwood–softwood differences are evident in ^{13}C spectra. Hardwood lignins contain syringyl (S) units with distinctive C-3/5 and C-2/6 signals, (see Figure 4), absent in softwoods, reflecting higher etherified β-O-4 content (see Figure 8) and fewer free phenolic groups (38,351). Softwoods are guaiacyl (G)-rich, with stronger signals from condensed structures such as phenylcoumaran (β-5) and biphenyl (5-5) linkages (see Figure 8) (38,342,343). These compositional differences influence lignin's reactivity and thermal behaviour.

Few signals in the ^{13}C NMR lignin spectrum are linked to specific lignin structures and instead are mostly sidechain carbon signals which are identified in the small chemical shift range (52-90 ppm). ^{13}C NMR encounters many of the same issues as ^{1}H NMR in the absence of full signal resolution. For instance, signal overlap can occur in both techniques, where peaks from different carbon or hydrogen atoms overlap, making it challenging to distinguish between them. Additionally, broadening of peaks can happen in both ^{13}C and ^{1}H NMR, leading to difficulties in accurately identifying specific atoms or functional groups. Another common issue is noise in the spectrum, which can obscure weaker signals and complicate the analysis of the molecular structure (346). Peak assignments for lignin subunits are summarised in Table 7.

Grass-type lignins, such as wheat straw, are typically G-rich but contain more p-hydroxyphenyl and ferulate units, resulting in higher carboxylic group content than in woody lignins (358,365). Interunit linkages including β-O-4, β-5, β-β′, β-1, diaryl ether, and 5-5′/4-O-β′ can be quantified using combined ^{13}C and HSQC methods (357,359,360). In spruce milled wood lignin, ~80 % of side-chain moieties have been identified, including dibenzodioxocin, phenyl coumaran, and pinoresinol structures, as seen in Figure 8 (359,360,366),

Table 7. ^{13}C NMR chemical shift assignments for lignin subunits and functional groups, collated from literature (38,80,364,365,304,342,343,357,358,361–363).

Lignin unit / group	δ ^{13}C (ppm)	Notes	References
S units	104–108 (C-3/5), 130–135 (C-1), 148–153 (C-2/6)	Two methoxy groups shift carbons downfield	(38,361,362)
G units	114–116 (C-3/5), 133–135 (C-1), 146–150 (C-4)	Often condensed (β-5, 5-5 linkages)	(38,304,363)
H units	115–120 (C-3/5), 130–132 (C-2/6)	No methoxy group	(80,304,361)
Methoxy (–OCH_3)	55–57	Abundant in hardwoods	(38,342,343)
Hydroxyl carbons	172–169.6 (primary-OH), 169.6–168.6 (secondary-OH), 169–167 (phenolic-OH)	From acetylation/derivatisation	(364)
Aliphatic methylene	~30	Common in side-chains	(358,365)
β-O-4 side-chain	89–78, 76–73, 63–60	From coniferyl alcohol units	(357)
Carbonyls	200–190 (aldehydes/ketones), 182 (quinone)	Includes cinnamaldehyde, α-keto groups	(80,361,362)
Carboxylic acids	175–168 (aliphatic COOR), 168–166 (conjugated COOR)	Higher in grasses due to ferulates	(80,361,362)

2.7.2.4. NMR spectroscopy of lignin in DMSO

Underivatised lignins are commonly dissolved in deuterated solvents of acetone-d_6/D_2O (9:1 solvent ratio) or DMSO-d_6, this is useful as the solvents are non-toxic and readily available. Chemical shifts can be influenced by solute concentrations, temperature, and the precise solvent composition (38,342,367,368). Higher temperatures can cause up field shifts by weakening

hydrogen bonding (350,368). Acetylation improves lignin solubility and reduces intermolecular interactions, producing sharper ^{13}C signals. Ralph *et al*., (342) reported acetone-d_6 as optimal for acetylated lignin, enabling better alignment between model compound shifts and actual lignin spectra.

Reviewing literature on NMR spectroscopy of lignin in DMSO is directly relevant to this study, as DMSO-d_6 was used as the deuterated solvent in the author's experiments. Existing research provides insight into DMSO's interaction with lignin and its impact on resolution and chemical shifts, aiding accurate interpretation of characteristic peaks and solvent effects. Comparing published methodologies and results supports validation of the current approach, ensures consistency with established findings, and highlights novel observations, thereby strengthening the credibility and context of the research.

2.7.2.5. NMR spectroscopy of lignin fibres

Foston *et al.*, used solid-state and solution NMR to study structural changes in hardwood lignin during oxidative thermo-stabilisation and carbonisation (79,305,369). Methoxy groups, β–O–4, phenylcoumaran, and resinol linkages (illustrated in Figure 8) were detected in native lignin (264,357).

NMR techniques revealed that the oxidative thermo-stabilisation of lignin fibre caused an increased presence of ester and anhydride functionality, most likely because of cross-linking within the oxidised lignin macromolecule (9,264). While carbonisation increased condensed aryl carbons and reduced oxygen-containing groups, especially above 800 °C (264,370,371).

2.7.2.6. HSQC NMR Spectroscopy of Lignin: Insights into functional groups and structural modifications

Heteronuclear single quantum coherence (HSQC) NMR is highly effective for qualitative and quantitative investigation of lignin, providing well-defined signals and resolving overlaps seen in 1D ^{1}H and ^{13}C spectra. This 2D technique correlates carbon and hydrogen atoms, offering detailed structural information, particularly for complex lignin fractions (302,342,372).

2D-HSQC NMR spectra of non-acetylated lignin samples are useful for determining the specific structures of C-O and C-C connections (335,342). A typical 2D-HSQC spectra of lignin consists of two distinct regions: the side-chain region (δC/δH=50–90/2.5–6.0 ppm) and the aromatic region (δC/δH=100–150/5.5–8.5 ppm). The side-chain area of the 2D-HSQC NMR spectra contains valuable data regarding the many linkages found in lignin, such as β-O-4, β- β, β-5 and β-1 (see Figure 8).

The correlation seen at δC/δH 103.8/6.7 ppm corresponds to the C2/C6 positions of the syringyl unit region (see Figure 4). Simultaneously, the guaiacyl (G) units exhibit distinct correlations for C2-H2 (δC/δH.104.8/7.3 ppm) and C5-H5 (δC/δH 115.5/6.8 ppm) (322,373). Furthermore, the p-hydroxyphenyl (H) units are located at the chemical shift values of δC/δH 130/7.2 ppm. Additionally, the correlations of p-coumarates can be observed in the δC/δH 130/7.5 ppm range (374).

The 2D-HSQC NMR spectra readily display cross-signals originating from H, S, and G units in the aromatic regions (335,342), as well as distinct p-coumarate and ferulate signals in the side-chain region of grass-derived lignins. In certain hardwoods, such as poplar and willow, p-hydroxybenzoate cross-signals are also present. S/G/H ratios can be determined directly from aromatic region integrals (296).

Alkyl groups, aliphatic/phenolic hydroxyl groups, methoxy groups, aromatic O/C/H structures, aldehydes, ketones, and β-O-4 substructures in lignin have all been extensively studied using simple ^{1}D, ^{1}H, and ^{13}C NMR (12,306). 2D HSQC due to its versatility in determining lignin subunits and interlinkages as well as lignin-carbohydrate complexes, is also significant in terms of lignin characterisation (375,376). Additionally, a variety of solvent systems, including DMSO-d_6 and pyridine have been used in gel-state and liquid-state 2D whole-cell-wall NMR techniques to shed light on the entire spectrum of polymers that make up plant cell walls (373,377,378).

Sette *et al*., (36,354), applied rapid quantitative HSQC NMR to measure inter-unit linkages in milled softwood, hardwood, and technical lignins, using guaiacyl C2 and syringyl C2/C6 signals (seen in Figure 3) as internal standards. as internal standards. This approach enabled quantitative identification of major linkages (except 4-O-5) in both native and technical lignins (36,354). Shi *et al*., (379), have also used NMR techniques (^{1}H-NMR, ^{13}C-NMR & HSQC) to characterise grass-type (HGS) lignin with high syringyl content (S/G ≈ 1.6) and ~79.5% β-O-4′ aryl ethers per 100 aromatic units, with no evidence of α-O-4′ or β-O-4′ cleavage. Wen *et al*., (335), reported the use of solution state NMR methods (^{13}C-NMR and 2D-HSQC techniques) to show that β-O-4 and ester bonds (acetyl and coumaryl residues) were the main linkages cleaved (seen in Figure 6) during organosolv pretreatment. both qualitatively and quantitatively characterise lignin, both isolated and native lignin. Amiri *et al*., (380), established lignin structure utilising quantitative ^{1}H-^{13}C HSQC-NMR spectroscopy. Reporting that ether linkages are not being

dispersed randomly in isolated lignin, unlike in natural lignin (261,354).
Overall, 2D-HSQC NMR is a powerful technique for identifying lignin's primary structural units, quantifying inter-unit linkages, and monitoring modifications in lignin fractions from various biomass sources and industrial processes.

2.7.3. Gel permeation chromatography (GPC)

GPC is a commonly employed technique in size exclusion chromatography for the determination of molecular weight (M_w) (381). The selection of columns, including their quantity, and the type of detector, are vital for achieving precise determination of molecular mass (382).

The molar mass arrangement of lignins is a crucial characteristic for understanding their characteristics and reactivity. GPC is a highly favoured method for analysing this distribution. During the GPC analysis, the molecular weight of the lignin polymers can be determined using the average (M_w), the average number molecular weight (M_n), and polydispersity index (PDI) (M_w/M_n) (383,384).
Analysis typically involves calibration with monodisperse polymer standards to generate a retention time-molecular weight curve. Since no lignin specific standards are commercially available, substitutes such as polystyrene, sodium polystyrene sulphonates, or poly(methyl methacrylate) are used, often leading to quantification errors (275).

Mobile phase selection depends on lignin type: hydrophilic lignins (e.g., lignosulfonates) dissolve in water, whereas hydrophobic lignins (e.g., Kraft lignin) require non-aqueous solvents such as tetrahydrofuran (THF) (385). Frequently, hydrophobic lignins undergo acetylation to enhance their solubility in the eluent (386). In order to precisely measure the molecular weight, a calibration curve is conducted by utilising the retention time, commonly employing polystyrene and veratrole as reference compounds (387). The molecular weight of lignin varies depending on the kind of feedstock, species, and extraction/purification methods employed (388).

Brosse *et al.*, (389), compared miscanthus organosolv lignin and milled wood lignin using acetylated samples in THF with polystyrene standards, finding organosolv treatment significantly degraded the macromolecular lignin structure. El Hage *et al.*, (390), studied organosolv delignification severity and observed that M_w and M_n values, when determined using polystyrene standards, were often overestimated (275). In order to address the limitations of GPC lignin analysis, a concept known as "universal calibration" has been suggested by Himmel *et al.,*

(391). This calibration is not reliant on the molar mass of a polymer, but rather on its hydrodynamic volume, which is obtained by viscometry (392).

Another problem that arises in lignin GPC analysis is the polymer association caused by polar interactions, which result in an overestimation of the molar mass, particularly when dealing with underivatised lignins (393,394). Tolbert *et al.*, (395), reported that such complex formation can triple molecular weight. To prevent aggregation, especially in Kraft, organosolv, or steam-explosion lignins; Constant *et al.*, (80,275), recommended using organic solvents (THF or DMF) and acetylation.

Lignin molecular weights typically range from 480 g/mol to 8300 g/mol (271,391). Isolation methods can alter this: alkaline treatments (e.g., Kraft pulping) generally depolymerise lignin by ether bond cleavage (see Figure 9), resulting in smaller molecular weight fragments (390,396). In contrast, some treatments increase molecular weight via cross-linking or condensation. Ethanol organosolv pulping, using ethanol and sulphuric acid, produces lignin with low PDI and small M_w (321,390). A compilation of GPC analysis data for lignin reported in the literature, including M_w, M_n, PDI, is presented in Table 8.

The M_n represents the mean molecular weight, calculated by dividing total polymer mass by molecule count, reflecting average chain size (397). PDI (Mw/Mn) describes molecular weight distribution: PDI = 1 indicates uniform chain lengths, while higher values indicate broader distributions (398). Elevated PDI values signify a wider dispersion, influencing the polymer's physical characteristics, processing behaviour, and ultimate performance (399).

Previous members of the University of Birmingham research group, Bongkot Hararak (404) and Inam Khan (405) investigated lignin fractionation methods. Single-solvent acetone fractionation reduced ash content and improved PDI, facilitating lignin electro-spinning (260). The acetone-soluble lignin had an ash concentration of 0.06% (w/v). The M_w was 4250 $g \cdot mol^{-1}$, whilst the polydispersity index was 1.73. On the other hand, the values for as-received lignin were 1.20% (w/v) and 6000 $g \cdot mol^{-1}$ and 2.22, respectively in the order aforementioned.

Table 8. GPC analyses of average molecular weight (M_w), average number molecular weight (M_n) and polydispersity (PDI) for acetylated lignin samples, as reported from literature (80).

Lignin	M_w (g/ mol)	M_n (g/ mol)	PDI (M_w/M_n)	References
Organosolv lignin-oil palm fronds	4023	1581	2.54	(313,400)
Organosolv lignin-oil palm fronds	822	411	2.00	(322)
Kraft lignin-Kenaf	1143	929	1.23	(401)
Organosolv lignin-Kenaf	968	930	1.04	(401)
Kraft lignin-empty fruit bunch	1564	597	2.62	(384)
Kraft lignin-pine	8700	2400	3.63	(308)
Organosolv lignin-tamarind	3100	1700	1.80	(308)
Soda lignin-flax fibres	2600	1500	1.80	(308)
Flax lignin	7620	2123	3.59	(402)
Oil palm fronds	2537	1212	2.09	(313)
Oil palm fronds	2876	1381	2.08	(400)
Oil palm fronds	3093	1647	1.88	(396)
Oil palm fronds	3624	1888	1.92	(396)
Oil palm fronds	784	460	1.70	(322)
Domtar BioChoice Kraft	6772	949	7.10	(403)
Domtar Indulin Kraft	6549	656	9.90	(403)

2.7.4. Thermal analysis

TGA and DSC are frequently employed to determine the thermal characteristics and degrading characteristics of lignins (27).

2.7.4.1. Thermogravimetric analysis (TGA)

TGA measures the reduction in weight of lignin as a function of temperature, under a nitrogen atmosphere. Essentially, the TGA curves of lignins exhibit two distinct stages of decomposition (329). During the initial degradation stage, there is a reduction in weight caused by the release of water, carbon monoxide, carbon dioxide, and other byproducts of pyrolysis. This occurs as a result of the breaking of the phenolic side chains at temperatures ranging from 30 to 120 °C (308,406). The second stage of degradation involves the loss of weight from hemicellulose components that are connected to the lignin structure. This occurs at temperatures between 180-350 °C and is a consequence of the precipitation of lignin (308,384,396). The primary deterioration of lignin weight loss demonstrates the breakdown of the intricate lignin composition within the temperature range of 300–400 °C, see Table 9. In this area, the breakdown of connections between phenolic hydroxyl, carbonyl groups, and benzylic hydroxyl is responsible for the destruction of the intricate lignin structure. This process results in the release of individual phenols into the vapour phase (407). At a temperature of 380 °C, there is a distinct maximum point associated with the process of hydrogenating methoxy groups on the aromatic ring, which subsequently leads to the release of methanol. Methane is a byproduct that can be released at temperatures around 350 °C and it ceases to exist at temperatures between 420 and 430 °C. In addition, the release of carbon dioxide (CO_2) occurs at temperatures ranging from around 200 °C to 640–690 °C as a result of the breaking of C–O–C and C=O bonds (292). Carbon monoxide (CO) is released between temperatures of 220 °C and 790 °C as a result of the decarbonylation reaction of alkyl side-chain carbonyl groups (328,330).

The weight loss observed prior to reaching a temperature of 150 °C can be attributed to the process of water evaporation and a minor degree of dehydration response (324).
Sun *et al.*, (408), reported that lignins exhibit a progressive decrease in weight over 400 °C (up to 900 °C) as a result of the degradation or condensation process of the aromatic rings within the lignin structures. Lignins exhibit stability at elevated temperatures due to their increased degree of branching and the production of densely packed aromatic structures, which can be evidenced by TGA thermal analyses.

In conclusion, the thermogravimetric analysis of lignin highlights its importance in understanding the thermal stability and decomposition characteristics of lignin. The reviewed studies provide valuable context for the current experimental results, allowing validation and comparison of results with established knowledge.

Table 9. The thermal analysis (TGA and DSC) from different biomass samples, as reported from literature (80).

Lignin type	**TGA analysis, DTG_{max} (°C)**	**DSC analysis, T_g (°C)**	**References**
Organosolv lignin-oil palm fronds	345	52	(313,400)
Autohydrolysed-oil palm fronds	368	46	(400)
Autohydrolysed-oil palm fronds	351	49	(313)
Soda lignin-sugar cane bagasse	350	N/A	(318)
Kraft lignin-pine	421	144	(308)
Soda lignin-flax fibres	356	138	(308)
Organosolv lignin-tamarind	413	100	(308)
Organosolv lignin-oil palm fronds	N/A	69	(409)
Kraft lignin-Kenaf	N/A	75	(401)
Organosolv lignin-Kenaf	N/A	66	(401)
Alfalfa lignin	331	N/A	(25)
Wheat straw lignin	328	N/A	(25)
Pine straw lignin	336	N/A	(25)
Flax fibre lignin	332	N/A	(25)

2.7.4.2. Differential scanning calorimetry (DSC)

DSC analysis is a key technique for determining the glass transition temperature (T_g) of polymers. For amorphous polymers such as lignin, T_g marks the transition from a glassy to a rubbery state, directly influencing their processing and industrial applications (409). Furthermore, there exists a correlation between the T_g value and the M_w, which can be elucidated in relation to the free volume idea, proposed by Hussin *et al*., (322). The term "free volume" refers to the unoccupied space within solid or liquid samples that is not taken up by polymer molecules (321).

The T_g of lignin is reached when the primary polymer chains have enough thermal energy to overcome intermolecular forces, allowing rotational and vibrational movements of the polymer segments. This process creates free volume in the material, which is characteristic of the glass transition (321).

The molecular weight of lignin also plays a significant role in this process. A higher molecular weight results in longer polymer chains, which are more constrained by entanglements and require more energy to rotate or move. As a result, lignin with a higher average molecular weight typically exhibits a higher T_g because it takes more thermal energy to activate the molecular motion necessary to transition from the glassy to the rubbery state (401,410).

DSC analysis therefore provides valuable insight into lignin's thermal behaviour, particularly its glass transition and melting characteristics.

2.7.5. Rheological characterisation

Viscosity, the property of a fluid that determines its resistance to flow, is a critical parameter in electro-spinning lignin solutions. Both lignin content and storage time significantly influence viscosity (411,412). Maintaining appropriate viscosity is essential for producing uniform fibres, as low viscosities can result in beading or irregular fibre formation (see Section 2.4.2), while excessively high viscosities hinder jet formation.

In rheology, sweep and ramp tests are commonly used to analyse flow and viscoelastic properties under varying stress, strain, or shear conditions. Sweep tests vary a single parameter, such as frequency, strain, or stress, within a defined range while keeping other parameters constant. Frequency sweeps, for instance, adjust oscillation frequency at constant strain or stress to evaluate viscoelastic behaviour across timescales (413,414).

Ramp tests gradually change stress, strain, or shear rate to assess viscosity changes. Stress ramps

determine how viscosity varies with increasing or decreasing applied stress, providing yield stress and flow curve data (415,416). Shear rate ramps generate flow curves by relating shear rate to viscosity. The shear rate is systematically varied over time in a linear manner in order to measure the resulting viscosity (416,417).

Akbari *et al.*, (324), investigated DMF solutions of softwood Kraft lignin polymer blends to evaluate lignin–polymer interactions. They observed a viscosity drop from 55 to 40 mPa·s over 5 days, suggesting molecular degradation, aggregation, or solvent evaporation during storage. This decline reduced electro-spinning performance and fibre quality, indicating that freshly prepared solutions are preferable. Increased polymer chain entanglement elevated viscosity, whereas reduced entanglement lowered it (418).

The chemical structure of lignin, rich in phenolic rings and hydroxyl groups, enables good solubility in DMF. However, DMF alone does not significantly depolymerise lignin without heat or catalysts (419). In some cases, cross-linking or condensation can increase molecular weight over time, while degradation processes reduce it (420).

2.7.5.1. Effect of solution viscosity on electro-spinning

Lignin, an intricate biopolymer, presents distinct obstacles for electro-spinning because of its viscosity and solubility. The viscosity of lignin solutions is affected by various factors, including the kind of lignin, its concentration, the choice of solvent, and the inclusion of additional compounds. Solutions possessing a moderate to high viscosity are often better suited for the process of electro-spinning (421). In electro-spinning, elevated viscosity is vital as it stabilises the Taylor cone, which is necessary for producing a uniform polymer jet (see Section 2.4). The Taylor cone is the conical structure of the polymer solution at the needle's apex when subjected to an electric field. For the polymer jet to be consistently ejected from the tip, viscosity must be appropriately calibrated; if viscosity is excessively low, the jet may fragment into droplets, resulting in beading instead of continuous fibre production. An increased viscosity imparts essential cohesion and stability to the jet, resulting in the formation of homogeneous fibres (422). This occurs due to viscosity influencing the molecular entanglement within the solution, which aids in maintaining the integrity of the polymer chains when an electric field is applied. Increased viscosity enables electrostatic forces to more efficiently elongate polymer chains into a fine jet, as opposed to inducing droplet formation. The steady Taylor cone and cohesive jet are essential for producing continuous and uniform fibres, hence enhancing control over the electro-spinning process and fibre shape. (423).

On the other hand, solutions with too high viscosity might cause problems in the creation of jets and increase the likelihood of clogging. Whilst solutions with excessively low viscosity can lead to weak fibre development and uneven diameters, as mentioned previously (229,240). Hence, it is necessary to attain an ideal viscosity range in order to ensure efficient electro-spinning.

The ideal viscosity range for efficient lignin electro-spinning can vary based on factors such as the solvent, lignin concentration, and specific electro-spinning conditions. Research suggests that lignin solutions with viscosities typically between 50 to 200 mPa·s are optimal for producing uniform fibres. For example, Kadla et al., (177), found that viscosities in the range of 100 to 150 mPa·s resulted in stable electro-spinning and smooth fibre formation, while Cintra et al., (424), reported that 50 to 100 mPa·s was ideal for maintaining jet stability and minimising beading. The precise viscosity required depends on the type of lignin and solvent system used.
The viscosity of common solvents, such as DMF, DMSO, and ionic liquids, is influenced in varying ways by their interactions with lignin (229,425). For instance, whereas solvents that effectively dissolve lignin may lead to solutions with decreased viscosity, they may not necessarily be optimal for electro-spinning. Therefore, it is essential to optimise the solvent solution in order to achieve the appropriate viscosity for successful fibre formation (426). Ultimately, the viscosity of lignin solutions play a critical role in the process of electro-spinning, impacting the creation, durability, and excellence of the resulting fibres. To enhance the electro-spinning process and broaden the applications of lignin-based nanofibres, it is imperative to comprehend and optimise viscosity by selecting the suitable lignin type, solvent, and additives.

2.7.6. Lignin fibre characterisation

Misra *et al.,* (263), produced electro-spun organosolv hardwood lignin-based fibres blended with PEO and cellulose acetate. These were thermostabilised, carbonised, and characterised using SEM, Raman spectroscopy, and TGA. SEM analysis showed that carbonisation significantly reduced fibre diameter, by 78% for lignin/PEO blends and 44% for lignin/cellulose acetate blends. Lignin/PEO fibres initially measured ~3 µm in diameter, decreasing to sub-micron sizes after carbonisation, while lignin/cellulose acetate fibres decreased from ~500 nm to 200–300 nm (427).
TGA results indicated that the thermal stability of thermostabilised fibres was similar to that of as-spun fibres, with ~40% residual mass. Degradation occurred in two stages; the first at ~337 °C (associated with PEO and lignin decomposition), and the second at ~750 °C. Carbonised fibres had improved thermal stability, leaving ~66% residual mass, and exhibited ~10% weight

loss at 100 °C due to moisture and volatile release. Raman analysis revealed that higher carbonisation temperatures increased graphitic content and structural alignment.(263).

Attia *et al.*, (426), electro-spun fibres from lignin extracted via catalytic organosolv treatment of palm fronds and banana bunches. Characterisation included SEM, TGA, FTIR, elemental analysis, and tensile testing. Carbonisation at 500 °C preserved fibre morphology but resulted in carbon content below 62% (w/v), indicating incomplete carbonisation. TGA and elemental analysis confirmed this, while tensile testing showed a strength of ~3.1 MPa and elongation at break of 69% (428,429).

These studies provide valuable context for the current work on electro-spun lignin nanofibres, enabling comparisons in morphology, thermal stability, and structural development.

2.7.7. Morphological assessment

Optical microscopy is useful for observing lignin dissolution in different solvents and assessing particle size and morphology (385,430). Mandlekar *et al.*, (431), employed this method to ascertain the average particle size of various technical lignins, specifically 71, 63, and 39 μm for alkali low sulfonate lignin, lignosulfonate, and Kraft lignin, respectively. SEM facilitates the examination of intricate surface morphology and microstructures of lignin-derived materials, elucidating the impact of processing parameters, including stabilisation and carbonisation temperatures, on the fibre diameters and porosity of lignin (236,432).

Akbari *et al.,* (324), examined lignin and lignin/polyamidoamine dendritic polymer (PAMAM) blend nanofibres before and after heat-setting. Blend fibres exhibited smaller diameters than neat lignin fibres due to the cationic charges of PAMAM, which lowered surface tension during electro-spinning (433). Additional diameter reduction (~10%) was attributed to chemical interactions between PAMAM cationic groups and lignin's anionic hydroxyl groups. Heat-setting increased the average diameter of both neat and blend fibres, likely due to water removal and hydroxyl group reactivity, which can promote cross-linking and increase viscosity. Conversely, these changes may also enhance chain alignment and reduce hydrogen bonding, facilitating fibre stretching. The final effect depends on the balance of these factors. Diameter variations may also result from depolymerisation and recondensation during heat-setting (434). Thermostabilisation, performed at higher temperatures than heat-setting, typically causes a greater diameter reduction (160).

SEM is also valuable for studying carbon nanofibres from softwood Kraft lignin. Schlee *et al*., (435), reported that stabilisation at 190 °C produced fibres with ~460 nm diameters, which remained stable at higher temperatures, whereas hardwood Kraft lignin showed a greater diameter decrease under the same conditions. Transmission electron microscopy (TEM) is effective for lignin nanoparticles, allowing clear visualisation of core–shell structures and internal features (436,437).

Overall, morphological assessment by SEM is crucial for evaluating electro-spun nanofibre quality, providing detail on diameter, texture, and uniformity. It helps identify bead formation, defects, and inconsistencies that can affect performance, thereby supporting optimisation of electro-spinning parameters and improving fibre quality (16,438).

2.8. Literature review conclusion

Lignin, a complex and heterogeneous polymer abundantly present in biomass, has attracted growing interest as a renewable resource for applications beyond its traditional status as a pulping by-product. This review examined key aspects of lignin research, including its occurrence in biomass, extraction and purification methods, cross-linking behaviour, solvent interactions, solubility in DMSO, and characterisation via NMR, FTIR, GPC, viscosity, morphological assessment, and thermal analysis (DSC and TGA).

Lignin content varies between biomass types, influencing extraction method selection. Established processes such as Kraft and soda pulping remain prevalent, but advanced methods; organosolv, steam explosion, and ionic liquids, offer improved yields with reduced environmental impact. Post-extraction purification, through techniques such as ultrafiltration and fractionation, tailors molecular weight and chemical properties for targeted applications.

Lignin's reactive phenolic groups enable cross-linking, enhancing mechanical and thermal properties in biopolymers. Solvent–lignin interactions, particularly with DMSO, are critical for both processing and structural analysis. DMSO's high solvating power supports detailed structural studies and facilitates the preparation of lignin-based blends.

NMR spectroscopy, including 1D (^{1}H, ^{13}C) and 2D HSQC, is indispensable for elucidating lignin structure, functional groups, inter-unit linkages, and changes induced by processing. Complementary techniques such as FTIR, GPC, rheology, SEM, DSC, and TGA further characterise lignin's chemical, physical, and thermal behaviour.

Future research should focus on improving extraction efficiency with minimal environmental footprint, advancing solvent systems, and developing scalable modification strategies. The versatility of lignin positions it as a key sustainable feedstock for applications in biopolymers, composites, pharmaceuticals, and energy storage. Realising this potential will require continued interdisciplinary innovation and optimisation across the entire value chain.

3. Experimental

3.1. Materials

(i) Lignin: Softwood Kraft lignin (Domtar BioChoice^{TM}) was purchased from UPM Biochemicals. BioChoice^{TM} lignin is a by-product of the Kraft pulping process, and it was dried in a vacuum oven with a liquid nitrogen trap at 80 °C for 6 hours at a decreased pressure of 1 bar to remove moisture. A photograph of the as-received lignin powder is shown in Figure 22.

Figure 22. Photograph of the BioChoice^{TM} lignin powder (531).

(ii) DMSO: 99.8% anhydrous DMSO was used as the solvent and was obtained from Alfa Aesar in the UK. Due to DMSO's hygroscopic properties, the container was sealed with a silicone rubber septum, and the solution was extracted using a hypodermic needle & syringe.

(iii) Deuterated DMSO: Dimethyl sulfoxide-d_6 "100%", 99.96 atom% D, was purchased from Sigma-Aldrich. This was necessary for dissolution in NMR sample preparation in order to assist in identify peaks.

(iv) Polyacrylonitrile: PAN was purchased from Goodfellow in powder form (230,000 g/mol), it was blended with lignin in DMSO solution before being electro-spun.

All polymer concentrations are expressed as % (w/v), referring to grams of polymer per 100 mL of DMSO. For example, a 10% (w/v) solution contains 10 g of polymer in 100 mL of solvent. This applies to both neat lignin and lignin:PAN blend solutions, with the "lignin:PAN" ratio (e.g., 30:70) indicating the composition of the total polymer content where relevant. Throughout this thesis, the term "lignin/DMSO" refers specifically to neat lignin dissolved in DMSO, without the inclusion of any co-polymers.

3.2. Characterisation

The methods employed to characterise the lignin as-received, the electro-spinning solutions, and the electro-spun fibres are summarised in the section that follows.

(i) Differential scanning calorimetry (DSC): Using a differential scanning calorimeter (Perkin-Elmer DSC-7), melting points, glass transitions, and heat of fusion were precisely measured for lignin samples in crimped double pierced aluminium pans. A crimped pan without the lignin was used as the reference. The sample and the reference lids were pierced with two holes to permit the release of volatiles during the heating cycle. The instrument was calibrated using indium and tin. Lignin samples were examined in a nitrogen environment, with the flow rate of 50 mL/min throughout. To determine the thermal characteristics of the lignins, samples of 5–10 mg weight were heated at a rate of 20 °C min^{-1} between 20 and 220 °C, two successive cooling and heating cycles were conducted, with three consecutive DSC scans performed per sample. These measurements were conducted as one-off experiments, and therefore no replicate data or error bars are reported.

(ii) Thermo-gravimetric analysis (TGA): The thermogravimetric analyser (Perkin-Elmer TGA 8000) is suitable for organics and determining the degradation temperature for the lignin samples tested. Approximately 10 mg of each lignin sample was placed in a platinum pan and heated from 100 °C to 800 °C at a rate of 20 °C min^{-1} under a nitrogen atmosphere. The nitrogen flow rate was maintained at 20 mL/min throughout the run. A blank reference pan was used for baseline correction. These measurements were conducted as one-off experiments, and therefore no replicate data or error bars are reported.

(iii) Fourier transform infrared spectroscopy (FTIR): FTIR spectroscopy was conducted using a Thermo Scientific Nicolet iS50 FT-IR spectrometer equipped with a PIKE Technologies GladiATR single-reflection diamond ATR accessory. This system utilises a monolithic diamond crystal, allowing direct analysis of solid and semi-solid samples without the need for additional preparation. Spectra were recorded for three sample types: as-received lignin, vacuum-dried lignin, and vacuum-dried electro-spun lignin fibres. A small amount of each sample was placed onto the ATR crystal, and a pressure arm was applied to ensure consistent contact with the surface. All spectra were collected over a range of 4000–400 cm^{-1}, using an average of 100 scans per sample at a resolution of 4 cm^{-1} to enhance signal quality. A background spectrum was obtained before each measurement. OMNIC 8.1 software was used for spectral acquisition, baseline correction, and data analysis. All FTIR measurements were performed as single-run, one-off experiments due to limited material availability.

(iv) Elemental analysis: Elemental analysis of lignin samples was conducted via a CHNS elemental analyser (model EA111 Carlo Erba Instruments, UK). The samples underwent freeze-drying for one week before the analysis was performed. The organic elemental composition was measured using combustion elemental analysis according to the Pregl-Dumas method (439,440). The absolute content of carbon, hydrogen, nitrogen, and sulphur percentage in each sample of lignin was then determined. For each sample, two measurements were performed, and the resulting percentage values were averaged to obtain the final reported values. All elemental analysis values are reported as the mean ± standard deviation of two measurements, rounded to two decimal places for consistency.

(v) Nuclear magnetic resonance spectroscopy (NMR): Solution-state NMR spectroscopy was employed to investigate the structural features and chemical modifications of lignin samples, due to its high sensitivity and versatility for characterising complex macromolecules. All NMR measurements were performed using a Bruker AVANCE 600 MHz spectrometer, capable of acquiring both one-dimensional (1D) and two-dimensional (2D) spectra. Lignin samples (~10 mg) were dissolved in 0.75 mL of deuterated dimethyl sulfoxide (DMSO-d_6), in accordance with established protocols (357,358,365). Chemical shifts for both ^{1}H and ^{13}C nuclei were referenced to the residual solvent peak of DMSO-d_6 and reported relative to tetramethylsilane (TMS) in parts per million (ppm).The operating frequencies were 600.13 MHz for ^{1}H and 150.90 MHz for ^{13}C nuclei, with experiments conducted at a constant temperature of 295 K. Two-dimensional spectra were acquired using standard pulse sequences. COSY (Correlation Spectroscopy) experiments were recorded with a spectral width of 6 kHz in both dimensions, using 256 increments, 32 scans per increment, and 1024 data points in the direct dimension. The relaxation delay was set to 1.5 s, and the ^{1}H pulse width was 9.3 μs.

(vi) Rheology: A cone-and-plate rheometer (Discovery Hybrid Rheometer, model HR-1, TA instrument, UK) was used to measure the viscosity of the neat DMSO (Alfa Aesar), lignin:PAN in DMSO and lignin/DMSO solutions. The plates had a 40 mm diameter and a 4° cone angle. The shear viscosity was measured at room temperature (25 °C) and the electro-spinning chamber temperature (55 °C), whilst the rheometer was operated at 10 s^{-1}. Viscosity measurements for the solutions were conducted as single-run experiments for each formulation; consequently, no error bars are included in the reported data.

(vii) Electrical conductivity: A bench conductivity metre (model 4510, Jenway, UK) was used to determine the electrical conductivity of the DMSO and lignin/DMSO solutions. A sodium chloride conductivity standard solution (HI7033, Hanna Instrument) was used to calibrate the instrument. Once the probe was immersed in the glass vial, the top was sealed with a rubber septum to minimise the interaction of the solution with atmospheric moisture. The temperature of the solutions was regulated by part-immersing the glass vial housing the solution in a temperature-regulated water bath (Grant, UK). The electrical conductivity of DMSO was determined from 25 and 60 ºC in increments of 5 minutes with a dwell of 10 minutes at each temperature where five readings were taken and averaged. The same procedure was performed for the lignin:PAN in DMSO and lignin/DMSO solutions.

(viii) X-ray diffraction (XRD): XRD is a non-destructive analytical method for learning about a compound's crystalline structure. Lignin samples, as-received powder and carbonised electro-spun nano-fibres were characterised by XRD analysis. Using Cu K radiation (λ=1.54) and a Panalytical Empyrean diffractometer with a Ni filter, XRD patterns were captured. The scanning ranged from 0° to 90° with steps of 2 s and 0.02°. Utilising the ICDD database and the X'Pert Highscore Software (version 2.2), chemical compound identification was carried out for the lignin samples. XRD measurements for the lignin samples were conducted as single-run experiments; consequently, no error bars are included in the reported data.

(ix) Scanning electron microscopy and image analysis: A scanning electron microscope (HITACHI TM-3030, Japan) that was operated at 15 kV with a current of 0.8 nA was used to study the morphology of the as-received lignin and the electro-spun fibres. An adhesive carbon tape was used to place the sample on the SEM stub, prior to inspecting the samples on the scanning electron microscope. The samples were coated with a gold/palladium alloy using an Emscope SC 500 vacuum sputter-coater for three minutes at 25 mA and a vacuum of 1 mTorr. The diameters and alignment of electro-spun fibres was measured using image analysis using Image J software (NIH, USA). 150 measurements were obtained per sample for the fibre diameter measurements. 100 measurements were made per sample to determine degree of alignment of fibres. The fibre direction angles recorded in ImageJ were normalised by establishing the mean fibre direction at 0°, thereafter computing the variation in degrees of all fibre direction observations from this reference point. For consistency, all SEM measurements were conducted at a magnification of 1000×, allowing direct comparison of fibre morphology between samples.

(x) Gel permeation chromatography (GPC): Arkadios Marathianos of the University of Warwick used GPC to determine the lignin's molecular weight distribution. The lignin samples were dissolved at a concentration of 5 mg/mL in DMF, which was acquired from Sigma-Aldrich. At 50 °C, DMF was utilised as the mobile phase eluent at a flow rate of 1 mL/min. The column was filled with 80 µL of dissolved lignin sample in DMF at a concentration of 1 mg/mL. GPC (Agilent 1260 Infinity II-MDS) was used to determine the molecular weight distribution. Elira He, a colleague researcher from the University of Birmingham, conducted the analysis of the GPC data.

(xi) Thermostabilised lignin powder was prepared by initially drying as-received softwood Kraft lignin (BioChoice) in a vacuum oven at 100 °C for 4 hours. The vacuum-dried lignin powder was then transferred to an alumina combustion boat (Almath Crucibles Ltd, UK) and placed at the centre of a tube furnace (PYRO THERM Furnaces, UK). Prior to thermal treatment, the tube was purged with the appropriate process gas, either dry nitrogen or dry compressed air, at a flow rate of 50 mL/min for 30 minutes. The thermal protocol began with a 1 hour hold at 100 °C, followed by a controlled temperature ramp of 1 °C min^{-1} up to the target temperature of 260 °C. The sample was then held at this temperature for 2 hours. Following the heat treatment, the sample was allowed to cool naturally to room temperature (25 °C) under the same gas atmosphere used during the process. The temperature was measured using a thermocouple (R-Type) and recorded using a Pico TC-08 data logger and Picolog data logging software (Pico Technology, UK). Siheng Shao and Elira He, colleague researchers from the University of Birmingham, conducted the thermostabilisation of the lignin powder samples in the tube furnace.

(xii) Lignin fibre thermostabilisation and carbonisation: Electro-spun lignin fibre mats (3.5 cm × 5 cm), prepared from a 100 % (w/v) neat lignin solution in DMSO refluxed for 4 hours at 100 °C prior to electro-spinning, were cut and placed between alumina ceramic plates to preserve morphology during thermostabilisation. The assembly was positioned at the centre of a tubular furnace (PYRO THERM Furnaces, UK), which was purged with dry nitrogen. The samples were first held at 100 °C for 1 hour, then heated to 260 °C at a rate of 1 °C min^{-1} and held for 2 hours to complete stabilisation. The carbonisation of the fibre samples was carried out directly after the stabilisation process without removing the sample from the tube furnace. The temperature was increased at the same heating rate to the target carbonisation temperatures of 600 °C, 900 °C, or 1200 °C, with each sample held for 2 hours under continuous nitrogen flow of 50 mL/min. The furnace was then allowed to cool naturally to room temperature under nitrogen. Siheng Shao and

Elira He, colleague researchers from the University of Birmingham, conducted the carbonisation of the lignin fibre in the tube furnace.

3.3. Preparation of lignin:PAN blend DMSO solutions

Blend solutions of lignin and PAN were prepared using DMSO as the solvent. The lignin was first dried in a vacuum oven with a liquid nitrogen trap at 80 °C for 6 hours, ground using a pestle and mortar, and then dissolved in DMSO with continuous agitation using a magnetic stirrer. Similarly, PAN was dissolved in DMSO under constant stirring. The individual solutions were filtered using a Buchner funnel with 1.2 µm glass fibre filter paper before being combined according to the desired blend ratios. By varying the blend composition and processing parameters, highly aligned fibres were successfully produced from 30:70, 50:50, and 70:30 lignin:PAN blends. Following the electro-spinning of blend fibres, neat lignin fibres were spun separately to compare morphology and structural properties.

3.4. Preparation of lignin/DMSO solutions for identifying the optimum concentration

To find the best lignin concentration for electro-spinning, a variety of lignin solutions in DMSO were created. The lignin polymer concentrations made were 50, 60, 70, 75, 80, 90, 95 and 100 % (w/v) in DMSO. The lignin was dissolved and homogenised using an overhead stirrer for 6 hours at room temperature. During the dissolution process, the beaker containing the lignin DMSO mixture was part-covered using Parafilm (Parafilm®, Medium, Phillip Harris, UK) to minimise the absorption of atmospheric moisture After the dissolution of lignin, the solution was kept in an airtight container until it was needed for characterisation or electro-spinning.

3.5. Heat treatment temperatures for the 100% (w/v) lignin/DMSO solutions

The rationale for selecting the 100% (w/v) lignin/DMSO is presented in a subsequent section (see Section 4.4.4). The research hypothesis was that the tendency for lignin to cross-link during thermal treatment could be used to increase its molecular weight to enable it to be electro-spun without requiring fractionation or blending. The refluxing of the lignin/DMSO solution was conducted in a 100 mL three-neck round-bottom flask where the central neck was used to house a condenser, shown in Figure 23. The other two necks were capped with a silicone rubber septum, and one housed a digital thermocouple (TFA Dostmann Professional Digital Thermometer with Probe) and the other a hypodermic metal needle through which nitrogen gas (inert atmosphere compressed air) was bubbled into the solution at 30 mL min^{-1}. A magnetic stirrer was also used to stir the solution. The temperatures selected were 80, 100, 120, 140 and

160 °C. These temperatures were selected based on the DSC where the glass transition temperature showed a sequential increase after three consecutive scans.

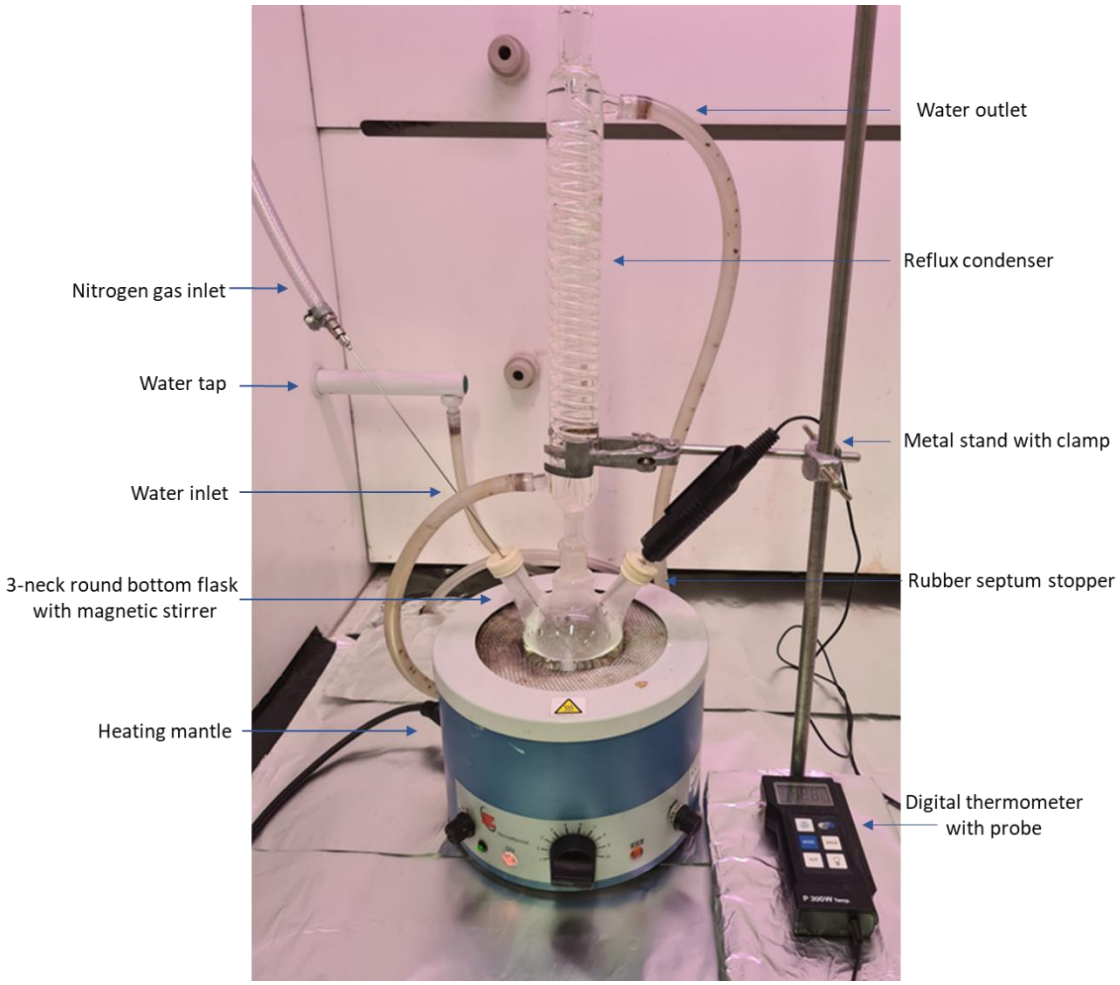

Figure 23. Photograph of the reflux system set-up used to dissolve lignin in DMSO.

3.6. Electro-spinning

A schematic diagram of the custom-made electro-spinner that was used is shown in Figure 24 (19). The key coded components in Figure 24 are: (i) Liquid dispenser (AL1010, World Precision Instruments). (ii) A disposable syringe (Terumo, UK) and a flat-tip 25-gauge needle (AD725025, Adhesive Dispensing Ltd, UK) with outer and inner bore diameters of 0.3 and 0.5 mm respectively, needle assembly with a lock (16.5 mm length). (iii) A Teflon tube (PTFE) of dimensions (20 mm length), inner and outer bore diameters of 5.42 and 1.65 mm respectively with PTFE lock adapters; syringe end (25 mm length, 5 mm inner diameter) & needle end (22 mm length, 5mm inner diameter) at both ends; (iv) a ring-adapter for connecting the tip of the needle to a high-voltage power supply (DC, 73030 Genvolt, UK). (v) A square copper grounded

collector plate of dimensions 10 x 10 x 0.5 cm. A crimp-free aluminium foil was placed in intimate contact on the surface of a grounded copper plate.

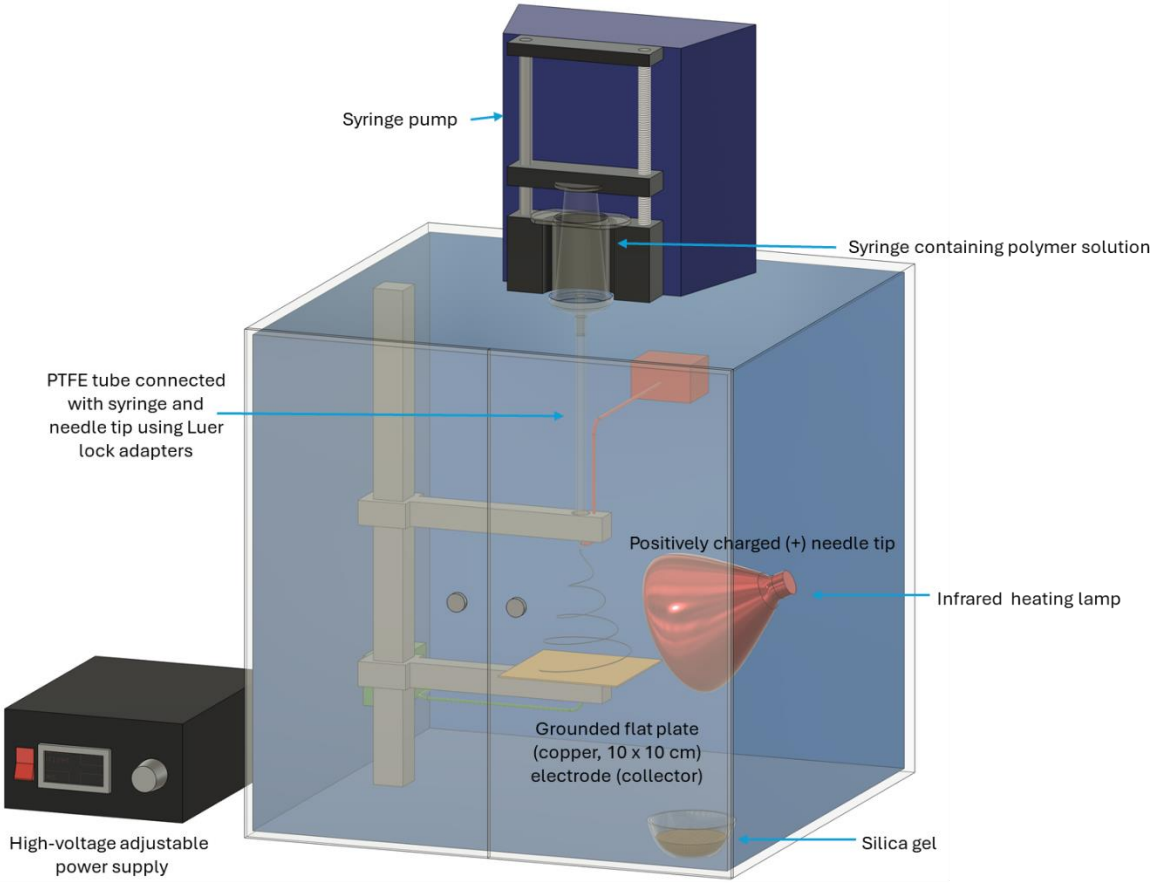

Figure 24. Schematic illustration of electro-spinning setup with a flat plate ground-electrode for collecting random orientated lignin fibres (19).

The applied voltage ranged from 10-12 kV, and the working distance between the tip of the needle and the grounded electrode was maintained at 8 cm. The liquid dispenser was set to operate at 0.5 mL hour^{-1}, but it was adjusted as required to maintain a pendant drop of the polymer solution at the tip of the needle. The chamber's temperature was held between 55 and 60 °C and maintained for the entire duration of electro-spinning, for each sample ten minutes.

This was achieved using a 175 W infrared lamp (IR 175R E27 Infrared Bulb, Phillips, UK). The infrared lamp was turned on during electro-spinning and was located on one side of the chamber. It was turned off just before electro-spinning. Silica gel (Bluestar Packaging Supplies Ltd), in combination with the temperature were to maintain the humidity within the chamber to between 8.5% and 10%. A digital thermometer-hygrometer was used to measure the temperature and humidity (RS Pro, RS Components, UK) within the chamber. Each solution was electro-spun for

10 minutes. Three collector geometries were used: a grounded copper plate (10cm x 10cm x 1mm), a parallel electrode (4cm and 8cm gap) and the custom-made PTFE Vee-shield.

The flat plate collector and a parallel electrode collector are shown in Figure 25. The flat plate setup (Figure 25a) consisted of a grounded aluminium foil-covered metal plate that enabled uniform fibre deposition with randomly oriented fibre mats. This served as the standard collector for initial electro-spinning trials. In contrast, the parallel electrode collector (Figure 25b) featured two grounded metallic strips mounted on either side of a non-conductive substrate, creating a concentrated electric field across the gap. This configuration was employed to induce fibre alignment and evaluate the effect of directional electric fields on fibre orientation. Both collectors were used within the same custom-built electro-spinning chamber under identical environmental conditions.

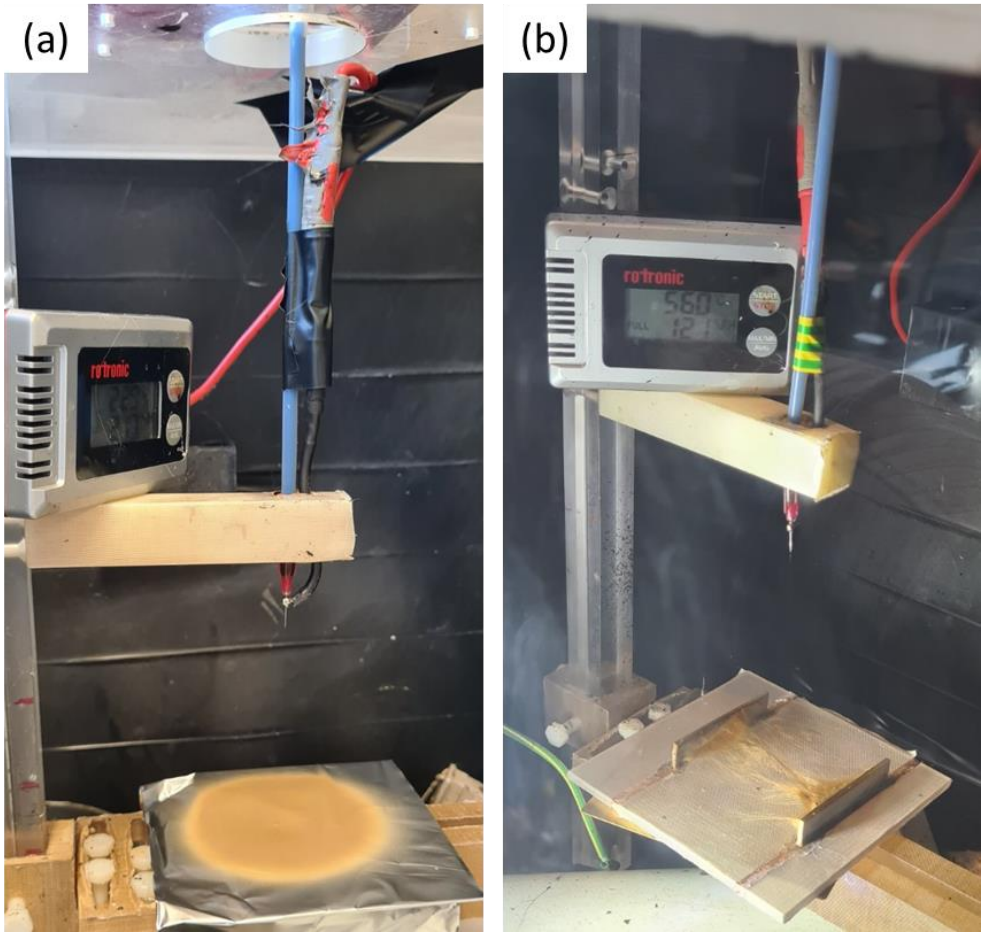

Figure 25. Close-up images of the two initial collector configurations used during electro-spinning; (a): Flat plate collector with aluminium foil for random fibre deposition, and (b): Parallel electrode collector designed to promote fibre alignment across the gap.

Following initial electro-spinning trials using a flat plate and parallel electrode collectors, a third configuration, a custom-made Vee-shaped shield collector, was employed to improve fibre alignment (19). As shown in Figure 26, the setup consists of two grounded PTFE arms arranged in a "Vee" formation, designed to focus the electric field and promote more directed fibre deposition across the angled gap. This Vee-shield configuration proved more effective in producing aligned fibre mats compared to the previous setups, likely due to the converging field lines encouraging uniaxial stretching and orientation of the electro-spun fibres (220–222). The collector was integrated into the same custom-built chamber used for earlier experiments, maintaining consistent environmental control and needle-to-collector distance. This refinement in collector geometry was crucial for enhancing alignment in subsequent electro-spun lignin fibre samples.

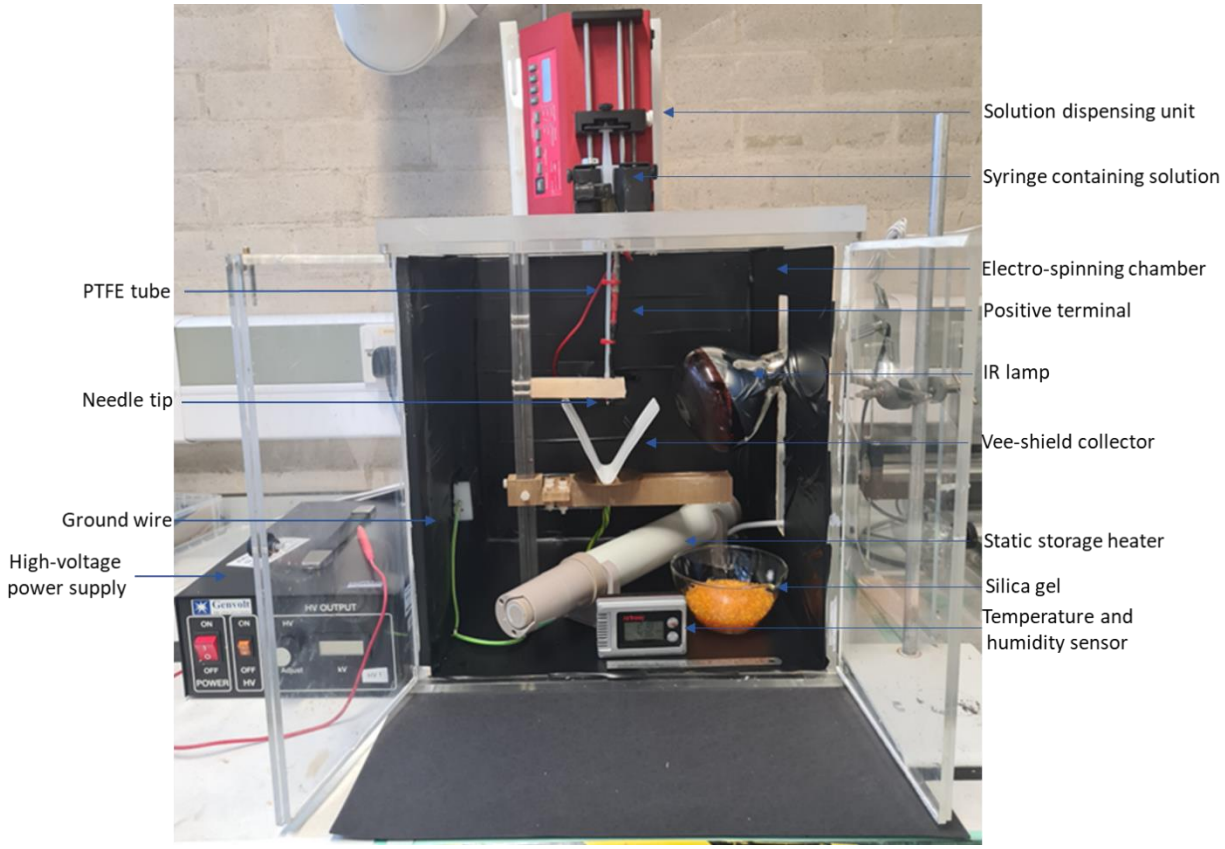

Figure 26. Photograph of Vee-shield electro-spinning setup.

4. Results & discussion

4.1. Characterisation of softwood Kraft lignin powder

Comprehensive characterisation of the softwood Kraft lignin (BioChoice) powder, as-received and vacuum dried (at 80 °C for 6 hours), was carried out using FTIR, NMR spectroscopy, elemental analysis, XRD, DSC, TGA and GPC techniques.

4.1.1. Fourier-transform infrared spectroscopy of lignin powder samples

FTIR spectroscopy was utilised to define the chemical structure of the lignin samples and determine the functional groups contained in the material. This approach elucidates the molecular interactions within the lignin structure by identifying unique absorbance bands linked to essential functional groups, including hydroxyl (-OH), carbonyl (C=O), and aromatic (C=C) groups, as shown in Figure 8. The acquired spectra were evaluated by comparing peak intensities and positions with literature data, facilitating a thorough comprehension of lignin's chemical makeup and its appropriateness for fibre synthesis. The FTIR absorption peaks observed for the tested lignin samples were consistent with those reported in the literature, see Table 6, confirming the expected functional group assignments.

The FTIR spectra for the as-received lignin powder sample is shown in Figure 27.

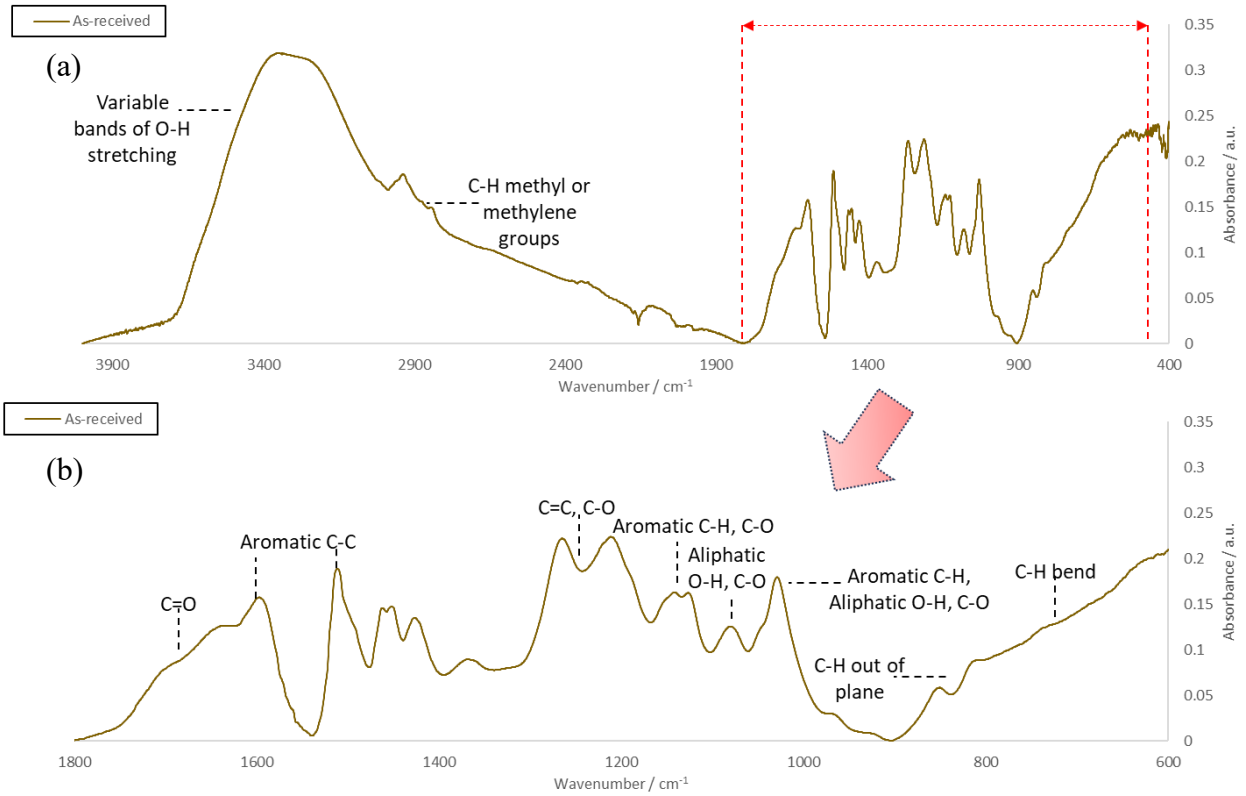

Figure 27. FTIR spectra of as-received lignin; (a) whole spectral range 4000-400 cm^{-1}, and (b) enlarged spectral view from 1800-600 cm^{-1}.

The FTIR spectra for the as-received lignin sample and the vacuum dried 80 °C for 6 hours lignin sample are shown in Figure 28, covering the region of 4000 to 400 cm^{-1} wavenumber.

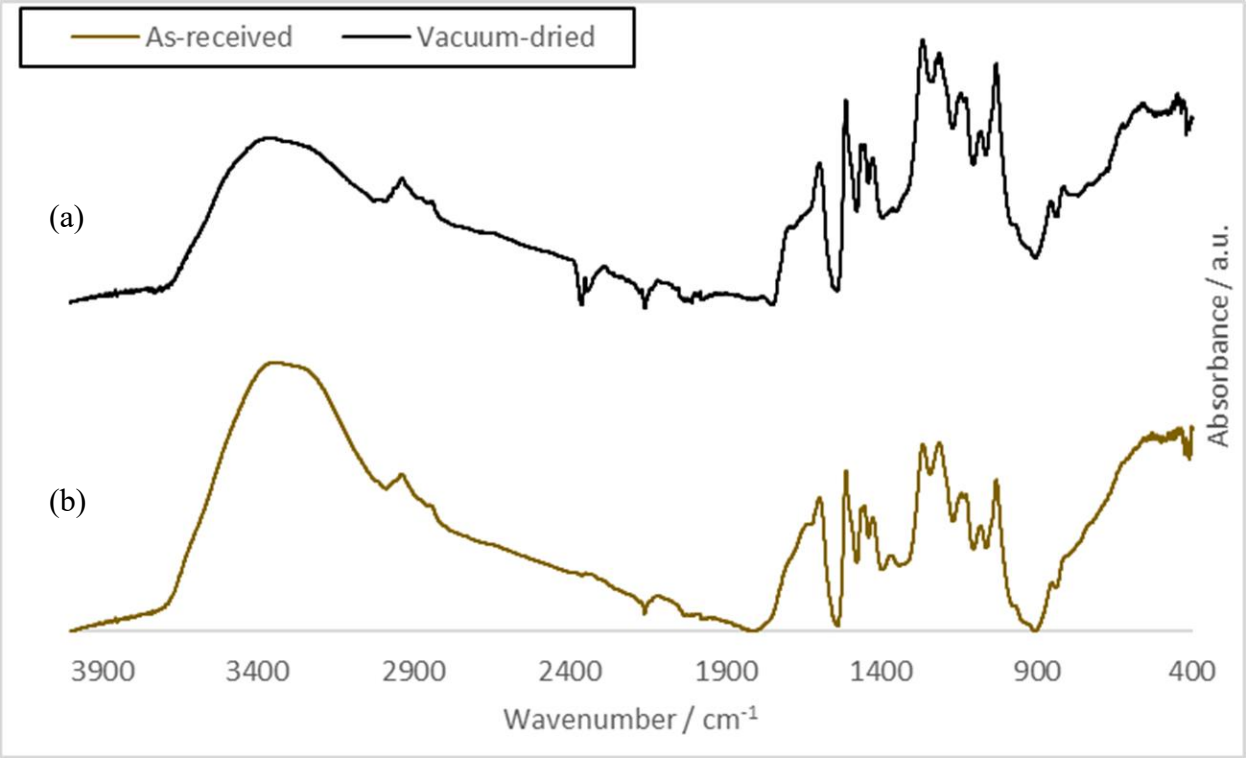

Figure 28. The FTIR spectra for the: (a): the vacuum dried 80 °C for 6 hours lignin sample and (b): as-received lignin sample, offset by absorbance to enable comparison.

Both spectra are plotted separately to highlight any structural or chemical changes occurring due to the drying process at 80 °C for 6 hours in the vacuum oven. The analysis focuses on identifying functional group variations between the samples, which can indicate potential alterations in lignin structure or moisture content resulting from the vacuum drying.

The spectra of the as-received and vacuum dried lignin were both identical as expected, except for the reduction of O-H (water peak) at 3400 cm^{-1} for the latter sample, with peak assignments tabulated in Table 10. This is because, unlike the as-received lignin, the sample that underwent vacuum drying at 80 °C for 6 hours had its moisture content significantly reduced, along with the removal of other contaminants such as sodium and potassium (260).

This region at 3400 cm^{-1} is associated with O-H stretching vibrations, which are predominantly attributed to hydroxyl groups in lignin and absorbed water. The marked decrease in intensity at this wavenumber in the vacuum-dried sample suggests substantial water loss due to the drying process (441).

Figure 29 compares the spectral changes from wavenumber 1900-400 cm^{-1}, which encompass the fingerprint region 1400-600 cm^{-1}. Comparing the lignin changes within this region is critical in identifying unique lignin structural features. Changes here can indicate structural modifications, such as hydrogen bonding rearrangements or minor degradation. Between 1900–400 cm^{-1}, the FTIR spectra of the as-received and vacuum-dried lignin samples show no significant changes, indicating that the core lignin structure remains intact.

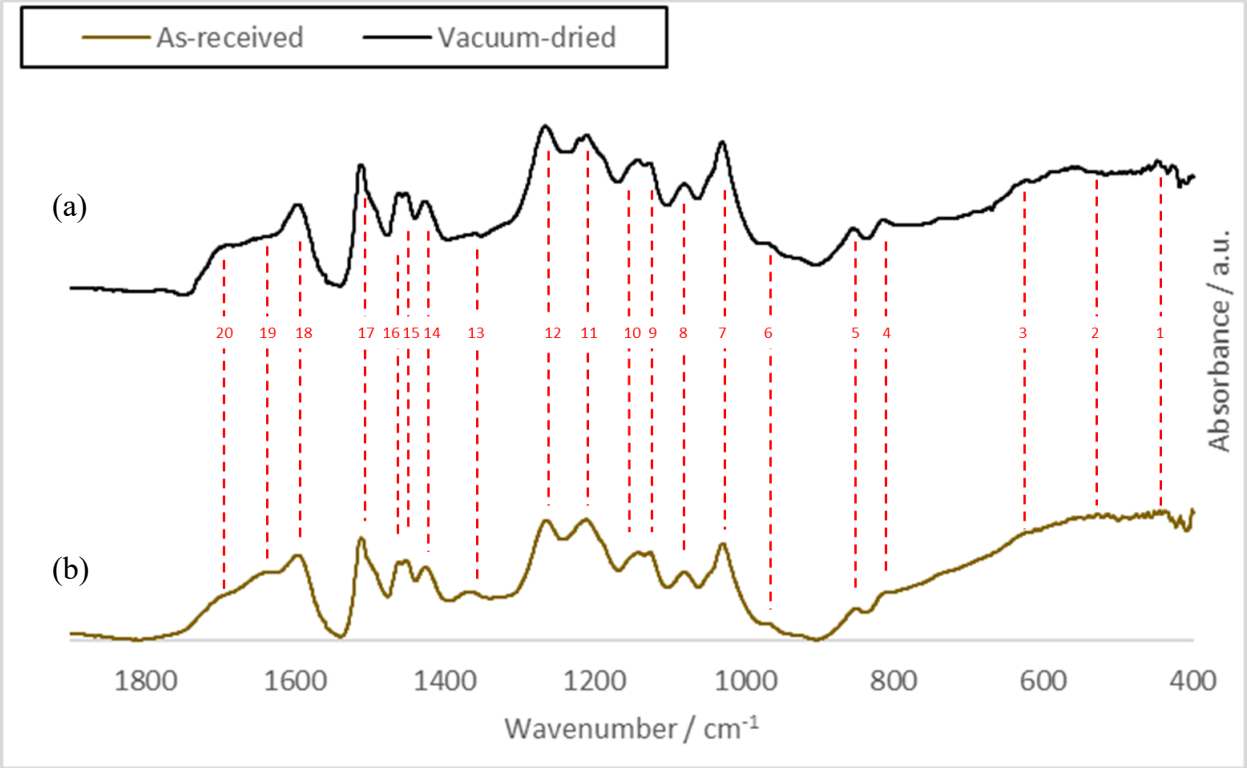

Figure 29. The FTIR spectra from wavenumber 1900-400 cm^{-1} for the: (a): the vacuum dried 80 °C for 6 hours lignin sample and (b): as-received lignin sample, offset by absorbance to enable comparison.

The characteristic peaks associated with aromatic ring vibrations (1500-1600 cm^{-1}), C-H stretching (400-700 cm^{-1}), and C-O ether linkages (1000-1200 cm^{-1}) remain unchanged, suggesting that vacuum drying primarily affects moisture content without altering the fundamental chemical composition of lignin.

The distinct peak at 1270 cm^{-1} signifies guaiacol lignin moieties, shown in Figure 3, which are linked to the interplay of C-O and C=O vibrations alongside C-C, C-O, and C=O stretching vibrations, respectively. The characteristic bands at 850 cm^{-1} signify C-H out-of-plane deformation typical of G-lignin units (442). The characteristic C=O stretching vibration (1700 cm^{-1}) remains unchanged, indicating that any carbonyl-containing groups, such as conjugated ketones, esters, or carboxyl groups, are unaffected by drying (443). The aromatic skeletal

vibrations C-C (1600, 1500, and 1420 cm^{-1}) also remain stable, confirming that the lignins aromatic backbone is retained (444,445). The as-received and vacuum dried lignin samples within the region of 1900-400 cm^{-1} are similar with no noticeable change in the spectra within this highlighted region.

Figure 30 compares the functional group region from 4000-1900 cm^{-1}, for the as-received and vacuum dried lignin powder samples.

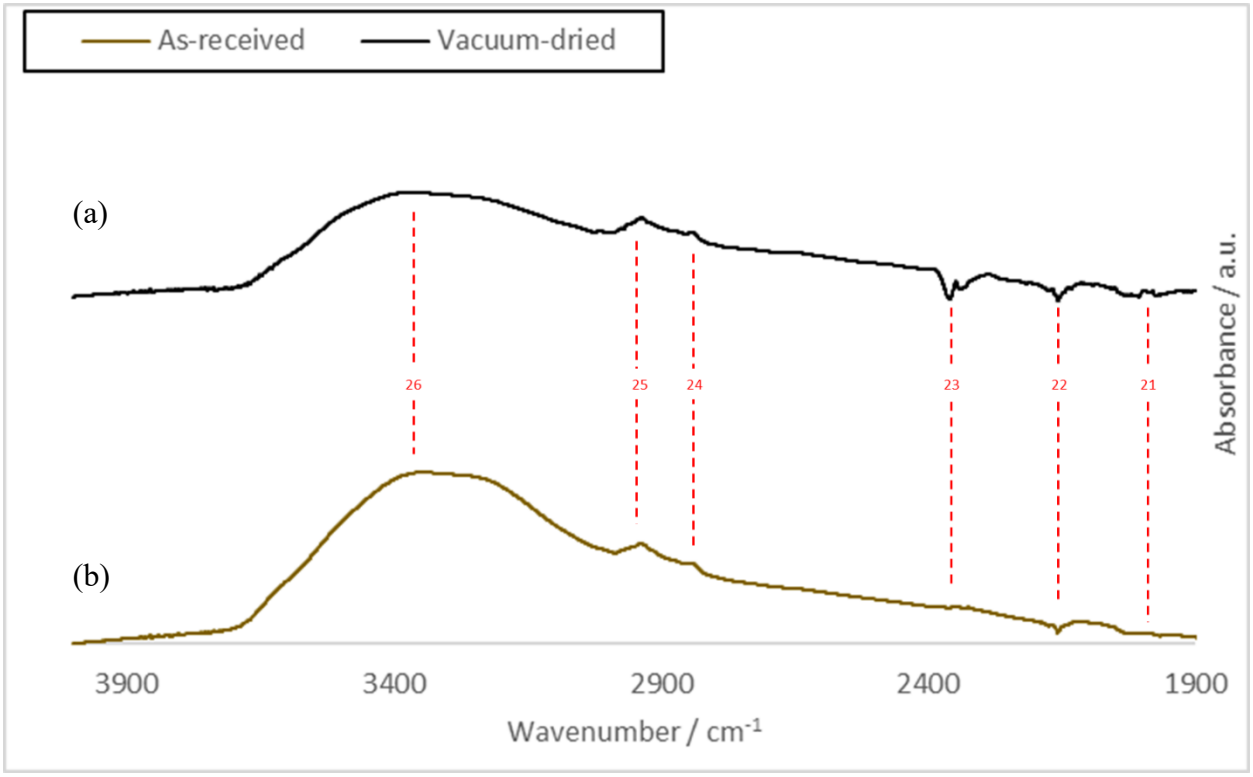

Figure 30. The FTIR spectra from wavenumber 4000-1900 cm^{-1} for the: (a): the vacuum dried 80 °C for 6 hours lignin sample and (b): as-received lignin sample offset by absorbance to enable comparison.

The region from 4000-1900 cm^{-1} contains absorption bands related to major functional groups such as O-H and C=O stretching vibrations (446,447). The most significant difference between the two spectra is observed around 3400 cm^{-1}, corresponding to the O-H stretching vibration.

The as-received lignin spectra show a broad, intense peak due to hydrogen-bonded hydroxyl groups, primarily from absorbed moisture. After vacuum drying, this peak is significantly reduced, confirming the removal of water during the drying process (448,449). In the 2950–2850 cm^{-1} range, characteristic aliphatic C-H stretching vibrations from methyl ($-CH_3$) and methylene ($-CH_2-$) groups are present. These peaks remain largely unchanged between the two samples, indicating that vacuum drying does not affect the lignin's aliphatic backbone.

Table 10. Peak assignment for as-received and vacuum dried lignin (80 °C for 6 hours) FTIR spectra (324,444,445).

Peak Number	FTIR Frequencies (cm^{-1})	Peak Assignments
1	430-460	C-H bend weak
2	500-545	C-H bend weak
3	720-740	C-H medium
4	800-815	C-H medium
5	850-920	C-H out of plane
6	955-965	C-H stretching
7	1025-1035	C-O stretching (sharp)
8	1075-1088	Aromatic C-H, Aliphatic O-H, C-O stretching
9	1125	C-O stretching
10	1135	Aromatic C-H, C-O stretching
11	1205-1220	C-C stretching (lignin)
12	1270	C-O stretching guaiacol lignin, C=O
13	1370	Weak aromatic stretching C-C
14	1420-1440	Aromatic stretching C-C
15	1450	O-H in plane bending (cellulose, hemicellulose)
16	1460	O-H in plane bending (cellulose, hemicellulose)
17	1506	Aromatic ring C-C skeletal vibration (sharp)
18	1600	Aromatic ring C-C skeletal vibration
19	1645	Aromatic ring C-C skeletal vibration (broad)
20	1700	C=O stretching (broad)
21	1970	Weak aromatic ring C-C skeletal vibration
22	2000-2130	C=C stretch vibration broad
23	2300	C-O stretching
24	2830	C-H stretching (CH_2 & CH_3 groups)
25	2936	C-H stretching (CH_2 & CH_3 groups)
26	3411	O-H water stretching

Between 2400 and 1900 cm^{-1}, weak overtone and combination bands are observed, which arise from aromatic ring vibrations (444,445). No significant differences are seen in this region, reinforcing that the overall chemical structure of lignin remains intact after vacuum drying. The primary change in the spectra is the reduction in hydroxyl (-OH) absorbance, confirming moisture loss, while other functional groups remain unaffected.

Thermostabilised lignin powder was also characterised by FTIR to investigate chemical changes during thermal treatment, as shown in Figure 31. Lignin powder was thermostabilised by heating to 260 °C and held for 2 hours in air and nitrogen atmospheres, respectively.

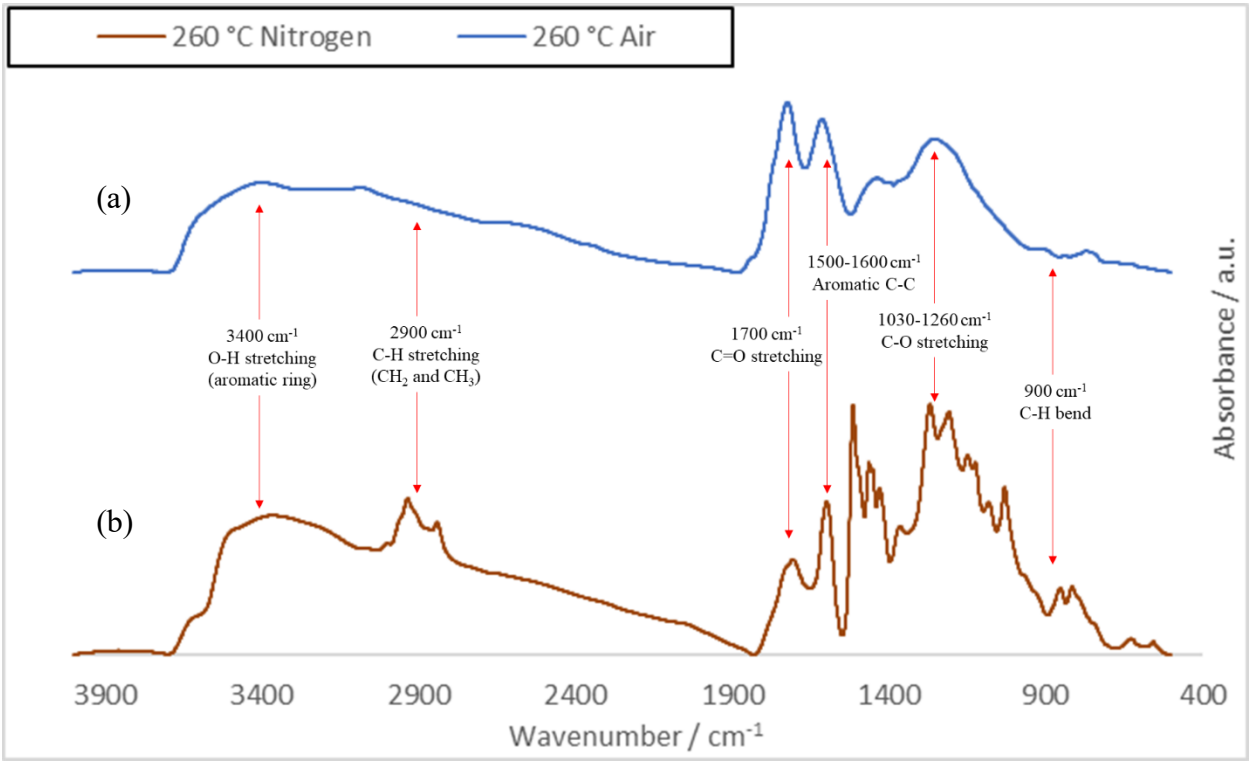

Figure 31. The FTIR spectra for the: (a): 260 °C thermostabilised lignin in air and (b): 260 °C thermostabilised lignin in nitrogen, offset by absorbance to enable comparison.

Both thermostabilised samples exhibited a broad O–H stretching band around 3400 cm^{-1}, corresponding to hydroxyl groups from phenolic and aliphatic alcohols (442). This band was more pronounced in the nitrogen-treated lignin, suggesting increased hydroxyl content due to oxidative cleavage of ether bonds, see Figure 6. C–H stretching bands near 2900 cm^{-1}, attributed to aliphatic $–CH_2$ and $–CH_3$ groups , were also more pronounced in the nitrogen-treated sample, indicating breakdown of side chains in air by comparison (444,445).

A reduced carbonyl region (~1700–1750 cm^{-1}), was seen in the nitrogen-treated sample, whilst the air-treated sample displayed a strong absorbance band associated with C=O stretching vibrations of conjugated ketones, aldehydes, and carboxylic acids (443). Aromatic skeletal vibrations around 1510–1600 cm^{-1}, typical of lignin's guaiacyl and syringyl units (442), were more distinct in the nitrogen-treated lignin, indicating better preservation of the aromatic structure. The C–O stretching vibrations in syringyl and guaiacyl units (1220–1260 cm^{-1} and 1030–1120 cm^{-1}, respectively) were also more intense in the nitrogen sample, while significantly diminished in the air-treated lignin, suggesting oxidative cleavage of ether linkages in the latter, see Figure 9 (441). Overall, these spectral differences confirm that thermostabilisation in air leads to more extensive chemical modification of lignin, particularly oxidation and degradation of aromatic and aliphatic structures. In contrast, treatment under nitrogen better preserves the native lignin backbone by limiting oxidative reactions (442).

FTIR analysis highlighted distinct chemical differences among the as-received, vacuum-dried, and thermostabilised lignin powders. The as-received lignin exhibited characteristic bands for hydroxyl (–OH) groups (~3400 cm^{-1}), aliphatic C–H stretching (~2900 cm^{-1}), and aromatic skeletal vibrations (~1510–1600 cm^{-1}), typical of lignin (442,450). Upon vacuum drying, these peaks remained largely unchanged, but their overall intensity decreased, suggesting minimal structural alteration apart from moisture removal. Notably, the –OH band became narrower, consistent with reduced hydrogen bonding due to water loss (260).

In contrast, thermostabilisation at 260 °C resulted in pronounced spectral changes. The sample treated in air showed a significant increase in absorbance around 1700–1750 cm^{-1}, corresponding to carbonyl (C=O) stretching vibrations, indicating oxidative degradation and formation of aldehyde, ketone, or carboxylic acid groups (443). Additionally, a broadening and increase in the –OH stretching region suggested the formation of new hydroxyl functionalities from bond cleavage (441). In the nitrogen-treated lignin, these oxidative features were less pronounced, and the aromatic skeletal bands (1510–1600 cm^{-1}) and C–O ether vibrations (1030–1260 cm^{-1}) were better retained compared to the air-treated sample (442). This suggests that nitrogen atmosphere helped preserve the lignins native aromatic and ether structures by suppressing oxidative reactions. Together, these spectra demonstrate that air thermostabilisation promotes oxidation, leading to more significant chemical modifications, whereas nitrogen treatment results in a more thermally preserved lignin structure, with less disruption to its core functional groups.

4.1.2. NMR spectroscopy of lignin powder

NMR spectroscopy was conducted to characterise the structural features of lignin in different forms. The samples analysed included as-received lignin, vacuum-dried lignin, and vacuum-dried electro-spun lignin fibres. A comprehensive NMR approach was employed, utilising ^{1}H NMR, ^{13}C NMR, ^{1}H-^{1}H COSY (correlation spectroscopy), and ^{1}H-^{13}C HSQC spectroscopy for each sample. ^{1}H NMR was used to identify and quantify the different proton environments within the lignin structure, while ^{13}C NMR provided insights into the carbon backbone and functional groups. The ^{1}H-^{1}H COSY spectra enabled the correlation of coupled protons, aiding in the identification of linkage patterns and side-chain structures. Finally, the ^{1}H-^{13}C HSQC spectra allowed for the assignment of cross-peaks between proton and carbon signals, facilitating a more detailed analysis of lignins aromatic and aliphatic regions. This combination of techniques enabled a detailed structural assessment, allowing for the identification and quantification of key functional groups, linkages, and molecular interactions within the lignin samples. By comparing the spectra, insights into the effects of drying and electro-spinning on lignins chemical structure were obtained. The following lignin structural characteristics can be measured by proton-NMR: carboxylic acid (δ 12.6-13.5 ppm), aldehyde (δ 9.4-10.0 ppm), phenolic hydroxyl (δ 8.0-9.4 ppm), -5 phenolic hydroxyl (δ 8.99 ppm), syringyl C5 phenolic hydroxyl (δ 8.0-8.5 ppm), aromatic protons (δ 6.3–7.7 ppm), and aliphatic protons (333,342,451). Shown in Figure 32 is the standard structure for softwood lignin adapted from literature with interunit linkages highlighted.

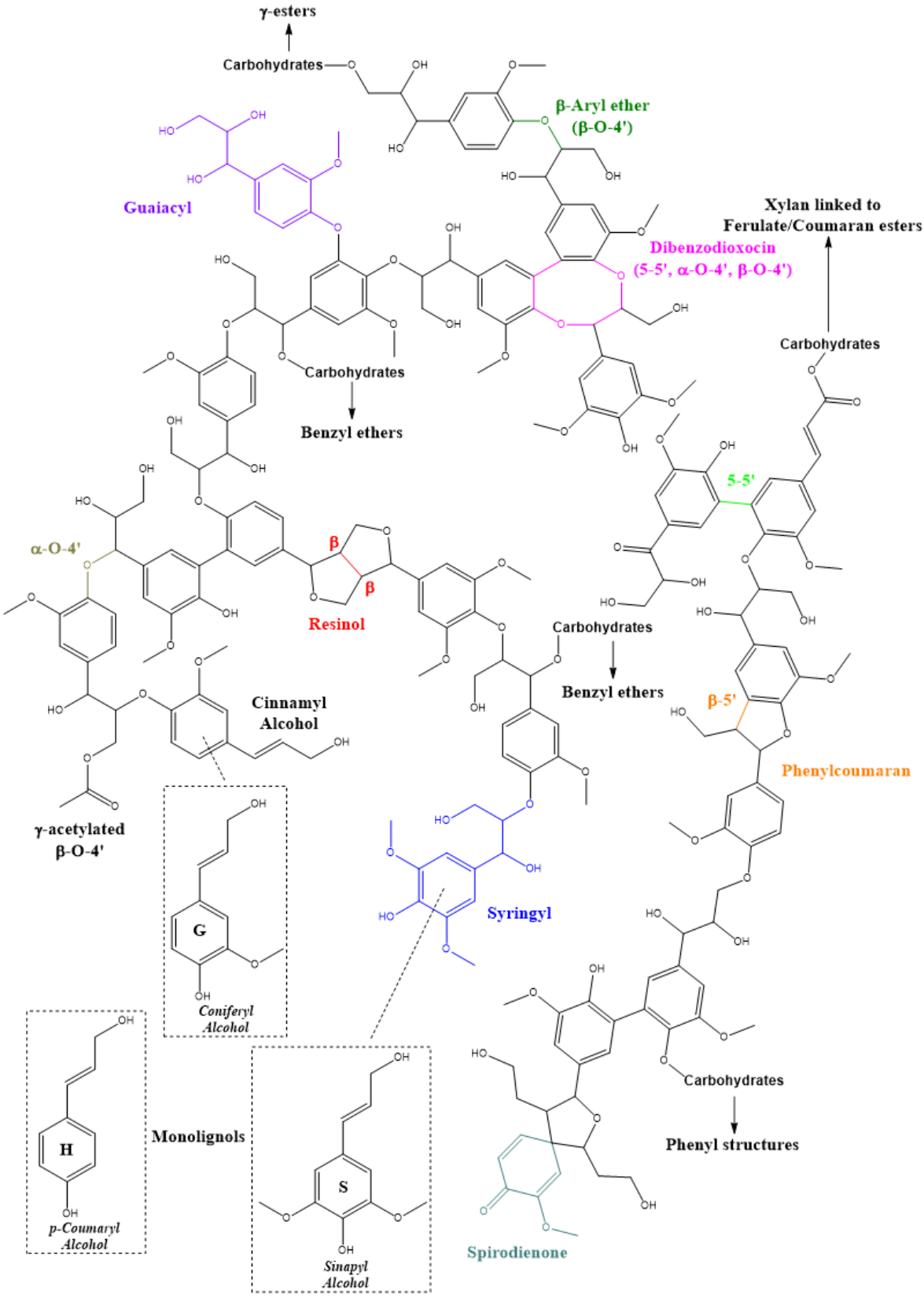

Figure 32. Proposed structure of softwood lignin with interunit linkages highlighted, adapted from literature source, Suota et al., (271).

4.1.2.1. NMR of as-received lignin powder

NMR spectroscopy was employed to characterise the structural features of as-received lignin powder. Shown in Figure 33, is the ^{1}H NMR spectra of as-received lignin powder.

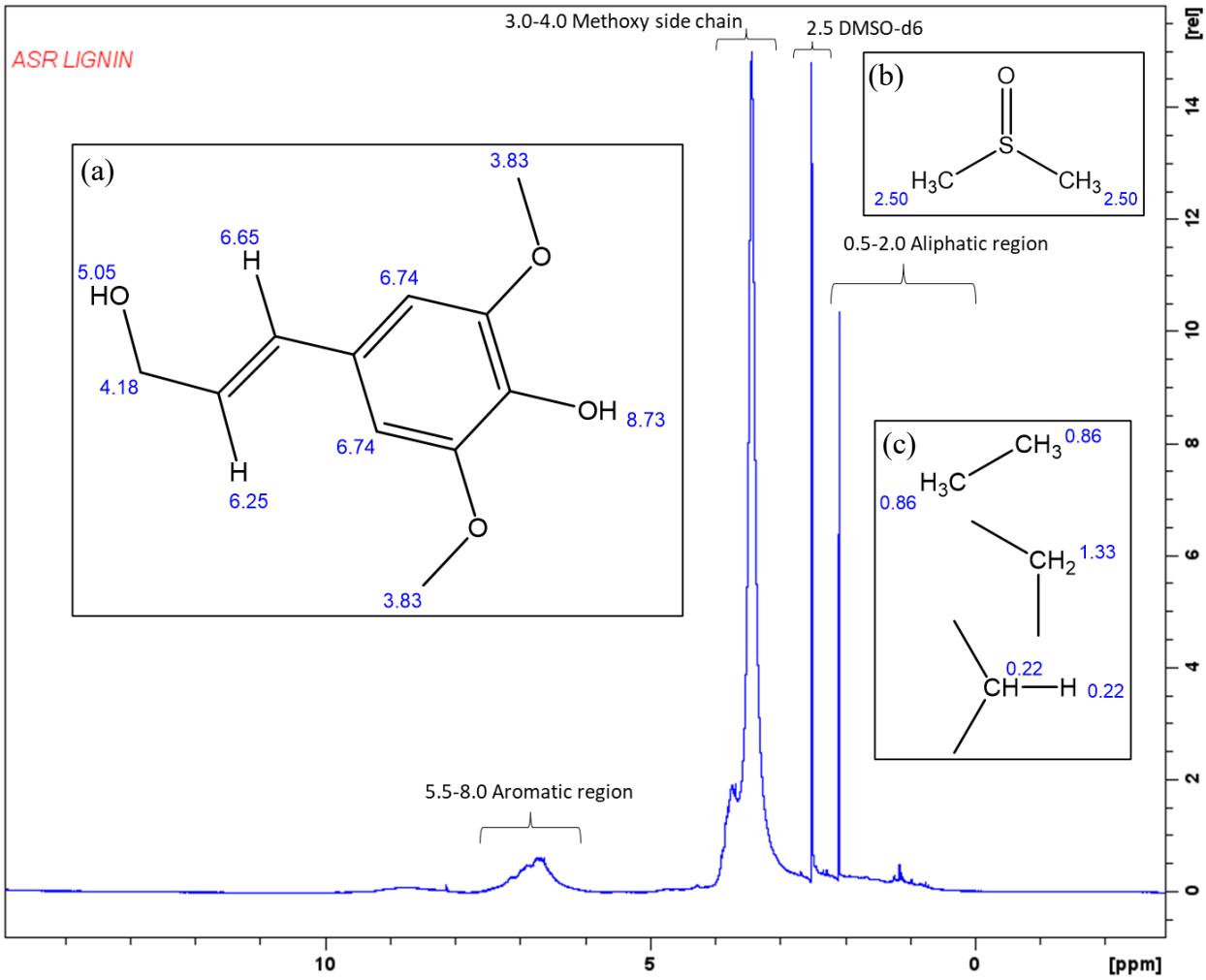

Figure 33. ^{1}H NMR spectra of as-received lignin, and assignments of the structural features with labelled literature ppm values: (a): sinapyl alcohol repeating lignin monomer including methoxy side chain, (b): DMSO solvent structure and (c): aliphatic region containing methyl (-CH_3), methylene (-CH_2 and methine group (-CH) (333,342,451).

Characteristic peaks for lignin were seen in the as-received lignin, as anticipated. The aromatic region was seen from 5.0-8.0 ppm, methoxy side chain from 3.0-4.0 ppm, DMSO-d_6 solvent peak seen as expected from a quintet splitting at 2.50 ppm & the aliphatic region containing residual proton and ethyl groups from 0.5-2.0 ppm.

A zoomed-in ^{1}H NMR spectrum of as-received lignin powder is presented in Figure 34, highlighting key spectral regions relevant to lignin's structural composition. The aromatic region, which corresponds to proton signals from lignin's phenylpropanoid units, is distinctly observed. Additionally, the peak for methoxy side chain protons, characteristic of syringyl and guaiacyl units, are expanded, see Figure 3 for monolignol schematics. A broad water peak is present, likely due to residual moisture in the as-received lignin powder sample.

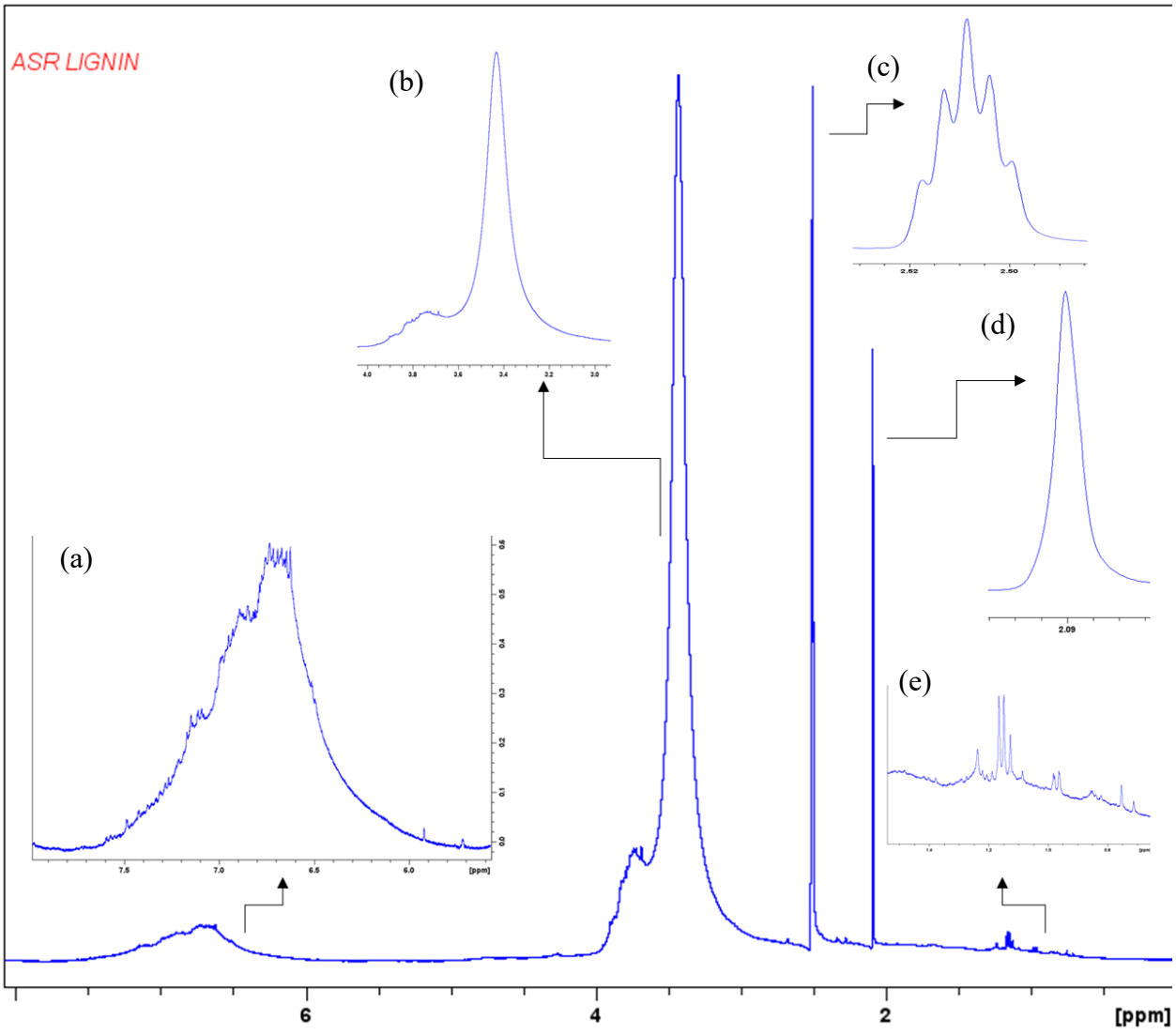

Figure 34. Zoomed in ^{1}H-NMR spectrum of as-received lignin powder in DMSO-d_6, highlighting key spectral regions. (a): the aromatic region was seen from 5.0-8.0 ppm, (b): methoxy side chain from 3.0-4.0 ppm, (c): DMSO-d_6 solvent peak seen at 2.50 ppm, (d): the aliphatic region seen at 2.05 ppm and (e): region containing residual proton and ethyl groups from 0.5-2.0 ppm.

The DMSO-d_6 solvent quintet peak is also marked, along with a methyl singlet and the residual proton region, providing a comprehensive overview of the proton environment in the sample.

A selection of lignin inter-unit linkages such as aryl ether linkages, condensed and uncondensed aromatic and aliphatic carbons, as well as other structural details about lignin can all be obtained using the method of ^{13}C NMR spectroscopy. Similar expected peaks were seen for the corresponding ^{13}C NMR for as-received lignin as previously elucidated in ^{1}H NMR, as seen in Figure 35.

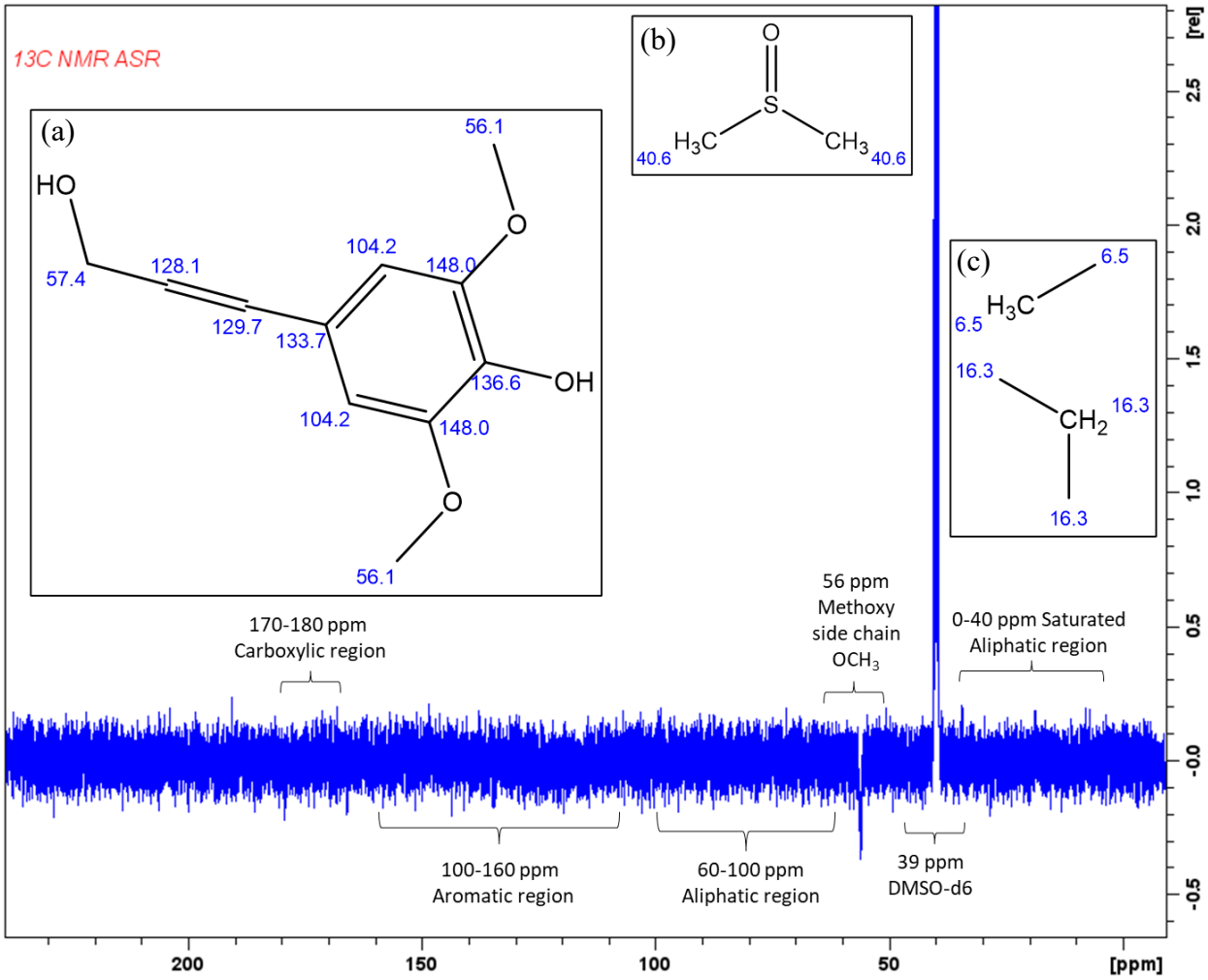

Figure 35. ^{13}C NMR spectra of as-received lignin, and assignments of the structural features with labelled literature ppm values: (a): sinapyl alcohol repeating lignin monomer including methoxy side chain, (b): DMSO solvent structure and (c): aliphatic region containing methyl ($-CH_3$), methylene ($-CH_2$ and methine group ($-CH$) (333,342,451).

The noisy spectra observed in the ^{13}C NMR, despite multiple repeats, were attributed to instrumentation issues at the University of Birmingham; however, the listed regions were confidently assigned based on the HSQC spectra for as-received lignin shown in Figure 36. Despite the resolution of ^{13}C NMR and the sensitivity of ^{1}H NMR in revealing a variety of

structural properties of lignin, the measurement of these traits is challenging for several reasons. These elements consist of relaxation rates, carbon purse offset effects, coupling constant variations, and proton homonuclear coupling effects (342,403,451).

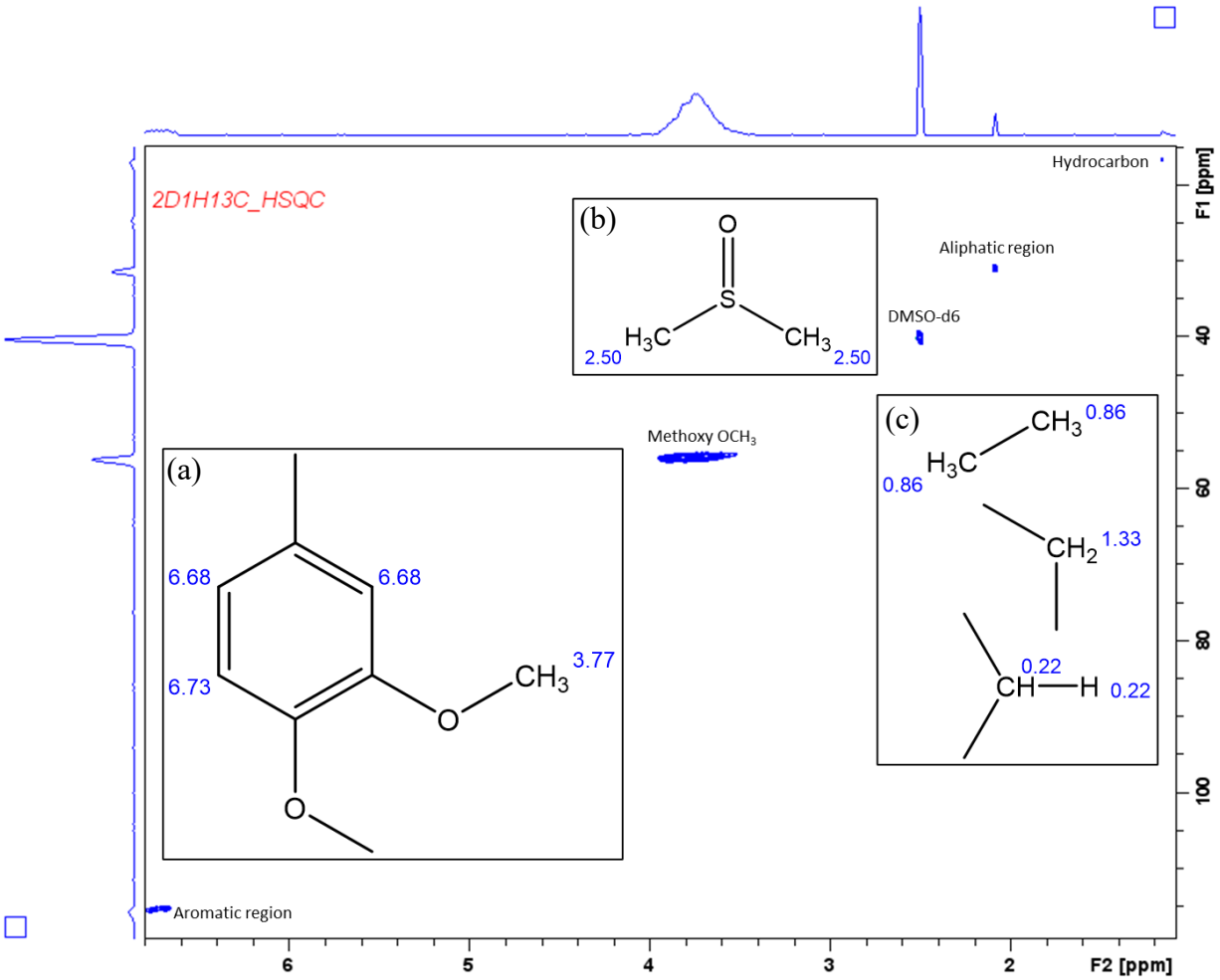

Figure 36. $^{1}H^{13}C$ – HSQC spectra for as-received lignin, and assignments of the structural features with labelled literature ^{1}H NMR ppm values: (a): guaiacyl lignin repeating unit including methoxy side chain, (b): DMSO solvent structure and (c): aliphatic region containing methyl ($-CH_3$), methylene ($-CH_2$ and methine group ($-CH$) (333,342,451).

The 2D $^{13}C/^{1}H$-correlated HSQC spectroscopic technique thus confirms the correspondence between the ^{1}H and ^{13}C spectra. The hydrocarbon (^{1}H=1.15 ppm, ^{13}C=16.82 ppm), aliphatic region (^{1}H=2.08 ppm, ^{13}C=31.20 ppm), DMSO-d_6 solvent peak hydrocarbon (^{1}H=2.50 ppm, ^{13}C=39 ppm), methoxy side chain OCH_3 (^{1}H=3.74 ppm, ^{13}C=56 ppm) and the carbon aromatic region (^{1}H=6.71 ppm, ^{13}C=115.90 ppm).

Interunitary linkages, shown in Figure 32, are discernible from the HSQC spectra, particularly in the vicinity of oxygenated aliphatic carbons (^{13}C:50–65 ppm/ ^{1}H: 3.0–4.5 ppm) & aromatic carbons (^{13}C:100–125 ppm/ ^{1}H: 6.0–7.0 ppm) by further investigation of the HSQC spectra. The

main structural features are identified according to previous designations in the literature (349,354,359,403,452), with spectra shown in Figure 37.

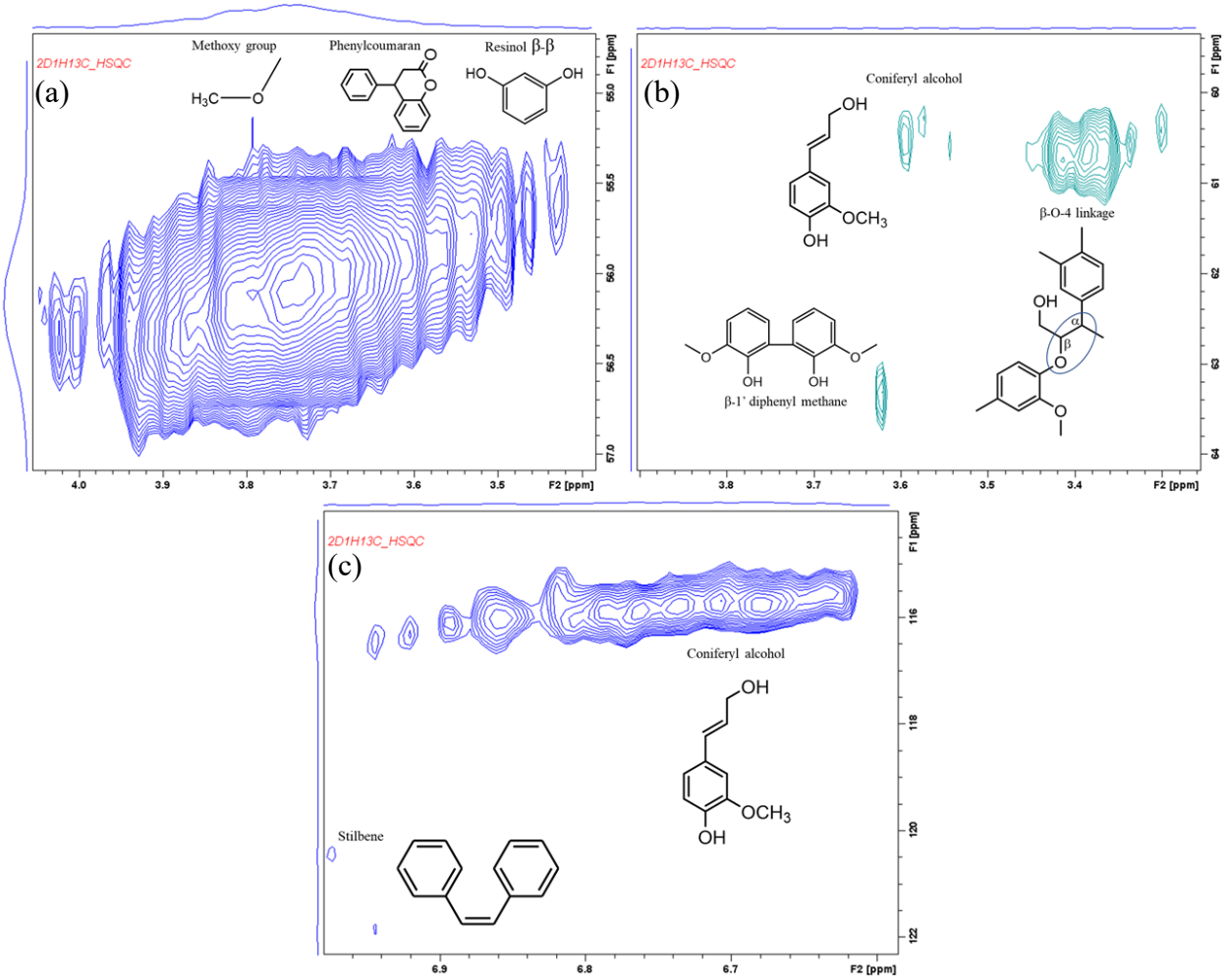

Figure 37. Zoomed in $^{1}H^{13}C$ – HSQC spectra with structures for the: (a) and (b): aliphatic regions and (c): aromatic regions of as-received lignin.

The aliphatic structures identified, (shown in Figure 8), are resinol β-β linkage (^{1}H=3.45 ppm, ^{13}C=55 ppm), phenyl coumaran unit (^{1}H=3.60 ppm, ^{13}C=56 ppm), methoxy side chain (^{1}H=3.74 ppm, ^{13}C=60 ppm), coniferyl alcohol unit (^{1}H=3.59 ppm, ^{13}C=60 ppm), β-O-4 linkage (^{1}H=3.38 ppm, ^{13}C=61 ppm), β-1 diphenyl methane linkage (^{1}H=3.62 ppm, ^{13}C=63 ppm). The aromatic structures identified are the guaiacyl unit (^{1}H=6.76 ppm, ^{13}C=115 ppm) & the stilbene unit (^{1}H=6.99 ppm, ^{13}C=118 ppm).

To investigate the effect of solvent on the NMR spectrum of lignin, the as-received sample was dissolved in THF instead of DMSO-d_6 and analysed using ^{1}H NMR, enabling clearer characterisation of aromatic and aliphatic proton environments without interference from the dominant DMSO peak. The ^{1}H NMR spectra for as-received lignin dissolved in THF is shown in

Figure 38. The typical solvent peak for DMSO at 2.50 ppm is no longer present, confirming the absence of DMSO in the sample. Instead, strong peaks characteristic of THF are now observed at approximately 1.841 ppm (methylene protons) and 3.727 ppm (oxymethylene protons) (273).

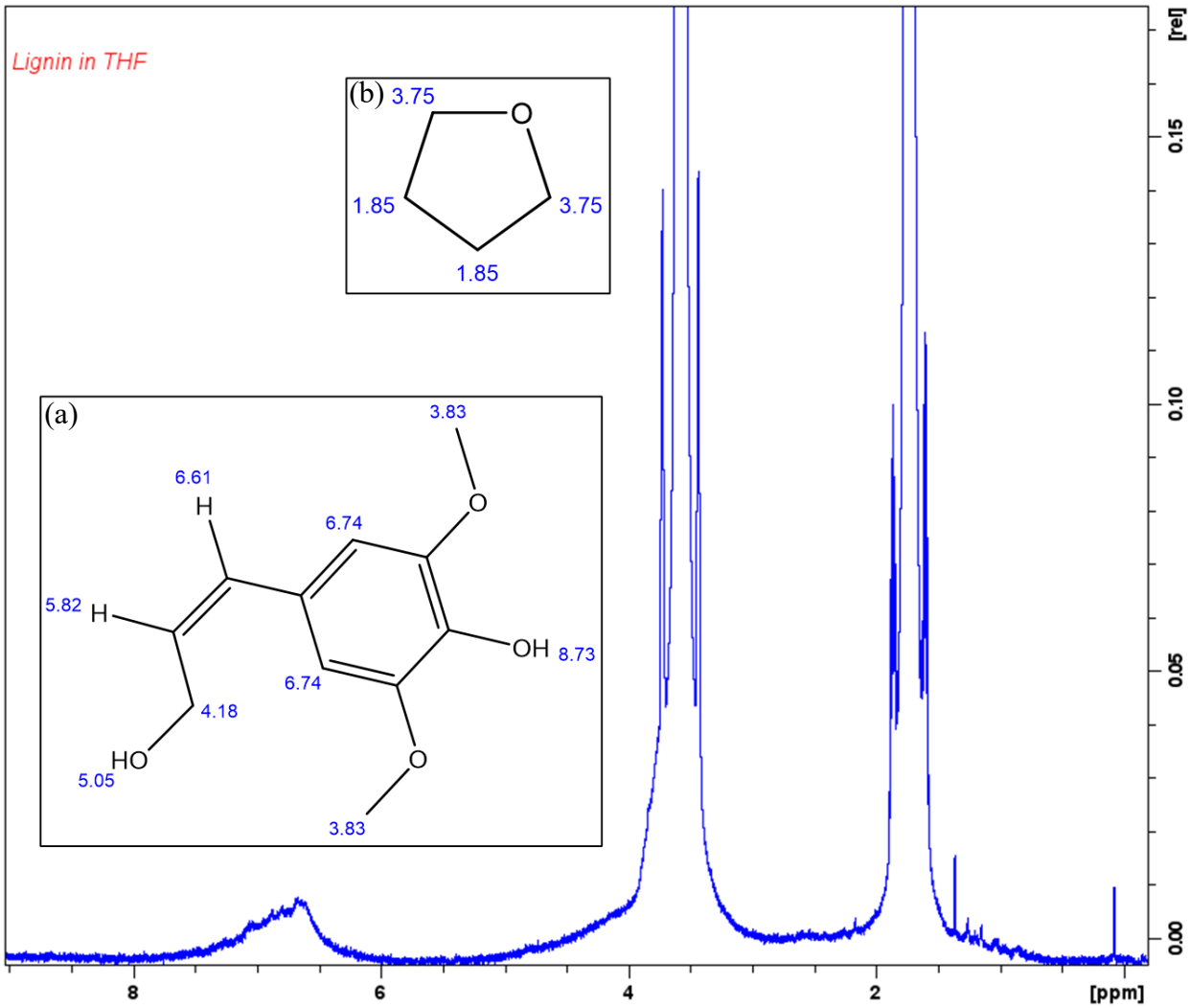

Figure 38. [1]H NMR spectra of as-received lignin dissolved in THF, and assignments of the structural features with labelled literature ppm values; (a): sinapyl alcohol repeating lignin monomer including methoxy side chain, (b): THF solvent structure (333,342,451).

Alongside these solvent peaks, the typical lignin peaks previously identified using the DMSO-d_6 solvent are still present, indicating that the fundamental structural components of lignin remain unchanged regardless of the solvent. As previously mentioned, the aromatic region of lignin is seen between 6.0-8.0 ppm, whilst the rest of the peaks are similar to previously reported as expected for as-received lignin. However, noticeable differences in chemical shift and peak intensity between the spectra can be attributed to variations in solvent–lignin interactions (453). DMSO is known to form strong hydrogen bonds with the hydroxyl groups in lignin, which alters the local chemical environment and leads to changes in signal intensity. In contrast, THF

exhibits a weaker hydrogen-bonding capacity, resulting in reduced interaction with lignin's hydroxyl groups. This difference is supported by their respective donor numbers, with DMSO having a significantly higher value (29.8) compared to THF (20.0), indicating stronger solvation of hydroxyl protons in DMSO (185,454). Consequently, using THF minimises these interactions, producing sharper signals and less downfield shifting in the lignin proton spectrum.

4.1.2.2. NMR of vacuum dried lignin powder

NMR spectroscopy was employed to characterise the structural features of vacuum dried lignin powder. The vacuum dried lignin sample shows similar ^{1}H NMR peaks as expected in comparison to the as-received lignin sample, with a reduction in the (OH) water peak at 3.80 ppm which is to be expected, attributable to the elimination of moisture during the drying process, illustrated in Figure 39.

As-received lignin typically contains water due to its hygroscopic properties, resulting in hydrogen bonding interactions with hydroxyl groups within the lignin, between hydroxyl (-OH) groups and adjacent ether or phenolic oxygen atoms, see Figure 6. The presence of water is identified as an OH-related signal in the NMR spectrum at around 3.80 ppm, corresponding to the proton environment of water molecules (360).

Upon drying lignin, particularly under vacuum at 80 °C for 6 hours, moisture is reduced, leading to a reduction of the water peak at 3.80 ppm (a reduction of water peak intensity of 87% from the as-received sample to the vacuum dried lignin sample). The same decrease in -OH peak is seen from the as-received to vacuum dried FTIR spectra (see Section 4.1.1). In the absence of water, the concentration of hydrogen atoms in that particular environment diminishes, resulting in a weakened or absent signal at this location (343).

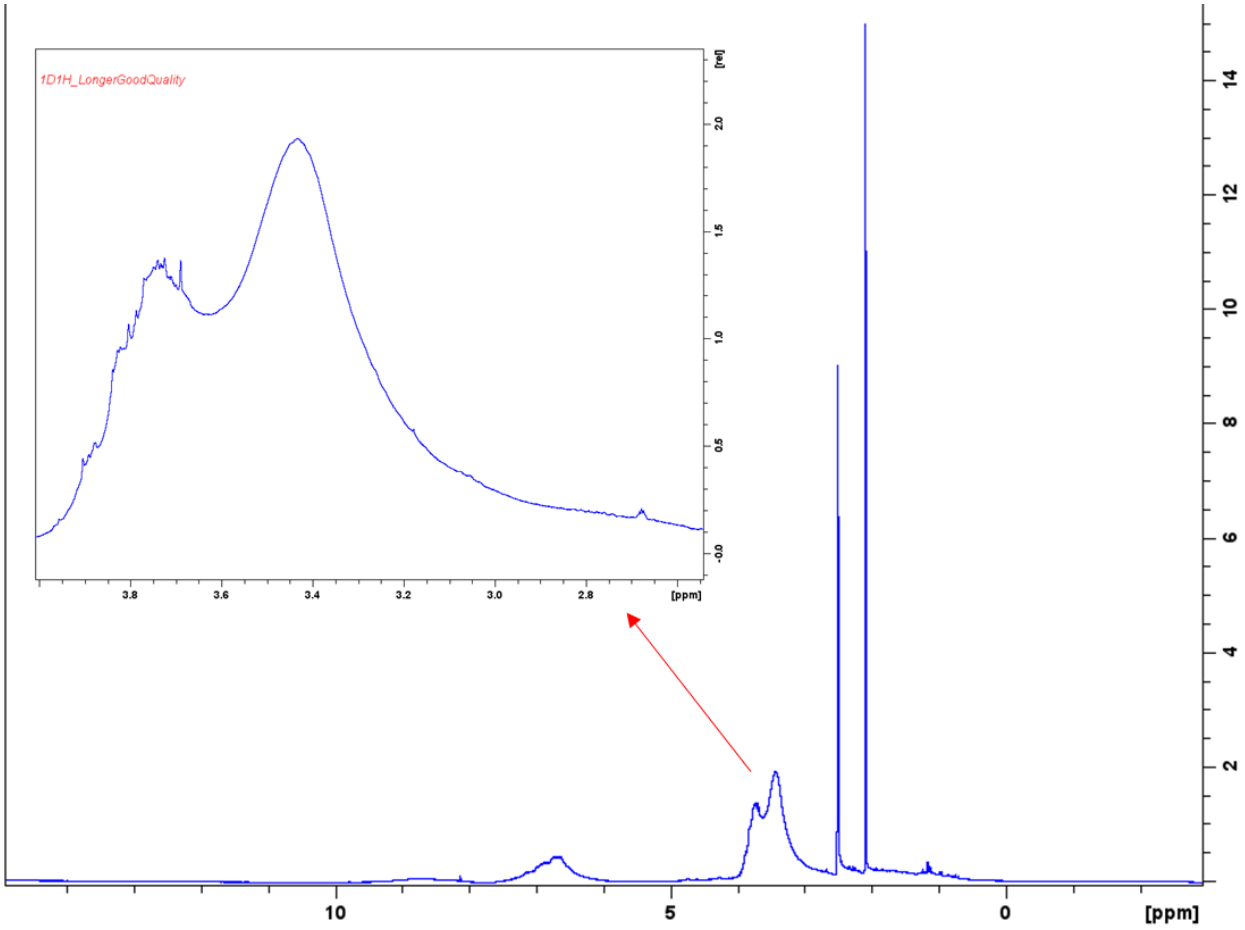

Figure 39. [1]H NMR spectra of vacuum dried lignin, with zoomed region around 3.80 ppm to demonstrate reduction in water peak.

The water content of lignin significantly influences its processing behaviour and the structural integrity of electro-spun fibres. Water acts as a plasticiser, reducing the glass transition temperature of lignin, seen in Section 2.7.4.2 (455). An optimal moisture level is key; as excessive water can disrupt the formation of a stable jet during electro-spinning, leading to bead formation or fibre breakage, while insufficient water may increase brittleness, hindering the formation of continuous, uniform fibres (see Section 2.4.2) (251). The drop in moisture content indicated by the ^{1}H NMR data's water peak intensity reduction, suggests that the drying procedures successfully lower the amount of bound or free water in the lignin matrix (see Section 2.1.2) (66,67).

Vacuum dried lignin sample also has similar ^{13}C NMR peaks, shown in Figure 40, in comparison with the as-received lignin sample, which is to be expected. The HSQC spectra for the vacuum dried lignin powder (80 °C for 6 hours) is also shown in Figure 41.

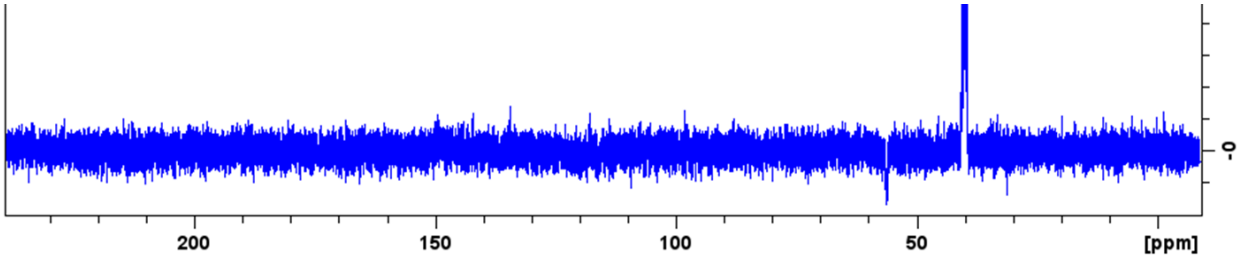

Figure 40.^{13}C NMR spectra of vacuum-dried lignin powder (80 °C for 6 hours).

Many structural features are clearly identifiable in the HSQC spectra for vacuum dried lignin, particularly in the region of oxygenated aliphatic carbons (δC/δH:50–100/2.5–5.5 ppm). Peak areas are identified and labelled in Figure 42.

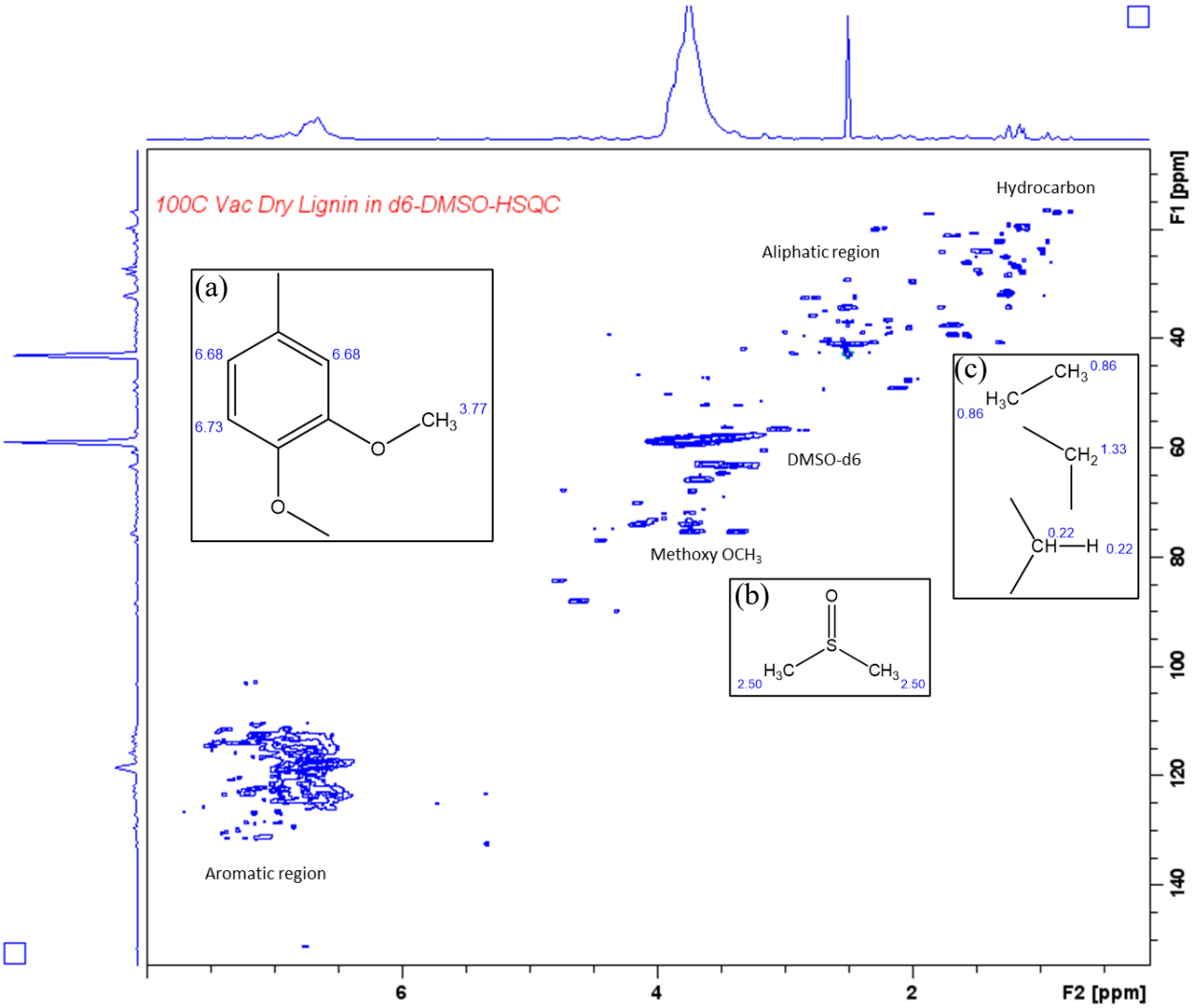

Figure 41. $^{1}H^{13}C$ – HSQC spectra for vacuum dried lignin (80 °C for 6 hours), and assignments of the structural features with labelled literature ^{1}H NMR ppm values: (a): guaiacyl lignin repeating unit including methoxy side chain, (b): DMSO solvent structure and (c): aliphatic region containing methyl (-CH_3), methylene (-CH_2 and methine group (-CH) (333,342,451).

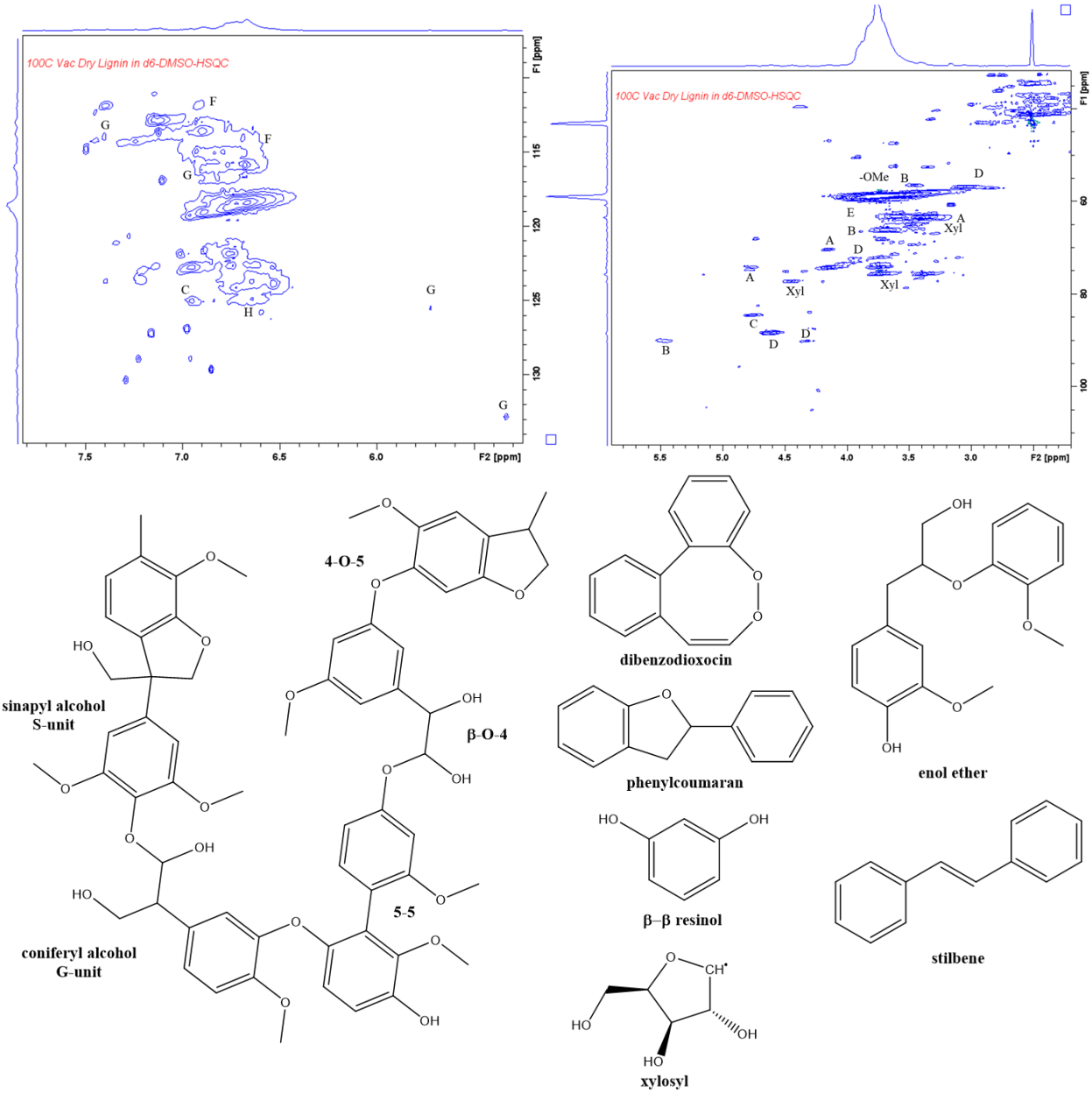

Figure 42. $^{1}H^{13}C$ – HSQC spectra for vacuum dried lignin with peak areas labelled and shown schematically; (a): ß-O-4, (b): Phenylcoumaran, (c): Dibenzodioxocin, (d): Resinol, (e): Coniferyl alcohol, (f): Enol ether, (g): Guaiacyl unit, (h): Stilbene, (Xyl): Xylosyl units (403) (271).

Major structures identified (see Figure 32) include; stilbene moieties (δC/δH, δ128/7.0–7.3 ppm), β-vinyl ether (δC/δH, δ144/7.3 ppm, δ109/5.5 ppm, and δ112/6.1 ppm), coniferyl alcohol (δC/δH, δ128/6.5 ppm), resinol type (δC/δH, δ33.8/2.5 ppm, δ42.4/1.9 ppm), β-O-4' linkage (δC/δH, δ60.4/3.5 ppm, δ71.3/4.9 ppm, δ84/4.3 ppm), β-β' linkage (δC/δH, δ71.1/4.2 ppm, δ84/4.3 ppm, δ84.9/4.6 ppm), and β-5' linkage (δC/δH, δ86.4/5.5 ppm) (271,403).

Even at elevated vacuum drying temperatures of 140 °C and 160 °C, the ^{1}H NMR spectra of lignin powder remained consistent with that of the sample dried at 100 °C, showing no significant changes; characteristic peaks associated with aromatic protons, methoxyl groups, residual DMSO, and aliphatic side chains were preserved across all samples, see Figure 43.

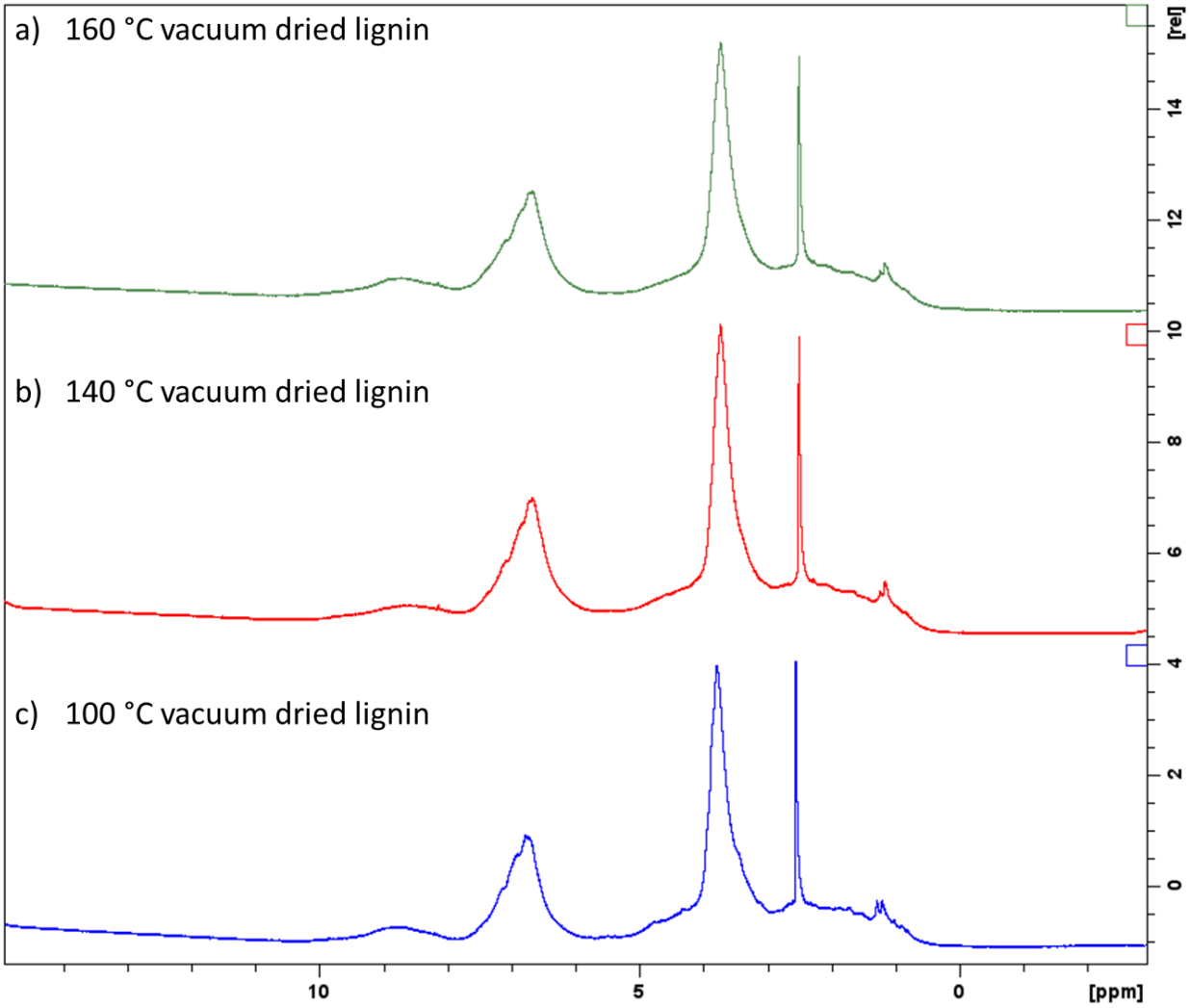

Figure 43. 1H NMR comparison of vacuum dried lignin powder for 4 hours each; a): 160 °C, b) 140 °C and c) 100 °C, respectively.

Although no significant structural changes were observed in the NMR spectra with increasing vacuum drying temperature, with characteristic peaks for aromatic protons, methoxyl groups, residual DMSO, and aliphatic side chains remaining consistent. GPC analysis revealed a gradual increase in molecular weight with heat treatment (see Section 4.1.7). This molecular weight increase, together with observed rises in solution viscosity (see Section 4.3.1) and conductivity (see Section 4.3.2), likely facilitates the improved electro-spinnability of neat lignin at elevated temperatures, as these properties are critical for stable jet formation during electro-spinning.

4.1.3. Elemental analysis of lignin powder

Elemental analysis was conducted to evaluate changes in carbon (C), hydrogen (H), nitrogen (N), and sulphur (S) content across different lignin samples, including the as-received lignin powder, vacuum-dried lignin powders at 80 °C and 100 °C for 6 hours each, and electro-spun fibres prepared from lignin/DMSO solutions refluxed at temperatures between 80 °C and 160 °C, each respectively. This analysis provides insight into the chemical modifications occurring during thermal drying and electro-spinning.

The elemental composition of lignin powder was analysed before vacuum drying as-received and after vacuum drying at 80 °C and 100 °C for 6 hours, respectively, which yielded changes in the carbon and hydrogen content, with minor variations in nitrogen and sulphur percentages. The elemental analysis percentage values for the lignin powder samples are shown in Table 11 and displayed in Figure 44.

Table 11. Elemental analysis percentage values for the as-received lignin powder, vacuum-dried lignin powders at 80 °C and 100 °C for 6 hours each.

	C (%)	**H (%)**	**N (%)**	**S (%)**
As-received	51.32 ± 0.46	6.32 ± 0.25	0.30 ± 0.01	2.59 ± 0.33
80 °C vacuum dried	60.56 ± 0.16	5.67 ± 0.08	0.26 ± 0.01	2.36 ± 0.21
100 °C vacuum dried	85.08 ± 0.00	7.09 ± 0.00	0.00 ± 0.00	2.67 ± 0.00

The as-received lignin powder exhibited a carbon content of 51.32%, hydrogen content of 6.32% and nitrogen content 0.30%. Upon vacuum drying at 80 °C, the carbon content significantly increased to 60.56%, while both hydrogen and nitrogen decreased (5.67% and 0.26%, respectively), suggesting effective removal of residual moisture. Lignin naturally contains bound water, and drying at elevated temperatures would lead to the evaporation of both free and some bound water molecules, reducing the overall hydrogen percentage (68). Since lignin contains oxygen-rich functional groups (e.g., hydroxyl, methoxy, and carbonyl groups), the observed rise in carbon percentage is likely due to the preferential loss of these oxygenated species along with water during the drying process (314).

A further increase in vacuum drying temperature to 100 °C led to a dramatic rise in carbon content, 85.08%, and hydrogen content, 7.09%, while nitrogen was undetectable at 0.00%. This sharp increase may indicate partial carbonisation or condensation reactions occurring during high-temperature vacuum drying, which reduce heteroatom content and enrich the sample in fixed carbon (15,456). Sulphur content across all three powder samples remained relatively consistent (2.36–2.67 % (w/v)), suggesting minimal sulphur volatilisation under these conditions (456).

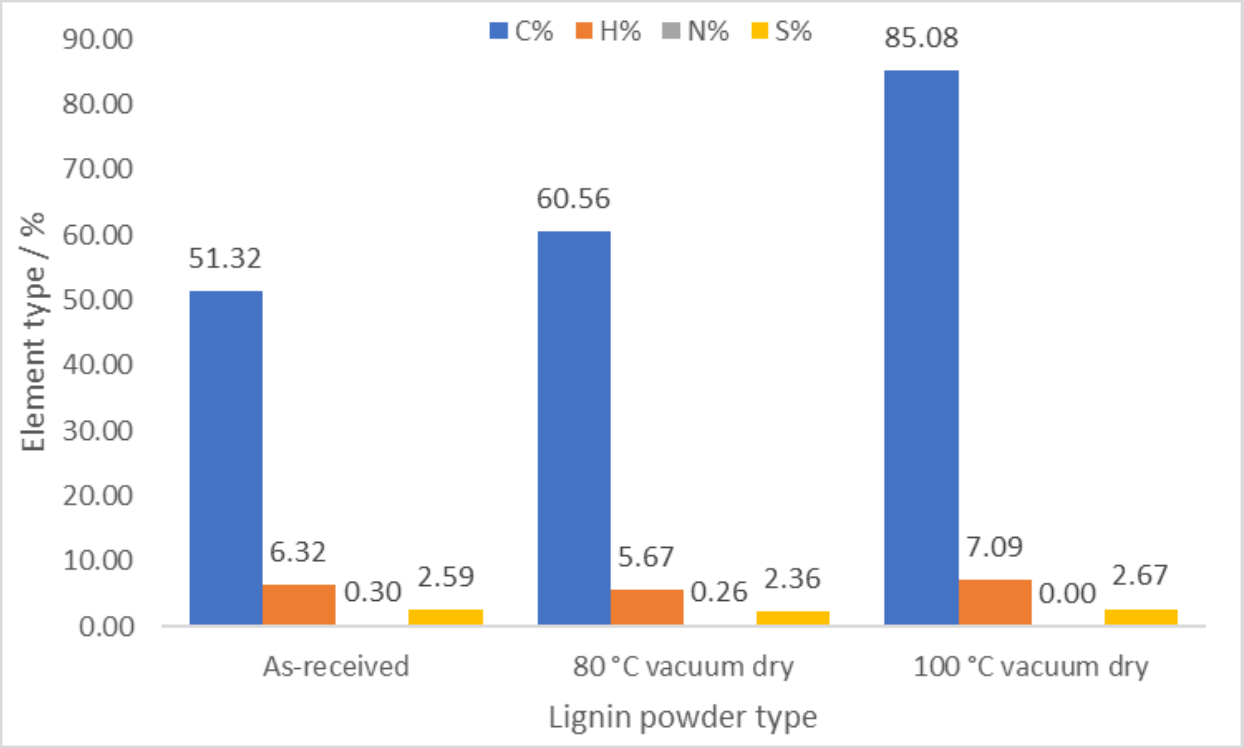

Figure 44. Elemental analysis (C, H, N, S) percentile values for the as-received lignin powder, vacuum-dried lignin powders at 80 °C and 100 °C for 6 hours each.

The electro-spun fibres produced from lignin solutions refluxed in DMSO showed consistent elemental profiles across all temperatures (80 °C, 100 °C, 120 °C, 140 °C and 160 °C, each respectively), elemental percentage values shown in Table 12.

Carbon content ranged narrowly from 60.00% to 61.87%, with a slight maximum at the 80 °C reflux temperature. Hydrogen content remained between 5.40% to 5.75%, and nitrogen was consistently low, between 0.16% to 0.18%, indicating stable composition and effective nitrogen removal during DMSO processing and electro-spinning.

Table 12. Elemental analysis percentage values for the electro-spun fibres prepared from lignin/DMSO solutions refluxed at temperatures 80 °C, 100 °C, 120 °C, 140 °C and 160 °C.

	C (%)	H (%)	N (%)	S (%)
80 °C reflux	61.87 ± 0.11	5.67 ± 0.02	0.17 ± 0.00	3.54 ± 0.07
100 °C reflux	60.77 ± 0.15	5.75 ± 0.07	0.17 ± 0.00	5.46 ± 0.10
120 °C reflux	61.20 ± 0.14	5.40 ± 0.23	0.16 ± 0.00	5.85 ± 0.21
140 °C reflux	60.95 ± 0.10	5.49 ± 0.13	0.18 ± 0.02	6.62 ± 0.05
160 °C reflux	60.00 ± 0.24	5.51 ± 0.25	0.16 ± 0.01	5.14 ± 0.11

Notably, sulphur content increased with increasing reflux temperature, from 3.54% at 80 °C to a peak of 6.62% at 140 °C, before dropping slightly to 5.14% for the 160 °C reflux temperature sample. The increase in sulphur content for the electro-spun fibre samples from lignin/DMSO reflux, average sulphur content 5.32%, in comparison to the lignin powder samples sulphur elemental composition, average sulphur content in powders, 2.54%, is due to increased incorporation or retention of sulphurated lignin fragments at higher temperatures during the reflux process in DMSO (122). The electro-spinning process from refluxed lignin/DMSO solutions appears to control the elemental shifts as opposed to the dramatic elemental shifts observed in thermally treated powders, particularly at 100 °C under vacuum, which underwent significant compositional changes in carbon content, see Table 11, suggestive of partial pyrolysis, consistent with literature on thermal degradation (267,456).

4.1.4. X-ray diffraction of lignin powder

In this study, XRD was employed to characterise both as-received and vacuum-dried lignin, providing insights into its structural properties. The as-received lignin likely contains residual moisture and may exhibit a more amorphous structure, which could influence its overall crystallinity. In contrast, vacuum drying removes this moisture, potentially altering the molecular organisation of the lignin. By comparing the XRD patterns of these two powdered forms, the impact of drying on lignin's phase transitions, and structural order can be assessed. The lignin XRD patterns for the as-received and vacuum dried lignin powder samples are displayed in Figure 45.

The XRD patterns show minimal differences, with nearly identical features between the as-received and vacuum dried samples. This similarity is expected, as neither sample has undergone

oxidation or carbonisation, processes that could otherwise introduce structural rearrangements (267). Both XRD profiles display a broad diffraction peak centred around 2Θ = 20°, commonly associated in literature with the (002) reflection, associated with disordered stacking of aromatic domains in lignin (457).

This broad feature is characteristic of lignin's amorphous structure, reflecting its irregular and heterogeneous molecular arrangement (283). A smaller, broad signal observed near 2Θ = 44° may correspond to in-plane ordering within disordered carbon domains, associated with the (100/101) reflection, though it remains weak and diffuse. It has been reported that the intensity of these diffraction peaks increases gradually with temperature, which implies that the degree of graphitisation in turn also increases with increasing carbonisation temperature (457).

The similarity in XRD results across both powder samples suggests that the vacuum drying process alone does not significantly alter the lignin's structural arrangement at the molecular level. The broadness of the peak also reflects the complexity and irregularity of lignin's polymeric network, which consists of randomly linked phenolic monomers, seen in Figure 3 (37,38). In some cases, the intensity or shape of such broad features may vary depending on factors such as temperature, humidity, or chemical treatment. However, in this case, vacuum

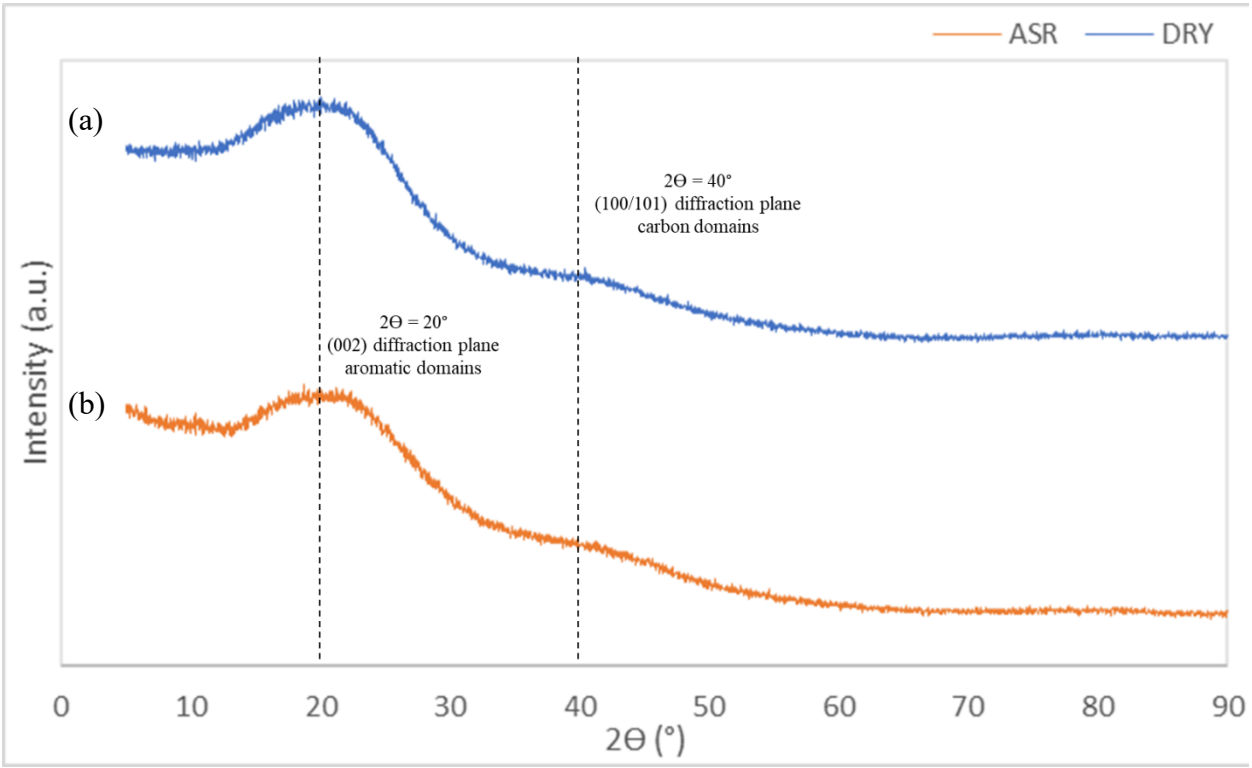

Figure 45. X-ray diffraction pattern for, (a): vacuum dried lignin powder (80 °C for 6 hours) and (b) as-received lignin powder, offset by intensity to enable comparison.

drying at 80 °C appears insufficient to induce any notable structural rearrangement within the lignin. While this temperature is effective for removing moisture in the lignin powder, it is not high enough to cause significant changes in the molecular organisation or aromatic domain interactions in the lignin matrix (457).

4.1.5. Differential scanning calorimetry of lignin powder

Using DSC, the thermal behaviour of lignin was investigated. The glass transition temperature (T_g) is a key parameter that provides valuable insights into the behaviour and properties of amorphous materials like polymers and glasses. T_g refers to the temperature at which, following heating or cooling, a material changes from a stiff, glassy condition to a more flexible, rubbery, or viscous state (308). T_g also indicates the molecular mobility of the material, influencing its ability to flow or undergo rearrangement. T_g plays a vital role in determining suitable processing conditions and thermal stability, as well as predicting the material's physical aging phenomena and long-term durability (9,457,458).

The DSC results for the as-received lignin sample from the first heating scan are shown in Figure 46, highlighting a significant endothermic transition associated with the T_g.

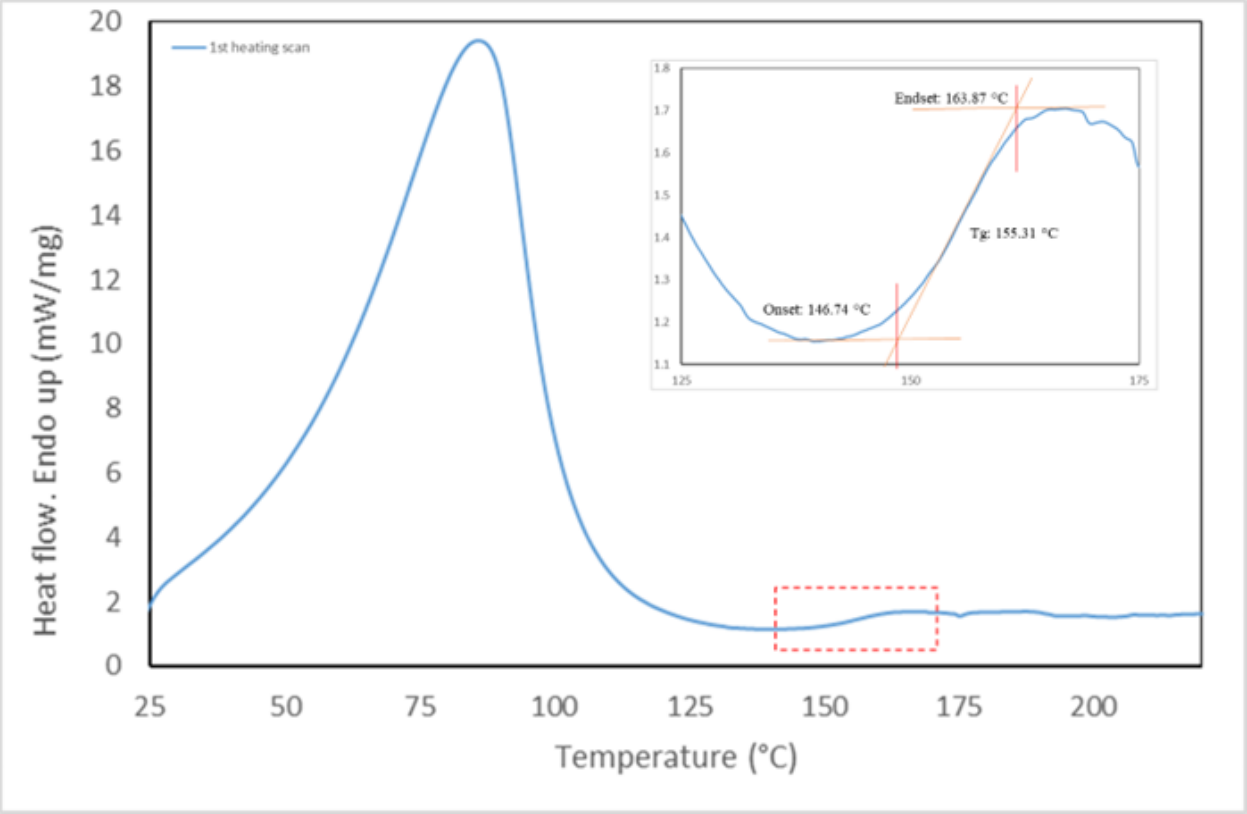

Figure 46. DSC thermogram for as-received lignin, 1st heating scan, with insert showing an expanded view between 125 °C and 175 °C.

The zoomed inset shows the calculation of the onset, T_g, and endset values, which were determined to be 146.7 °C (onset), 155.3 °C (T_g), and 163.9 °C (endset). The T_g value is similar to what is reported in literature for Kraft lignin, see Table 9.

This confirms the thermal softening behaviour of lignin, where the increase in molecular mobility at elevated temperatures result in a transition from a glassy to a rubbery state. The first heating scan for the as-received lignin demonstrates of a sizable endothermic peak between 50 and 120 °C. This is a result of the lignin's absorbed water and low molecular weight substances evaporating within this temperature range (25,27). This large peak is not seen in subsequent second and third heating scans suggesting it is moisture removal.

The DSC thermograms for the second and third heating scans for as-received lignin powder is shown in Figure 47. The first heating scan for the as-received lignin revealed a T_g of 155.3 °C, which increased slightly in the second and third heating scans to 156.2 °C and 162.7 °C, respectively. This shift suggests a degree of structural relaxation or molecular reorganisation upon repeated thermal treatment. The increase in T_g with repeated heating is consistent with the removal of residual moisture and the formation of stronger intermolecular interactions or partial cross-linking upon heating (459).

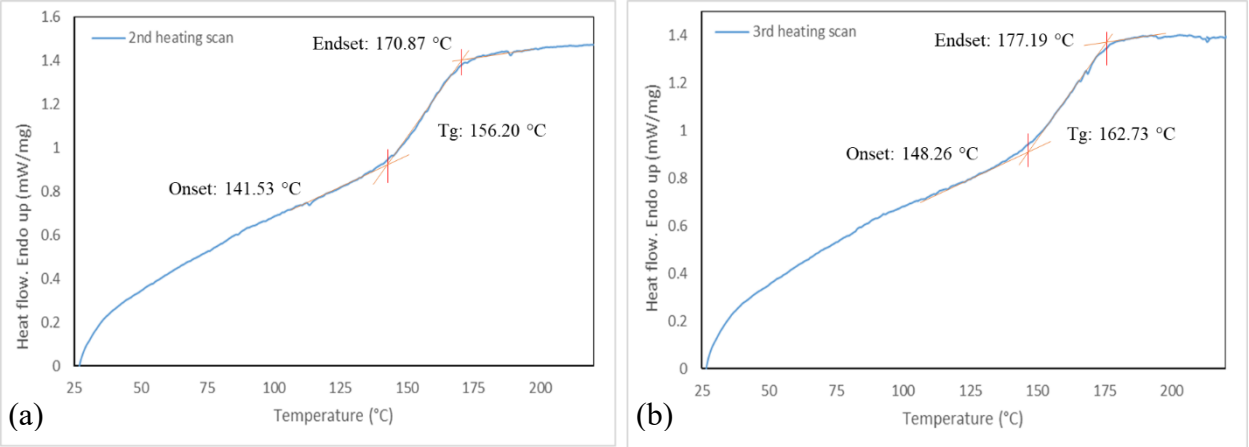

Figure 47. DSC thermograms for as-received lignin; (a): 2nd heating scan and (b): 3rd heating scan.

The three heating scans and calculated onset, endset and T_g values are shown in Figure 48. For the vacuum-dried lignin samples, the T_g values were consistently higher than those of the as-received lignin. The first heating scan for the vacuum-dried sample showed a T_g of 165.3 °C, increasing to 172.1 °C and 179.8 °C in the second and third scans, respectively. The higher T_g values for vacuum-dried lignin reflect the removal of moisture and volatile components (25). The removal of which is also seen in the FTIR and NMR data (see Sections 4.1.1 and 4.1.2.2,

respectively). The consistent increase in T_g across heating cycles for both as-received and vacuum-dried lignin suggests changes in molecular mobility, or the loss of moisture during thermal treatment (401).

The glass transition temperature of lignin can be affected by moisture content (460). In general, as-received lignin is likely to have a lower T_g than vacuum-dried lignin because it often contains more moisture. Moisture acts as a plasticiser, lowering the T_g by increasing the mobility of polymer chains (457,461). Vacuum-drying lignin, at 80 °C, removes a greater amount of moisture and volatile compounds. This reduction in plasticising agents can decrease chain mobility, which may contribute to the observed increase in Tg compared to the as-received lignin sample (285). The association T_g for the first, second and third heating scans for the as-received and vacuum dried lignin sample are presented in Table 13.

Table 13. T_g values for the as-received and vacuum dried lignin (80 °C for 6 hours) powder.

DSC lignin samples	**1st heating scan, glass transition T_g (°C)**	**2nd heating scan, glass transition T_g (°C)**	**3rd heating scan, glass transition T_g (°C)**
As-received lignin	155.3	156.2	162.7
Vacuum dried lignin (80 °C for 6 hours)	165.3	172.1	179.9

In Table 13, it is evident that the T_g rises from the first to the third scan, for all lignin samples. The increase in T_g across successive scans likely reflects structural changes within the lignin matrix induced by thermal history and rearrangement of molecular chains (401,462).

Cross-linking and condensation reactions can take place when lignin is heated to 220 °C. This occurs between aromatic rings and functional groups (such as hydroxyl and methoxy groups), (463,464). The enhanced molecular connectivity restricts chain mobility and raises the T_g in subsequent scans. In addition, the elevated heating may drive off residual moisture and low-molecular-weight volatiles, reducing the free volume within the lignin structure (465). This leads to increased chain packing and stronger intermolecular bonding, which can further contribute to an increase in T_g (131,271).

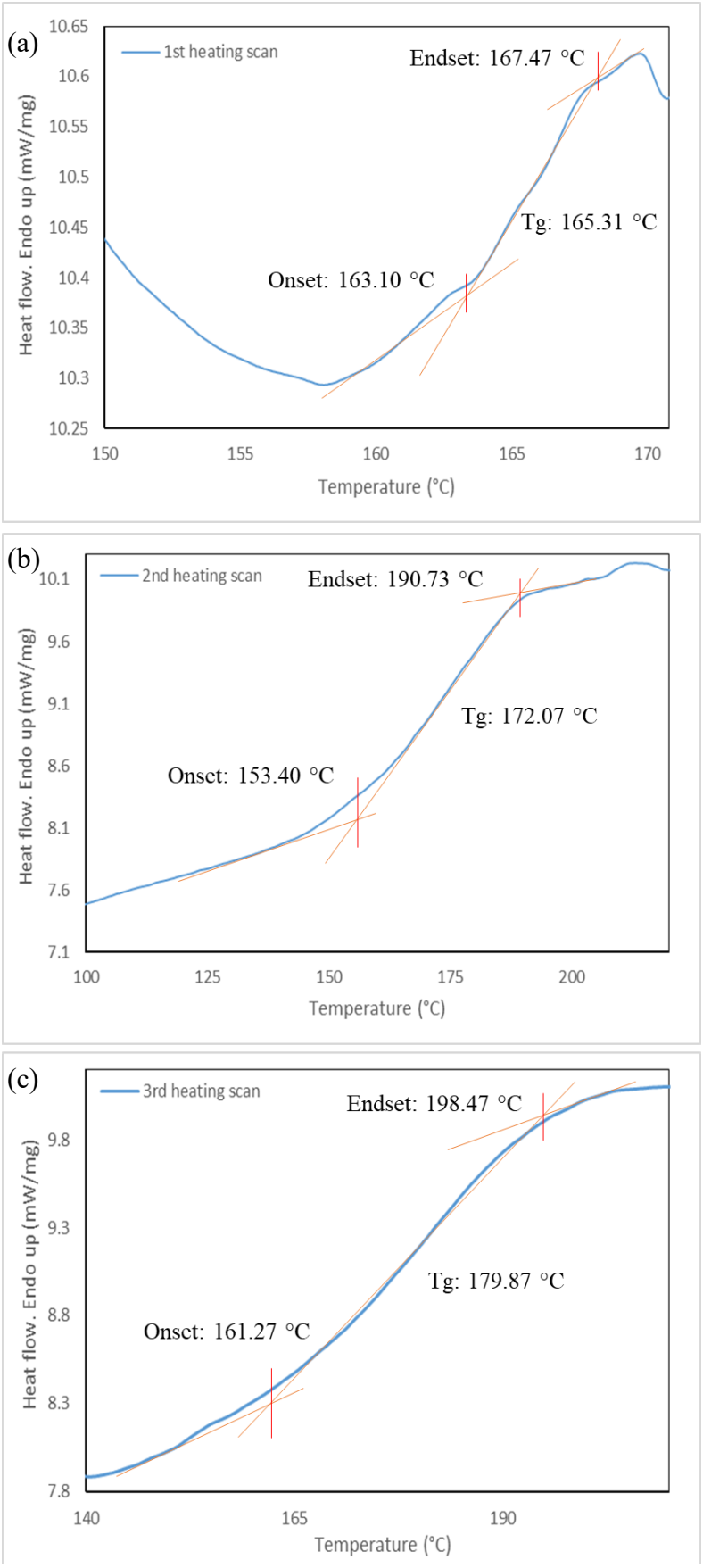

Figure 48. DSC thermograms for vacuum dried lignin; (a): 1st heating scan, (b): 2nd heating scan and (c): 3rd heating scan.

4.1.6. Thermo-gravimetric analysis of lignin powder

TGA is a method used for calculating how much a material changes in weight as a function of temperature. This research offers important details regarding the lignin material's thermal stability, composition, and degradation behaviour (27,466). Utilising thermogravimetric analysis (TGA Q 50, TA Instruments, USA), it was determined under nitrogen atmosphere whether the lignin samples were thermally stable, at a flow rate of 30 mL/min.

The thermal breakdown of lignin is known to occur in multiple stages throughout a wide temperature range of 160-900 °C. Conversely, wood components including cellulose and hemicellulose are recognised to decompose at temperatures exceeding 315-400 °C and 220-315 °C, respectively (27,326).

To examine the thermal stability of the materials, samples weighing less than 10 mg were heated at a rate of 15 °C min^{-1} from 100 to 800 °C. The instrument produced a weight loss against temperature curve. The TGA curve for the as-received lignin sample and vacuum dried lignin sample is shown in Figure 49.

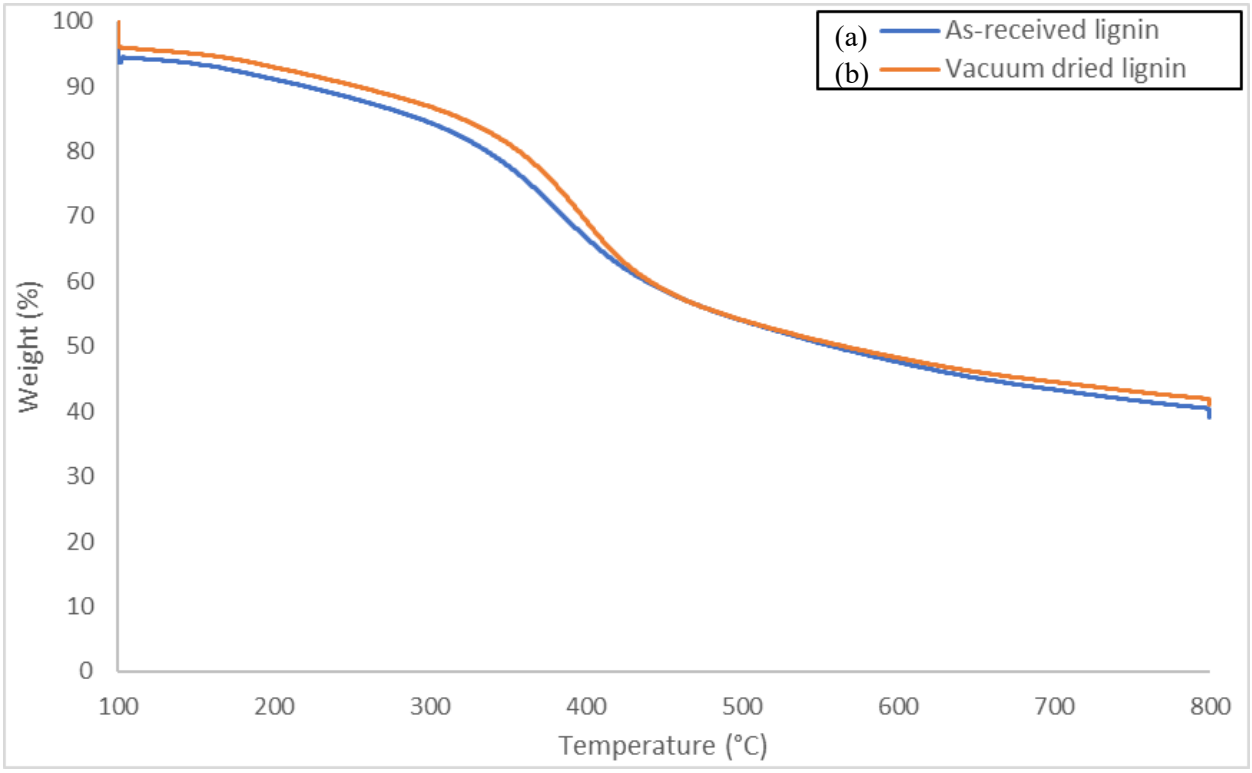

Figure 49. TGA thermogram with curves for the; (a): as-received and (b): vacuum dried lignin samples.

The TGA thermogram demonstrates that the major degradation of all lignins took place in a temperature range between 300-500 °C, with maxima at around 350 °C, as evidenced in the

curve. The TGA data is similar to what is reported in the literature for Kraft lignin, see Table 9. The percentage decrease in weight for the as-received lignin sample from the TGA thermogram is shown in Figure 50.

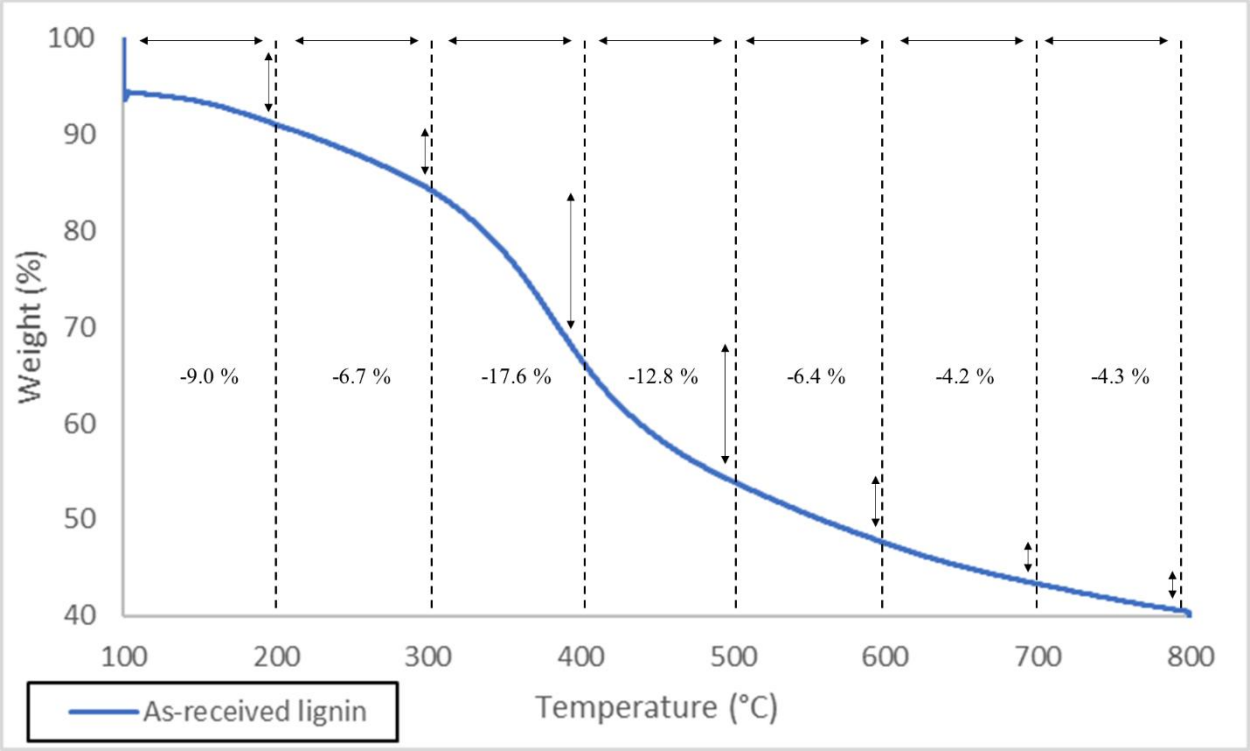

Figure 50. TGA thermogram for the as-received lignin sample showing weight loss percentage at each temperature interval.

The weight loss data for the as-received lignin sample at different temperature stages reflects the thermal decomposition behaviour of lignin. Between 100–200 °C, a weight loss of 9.0% was observed, which is likely due to the evaporation of absorbed moisture and the release of low-molecular-weight volatiles (25,329). This initial loss reflects the removal of physically bound water and small organic compounds. A smaller weight loss of 6.7% occurred between 200–300 °C, suggesting the onset of the breakdown of weakly bound functional groups such as hydroxyl and methoxy groups, along with some early-stage thermal degradation of lignins side chains (see Section 2.7.4.1). A significant weight loss of 17.6% was recorded between 300–400 °C, indicating the primary degradation of lignin's structural components, including the cleavage of ether and C–C bonds within the aromatic rings (292). This stage represents the most active thermal decomposition phase. Between 400–500 °C, a weight loss of 12.8% occurred, which

corresponds to further decomposition of aromatic rings and the formation of char, alongside the release of gases such as carbon monoxide, carbon dioxide, and methane (408).

The weight loss reduced to 6.4% between 500–600 °C, indicating the slower degradation of more thermally stable structures and the continued formation of char. A further weight loss of 4.2% between 600–700 °C reflects the gradual breakdown of the remaining thermally stable lignin components and the continued release of volatiles (25). Between 700–800 °C, the weight loss of 4.3% suggests the final stages of carbonisation, where the remaining organic material decomposes, leaving behind a carbon-rich residue (467,468). The total weight loss of 61.0% indicates that a significant portion of the lignin decomposes upon heating, with the remaining residue primarily consisting of carbonaceous material formed through the charring process.

The percentage decrease in weight loss for the vacuum dried lignin sample from the TGA thermogram is shown in Figure 51. The weight loss data for the vacuum-dried lignin sample shows a slightly different thermal decomposition pattern compared to the as-received sample, reflecting the effect of vacuum drying on lignins thermal stability.
Between 100–200 °C, the vacuum-dried sample exhibited a weight loss of 7.1%, which is lower than the 9.0% recorded for the as-received sample. This reduction suggests that vacuum drying effectively removed a portion of the absorbed moisture and low-molecular-weight volatiles prior to testing. In the 200–300 °C range, the vacuum-dried sample showed a weight loss of 6.1%, similar to the 6.7% seen for the as-received sample, indicating comparable early-stage decomposition of functional groups and side chains. A significant weight loss of 17.5% was observed between 300–400 °C, comparable to the 17.6% recorded for the as-received sample, reflecting the main thermal degradation phase where the breakdown of ether and C–C bonds occur. Between 400–500 °C, the vacuum-dried sample showed a higher weight loss of 15.3% compared to 12.8% for the as-received sample.

This suggests that the structural modifications caused by vacuum drying may have enhanced the breakdown of more stable aromatic structures at this stage (25,467,468). The weight loss decreased to 5.8% between 500–600 °C, slightly lower than the 6.4% seen for the as-received sample, indicating a slower rate of degradation of the remaining stable structures. Between 600–700 °C, the vacuum-dried sample lost 3.7% compared to 4.2% for the as-received sample, showing slightly reduced decomposition of thermally resistant lignin components. After 600 °C, the rate of weight loss slows, this phase likely involves dehydrogenation processes along with

the generation of condensable gases (e.g., acetaldehyde, acetic acid) and non-condensable gases (CO, CO_2), leading to the progressive breakdown into char (467,468).

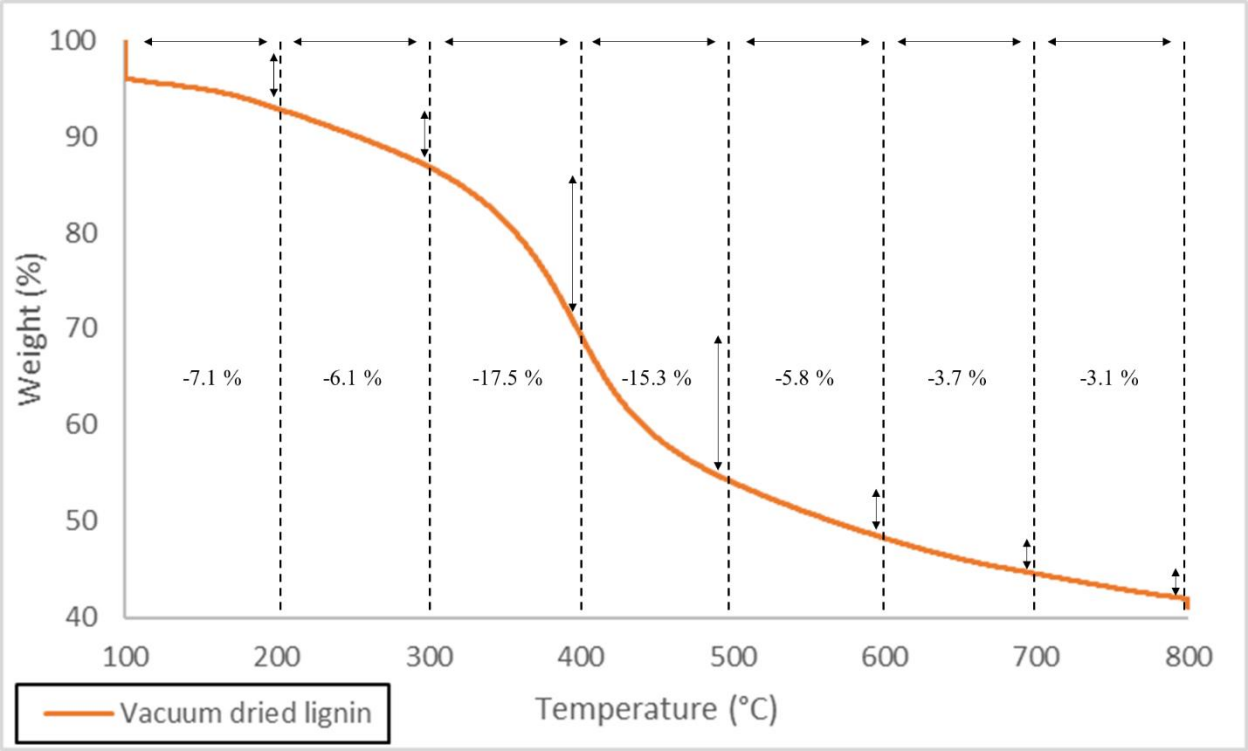

Figure 51. TGA thermogram for the vacuum dried lignin sample showing weight loss percentage at each temperature interval.

Dehydration of lignin and the thermal oxidative breakdown of lignin macromolecular chains, see Figure 17, can also contribute to the weight loss. In the final stage, from 700–800 °C, the vacuum-dried sample exhibited a weight loss of 3.1%, lower than the 4.3% for the as-received sample, suggesting a more stable char formation due to the structural changes induced by vacuum drying. The total mass loss for the vacuum-dried sample was 58.6%, slightly lower than the 61.0% recorded for the as-received sample, indicating that vacuum drying enhanced thermal stability by reducing the presence of volatile components and moisture within the lignin matrix.

In comparison with the work of previous researchers, such as Inam Khan and Bongkot Hararak (404,405), whose TGA data also investigated Domtar lignin, the findings from the current research align well with their observations. Both studies reveal similar thermal degradation patterns and weight loss behaviours, supporting the reproducibility and consistency of thermal profiles for Domtar lignin across different experimental setups.

4.1.7. Gel permeation chromatography of lignin powder

GPC analysis of the lignin was conducted by the Science City Research Alliance at the University of Warwick. The as-received lignin was pre-dried at 110 °C, ground, and sieved before further processing. For thermal treatment, samples were heated in a vacuum oven at set temperatures for 4 hours, followed by refluxing in DMF at 100 °C, 120 °C, or 140 °C for an additional 4 hours prior to being sent to the University of Warwick for GPC analysis.

The molecular weight distribution of as-received and vacuum-dried lignin samples was analysed using GPC, and the resulting chromatograms are shown in Figure 52, with corresponding values for number-average molecular weight (M_n), weight-average molecular weight (M_w), and polydispersity index (PDI) summarised in Table 14 (383,384).

Table 14. Molecular weight and polydispersity of lignin samples.

Lignin sample	**M_n (g/mol)**	**M_w (g/mol)**	**PDI (M_w/M_n)**
As-received	3047	5035	1.652
100 °C Vacuum Dried	3051	5160	1.691
120 °C Vacuum Dried	3137	5172	1.649
140 °C Vacuum Dried	3179	5462	1.718

The as-received lignin exhibited an M_n of 3047 g/mol and an M_w of 5035 g/mol, with a PDI of 1.652, indicating a broad molecular weight distribution typical of technical lignin. Upon vacuum drying at 100 °C, a slight increase in M_w to 5160 g/mol was observed, with M_n remaining nearly unchanged at 3051 g/mol, resulting in a marginally broader PDI of 1.691. Further thermal treatment at 120 °C and 140 °C led to continued increases in both M_n and M_w values. Notably, the sample treated at 140 °C showed the highest molecular weights (M_n = 3179 g/mol and M_w = 5462 g/mol) and the widest distribution (PDI = 1.718), suggesting structural rearrangement of lignin fragments at elevated temperatures. The GPC chromatograms support these observations, showing a consistent shift of the main peak toward slightly higher molecular weights with increasing drying temperature, along with a more pronounced high molecular weight shoulder in the 140 °C-treated sample. This behaviour indicates potential thermal-induced cross-linking or

aggregation (see Section 2.2.2), likely contributing to altered reactivity at higher treatment temperatures (135).

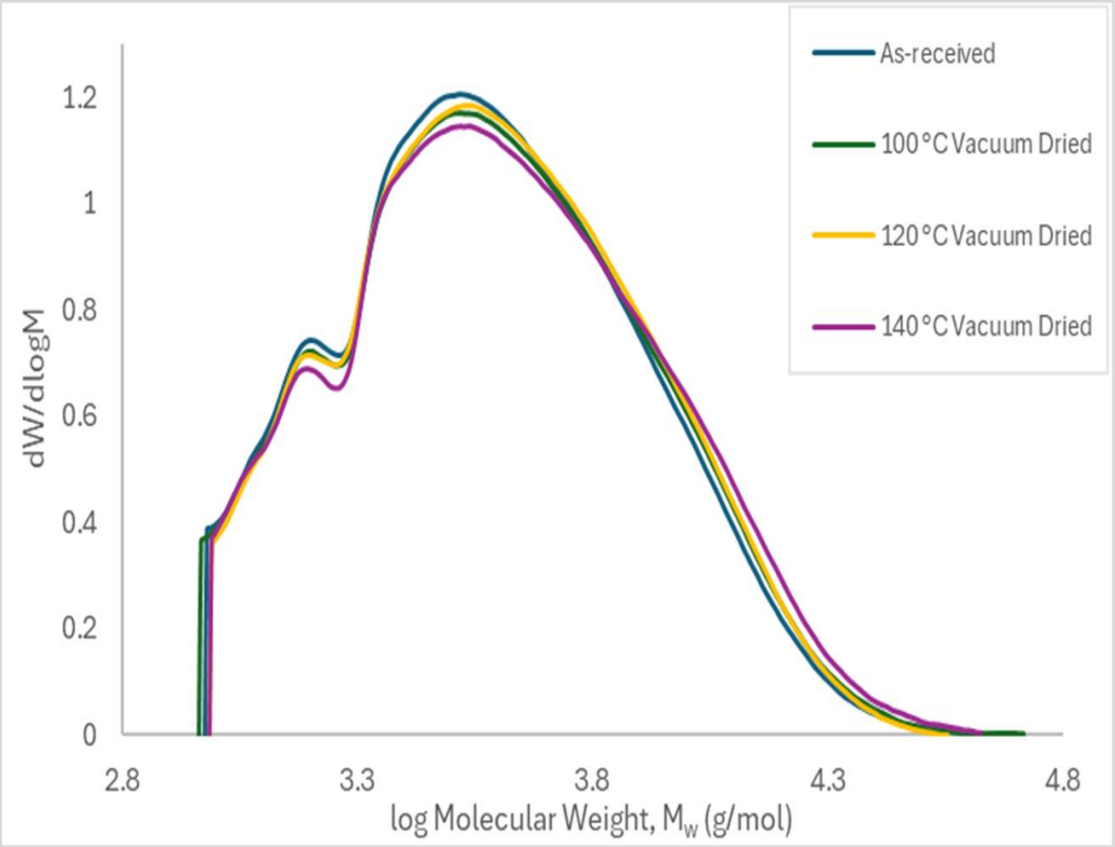

Figure 52. Molecular weight distribution traces for; (a): as-received lignin, (b): 100 °C vacuum dried lignin, (c): 120 °C vacuum dried lignin and (d): 140 °C vacuum dried lignin. Samples were all refluxed in DMF for 4 hours at 100 °C.

Previous members of the University of Birmingham research group, Bongkot Hararak (404) and Inam Khan (405) investigated lignin fractionation methods and characterised as-received Domtar lignin using GPC. The M_w for as-received lignin was 6000 $g \cdot mol^{-1}$, whilst the polydispersity index was 2.22, similar to the values reported in this study. The molecular weight and PDI values obtained in this study are also comparable to those reported in the literature for technical lignin samples analysed by GPC, see Table 8 for reported M_n, M_w and PDI literature values (80,403). In conclusion, the GPC data show a clear trend of increasing molecular weight and polydispersity in lignin with higher vacuum drying temperatures, likely due to thermal-induced condensation or cross-linking reactions that enhance molecular cohesion.

4.2. Characterisation of lignin:PAN blend solutions in DMSO

To evaluate the properties relevant to fibre formation and electro-spinning, lignin:PAN blend solutions in DMSO were characterised using SEM, shear viscosity rheology measurements, and solution conductivity analysis. These techniques were employed to assess the morphology of deposited fibres, the rheological behaviour and ionic characteristics of the solutions, respectively.

4.2.1. Electro-spinning of lignin using DMSO

This chapter presents a technique for electro-spinning softwood Kraft lignin exclusively utilising DMSO as the solvent, eliminating the necessity for polymer blending or chemical modification. DMSO is not toxic when compared to conventional solvents documented in the literature (for example, THF, DMF, DMAc), rendering it a safer and more environmentally friendly solvent option (3). The electro-spinning process parameters were optimised to generate bead-free and unfused lignin fibres, demonstrating the viability of utilising DMSO for electro-spinning neat lignin.

Furthermore, aligned electro-spun lignin fibres were effectively generated with a specially designed Vee-shaped polytetrafluorethylene “shield” that was co-located on a copper electrode. This accomplishment fills a gap in the literature, as the generation of fibres from neat softwood lignin using DMSO in a single-solvent system, has not been previously reported. Most prior research has concentrated on hardwood Organosolv lignin solubilised in ethanol or toxic solvents such as DMF (262), softwood lignin solvent blend systems in acetone (204), or softwood lignin composites with polymers such as PEO (469), PAN (411), or PVA (35). Softwood lignin is frequently deemed inadequate for spinning because of its insufficient viscoelasticity, necessitating the incorporation of additional polymers (284,470).

Electro-spinning of lignin requires dissolving in a suitable solvent (471–473). Researchers have routinely utilised DMF for this purpose, but its high toxicity and accompanying environmental and health issues pose considerable problems (472,474). DMSO provides a safer option while effectively facilitating lignin fibre production.

4.2.2. Selection of DMSO for electro-spinning

Previous work done by University of Birmingham researchers indicated that softwood Kraft lignin is soluble in acetone; nevertheless, its utilisation in electro-spinning is constrained by acetone's low boiling point (56 °C). The rapid evaporation of acetone was noted to induce the solidification of lignin at the needle tip, so interrupting the electro-spinning process. This was

solved by introducing a second co-solvent with a higher boiling point, DMSO. DMSO was used as the secondary solvent because of its mutual solubility and compatibility with lignin and acetone (204,404).

Following on, DMSO was chosen as the single-solvent for electro-spinning lignin in this study due to its unique combination of properties that enhance the processes efficiency and environmental safety. One of its key advantages is its high boiling point of 189 °C, which significantly reduces the evaporation rate of the lignin solution during electro-spinning. This ensures a stable spinning process compared to more volatile solvents, such as acetone, which as aforementioned can interrupt the electro-spinning process, because of solution evaporation at elevated temperatures.

In addition to its thermal properties, DMSO is a less toxic alternative to conventional solvents like DMF and DMAc, which pose significant environmental and health hazards. By selecting DMSO, the process aligns with greener and safer manufacturing practices while maintaining excellent solubility with lignin. This compatibility allows for the dissolution of lignin without the need for polymer blending or chemical modifications, simplifying the process and avoiding complications from insoluble residues (202,425).

Furthermore, DMSO's high dielectric constant plays a crucial role in electro-spinning, as it reduces the formation of beads, resulting in more uniform fibre production. Its low electrical conductivity also facilitates the formation of a stable Taylor cone, essential for the continuous expulsion of lignin jets during fibre formation (227,475). These characteristics make DMSO an ideal solvent for electro-spinning lignin alone, supporting the development of a simpler and more sustainable method for fibre production.

Table 15 illustrates the solvents that are frequently referenced in the literature for electro-spinning lignin, including DMF and DMAc, which exhibit toxicity. DMSO was advantageous in that the solvent mitigates the health and environmental hazards linked to hazardous solvents. DMSO provides benefits due to its reduced electrical conductivity and elevated dielectric constant relative to DMF. Solvents with elevated dielectric constants can significantly diminish bead production during electro-spinning (175,227). Nevertheless, additional parameters, including solution viscosity, surface tension, temperature, electrical conductivity, and dielectric constant, may also affect bead formation during electro-spinning, as discussed in Section 2.4.2.

Table 15. Solvents used for electro-spinning lignin and their selected properties (175).

Solvents	Toxicity*	Hansen Solubility Parameter δ_H ($MPa^{1/2}$)	Boiling point (°C)	Surface tension ($mN.m^{-1}$)	Electrical conductivity (µS/cm)	Dielectric constant
Acetone		7.0	56	23.3	5×10^{-5}	20.6
DMSO	Not hazardous	10.2	189	43.7	2×10^{-5}	46.6
DMF		11.3	153	35.0	6×10^{-5}	20.6
DMAc		10.2	166	34.0	2×10^{-5}	37.8
Ethanol		19.4	78	22.3	1×10^{-5}	22.4

*Toxicity hazard symbols:  :Serious health hazard,  :Flammable,  :Health hazards.

4.2.3. Transition from lignin:PAN blend to neat lignin electro-spinning in DMSO

The development of a method for electro-spinning neat lignin in DMSO was preceded by studies involving a 50:50 blend of lignin and PAN in the same solvent. This initial research phase aimed to address concerns regarding the processability of lignin as a standalone material for fibre production. PAN, known for its excellent viscoelastic and electro-spinnability properties, served as a model polymer to validate the potential of electro-spinning of neat lignin in DMSO. The successful production of lignin:PAN fibres confirmed the compatibility of DMSO as a solvent and the suitability of lignin as a precursor material when supported by a well-established polymer like PAN.

Building on the research group's previous work with lignin:PAN blends, this study strategically shifted towards a higher lignin content. Initial studies focused on electro-spinning lignin:PAN blends at a 30:70 polymer ratio, leveraging PAN's superior spinnability to ensure fibre formation and stability.

In the current work, the proportion of lignin was increased from 30% to 50% in the lignin:PAN blend, aiming to further evaluate the material's processability and behaviour at higher lignin concentrations. This transition was motivated by a desire to explore lignin's potential as a major fibre-forming component and to better understand its influence on fibre morphology and properties. The shift towards a 50/50 ratio not only provided insights into the compatibility of lignin with PAN but also allowed the study to assess whether lignin's inherent viscoelasticity

could sustain fibre formation under electro-spinning conditions with reduced reliance on synthetic polymers.

The findings from the 50/50 lignin:PAN electro-spinning experiments served as a stepping stone towards the goal of electro-spinning neat lignin fibres in DMSO, by then increasing the lignin content in the blend to 70%. By first demonstrating the feasibility of high lignin content in blends, this approach reduced the risk of process failure in transitioning to neat lignin, ensuring that both material properties and electro-spinning parameters could be optimised in a systematic and informed manner. This progression highlights the methodical approach of the study, moving incrementally from polymer blends to neat lignin fibres while refining techniques and understanding of lignin's spinnability.

Encouraged by these results, the research shifted focus to electro-spinning neat lignin in DMSO. This decision was driven by the goal of simplifying the fibre production process and avoiding the use of additional polymers. Neat lignin electro-spinning eliminates the need for blending, thus showcasing lignin's potential as an independent precursor material for fibre formation. The transition from a lignin:PAN blend to neat lignin also aligns with efforts to develop sustainable, single-component systems that reduce complexity and environmental impact.

By demonstrating that DMSO could effectively dissolve and support the electro-spinning of lignin, the research not only validated the use of this solvent but also advanced the understanding of lignin's viscoelastic properties and its capability for fibre production without reliance on synthetic polymers.

4.2.4. Electro-spinning of lignin:PAN blends in DMSO

PAN, a crude oil derivative, is the major precursor for carbon fibre synthesis (292). Lignin:PAN composites are significant as a largely renewable carbon fibre precursor material. Solutions were formulated using softwood Kraft lignin, PAN, and the non-toxic solvent DMSO. Nanofibres were produced using traditional electro-spinning techniques, followed by the application of an innovative Vee-shield technology to align the fibres (19). The addition of lignin to PAN/DMSO solutions reduced viscosity and enhanced conductivity, altering the homogeneity of the electro-spinning jet and fibre morphology. Highly aligned fibres were obtained from 30:70, 50:50, and 70:30 lignin:PAN blends by altering polymer blend content and processing conditions.

To begin with randomly deposited fibres of pure PAN in DMSO, % (w/v) of PAN in the solvent being 12% (w/v) and 14% (w/v), respectively, were generated via electro-spinning, as shown below in Figure 53. These PAN fibres were produced mostly bead free; beads were removed by increasing the polymer concentration from 12% (w/v) to 14% (w/v) in DMSO.

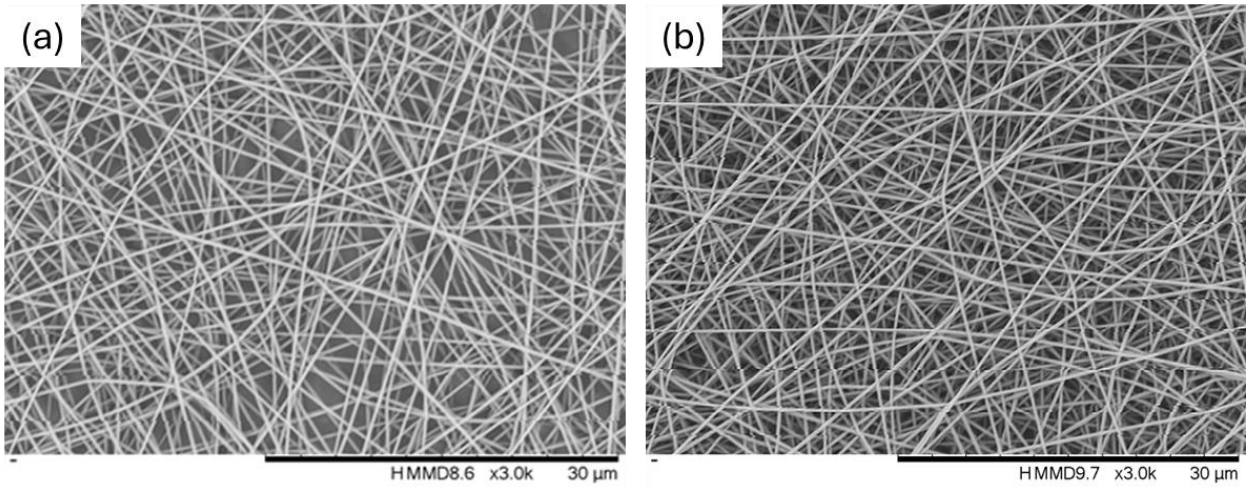

Figure 53. SEM micrographs of randomly deposited PAN fibres of (a): 12% (w/v) and (b): 14% (w/v) in DMSO alone.

Since it was found that increasing the polymer content reduced bead formation in electro-spun fibres, the following batch of lignin:PAN blend solutions to be electro-spun in DMSO were made at polymer concentrations of 14% (w/v) and 20% (w/v) of PAN in DMSO. To begin with, solutions were produced at polymer ratios of 30:70 lignin:PAN in DMSO and then 50:50 lignin:PAN in DMSO.

Figure 54 (a) and (b) are the micrographs for the 30:70 lignin:PAN blend polymer concentrations of 14% (w/v) in DMSO and 20% (w/v) in DMSO, respectively. As the polymer concentration was increased the number of droplets reduced on the fibre mat.

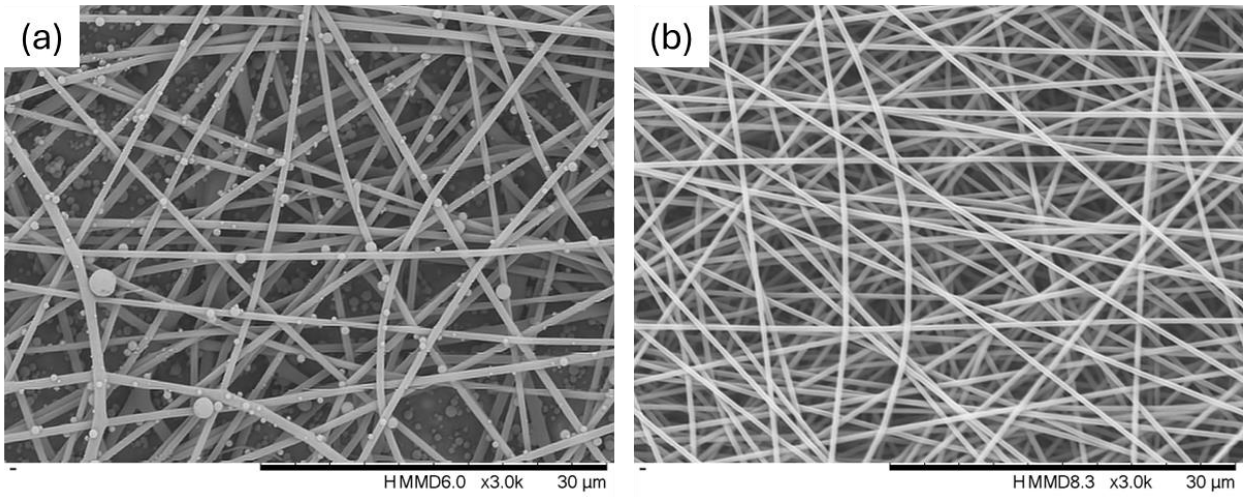

Figure 54. SEM micrographs of randomly deposited 30:70 lignin:PAN fibres in DMSO, of (a): 14% (w/v) and (b): 20% (w/v) polymer concentration.

Droplet formation was due to jet instability during the electro-spinning process leading to electro-spraying, this was reduced by increasing polymer concentration in the electro-spinning solution.

Droplet formation observed in the lower polymer concentration solution more closely resembled electro-spraying than fibre formation. This behaviour is likely due to insufficient chain entanglement and may also reflect partial material separation within the syringe during spinning, particularly if the solution had aged or remained in the tube for an extended period. Such instability can contribute to bead formation and poor fibre morphology. Following on, the lignin polymer concentration was increased in the electro-spinning solutions to a polymer blend of 50:50 lignin:PAN. Figure 55 (a) and (b), are the micrographs for the 50:50 lignin:PAN blend polymer concentrations of 14% (w/v) in DMSO and 20% (w/v) in DMSO, respectively.

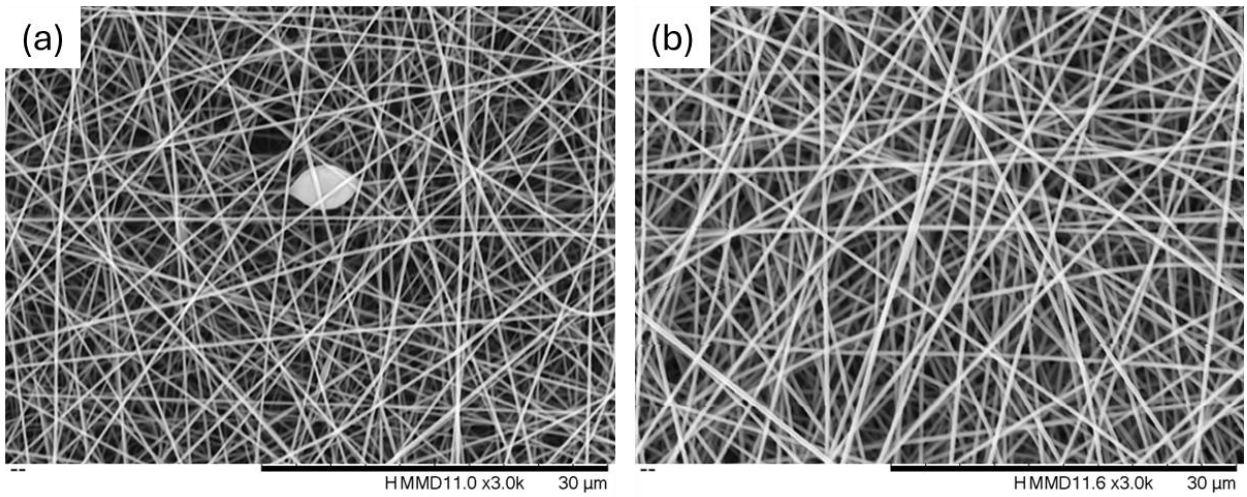

Figure 55. SEM micrographs of randomly deposited 50:50 lignin:PAN fibres in DMSO, of (a): 14% (w/v) and (b): 20% (w/v) polymer concentration.

As seen in the previous lignin:PAN blend of 14% (w/v), when the polymer concentration was increased the number of droplets reduced on the fibre mat. Droplet formation was also due to lack of homogeneity in the solution but is far less prevalent here in the 50:50 lignin:PAN solutions compared to the above 30:70 lignin:PAN solution at 14% (w/v) polymer concentration in DMSO.

Subsequently, the lignin ratio was increased further to 70:30 lignin:PAN. It was decided to adopt the 20% (w/v) polymer concentration in DMSO for subsequent experiments to avoid droplet formation as seen in for Figure 55 the 14% (w/v). Smooth, randomly oriented fibres were produced from the 70:30 lignin:PAN in DMSO solution 20% (w/v) polymer concentration, with no prevalent bead or droplet formation, as shown in Figure 56.

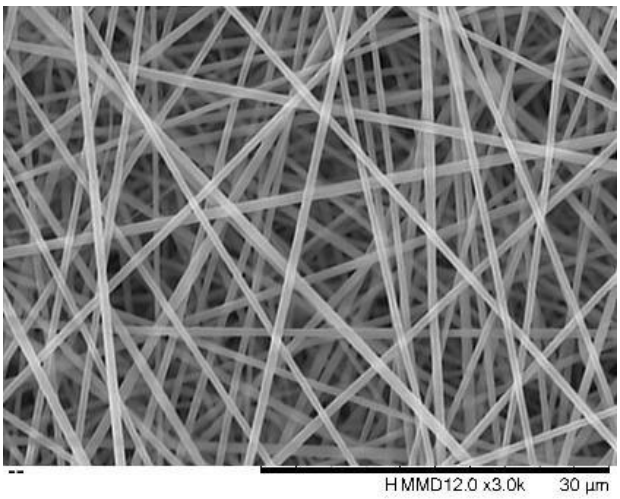

Figure 56. SEM micrograph of randomly deposited, 70:30 lignin:PAN fibres in DMSO of 20% (w/v) polymer concentration.

The fibres generated from a 14% (w/v) neat PAN solution exhibited smoothness, uniformity, and an absence of beads, the average fibre diameter was 451 nm, in accordance with findings from Shao *et al*., (19). Uniform and bead-free lignin:PAN fibres were similarly obtained with lignin content reaching 30%, while the overall polymer concentration remained constant. Raising the polymer concentration from 14 to 20% (w/v) resulted in an increase in average fibre diameter from 321 ± 76 nm to 425 ± 58 nm (see Table 16). At a lignin content of 50% and an overall polymer concentration of 14% (w/v), the emergence of beaded fibres was observed, accompanied by an increased distribution in fibre diameter to 586 nm.

Table 16. Average fibre diameter of randomly deposited lignin:PAN electro-spun fibres.

Polymer blend (lignin:PAN ratio, polymer concentration in DMSO, % (w/v))	0:100, 12% (w/v)	0:100, 14% (w/v)	30:70, 14% (w/v)	30:70, 20% (w/v)	50:50, 14% (w/v)	50:50, 20% (w/v)	70:30, 20% (w/v)
Mean fibre diameter (nm)	338	451	321	425	586	689	689

Bead formation is generally ascribed to inadequate molecular entanglement and the extensibility of polymer blends (243,461). The morphology and diameter of fibres are affected by the whipping behaviour of the jet (476). PAN, characterised by its long, linear molecular structure, can be readily elongated into thin fibres during the jet whipping process (477). The incorporation of lignin, which has its intricate ring and branched structures, enhances entanglement and diminishes stretchability. The blend can still be extruded into stretched fibres via electro-spinning; however, lignin restricts the reduction of fibre diameter and encourages bead formation.

4.2.5. Observed defects in randomly deposited fibres

The main observable defect in electro-spun lignin:PAN fibres at low overall polymer concentration is the formation of beads on the fibres, as illustrated in Figure 57. The removal of beads was achieved by increasing the overall polymer content in the solution.

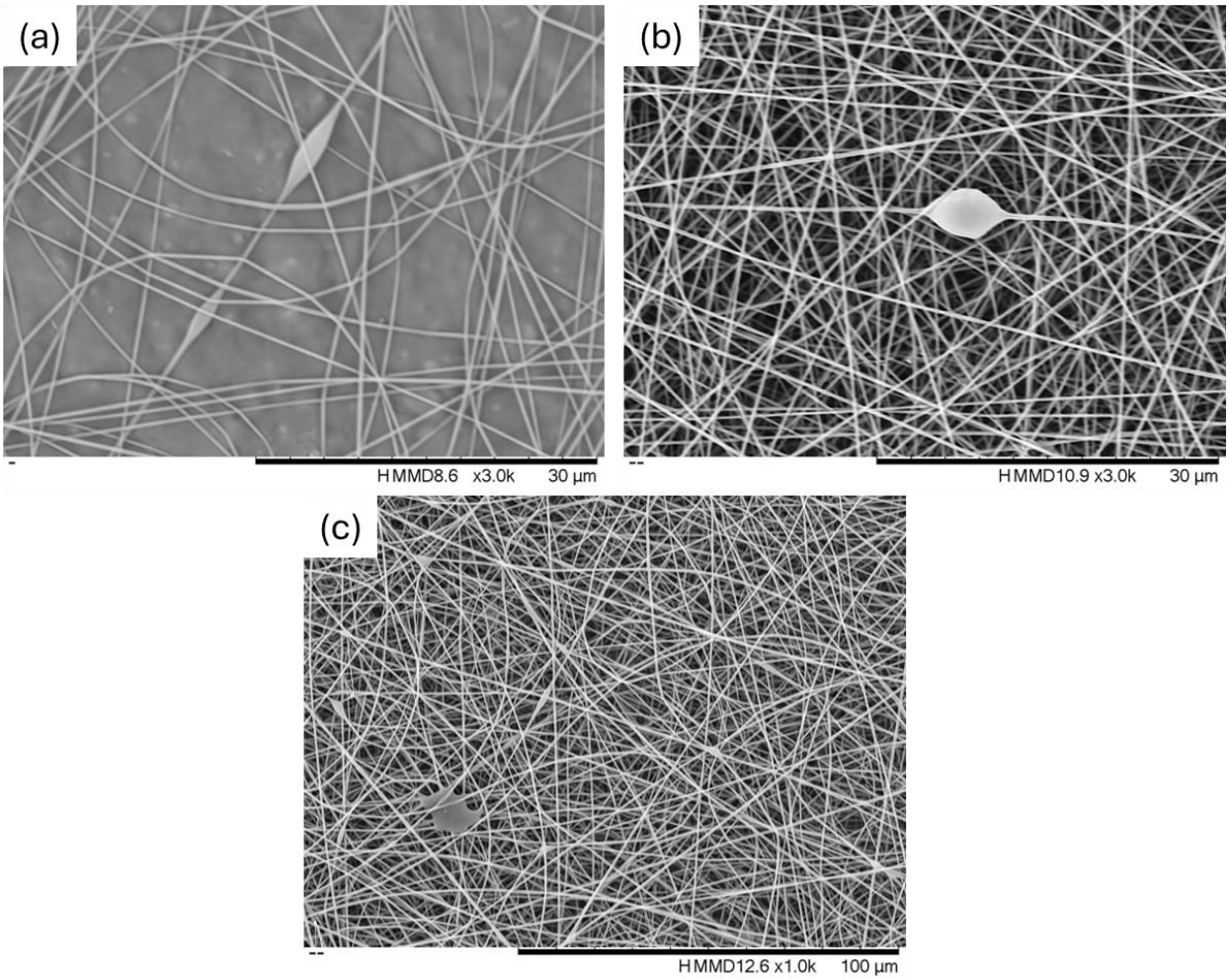

Figure 57. Beaded lignin:PAN electro-spun fibres on A: 0:100, 12% (w/v), B: 50:50, 14% (w/v) and 50:50, 20% (w/v).

The addition of lignin significantly disrupted jet stability, frequently resulting in electro-spraying, as seen in Figure 58.

The overall lignin polymer content was increased to manage this for the 20% (w/v) polymer concentration solution blends. Defect-free fibres were produced from the following lignin:PAN ratios: 0:100, 14% (w/v), 30:70, 14% (w/v), 50:50, 14% (w/v), and 70:30, 20% (w/v).

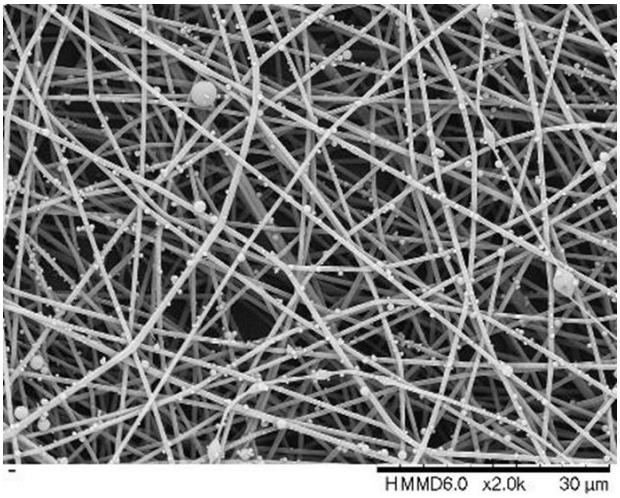

Figure 58. Electro-sprayed fibres of lignin:PAN blend 30:70, 20% (w/v) polymer concentration in DMSO.

Fibre fusing was observed in certain lignin:PAN electro-spun samples, where individual fibres joined at their intersections, forming fused regions, as shown in Figure 59. In the micrograph the fibres merge at a contact point due to unstable electro-spinning conditions (478).

This phenomenon was particularly prevalent in fibres produced from solutions with lower viscosity. During the electro-spinning process, lower-viscosity solutions exhibited unstable jet behaviour, leading to frequent jet breakage and the formation of droplets (234,238). These droplets, upon deposition onto the collected fibres, either partially dissolved the existing fibres or facilitated fusion at contact points, where individual fibres were no longer distinct, as seen in Figure 59.

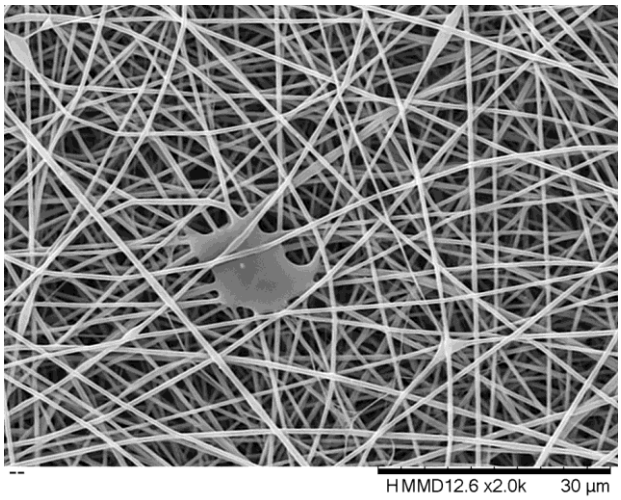

Figure 59. Fusing of electro-spun lignin:PAN fibres, 50:50, 20% (w/v).

The extent of fibre fusing was influenced by several key parameters, including solution viscosity, polymer concentration, applied voltage, and ambient humidity (284,466). Lower-viscosity

solutions generally led to higher instances of jet breakage, increasing the likelihood of droplet formation and subsequent fibre fusion. In contrast, higher-viscosity solutions produced more stable jets, reducing the occurrence of fused fibres (see Section 4.2.7).

4.2.6. Fibre alignment using the Vee-shield method

A novel method for producing highly aligned electro-spun fibres has been developed at the University of Birmingham, utilising a polytetrafluoroethylene (PTFE) Vee-shaped shield (19). This Vee-shield technique effectively aligned PAN fibres on both static and continuously hauled-off substrates. By optimising blend composition and processing parameters, highly aligned fibres were successfully produced from 30:70, 50:50, and 70:30 lignin:PAN blends are shown in Figure 60.

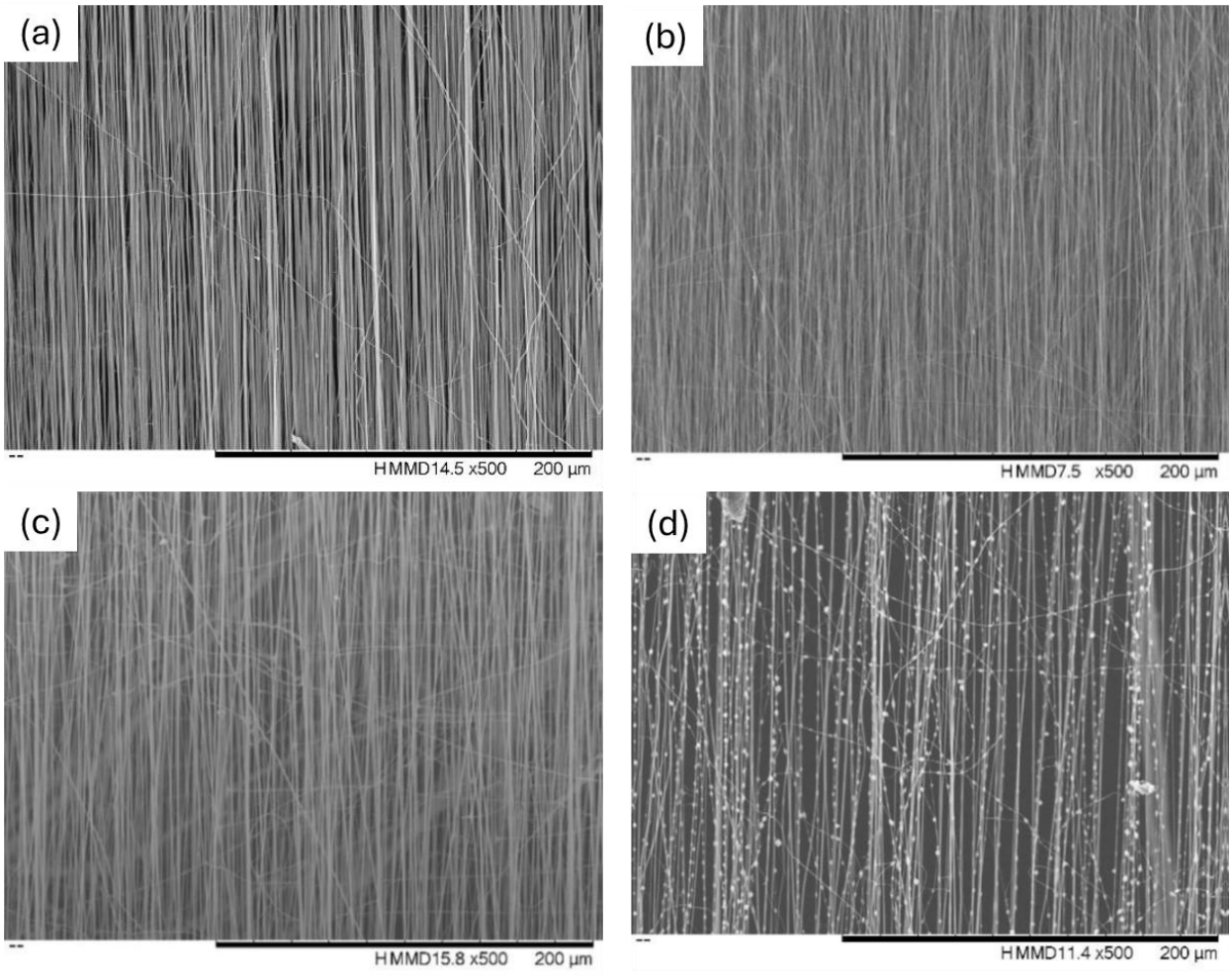

Figure 60. Vee-shield alignment of (a): 30:70, 14% (w/v), (b): 50:50, 14% (w/v), (c): 50:50, 20% (w/v) and (d) 70:30, 20% (w/v).

The fibre diameter was observed to increase with rising lignin content in the aligned lignin:PAN electro-spun fibres, as can be seen in Table 17, a trend consistent with the behaviour of the randomly oriented fibres. The lignin:PAN 30:70, 14% (w/v) sample, which contained the lowest

lignin concentration, exhibited the smallest average fibre diameter (312 nm). As lignin content increased in the blends, the fibre diameter progressively increased, with lignin:PAN 30:70, 20% (w/v) at 378 nm, lignin:PAN 50:50, 14% (w/v) at 535 nm, and the highest lignin content aligned sample, lignin:PAN 70:30, 20% (w/v), reaching an average diameter of 639 nm.

Table 17. Average fibre diameter of aligned lignin:PAN electro-spun fibres

Polymer blend (lignin:PAN ratio, polymer concentration in DMSO, % (w/v))	30:70, 14% (w/v)	30:70, 20% (w/v)	50:50, 14% (w/v)	70:30, 20% (w/v)
Mean fibre diameter (nm)	312	378	535	639

Additionally, higher lignin content enhances solution conductivity (see Section 4.2.7), which can influence charge distribution and jet stability, further contributing to diameter variations. This trend mirrors observations in the random fibre samples, where increased lignin content similarly led to thicker fibres, suggesting that the fundamental influence of lignin on solution properties affects both aligned and random fibre morphologies in a comparable manner. However, despite the increase in diameter, alignment was still maintained in the structured fibres, indicating that the Vee-shield method was effective in directing fibre deposition even as solution properties changed.

All lignin:PAN blends processed using the Vee-shield method exhibited significant fibre alignment. Increased lignin concentrations resulted in a broader distribution of fibre alignment. This may result from the enhanced conductivity of the solutions and the decreased viscosity (236).

The highest degree of alignment was observed in the lignin:PAN 30:70, 14% (w/v) blend, where more than 90% of fibres were oriented within 5 degrees of the mean fibre direction. Other blends showed slightly broader angular distributions, but in all cases, over 90% of fibres remained aligned within 10 degrees (Table 18).

Table 18. Fibre alignment distribution percentage using Vee-shield method of lignin:PAN fibres.

Polymer Blend (Lignin:PAN)	<1°	1°-2°	2°-3°	3°-5°	5°-10°	10°-20°	20°-45°	45°-90°
30:70, 14% (w/v)	53.5	23.9	9.1	5.7	1.9	3.8	0.9	1.3
50:50, 14% (w/v)	20.5	25.5	19.2	16.6	9.9	5.0	2.0	1.3
50:50, 20% (w/v)	25.8	18.2	19.9	18.2	11.9	2.6	1.3	2.0
70:30, 20% (w/v)	28.1	21.9	14.6	16.9	9.9	5.0	2.3	2.3

As the lignin content in the blend increased, so did the appearance of beads within the aligned fibres, as can be seen in Figure 60. This beading effect was particularly noticeable in higher lignin ratio blends, such as 70:30 lignin:PAN, where the fibre morphology exhibited a greater frequency of bead-like structures along the fibre length. The increase in lignin concentrations can lead to increased charge density variations and reduced chain entanglement, causing instability in the jet and promoting bead formation (43,479). Lignin's inherent conductivity may play a minor role in phase separation during electro-spinning, but bead formation is more likely driven by differences in solubility and viscosity between lignin and PAN in DMSO (252,480). At the 70:30 lignin:PAN ratio, phase separation was readily observable, with the solutions containing clumps of a more viscous material dispersed within a less viscous continuous phase. This phase separation indicates that lignin and PAN exhibit limited miscibility at this ratio, resulting in localised lignin-rich domains within a PAN-dominant matrix. The thermodynamic incompatibility between the two polymers, combined with potential differences in their solvation dynamics in DMSO, may lead to microphase separation. This heterogeneity can destabilise the electro-spinning jet, promoting defects such as bead formation and variations in fibre diameter (172,237,481). These results highlight the effectiveness of the Vee-shield method in achieving controlled fibre orientation. The observed variations in alignment across different blends suggest that lignin content influences fibre deposition dynamics, due to differences in viscosity, charge retention, and solvent evaporation rates when blended with PAN.

4.2.7. Lignin:PAN solution characterisation

Figure 61 shows the solution shear viscosity at 100 s^{-1} shear rate of the lignin:PAN blend solutions in DMSO measured at both 25 °C and 55 °C, highlighting the effects of polymer composition, total polymer concentration, and temperature on solution flow behaviour. Viscosity measurements for the lignin:PAN solutions were conducted as single-run experiments for each formulation; consequently, no error bars are included in the reported data. As anticipated, most formulations exhibited a decrease in viscosity with increasing temperature, due to enhanced chain mobility and reduced solvent viscosity at 55 °C (473). However, an anomaly was observed for the lignin:PAN 30:70 (14 % (w/v)) blend, where viscosity increased slightly from 8.13 Pa·s at 25 °C to 9.89 Pa·s at 55 °C.

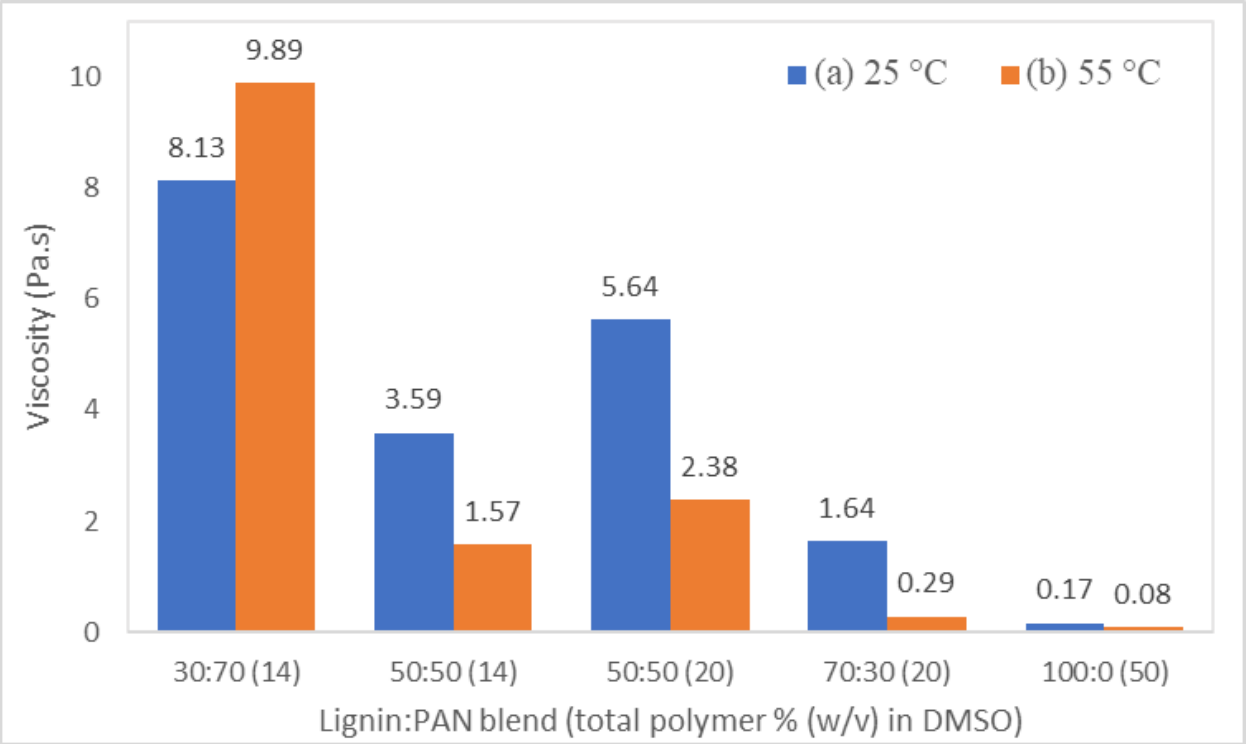

Figure 61. Lignin:PAN blend solution shear viscosity at; (a): room temperature (25 °C) and (b): electro-spinning chamber temperature (55 °C).

For all other blends, the viscosity decreased substantially at the electro-spinning chamber temperature of 55 °C. The lignin:PAN 50:50 blend at 14 % (w/v) dropped from 3.59 to 1.57 Pa·s, and at 20 % (w/v) from 5.64 to 2.38 Pa·s. The lignin:PAN 70:30 (20 % (w/v)) blend showed a significant reduction from 1.64 to 0.29 Pa·s, suggesting that higher lignin content supports efficient viscosity reduction with temperature, potentially enhancing spinnability at elevated chamber temperatures. The viscosity of the neat lignin solution (100:0 at 50 % (w/v)) also decreased markedly from 0.17 Pa·s to 0.08 Pa·s.

Increasing the lignin:PAN ratio in polymer blend solutions containing DMSO resulted in a reduction of solution shear viscosity, as shown in Figure 61. The reduction in solution shear viscosity can be attributed to the significant molecular weight disparity between PAN (230,000 g/mol) and lignin (5,000 g/mol) which results in a stark contrast in chain entanglement, with lignin exhibiting much lower entanglement density (466,482). Raising the total polymer concentration in the solution from 14% (w/v) to 20% (w/v) resulted in an approximate 30% increase in solution viscosity; from 1.57 Pa.s to 2.38 Pa.s for the 50:50 polymer blend solutions. At elevated lignin concentrations and reduced viscosity, the electro-spinning jet exhibited complete instability, resulting in the absence of a Taylor cone. No charged jet was present, and the solution was electro-sprayed (as seen in Figure 58). These solutions necessitated reduced feed rates to avoid dripping onto the fibre mat (as seen in Figure 59) and decreased applied voltages for stabilisation.

The solution conductivity of lignin:PAN blends, prepared in DMSO with varying polymer compositions and concentrations, is presented in Figure 62. The conductivity values for the lignin:PAN solutions were obtained by taking five individual measurements for each sample and reporting the averaged result to ensure accuracy and minimise experimental variability. A clear trend of increasing conductivity with higher lignin content was observed, highlighting lignin's contribution to the ionic strength of the solution.

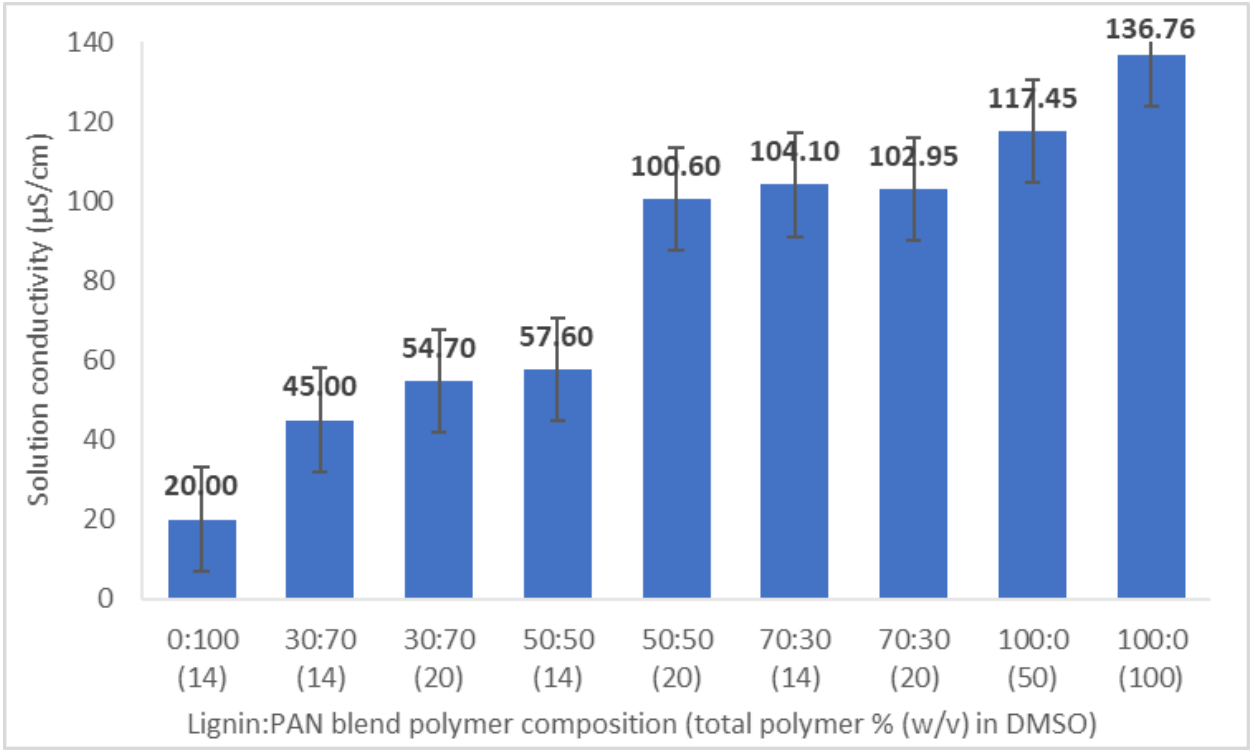

Figure 62. Lignin:PAN blend in DMSO solution conductivity, measured at 25 °C.

The pure PAN solution (0:100 blend, 14 % (w/v)) exhibited the lowest conductivity at 20.00 μS/cm, consistent with PAN's insulating nature and lack of ionisable functional groups (220). Introducing lignin into the blend led to a progressive rise in conductivity: the 30:70 blends showed values of 45.00 μS/cm and 54.70 μS/cm for 14 and 20 % (w/v) total polymer content, respectively, while further increasing lignin to a 50:50 ratio raised the conductivity to 57.60 μS/cm (14 % (w/v)) and 100.60 μS/cm (20 % (w/v)). The solution electrical conductivity increased with the overall polymer concentration, in accordance with similar trends which have been reported (19).

This trend suggests that not only does lignin contribute polar and potentially ionisable groups (e.g., phenolic hydroxyls and carboxylic acids seen in Figure 8), but that overall polymer concentration also enhances charge transport in the solution (243,483). Higher lignin concentration blends at 50:50 and 70:30 compositions (20 % (w/v)) yielded conductivities exceeding 100 μS/cm, with values of 100.60 and 102.95 μS/cm, respectively.

The highest conductivity was observed for neat lignin solutions, measuring 117.45 μS/cm (50 % (w/v)) and 136.76 μS/cm (100 % (w/v)). These values are significantly higher than those of any PAN-containing blends and highlight lignin's strong contribution to solution conductivity (219,480). This elevated conductivity is advantageous for electro-spinning, as it enhances jet stability and fibre formation through increased charge carrying capacity (213,227).

In DMSO, lignin's phenolic (-OH) and carboxyl (-COOH) groups can deprotonate, forming negatively charged species such as phenolates (Aromatic-O^-) and carboxylates (R-COO^-), which increase the availability of mobile charge carriers (484). Additionally, lignin often retains residual metal ions (e.g., Na^+, K^+, Ca^{2+}) from its isolation process, which act as mobile counterions, further promoting ionic dissociation and charge mobility (204,404).

The presence of highly polar functional groups in lignin (485) enhanced the conductivity of the polymer solution by acting as a more effective charge carrier. In contrast, PAN alone contributes less to solution conductivity, as it lacks these conductive functional groups; unlike lignin, which contains phenolic (-OH), carboxyl (-COOH), and aromatic π-conjugated systems which enhance charge transport and thus increase solution conductivity (271,477).

Highly conductive solutions necessitated experimental adjustments of spinning parameters, including voltage, feed rate, and working distance, to stabilise the Taylor cone jet which was obtained by trial and error during the experimental process. Higher conductivity solutions (100

μS/cm and above) typically necessitate applied voltages ranging from 4-8 kV, whereas less conductive solutions require voltages between 10-16 kV.

4.2.8. Lignin:PAN blend immiscibility

Polymer blend instability occurs when immiscible polymers separate or phase-separate due to factors like differences in viscosity, molecular weight and temperature sensitivity leading to a loss of uniformity and desired properties (486,487). Lignin:PAN blends demonstrated immiscibility characterised by a sea-island phase structure (488). Immiscibility in lignin:PAN solution blends resulted from inherent differences in chemical structures, solubility parameters, and intermolecular interactions among lignin, PAN, and the DMSO solvent. Lignin is an amorphous, highly branched polyphenolic polymer characterised by substantial hydrogen bonding capacity, while PAN is a linear synthetic polymer exhibiting strong dipole-dipole interactions attributed to its nitrile groups. The differences in molecular architectures and polarity may result in inadequate miscibility when combined in a common solvent like DMSO (284,285).

At reduced lignin concentrations, PAN demonstrates the ability to solvate and disperse lignin, resulting in a relatively uniform solution. As lignin content increases, its strong self-associating properties, influenced by hydrogen bonding and π-π interactions, may result in phase separation, creating lignin-rich domains within the PAN-rich matrix (489). This phenomenon appears as visible aggregates or clumps of highly viscous lignin distributed within a less viscous PAN-rich phase. Phase separation is significantly affected by factors such as polymer concentration, temperature, and solvent interactions (490). Increased temperatures can enhance solubility by promoting molecular motion; however, as the solution cools or solvent evaporates during electro-spinning, phase separation may become more evident, influencing fibre morphology (284).

Phase separation in electro-spinning solutions can result in defects, including beading, variations in fibre diameter, and inconsistent alignment, because it causes uneven distribution of the components, disrupting the solution's viscosity and surface tension, which in turn affects the stability and uniformity of the electro-spinning process (218,491). Increasing the lignin concentrations lead to electro-spraying, as seen in Figure 58, the formation of beaded fibres, as seen in Figure 57, or fused fibres as seen in Figure 59. Lignin:PAN blends exhibit phase separation above a 50:50 ratio, requiring continuous agitation to maintain solution homogeneity.

At 70% lignin in the polymer blend, the random fibres exhibited no defects, whereas the aligned fibres displayed beading. Establishing a steady jet in the electro-spinning system typically led to improved fibre morphology, this was done by running the electro-spinning at set conditions for 5 minutes prior to collecting fibres for analysis. The random fibre samples were generated following set-up runs, during which the jet had sufficient time to stabilise. The spinning time of the Vee-shield is significantly reduced due to its smaller substrate area.

The random fibres were consistently generated prior to the aligned fibres. The solutions typically necessitate mixing immediately prior to loading into the syringe for spinning to ensure a stable jet and uniform fibres. The incorporation of a magnetic stirring mechanism into the syringe would facilitate solution mixing during rotation, representing a pragmatic advancement for scale-up processes.

4.2.9. Lignin:PAN electro-spinning conclusions

Electro-spinning of lignin:PAN blends at a 70:30 ratio resulted in the production of randomly deposited and aligned fibres. Experimental adjustments to solution composition, processing methods, and spinning parameters successfully stabilised the Taylor cone jet across tested blend ratios. Increasing the lignin content in the lignin:PAN ratio from 0:100 to 100:0 resulted in an increase in both solution conductivity and solution viscosity. Lignin:PAN blends demonstrate phase separation at ratios exceeding 50:50, necessitating continuous agitation to avert phase separation. Additionally, increasing the lignin:PAN ratio from 0:100 to 70:30 resulted in a 103% increase in fibre diameter; from 338 nm to 689 nm. Aligned nanofibres were successfully produced from lignin:PAN blends at a 50:50 ratio without fibre defects using the Vee-shield method. Beaded fibres were spun from a 70:30 blend with alignment. 90% of all fibres were aligned within 10° of the mean measured aligned fibre direction.

4.3. Characterisation of neat lignin solutions in DMSO

The lignin/DMSO solutions were characterised using viscosity and conductivity measurements to assess their flow behaviour and ionic properties, respectively.

4.3.1. Rheology of neat lignin in DMSO solutions

Rheological measurements were conducted to assess the shear viscosity of polymer solutions of lignin dissolved in DMSO, providing insights into the flow behaviour of the solutions under different shear rates. Viscosity measurements for the lignin/DMSO solutions were conducted as single-run experiments for each formulation; consequently, no error bars are included in the reported data. Understanding the rheological properties of lignin solutions is critical for

optimising the electro-spinning process and producing defect-free fibres (492,493). The viscosity of the polymer solution plays a fundamental role in the electro-spinning process, as it directly affects fibre formation and morphology (494). If the viscosity is too low, the solution may produce beads instead of continuous fibres (see Section 2.4.2). Conversely, if the viscosity is too high, it can limit the stability of the jet, making fibre formation difficult and potentially leading to clogging and irregular deposition (17,495). Measuring the shear viscosity of lignin solutions allows for the identification of the optimal viscosity range for electro-spinning, ensuring the formation of continuous, bead-free neat lignin fibres.

5.2.1.1. Viscosity of 50-90% (w/v) lignin DMSO solutions

Lignin DMSO solution shear viscosities were measured using a HR-1 Discovery Hybrid Rheometer at room temperature. This section presents the rheological characterisation of neat lignin solutions in DMSO, with shear viscosities measured at room temperature for a series of increasing lignin concentrations; 50 % (w/v), 60 % (w/v), 75 % (w/v), 80 % (w/v), and 90 % (w/v), respectively. The shear viscosity of the lignin polymer solutions (50, 60, 75, 80 & 90% (w/v)) at 25 °C are shown in Figure 63. The data demonstrated an increase in solution shear viscosity with increasing lignin concentration, from lignin polymer concentrations 50 to 90% (w/v) in DMSO, at a shear rate of 100 s^{-1}.

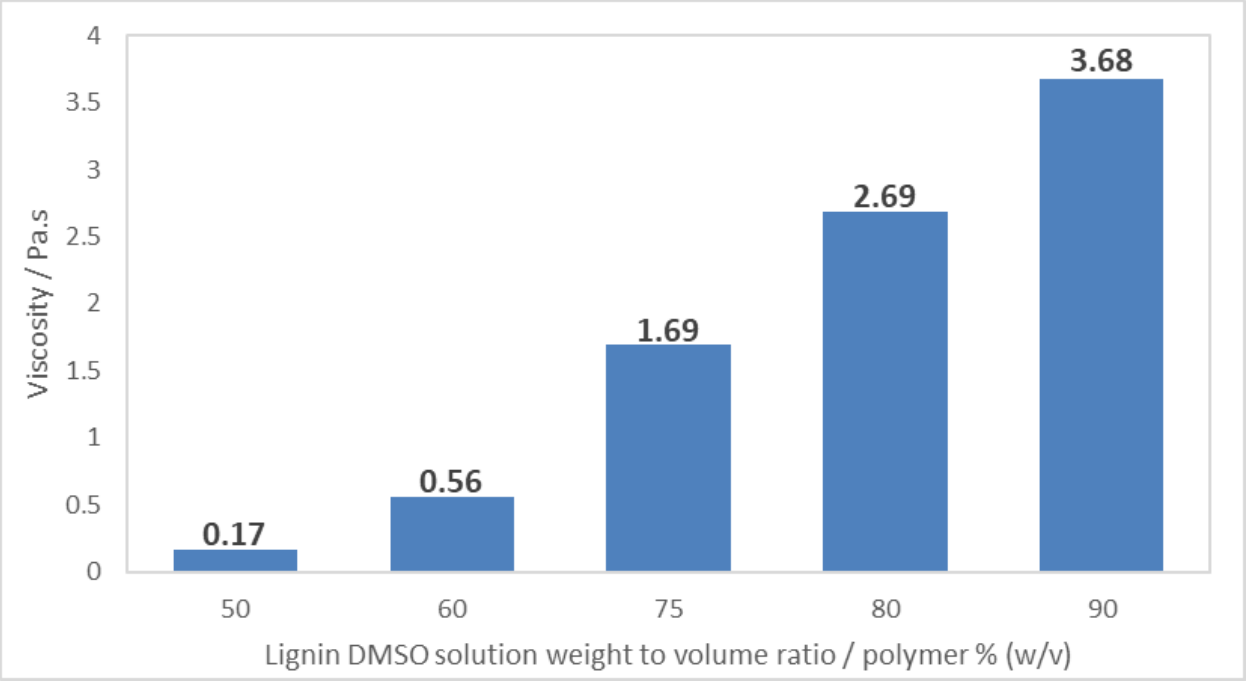

Figure 63. Lignin DMSO solution shear viscosity at room temperature for 50, 60, 75, 80 and 90% (w/v) solutions respectively

The viscosity increased from 0.17 Pa·s at 50% (w/v) to 3.68 Pa·s at 90% (w/v), reflecting a rapid rise in solution resistance to flow as the lignin content increased. This trend indicated that higher lignin concentrations lead to greater intermolecular interactions and entanglements within the solution, contributing to increased viscosity.

Lower viscosity at 50–60% (w/v) may result in insufficient chain entanglement, leading to bead formation rather than continuous fibre formation during electro-spinning, as seen in the micrographs for the 50% (w/v) electro-spun sample (Figure 68). At higher concentrations (75–90% (w/v)), the increased viscosity suggests stronger molecular interactions and network formation, which can stabilise the electro-spinning jet and facilitate the formation of smooth, uniform fibres (see Figure 70).

5.2.1.2. Viscosity of 100% (w/v) lignin DMSO solutions

This section details the rheological characterisation of neat lignin solutions in DMSO at 100 % (w/v), each subjected to a four-hour reflux heat treatment at set temperatures of 80 °C, 100 °C, 120 °C, 140 °C, and 160 °C. Shear viscosities were measured at 55 °C to simulate the temperature conditions within the electro-spinning chamber, data shown in Figure 64.

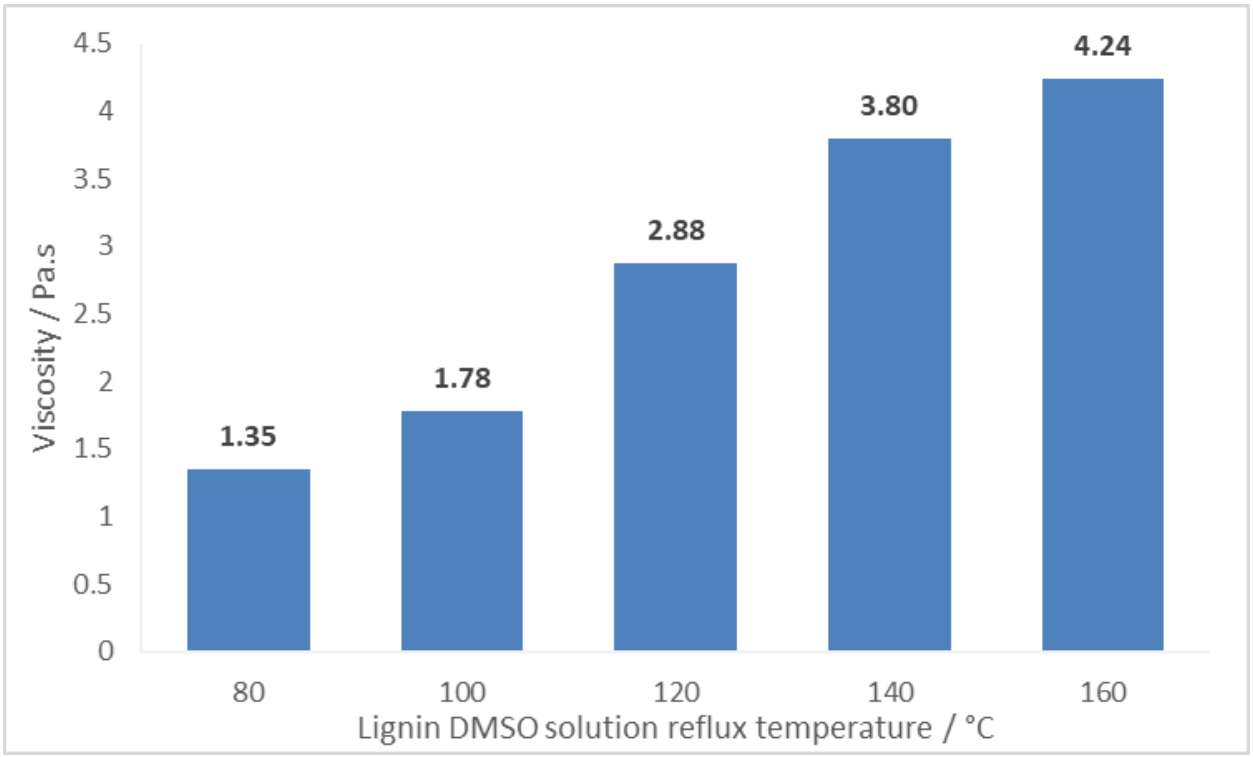

Figure 64. Sweep viscosity at 55 °C for the 100% (w/v) lignin DMSO refluxed solutions at each of the 5 set temperatures (80 °C, 100 °C, 120 °C, 140 °C, and 160 °C).

The data demonstrates a gradual increase in viscosity with increasing reflux temperature from 80 °C to 160 °C, rising from 1.35 Pa·s at 80 °C to 4.24 Pa·s at 160 °C. This increase reflects the

effect of thermal treatment on lignins molecular structure, where higher reflux temperatures will enhance solution viscosity (286,496). A similar trend was observed in the room temperature viscosity measurements, where the solutions demonstrated higher viscosities (~28 Pa·s), reflecting the decreased mobility of lignin chains at lower temperatures (273). In the context of electro-spinning, a viscosity of 2.88–3.80 Pa·s (at 120–140 °C reflux), provided optimal conditions for fibre formation, ensuring sufficient chain entanglement for jet stability while avoiding resistance to flow, which could otherwise cause jet breakage or fibre defects (492,497).

The viscosity ramp data shows a decrease in viscosity as the temperature increases from 25 °C to 65 °C. This reduction reflects the enhanced molecular mobility of lignin chains at elevated temperatures, which reduces intermolecular interactions and chain entanglement, thereby lowering solution viscosity (473). This trend helps explain why the 100 % (w/v) lignin/DMSO solutions could only be electro-spun at elevated temperatures; pre-heating the electro-spinning chamber to 55 °C reduces the solution viscosity sufficiently to enable stable jet formation and uniform fibre production, which was not achievable at room temperature (273). The shear ramp data for the lignin/DMSO reflux solutions is presented in Figure 65, illustrating the variation in viscosity with shear rate following thermal treatment at different reflux temperatures.

As shown in Figure 65, the viscosity of the 120 °C and 140 °C refluxed lignin solutions decrease from approximately 28 Pa·s at room temperature to around 2 Pa·s at 65 °C, highlighting the temperature-dependent thinning effect (498). Notably, the lignin solutions subjected to higher reflux temperatures, at 160 °C, exhibited progressively lower viscosities at all measurement points, from 13Pa.s at room temperature to around 1 Pa·s at 65 °C, which could indicate significant structural changes induced by thermal treatment (456). The viscosity ramp data revealed an inverse relationship between temperature and solution viscosity for lignin/DMSO systems. Across all samples, including the 80 °C and 100 °C refluxed samples, ramp viscosity decreased with increasing temperature (237). The trend observed in Figure 65 closely follows the behaviour predicted by the Arrhenius equation, where viscosity decreases with increasing temperature due to the thermally activated nature of molecular flow (326).

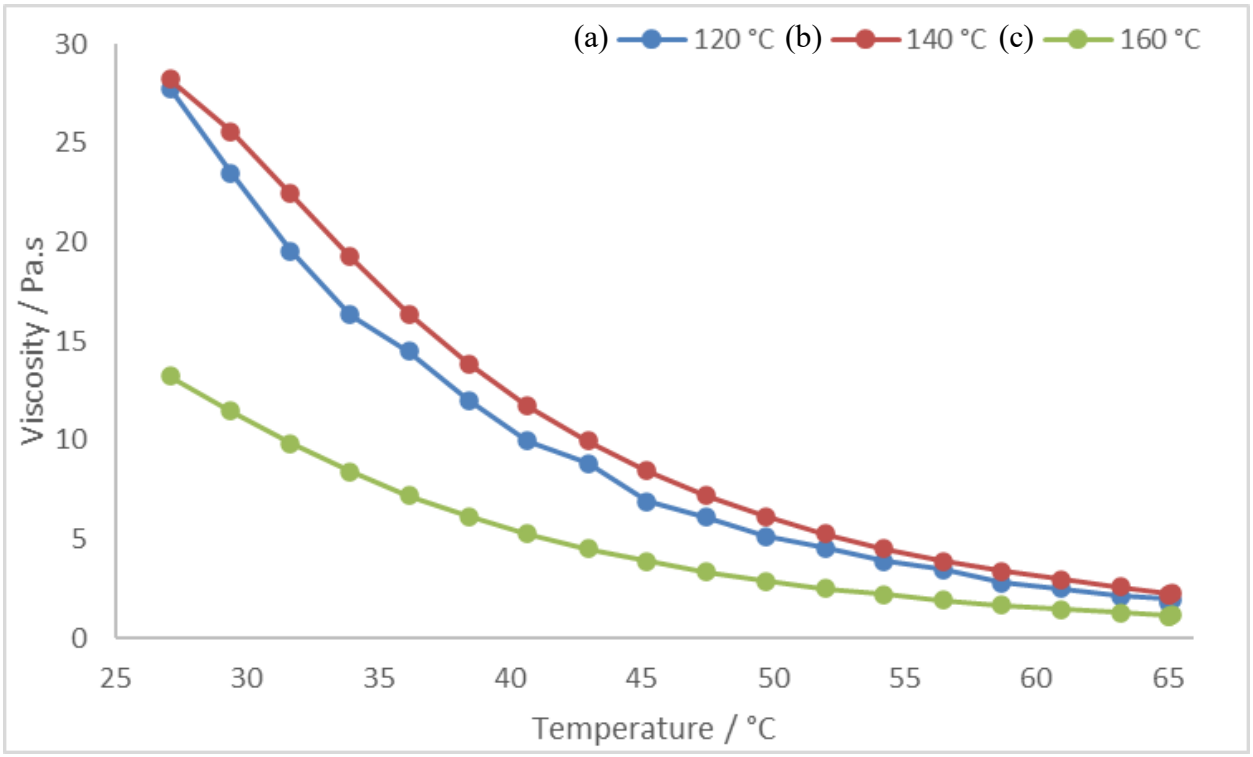

Figure 65. Viscosity of lignin DMSO solutions during temperature ramp 25 °C to 65 °C for the (a): 120 °C, (b): 140 °C and (c) 160 °C refluxed samples.

The rheological characterisation of lignin DMSO solutions provided valuable insights into the influence of concentration, thermal treatment, and temperature on solution viscosity, which are critical for optimising the electro-spinning process (17,233). The increase in viscosity with rising lignin concentration from 50 % (w/v) to 90 % (w/v) is primarily due to the greater amount of polymer present in solution, which promotes increased intermolecular interactions and chain entanglements. These effects are crucial for stabilising the electro-spinning jet and facilitating the formation of uniform, bead-free fibres (17,233).

The effect of thermal treatment was also evident, with refluxed 100% (w/v) lignin DMSO solutions showing an increase in viscosity with increasing reflux temperature from 80 °C to 160 °C. This increase suggests that higher reflux temperatures lead to greater chain entanglement and enhanced solution viscosity (237). Optimal electro-spinning performance was observed at solution viscosities; 2.88–3.80 Pa·s, for solutions refluxed at 120–140 °C, where sufficient chain entanglement stabilises the jet without excessive flow resistance (4,243).

Temperature-dependent viscosity ramp measurements further demonstrated a consistent decrease in viscosity with increasing temperature from 25 °C to 65 °C, reflecting enhanced molecular mobility and reduced chain interactions at elevated temperatures (247). This explains the

improved electro-spinning performance at 55 °C, where reduced viscosity allows for smoother jet formation and improved fibre morphology. The rheological data therefore highlights the importance of carefully tuning lignin concentration, solution temperature, and electro-spinning chamber temperature to achieve consistent, bead-free neat lignin fibre production.

4.3.2. Electrical conductivity of neat lignin in DMSO solutions

Conductivity measurements were conducted to evaluate the electrical properties of lignin DMSO solutions, which are important for understanding their behaviour during electro-spinning. Electro-spinning relies on the application of a high voltage to generate a charged jet from the polymer solution, and the conductivity of the solution directly influences the stability and formation of the jet (227). Higher solution conductivity improves the charge-carrying capacity of the electro-spinning fluid, enabling more efficient charge transfer and stronger electrostatic stretching forces during jet formation. This promotes jet elongation and thinning, resulting in finer, more uniform fibres and reduced bead formation (see Section 2.4.2) (461,499). In contrast, low conductivity limits charge mobility, weakening the stretching forces and often leading to bead defects or inconsistent fibre morphology due to insufficient jet stability (4,213,245).

The conductivity of lignin DMSO solutions was tested at room temperature (25 °C) and the electro-spinning temperature (55 °C) to investigate the effect of temperature and thermal treatment on solution conductivity. The conductivity values for the lignin/DMSO solutions were obtained by taking five individual measurements for each sample and reporting the averaged result to ensure accuracy and minimise experimental variability. The solutions tested were prepared from lignin that had been refluxed separately at different temperatures (80 °C, 100 °C, 120 °C, 140 °C, and 160 °C) to assess whether thermal treatment influences the solution conductivity of the resulting solutions.

The electrical conductivity of pure DMSO was measured over a range of temperatures from 25.4 °C to 79.4 °C to establish a baseline for comparison with lignin DMSO solutions, shown in Figure 66.

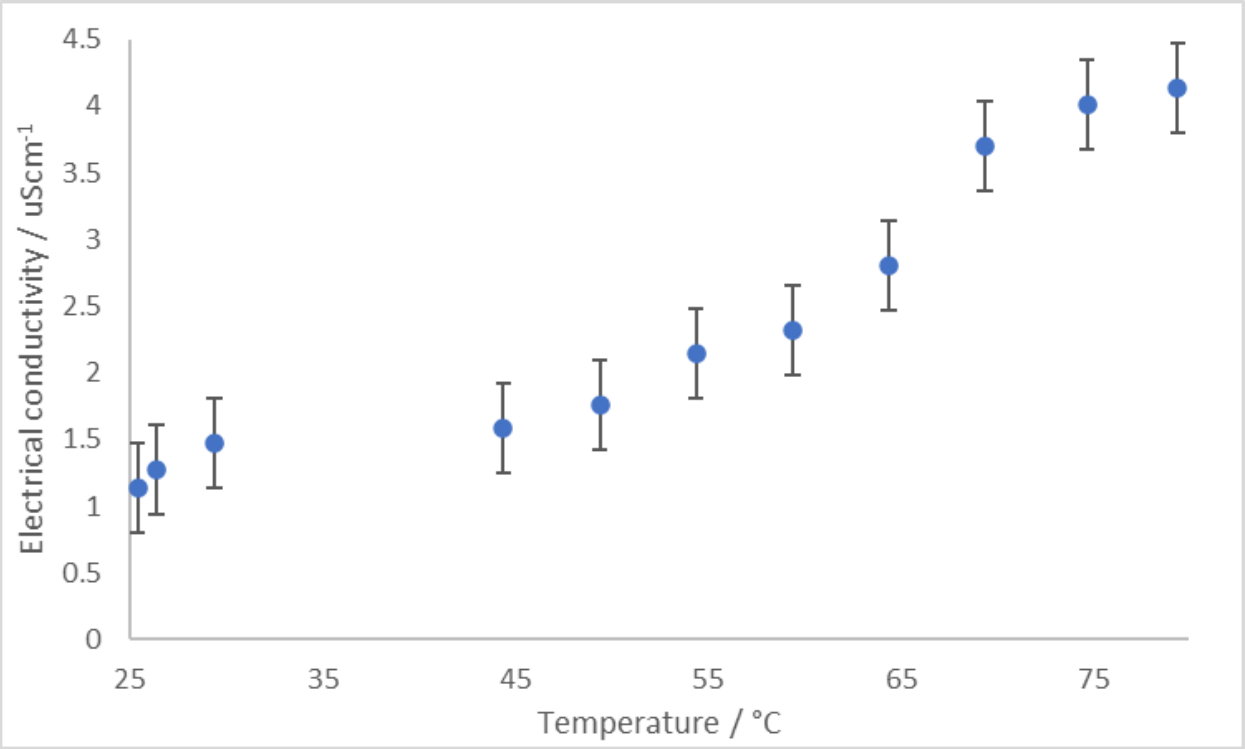

Figure 66. Electrical conductivity of pure DMSO measured from 25 °C to 79 °C.

The data shows a positive correlation between temperature and conductivity, with conductivity increasing progressively from 1.14 µS/cm at 25.4 °C to 4.14 µS/cm at 79.4 °C. This trend reflects the enhanced ionic mobility and reduced viscosity of DMSO at higher temperatures, which facilitate improved charge transport. The gradual increase in conductivity with temperature is consistent with the known behaviour of solvents, where thermal energy promotes the dissociation of ionic species and reduces intermolecular interactions, allowing for easier ion movement (219). A notable increase in conductivity is observed above 54.4 °C (2.15 µS/cm), which aligns with the reduction in viscosity at elevated temperatures (see Section 4.3.1).

This baseline data indicates that increasing the temperature of lignin DMSO solutions during electro-spinning is expected to similarly increase solution conductivity. The improved conductivity at higher temperatures would enhance the stretching and thinning of the charged polymer jet during electro-spinning, contributing to better fibre formation and reducing the likelihood of bead formation (see Section 2.4.2) (17,495). Consequently, the increase in conductivity with temperature observed in the lignin DMSO solutions can be partly attributed to the intrinsic temperature dependence of DMSO conductivity, as demonstrated by this control data (247).

The electrical conductivity of the refluxed lignin DMSO solutions was measured at both room temperature (25 °C) and the electro-spinning temperature (55 °C), as shown in Figure 67. The data reveals a notable difference in conductivity between the two temperatures, with all solutions exhibiting significantly higher conductivity at 55 °C compared to 25 °C.

At room temperature, the conductivity values ranged between 14.32 – 20.37 µS/cm, showing minimal variation across the refluxed samples. The slight increase observed at higher reflux temperatures (20.37 µS/cm for the 120 °C sample) suggests that thermal treatment may have marginally increased the ionic content or improved the dissociation of ionic species within the lignin structure, such as from phenolic groups (Aromatic-O^-) or carboxylic groups (COO^-) (500).

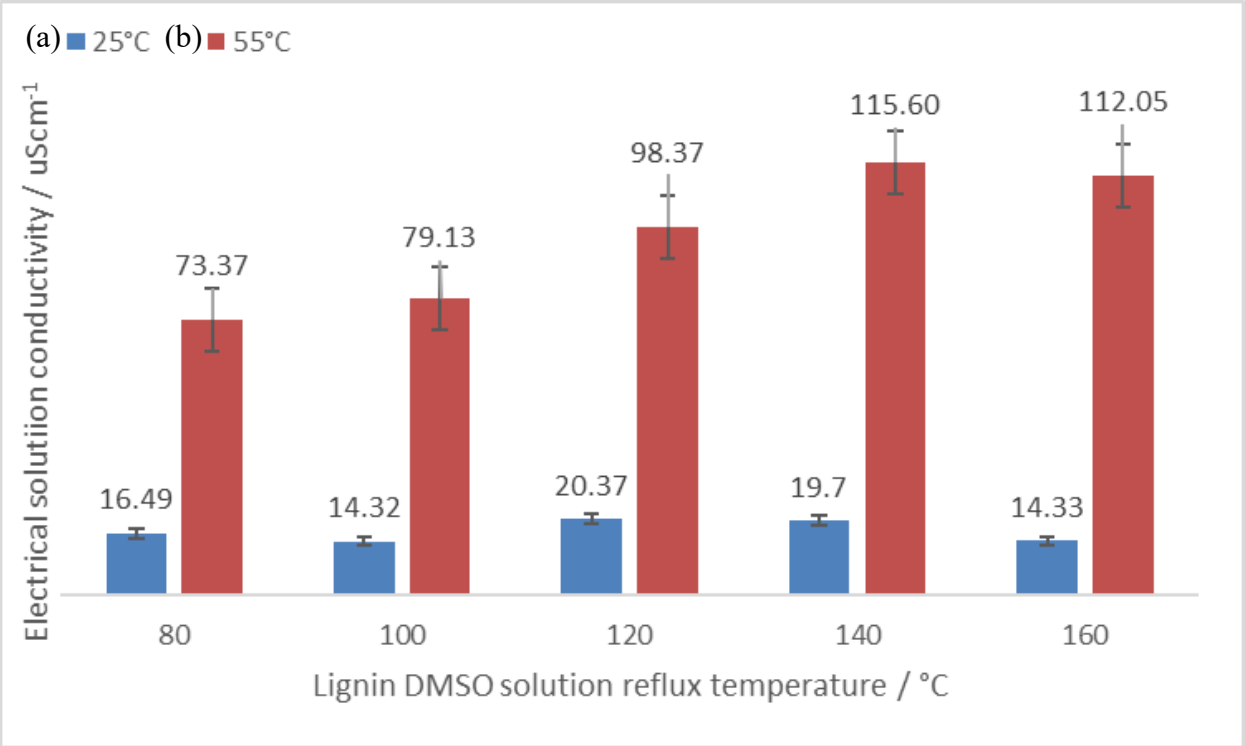

Figure 67. Electrical conductivity of refluxed lignin DMSO solutions at, (a): room temperature (25 °C) and (b): electro-spinning chamber temperature (55 °C).

This could result from thermally induced cleavage of ether linkages, shown in Figure 6, exposing more ionisable sites and increasing the availability of free anions (501). However, the differences at room temperature are relatively small, indicating that reflux temperature has a limited impact on solution conductivity under these conditions (212).

In contrast, the conductivity values at 55 °C were markedly higher, ranging between 73.37 – 115.60 µS/cm. The increase in conductivity with temperature is attributed to improved ionic mobility within the solution (474). Heating the solution reduced the solution shear viscosity (see

Section 4.3.1), facilitating better ion transport and increasing the overall conductivity (500,502). Notably, the 140 °C refluxed sample displayed the highest conductivity (115.60 µS/cm), suggesting that higher reflux temperatures may increase the availability of charged species in solution (219). The higher conductivity also corresponded to the 140 °C reflux lignin/DMSO solution producing the bead free aligned fibres from electro-spinning (see Figure 81). Interestingly, the conductivity for the 160 °C refluxed sample (112.05 µS/cm) was slightly lower than the 140 °C sample, despite following a similar trend. This could indicate structural changes or partial degradation of ionic components which occur at extreme reflux conditions, reducing the overall ion mobility (267).

The pronounced increase in conductivity at the elevated electro-spinning temperature is significant for the electro-spinning process (473). Higher conductivity is advantageous as it enhances the stretching and thinning of the charged polymer jet, promoting uniform fibre formation and reducing bead defects (see Section 2.4.2). The increase in conductivity, combined with reduced shear viscosity at the electro-spinning chamber temperature of 55 °C, aligns with the improved electro-spinning behaviour observed for these solutions. Overall, the results highlight that operating at an elevated electro-spinning temperature is essential for optimising solution conductivity, ensuring stable jet formation, and achieving consistent, bead-free lignin fibres.

4.4. Characterisation of electro-spun lignin fibres

Following electro-spinning, the resulting lignin fibres were characterised by SEM to evaluate morphology, and by FTIR and NMR spectroscopy to analyse chemical structure. Thermal properties were assessed using DSC and TGA.

4.4.1. Electro-spinning of neat lignin in DMSO

The investigation of lignin:PAN blends led to an exploration of the electro-spinning of neat lignin in DMSO, to evaluate its spinnability and the resulting fibre morphology. In contrast to PAN, which easily produces uniform fibres owing to its larger molecular weight and chain entanglements, lignin presents considerable difficulties for electro-spinning because of its amorphous, highly branched architecture and polydisperse molecular weight distribution (291,503). In lignin:PAN blends, PAN serves as a structural support, enhancing fibre formation and minimising defects like beading. In the absence of PAN, lignin's capacity to form continuous fibres is significantly affected by its solubility, solution viscosity, and conductivity (160,185).

DMSO was chosen as the solvent because of its strong solvating ability for lignin, which facilitates the dissolution of different lignin fractions while preserving an electro spinnable solution (229,425). The electro-spinning process of neat lignin poses challenges such as phase separation, solution instability, and increased beading (218,491). The stability of the electro-spinning jet is primarily affected by the limited polymer chain entanglement of lignin. Furthermore, the increased conductivity of lignin relative to PAN solutions may affect fibre formation by modifying charge distribution and jet dynamics (485).
Investigating the electro-spinning behaviour of neat lignin is essential for assessing its viability as an independent material for fibre production. The findings from these experiments can guide strategies for optimising processing conditions, including modifications to solution concentration, solvent selection, and electro-spinning parameters, to enhance fibre quality.

4.4.2. Electro-spinning bead-free neat lignin fibres in DMSO

After successfully electro-spinning smooth, bead-free fibres from lignin:PAN blends in/DMSO, attention was given to the electro-spinnability of neat lignin/DMSO solutions, gradually increasing the lignin concentration from 50 to 100% (w/v), of lignin in DMSO. The electro-spinning parameters included a feed rate of 0.5 mL/hour, a working distance of 13 cm, and an applied voltage of 13 kV. Initially, electro-spinning experiments were conducted at room temperature; however, the high viscosity of lignin/DMSO solutions led to needle clogging, preventing stable fibre formation. The high viscosity restricted the solution flow, causing intermittent jet formation and uneven deposition. To address this, experiments were conducted at an elevated temperature of 55 °C, similar to the conditions used for lignin:PAN solutions in DMSO solvent. Partial electro-spinning was achieved in the heated chamber, improving solution flow and jet stability. As a result, it was decided that all future experiments would be carried out at the electro-spinning chamber temperature 55 °C to ensure consistent fibre formation.
At the outset, attempts to electro-spin bead-free neat lignin fibres were unsuccessful from 50 to 70% (w/v) in DMSO. Fibres electro-spun from the 50% (w/v) solution exhibited a bead-on-string structure as seen in Figure 68.

Although electro-spinning at 50% (w/v) lignin in DMSO produced beaded fibres, the lignin content was increased to 75% (w/v) to maximise lignin loading in the solution. Higher lignin concentrations are desirable to enhance fibre yield and reduce the need for synthetic polymer additives while maintaining electro-spinnability. At 75% (w/v) lignin in DMSO, electro-spinning successfully produced smooth, bead-free fibres with uniform morphology, as seen in Figure 69.

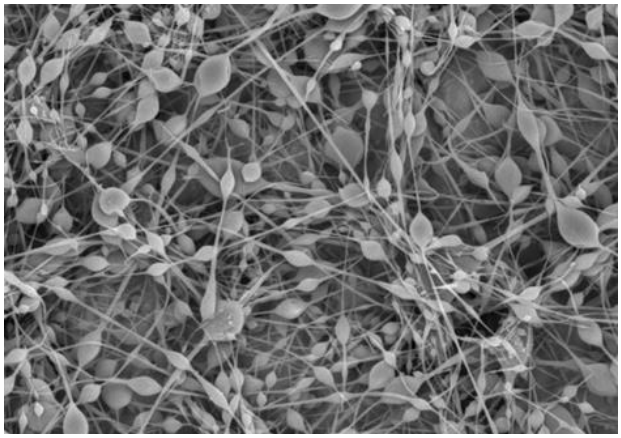

Figure 68. SEM micrograph of 50% (w/v) electro-spun bead on string lignin fibres.

Figure 70 displays magnified micrographs of the unfused, randomly oriented bead-free fibres in DMSO at a concentration of total lignin polymer of 75% (w/v). For the first time, electro-spinning of vacuum-dried neat lignin was performed in a repeatable manner utilising simply DMSO as the solvent. The 75% (w/v) lignin concentration provided an optimal balance between viscosity and electro-spinnability (see Section 4.3.1), allowing for stable jet formation and repeatable fibre production.

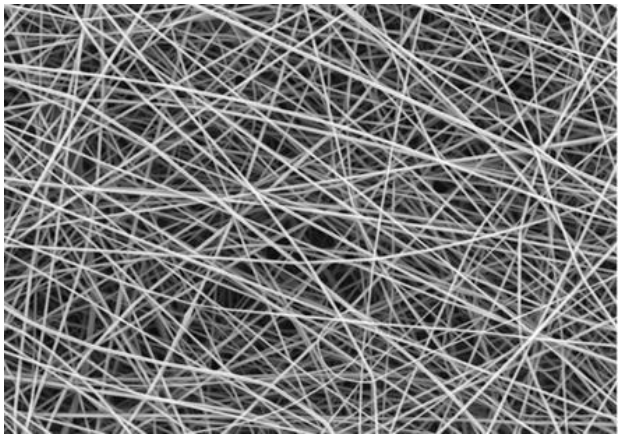

Figure 69. SEM micrographs for bead-free electro-spun 75% (w/v) neat lignin fibres.

This is significant since lignin typically requires a polymer blend, like PAN, or a binary solvent, like acetone/DMSO, to be appropriate for electro-spinning (204). Blending lignin with polymers like PAN and PVP can be disadvantageous leading to phase separation, which can occur due to lignin's immiscibility with synthetic polymers, affecting fibre uniformity. In addition, differences in solubility and viscosity hinder preparation of uniform solutions, leading to fibre defects during electro-spinning (236,239). The lignin/DMSO solution was prepared by heating and mixing vacuum dried as-received lignin in DMSO solution with constant stirring. The 75% (w/v) air-circulating oven heat treated lignin (120 °C for 2 hours) DMSO solution electro-spun fibres had an average fibre diameter of 830 nm.

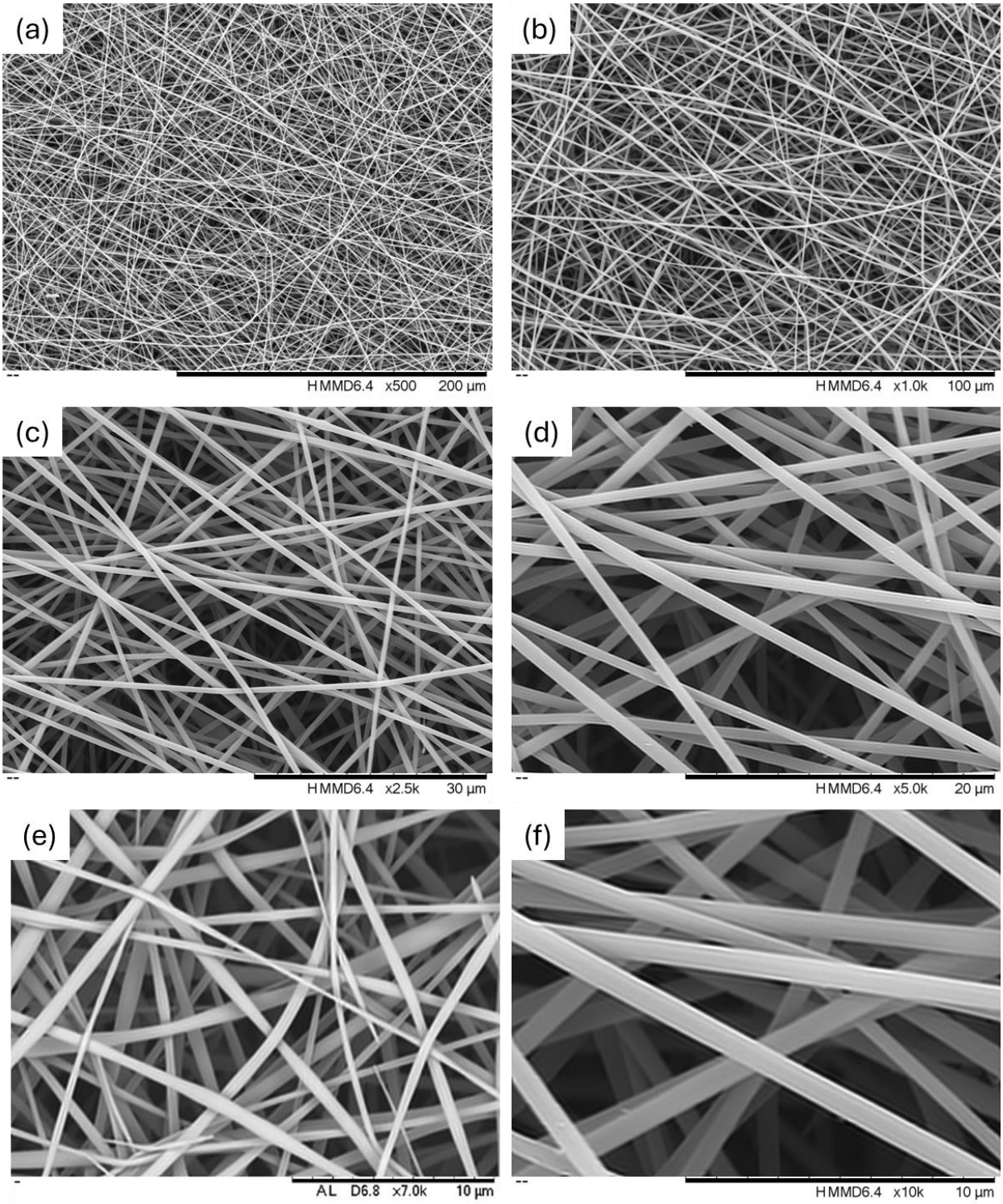

Figure 70.Magnified SEM images of electro-spun lignin fibres produced using 75% (w/v) vacuum dried lignin in DMSO polymer solution; from left to right: (a): x500, (b): x1000, (c): x2500, (d): x5000, (e): x7000 and (f): x10000 magnifications.

4.4.3. Neat lignin electro-spun fibre alignment using 75% (w/v) in DMSO solution

Endeavours were made to align fibres electro-spun from 75% (w/v) lignin in DMSO using both parallel electrode configurations and a custom-made PTFE Vee-shield. Electro-spinning was conducted with parallel electrodes spaced at 4 cm and 8 cm to create an electric field that would encourage fibre alignment. The parallel electrode method utilises a pair of grounded metallic electrodes with an air gap between them, which modifies the electric field distribution. This alteration in the field causes the polymer jet to oscillate between the electrodes, facilitating fibre alignment. Additionally, the residual charge on the suspended fibres plays a role in repelling newly arriving charged fibres, further contributing to their organised deposition (241,504). However, while some degree of orientation was observed, fibre deposition remained largely random due to disturbances in the electro-spinning jet. In contrast, the PTFE Vee-shield proved to be the most effective method, as its geometry concentrated the electric field, guiding fibre deposition along a more controlled path. This resulted in improved fibre alignment, demonstrating that the Vee-shield design effectively enhanced the uniformity and directionality of the neat electro-spun lignin fibres.

4.4.3.1. Fibre alignment using 4 cm parallel electrode

Attempts to align fibres using the 4 cm parallel electrode configuration were unsuccessful, resulting in randomly deposited fibres rather than a well-ordered structure. As seen in the attached SEM micrographs, see Figure 71, the fibres exhibit a highly entangled, non-uniform arrangement with no clear directional alignment.

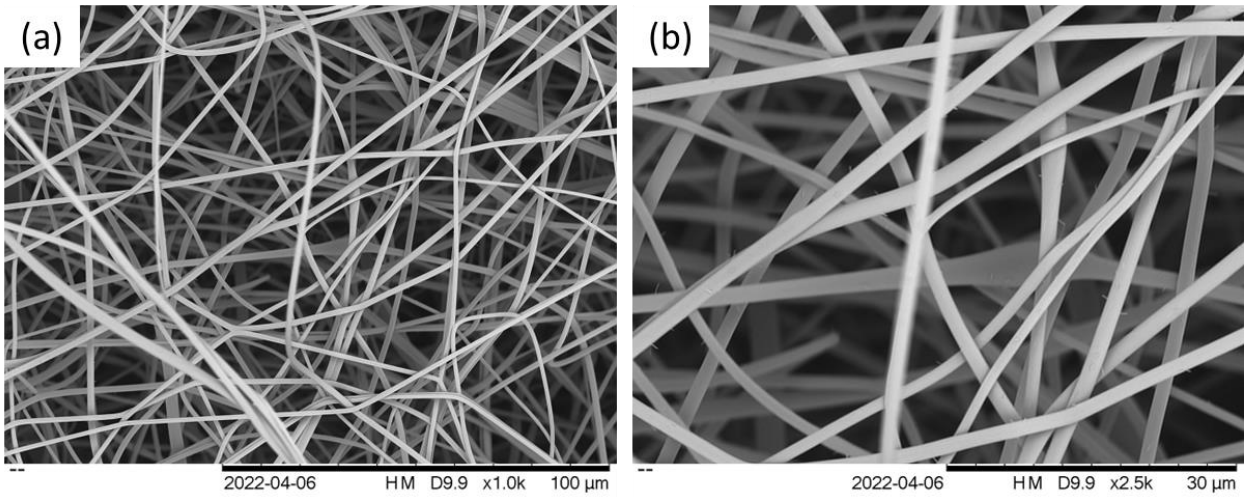

Figure 71. SEM micrographs for 75% (w/v) lignin in DMSO electro-spun aligned fibres using 4cm parallel electrode for magnifications; (a): x1000 and (b): x2500.

For electro-spun 75% (w/v) lignin/DMSO fibres aligned using a parallel electrode configuration with a 4 cm gap, the average fibre diameter was 1340 nm. The degree of fibre alignment, as measured by the angular deviation of fibres from the preferred orientation, showed a predominance of misaligned fibres, indicating that this setup did not effectively guide fibre deposition, fibre alignment shown in Table 19.

Only 3% of fibres were highly aligned, falling within the <1° deviation range, while no fibres were recorded within the 1–2° range, highlighting the inefficiency of this method in producing well-oriented fibres. A small fraction of fibres (4%) exhibited deviations between 2–3°, with a further 3% falling within the 3–5° range, suggesting that only a minor proportion of fibres achieved a level of alignment. Additionally, 5% of fibres deviated between 5–10°, and 10% were within the 10–20° range, showing some degree of orientation but still far from optimal alignment. The majority of fibres displayed significant misalignment, with 39% deviating between 20–45° and 36% exceeding 45°, highlighting a largely random fibre deposition pattern. This lack of alignment suggests that the 4 cm gap between the parallel electrodes did not generate a sufficiently strong or focused electric field to guide fibre orientation effectively. The broad angular distribution indicates jet instability and poor field focusing, leading to unpredictable fibre placement and reduced control over the electro-spinning process.

The chaotic distribution suggests that the electric field created by the 4 cm electrode spacing was insufficient to guide fibre deposition in a controlled manner. As a result, the fibres were deposited they settled in an unpredictable fashion, likely due to instabilities in the electro-spinning jet and the lack of a strong enough alignment force during electro-spinning. This outcome highlights the limitations of using closely spaced parallel electrodes for fibre orientation and suggests the need for alternative alignment strategies.

4.4.3.2. Fibre alignment using 8 cm parallel electrode

When using the 8 cm parallel electrode configuration, fibre alignment improved compared to the 4 cm setup, with more fibres orienting in a preferred direction. However, as seen in the SEM micrographs, shown in Figure 72, fibre deposition was significantly reduced, likely due to weaker electrostatic forces over the wider electrode spacing (505).

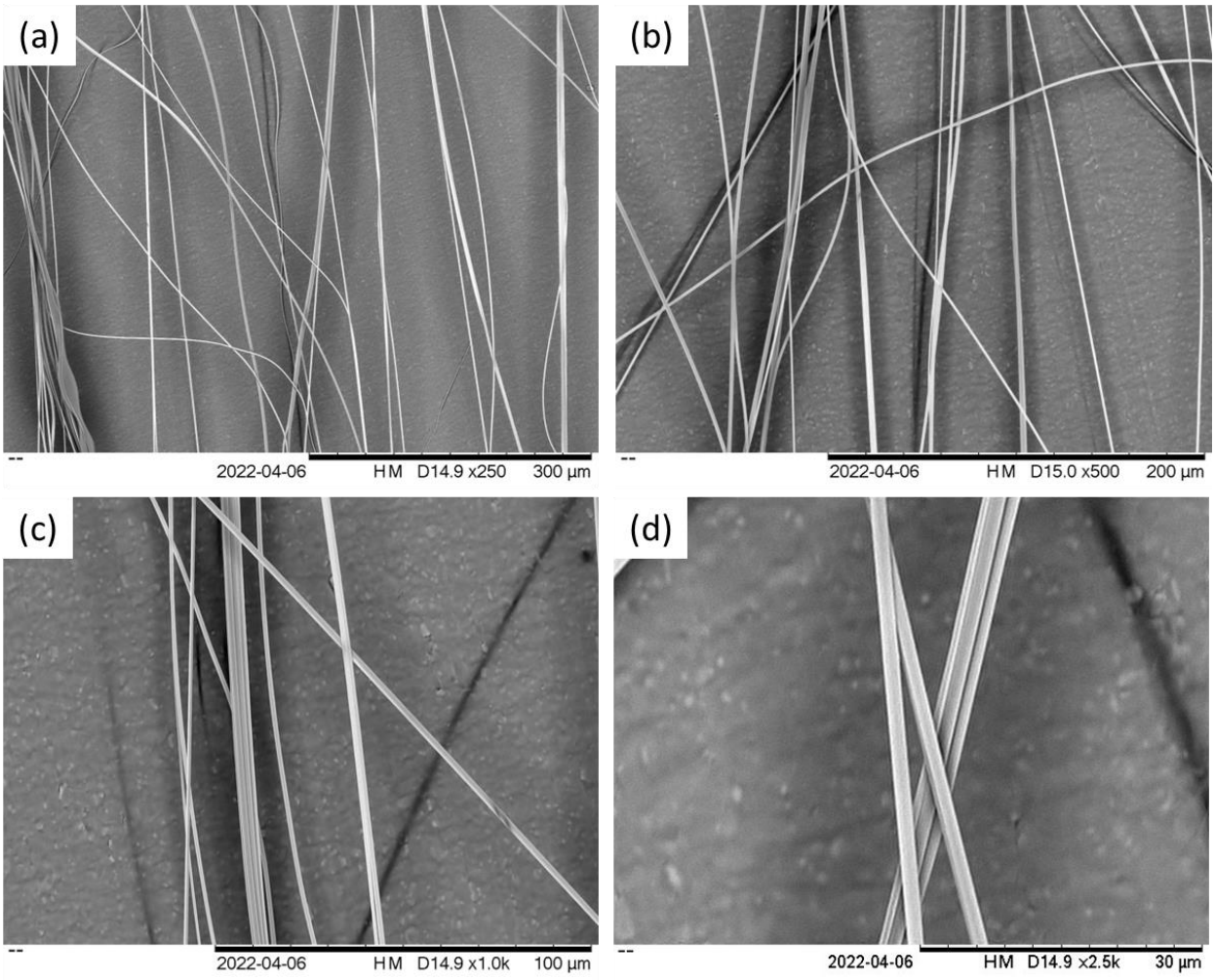

Figure 72. SEM micrographs for 75% (w/v) lignin in DMSO electro-spun aligned fibres using 8cm parallel electrode for magnifications; (a): x250, (b): x500, (c): x1000 and (d): 2500.

For electro-spun 75% (w/v) lignin/DMSO fibres aligned using a parallel electrode configuration with an 8 cm gap, the average fibre diameter was 1650 nm, slightly larger than the fibres produced with the 4 cm gap. The degree of fibre alignment showed a shift towards improved orientation compared to the 4 cm configuration, though a significant proportion of fibres still exhibited misalignment, as seen in Table 19.

No fibres were recorded within the <1° range, indicating that perfect alignment was not achieved. However, 8% of fibres fell within both the 1–2° and 2–3° deviation ranges, suggesting

that some fibres were more successfully oriented than with the 4 cm gap. Additionally, 4% of fibres deviated between 3–5°, while a larger proportion (32%) exhibited deviations between 5–10°, indicating an intermediate level of alignment. A further 12% of fibres fell within the 10–20° range, showing continued improvement in orientation.

Despite these enhancements, 36% of fibres deviated between 20–45°, demonstrating persistent misalignment, though notably, no fibres exceeded 45°, marking an improvement over the 4 cm configuration. The absence of fibres in the >45° range suggests that the increased electrode spacing provided better electrostatic guidance, reducing extreme misalignment. However, the overall spread of fibre orientation indicates that while the 8 cm parallel electrode gap improved fibre alignment, it was still insufficient for achieving highly ordered fibre deposition, likely due to continued jet instability and uneven electric field distribution.

Additionally, many fibres appeared fragile and exhibited breakage, suggesting that the increased alignment came at the cost of mechanical integrity. These observations suggest that although increasing electrode spacing can enhance fibre alignment, it may also compromise fibre quality and deposition efficiency, due to the fibres having a relatively low failure strain, making them more prone to breakage or instability during deposition (170).

4.4.3.3. Fibre alignment using PTFE Vee-shield

The use of the PTFE Vee-shield vastly improved fibre alignment and deposition compared to the parallel electrode configurations. As observed in the SEM micrographs, shown in Figure 73, the fibres exhibited a higher degree of orientation, with significantly reduced randomness in their arrangement.

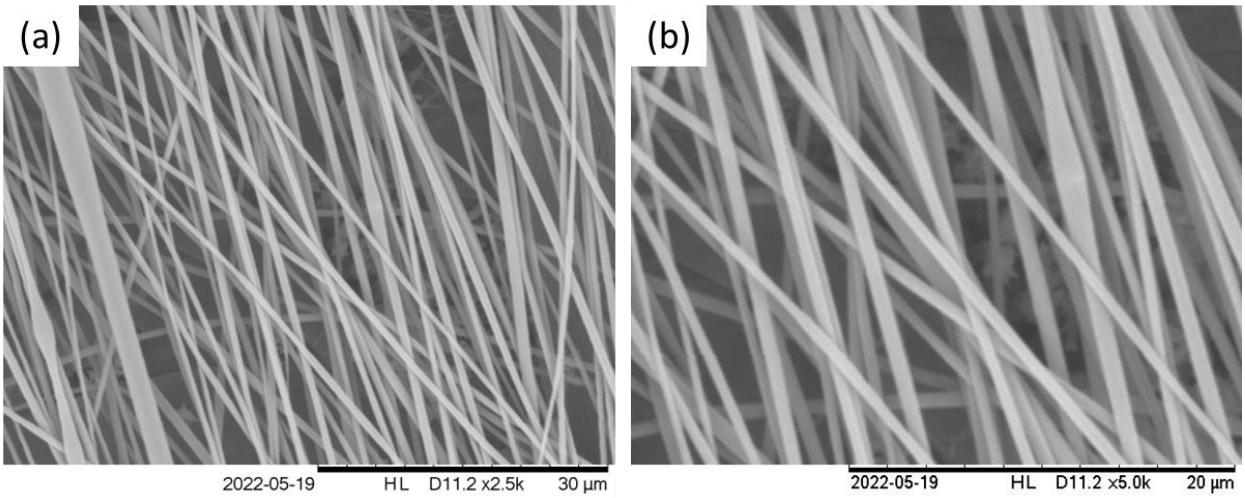

Figure 73. SEM micrographs for 75% (w/v) lignin in DMSO electro-spun aligned fibres using Vee-shield, for magnifications; (a): x2500 and (b): x5000.

For electro-spun 75% (w/v) lignin/DMSO fibres aligned using the PTFE Vee-shield with a 1 cm substrate fibre collector gap, the average fibre diameter was 755 nm, significantly smaller than fibres produced with parallel electrode configurations. The alignment results demonstrated substantial improvement, with a larger proportion of fibres falling within lower deviation angles, indicating a more controlled and directed deposition, as seen in Table 19.

A notable observation was that 8% of fibres exhibited near-perfect alignment (<1° deviation), marking a significant advancement over the parallel electrode setups. Additionally, 4% of fibres were deposited within the 1–2° range, while another 8% were within 2–3°, highlighting a greater concentration of highly aligned fibres. The proportion of fibres deviating between 3–5° was 7%, followed by a dominant 33% within the 5–10° range, indicating strong fibre orientation.

Further assessment showed that 22% of fibres deviated between 10–20°, while 18% fell within the 20–45° range. Importantly, no fibres were recorded with deviations exceeding 45°, confirming that the PTFE Vee-shield effectively minimised extreme misalignment. Compared to the parallel electrode setups, the Vee-shield generated superior alignment due to its ability to concentrate the electric field along a more controlled path, improving the uniformity of fibre deposition (19). The significantly reduced fibre diameter also suggests that the Vee-shield setup facilitated more stable jet elongation, contributing to the production of smoother, more uniform fibres.

Table 19. Fibre alignment percentage for 75% (w/v) neat lignin in DMSO electro-spun aligned fibres using 4 cm electrode, 8 cm electrode and 1 cm Vee-shield.

Fibre alignment (%)	**<1°**	**1°-2°**	**2°-3°**	**3°-5°**	**5°-10°**	**10°-20°**	**20°-45°**	**>45°**
4 cm electrode	3	0	4	3	5	10	39	36
8 cm electrode	0	8	8	4	32	12	36	0
1 cm Vee-shield	8	4	8	7	33	22	18	0

Fibre alignment percentage for 75% (w/v) neat lignin in DMSO electro-spun fibres under different collector configurations, parallel electrodes and Vee-shield, is shown in Figure 74.

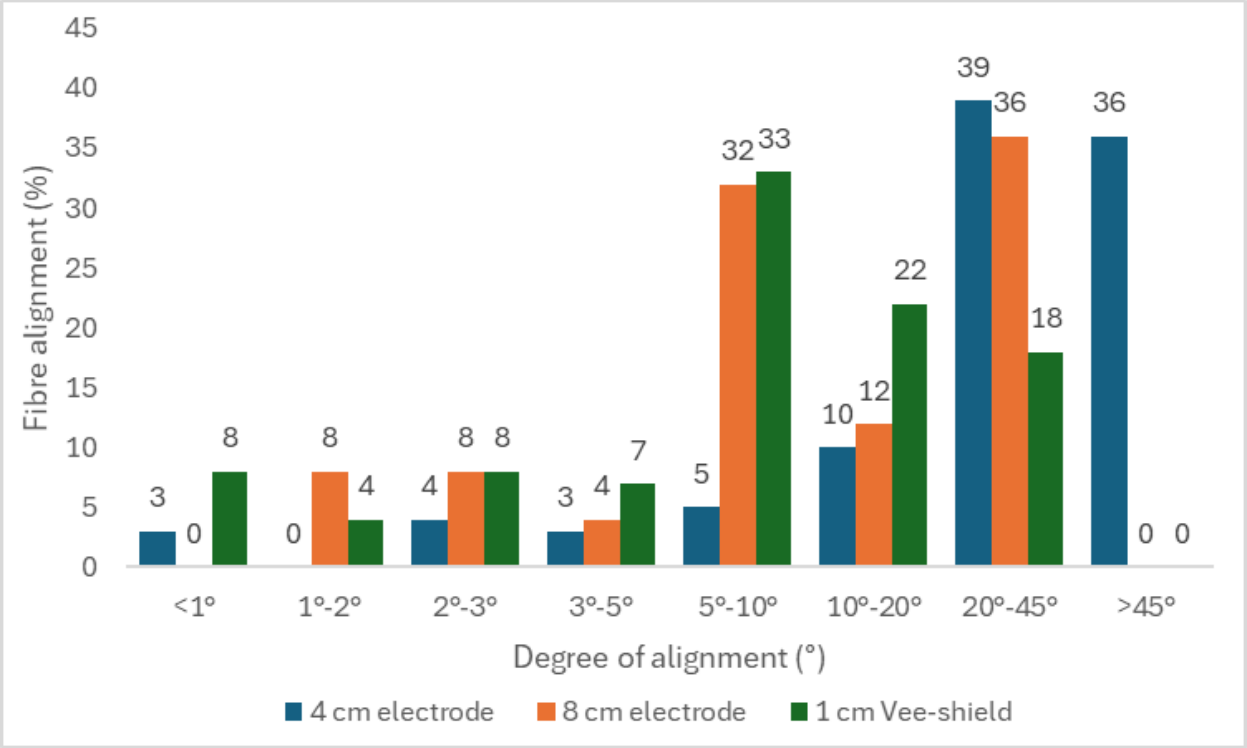

Figure 74. Fibre alignment distribution (%) for electro-spun 75% (w/v) neat lignin in DMSO using three collector setups: 4 cm electrode, 8 cm electrode, and 1 cm Vee-shield.

The fibre deposition was notably improved by using Vee-shield collector, with a denser and more uniform fibre mat forming on the collector. The fibres appeared smooth and continuous, indicating improved jet stability during electro-spinning. This suggests that the Vee-shield provided the optimal conditions for producing well-aligned, high-quality lignin fibres, in comparison to the parallel electrode alignment method.

4.4.4. Optimisation of 100% (w/v) lignin/DMSO solutions for electro-spinning

When increasing the lignin polymer weight in DMSO above 75% (w/v), beaded and fused fibres were observed via SEM analysis. However, at 80% (w/v), beaded fibres formed instead of uniform fibres. By gradually increasing the lignin concentration to 95% (w/v) in DMSO, a significant reduction in fibre beading was observed, as seen in Figure 75, indicating improved electro-spinnability.

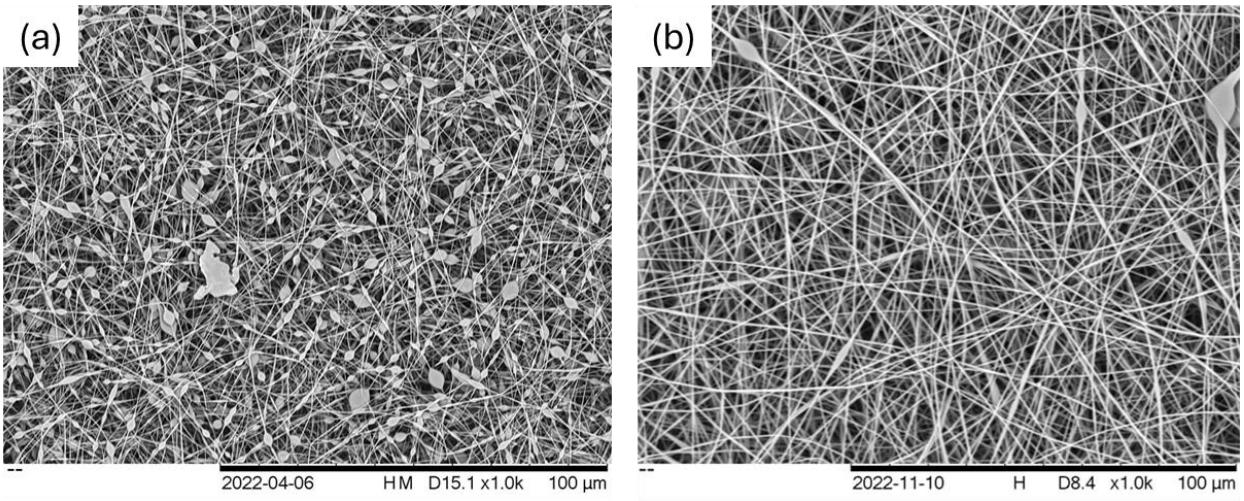

Figure 75. SEM micrographs for, (a): beaded electro-spun 80% (w/v) lignin fibres in DMSO & (b): reduced beaded electro-spun 95% (w/v) lignin fibres in DMSO.

At 80% (w/v) lignin concentration in DMSO, the average fibre diameter of the electro-spun fibres was relatively small at 280 nm. However, this was likely influenced by the presence of a large number of beads, which had an average bead diameter of 1488 nm. The high occurrence of beading suggests that the electro-spinning jet was unstable, leading to thinner fibres alongside the formation of large droplets (see Section 2.4.2). In contrast, at 95% (w/v), where bead formation was significantly reduced, the average fibre diameter increased to 550 nm, while the average bead diameter was reduced to 1264 nm, indicating a more uniform and stable jet during electro-spinning with improved fibre formation with fewer and smaller beads. For comparison, at 75% (w/v), where only minimal beading was observed, the average fibre diameter was 830 nm, demonstrating that a reduction in bead formation correlated with an increase in fibre diameter due to improved solution spinnability and chain entanglement. Evidence for the solution shear viscosity is presented in Section 4.3.1 and solution electrical conductivity in Section 4.3.2.

Whilst, at concentrations above 100% (w/v), electro-spraying occurred with limited fibre formation due to the high solution viscosity, making it unsuitable for electro-spinning. The ideal polymer concentration was determined to be 100% (w/v) neat lignin in DMSO.

At 100% (w/v) lignin in DMSO, most of the beading was eliminated, resulting in significantly improved fibre uniformity. However, some inconsistencies in fibre formation remained, prompting the decision to further optimise the solution through thermal treatment. In contrast to lower concentrations, where insufficient polymer interactions led to capillary breakup and bead formation, the higher lignin content provided the necessary viscoelastic properties for smooth jet

elongation and fibre deposition, limiting bead formation (246,251). The thermal processing step further enhanced solubility and ensured uniform solution properties, preventing premature jet breakup and improving fibre morphology. The presence of beads within the fibre structure can notably compromise the mechanical integrity and functional performance of the resulting fibre mat, serving as locations of structural weakness and defects (245). Optimising electro-spinning parameters is essential to mitigate this issue and achieve a uniform, bead-free fibre morphology (506).

At 100% (w/v) lignin in DMSO, electro-spinning was initially carried out at room temperature (25 °C) and then at an elevated chamber temperature of 55°C. The application of heat during electro-spinning significantly improved fibre formation, reducing bead defects and promoting more uniform fibre morphology, as seen in Figure 76.

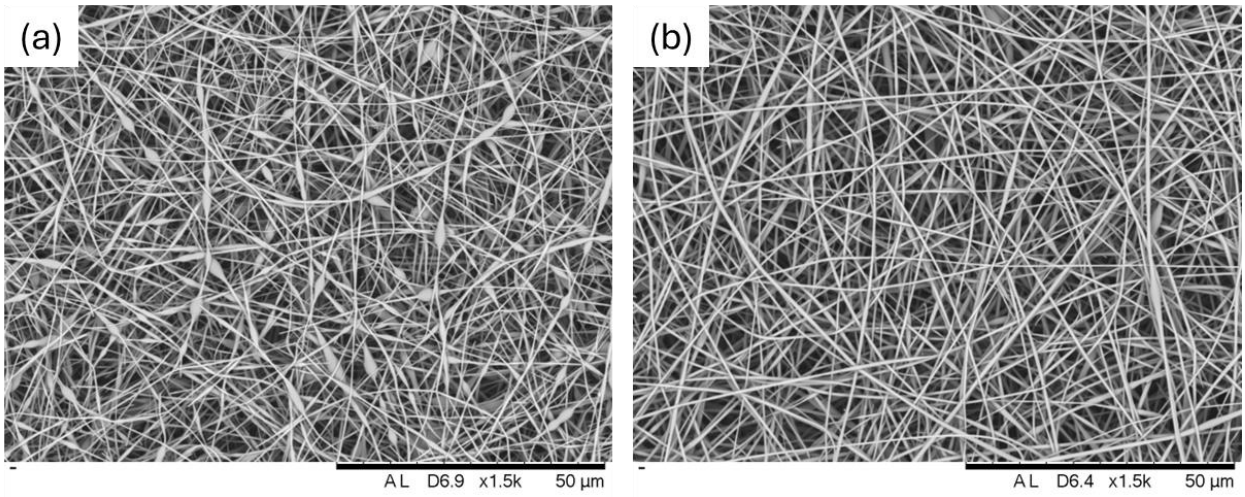

Figure 76. SEM micrographs for 100% (w/v) lignin in DMSO electro-spun fibres for chamber temperatures, (a): 25 °C & (b): 55 °C.

For electro-spun fibres produced from the 100% (w/v) lignin/DMSO solution at a room temperature (25 °C) electro-spinning chamber, the average fibre diameter was 528 nm, with a high degree of beading observed, 10 beads per 50 µm², with an average bead diameter of 1800 nm. However, when electro-spinning was conducted in a heated electro-spinning chamber at 55 °C, the fibre diameter slightly decreased to 510 nm, but with significantly fewer beads, only 6 beads per 50 µm², and a much smaller average bead diameter of 1116 nm.

The reduction in beading and bead size in the heated chamber is likely due to improved solution homogeneity, faster solvent evaporation and reduced surface tension (473). At elevated temperatures, the viscosity of the lignin/DMSO solution was reduced (see Section 4.3.1),

enhancing jet stability and reducing droplet formation. However, the slight decrease in fibre diameter suggests that the stretching forces acting on the jet were enhanced at the higher temperature, leading to finer fibre formation (422,492).

The increased chamber temperature lowered the solution viscosity, enhancing jet stability and fibre elongation. Given the positive effect of heat on electro-spinnability, further investigation into thermal treatment was pursued using reflux processing. This approach aimed to improve lignin solubility and solution homogeneity, ensuring consistent fibre formation at high concentrations.

At 80% (w/v) lignin in DMSO, electro-spinning resulted in beaded fibres rather than smooth, continuous fibres. When the concentration was further increased beyond 90% (w/v), electro-spraying became the dominant process, with limited fibre formation due to the excessively high viscosity of the solution. The increased viscosity restricted stable jet formation, preventing the elongation and thinning necessary for fibre production, making these concentrations unsuitable for electro-spinning (507).

To overcome this limitation and increase lignin solubility in DMSO, the subsequent lignin/DMSO solutions were heated at 120 °C prior to electro-spinning. Heating was intended to reduce solution shear viscosity and enhance the electro-spinnability of high-concentration lignin solutions. The initial dissolution of lignin at 100% (w/v) in DMSO was performed on a magnetic stirrer hotplate, ensuring a homogeneous solution. To further improve spinnability, the solution was then heated in an air-circulating oven at 120 °C for 2 hours while covered with aluminium foil to minimize solvent loss. Electro-spinning was carried out immediately after heating, when the viscosity was expected to be lower. Additionally, the electro-spinning chamber was maintained at 55 °C to sustain improved solution flow and jet stability during the electro-spinning process.

The micrographs in Figure 76, illustrate that heating the 100% (w/v) lignin/DMSO solution (at 120 °C for 2 hours) prior to electro-spinning resulted in the successful formation of smooth, mostly bead-free neat lignin fibres. To further investigate the effect of thermal treatment on lignin solubility and fibre formation, a series of controlled experiments were conducted. Lignin was dissolved in DMSO under reflux in a nitrogen atmosphere at temperatures of 80, 100, 120, 140, and 160 °C for 4 hours. Nitrogen gas agitation was introduced during reflux primarily to create an inert atmosphere and prevent unwanted oxidative degradation of lignin at elevated

temperatures and to minimise any interactions with atmospheric moisture (405). Lignin contains phenolic and aliphatic hydroxyl groups, which can undergo oxidation when exposed to air, potentially leading to structural changes that affect solubility and electro-spinnability (508). The solutions were then electro-spun, and the resulting fibres were characterised to assess morphological differences. Further characterisation, including viscosity and electrical conductivity, would provide deeper insight into the influence of thermal treatment on lignin's electro-spinning behaviour.

4.4.5. Electro-spinning of reflux heat treated 100% (w/v) neat lignin in DMSO solutions

Reflux heat treatment was introduced to further enhance the electro-spinnability of 100% (w/v) lignin in DMSO solutions by improving their solubility and reducing solution viscosity, enabling electro-spinning of a higher polymer concentration of neat lignin from 75% (w/v) to 100% (w/v) in DMSO. By subjecting the lignin/DMSO solution to reflux under controlled temperatures (80, 100, 120, 140, and 160 °C for 4 hours), the aim was to modify the solution properties to enable the formation of uniform, bead-free fibres during electro-spinning. The electro-spun fibres obtained from the reflux-treated solutions were analysed to assess the impact of heat treatment on fibre morphology, alignment, and uniformity.

The SEM micrographs reveal a clear trend in fibre morphology as a function of reflux heat treatment temperature. Beading was prevalent in fibres electro-spun from solutions treated at 80 °C and 100 °C, indicating insufficient modification of the lignin/DMSO solution properties at these temperatures, seen in Figure 77.

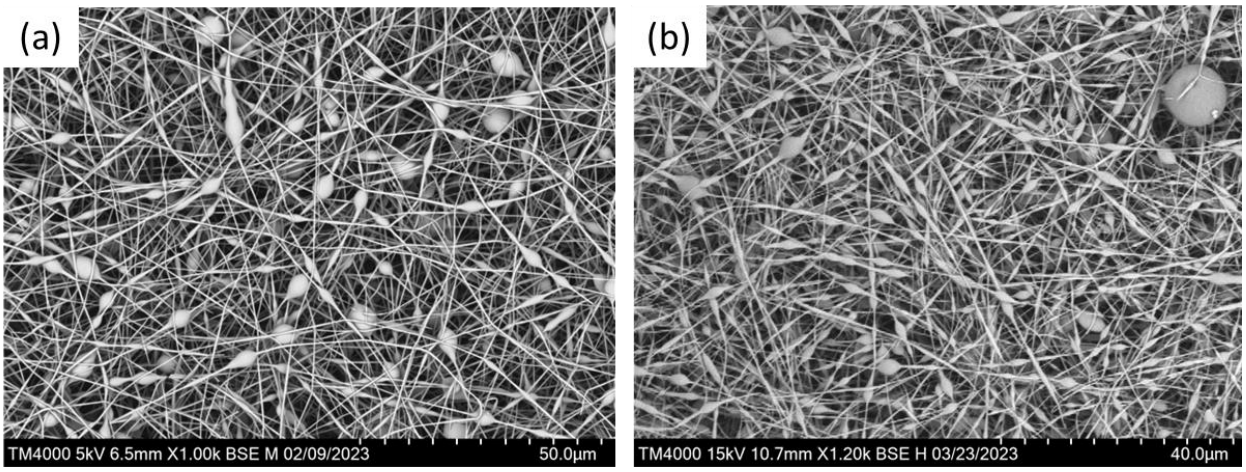

Figure 77. SEM micrographs for 100% (w/v) lignin in DMSO electro-spun fibres from reflux temperatures; (a): 80 °C and (b): 100 °C.

The number of beads observed in the electro-spun fibres from the 100% (w/v) lignin/DMSO solution decreased as the reflux temperature increased from 80 °C to 100 °C. At 80 °C, an

average of 40 beads per 50 µm² was recorded, which reduced to 35 beads per 50 µm² at 100 °C, indicating a decline in bead formation with increased reflux temperature.

Additionally, a noticeable reduction in bead diameter was observed. At 80 °C, the average bead diameter measured 2320 nm, whereas at 100 °C, the bead size significantly decreased to 1126 nm. This suggests that higher reflux temperatures contributed to a more uniform solution, likely reducing phase separation and minimising bead formation. Alongside these changes, the fibre diameter also decreased with increasing reflux temperature. At 80 °C, the average fibre diameter was 416 nm, which reduced to 269 nm at 100 °C. This reduction in fibre size indicates that higher reflux temperatures improved solution homogeneity, leading to finer, more uniform fibres and a noticeable reduction in beading (478,509). The 80 °C reflux solution, had a solution shear viscosity of 1.35 Pa.s and a solution electrical conductivity of 73.37 $uScm^{-1}$.

However, despite this improvement in fibre production, 100 °C was still not the optimal temperature for pre-treating the lignin solutions, as beading was still present, and the electro-spinning jet remained inconsistent, electro-spraying after 5 minutes. This was evident from the SEM micrographs, where large droplets were observed in the 100 °C sample (top right of image (b) from Figure 77), indicating that the solution shear viscosity (1.78 Pa.s) and solution electrical conductivity (79.13 $uScm^{-1}$) were still insufficient for stable fibre formation.

At 120 °C, beading was significantly reduced, suggesting that higher thermal processing facilitated better dissolution. Although the fibres here were broken and ribbon like, indicating that the electro-spinning solution still required optimisation to improve fibre morphology, as seen in Figure 78.

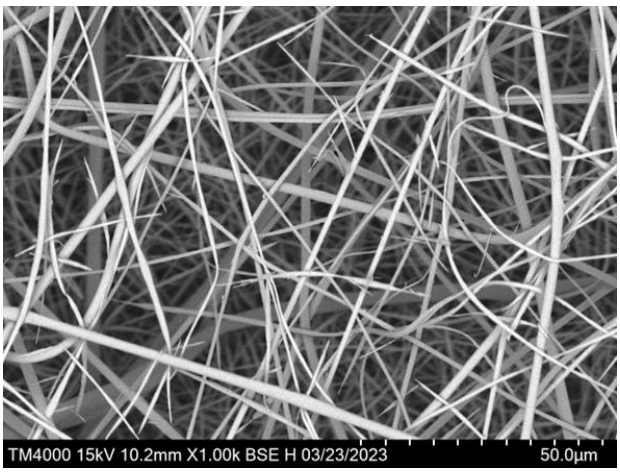

Figure 78. SEM micrograph for 100% (w/v) lignin in DMSO electro-spun fibres from reflux temperature 120 °C; magnification, x1000.

At a reflux temperature of 120 °C, the electro-spun fibres exhibited an average fibre diameter of 1094 nm with relatively few beads (8 beads per 50 µm²), marking a significant reduction in beading compared to the fibres produced at 80 °C and 100 °C (see Figure 77). The bead diameter at this temperature measured 1467 nm, showing a slight increase from the 100 °C solution but still lower than that of the 80 °C fibres.

However, despite the reduction in beading, the fibre morphology was highly inconsistent. The fibres were ribbon-like, broken, and unevenly distributed, leading to weak, fragmented structures. This irregularity in fibre formation suggests that while the 120 °C reflux treatment improved the solution properties (2.88 Pa.s solution shear viscosity and solution electrical conductivity 98.37 $uScm^{-1}$) to reduce beading, it was not sufficient to produce continuous, uniform fibres. Due to these structural weaknesses, further increasing the reflux temperature to 140 °C and 160 °C was necessary to improve fibre continuity, alignment, and mechanical integrity while maintaining the benefits of reduced bead formation.

At 140 °C and 160 °C, beading was eliminated, and smooth, uniform fibres were obtained at 100% (w/v) lignin in DMSO, as shown in see Figure 79. This can be attributed to enhanced reflux temperature, which further improved lignin solubility and the lignin/DMSO solution electro-spinning process. Though broken fibres were still observed at both the 140 °C and 160 °C reflux temperatures. The 140 °C reflux solution, had a solution shear viscosity of 3.80 Pa.s and a solution electrical conductivity of 115.60 $uScm^{-1}$. Whilst the 160 °C reflux solution, had a solution shear viscosity of 4.24 Pa.s and a solution electrical conductivity of 112.05 $uScm^{-1}$.

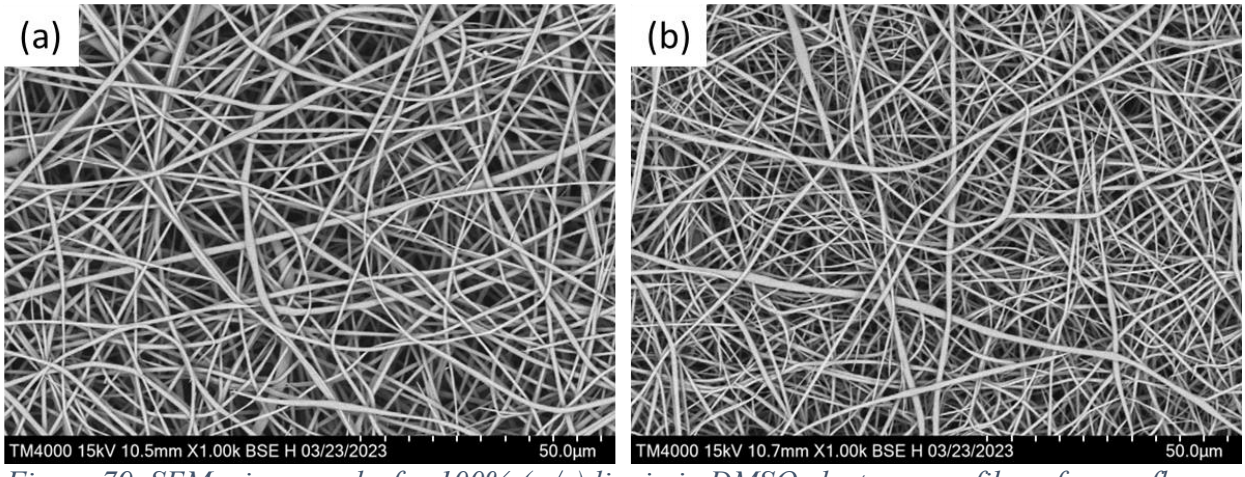

Figure 79. SEM micrographs for 100% (w/v) lignin in DMSO electro-spun fibres from reflux temperatures; (a): 140 °C and (b): 160 °C.

At 100% (w/v) lignin in DMSO, smooth and uniform fibres were produced at both 140 °C and 160 °C. This outcome reflects the positive influence of the heat treatment, as it allowed for a

more consistent fibre formation. The reduction in fibre defects and beading is a clear sign that higher temperatures contributed to better solution viscosity and electrostatic properties. Additionally, there was a noticeable reduction in the fibre diameter from 839 nm at 140 °C to 620 nm at 160 °C. This suggests that the higher reflux temperature, applied during solution preparation, reduced viscosity and improved polymer solubility, enabling the formation of thinner fibres during electro-spinning at 55 °C. Typically, lower viscosity allows for finer fibres due to easier jet thinning during electro-spinning (492). The reduced number of broken fibres at both 140 °C and 160 °C further highlights the positive effect of the heat treatment. The improved fibre stability at these temperatures is likely due to enhanced molecular alignment following heat treatment and improved lignin/DMSO solvent–polymer interactions (see Section 2.3.2), resulting in fewer defects during the electro-spinning process.

Overall, the reflux heat treatment from 80 °C to 160 °C positively influenced the electro-spinning of lignin by improving the solution's properties. This resulted in smoother, more uniform fibres with fewer defects and a smaller fibre diameter. The heat treatment facilitated a better balance between solvent evaporation and fibre formation, making it possible to obtain high-quality fibres at higher lignin concentrations (100% (w/v)).

Additionally, potential cross-linking or structural modifications at these elevated temperatures may have contributed to improved fibre integrity. These findings indicate that reflux heat treatment plays a crucial role in optimising lignin/DMSO solutions for electro-spinning by modifying solution properties to support bead-free fibre formation.

4.4.6. Electro-spun fibre alignment using reflux heat treated solutions of 100% (w/v) neat lignin in DMSO

Electro-spinning of reflux heat-treated 100% (w/v) lignin/DMSO solutions was carried out using a custom-made PTFE Vee-shield to promote fibre alignment. Previous experiments (see Section 4.4.3) had demonstrated that the Vee-shield was the most effective method for guiding fibre deposition and enhancing fibre uniformity. Given the improved solution properties following thermal treatment, the Vee-shield was employed to further refine fibre alignment and structure. The concentrated electric field generated by the shield facilitated the controlled deposition of fibres, minimising random orientation and enhancing directional alignment. This approach ensured that the thermally processed lignin solutions produced well-aligned, smooth, and uniform fibres, further validating the efficacy of reflux heat treatment in improving electro-spinnability.

Initial attempts to align fibres electro-spun from the 120 °C reflux heat-treated lignin/DMSO solution were unsuccessful, resulting in randomly oriented, beaded and broken fibres. Despite the improved solution properties from thermal treatment, fibre deposition remained inconsistent, with significant fibre breakage observed in the SEM micrographs, as shown in Figure 80.

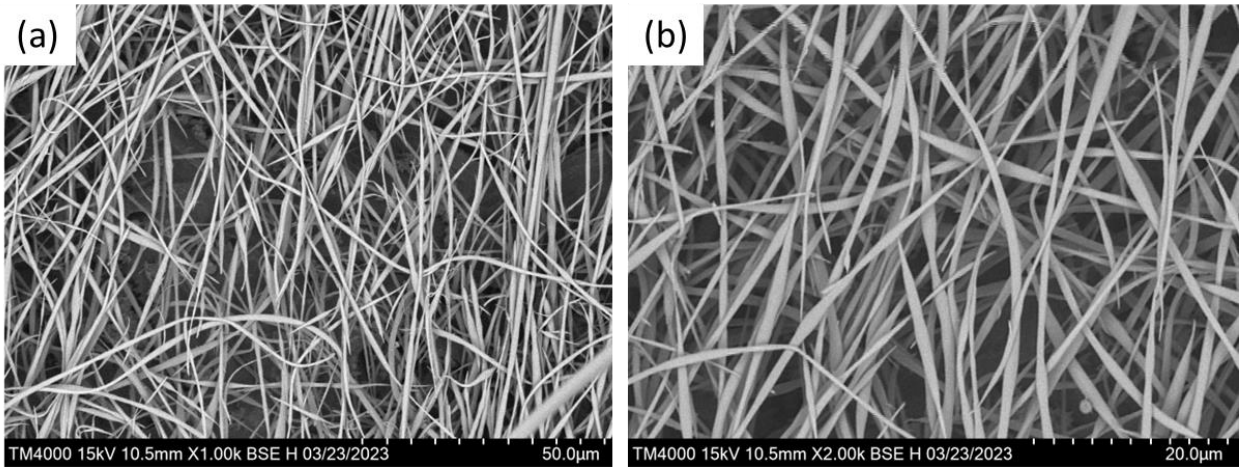

Figure 80. SEM micrographs for aligned attempt Vee-shield 100% (w/v) lignin in DMSO electro-spun fibres from reflux temperature 120 °C; magnifications (a): x1000 and (b): x2000.

At a reflux temperature of 120 °C, the aligned fibre electro-spinning process using the Vee-shield resulted in fibres with an average diameter of 789 nm and beads with a diameter of 1398 nm, with an average of 8 beads per 50 µm² was recorded. The fibres were predominantly random, beaded, and broken, which suggests that the electro-spinning conditions were not entirely optimised at this temperature. The high frequency of beading and broken fibres was not optimal for aligned fibre formation.

These fibre alignment results, shown in Table 20, illustrate that fibre alignment at 120 °C reflux temperature was somewhat scattered, with the highest percentage of alignment occurring in the 20-45° range (38%), followed by the 10-20° range (21%). However, the overall alignment was still quite random, with a notable portion of fibres in the lower alignment categories, such as 5% for <1° and 3% for both the 1-2° and 2-3° categories. The fibre alignment in the higher ranges (above 45°) was comparatively low at 12%, suggesting that while some fibres were more aligned, there was a significant amount of random and misaligned fibre formation.

Table 20. Fibre alignment percentage for 100% (w/v) electro-spun aligned fibres from 120 °C reflux temperature, using 1 cm Vee-shield.

Fibre alignment (%)	**<1°**	**1°-2°**	**2°-3°**	**3°-5°**	**5°-10°**	**10°-20°**	**20°-45°**	**>45°**
120 °C reflux temperature	5	3	3	4	14	21	38	12

The presence of a relatively high percentage of random and misaligned fibres, combined with the beading and broken fibres, indicates that 120 °C was not an ideal temperature for achieving a uniform, well-aligned fibre structure. Further optimisation of temperature or electro-spinning conditions may be required to achieve better alignment and minimise defects.
The electro-spinning jet appeared unstable, likely due to insufficient chain entanglement or inadequate viscosity for maintaining continuous fibre formation (215,227). As a result, the fibres lacked mechanical integrity and failed to exhibit the desired alignment, indicating that further optimisation of solution processing conditions was necessary to achieve uniform, well-aligned fibres.

Alignment was successfully optimised for fibres electro-spun from the 140 °C reflux heat-treated lignin/DMSO solution, producing smooth, bead-free fibres with continuous formation and improved deposition, as seen in Figure 81. The enhanced solution properties at this temperature facilitated stable jet formation, allowing for uniform fibre production without breakage (19,215,510). The PTFE Vee-shield effectively concentrated the electric field, guiding fibre deposition along a controlled path, resulting in well-aligned fibres. Unlike the lower reflux temperatures, no beading or fibre fragmentation was observed for the 140 °C reflux solution fibres.

At a reflux temperature of 140 °C, using an aligned Vee-shield, the electro-spinning process resulted in uniform, bead-free, and well-aligned fibres. The fibre diameter was measured at 1782 nm, indicating that the fibres were relatively thick compared to those produced at lower temperatures. The alignment of the fibres was notably improved, with no bead formation, suggesting that the electro-spinning conditions and the alignment shield contributed significantly to the quality of the fibres (19,241).

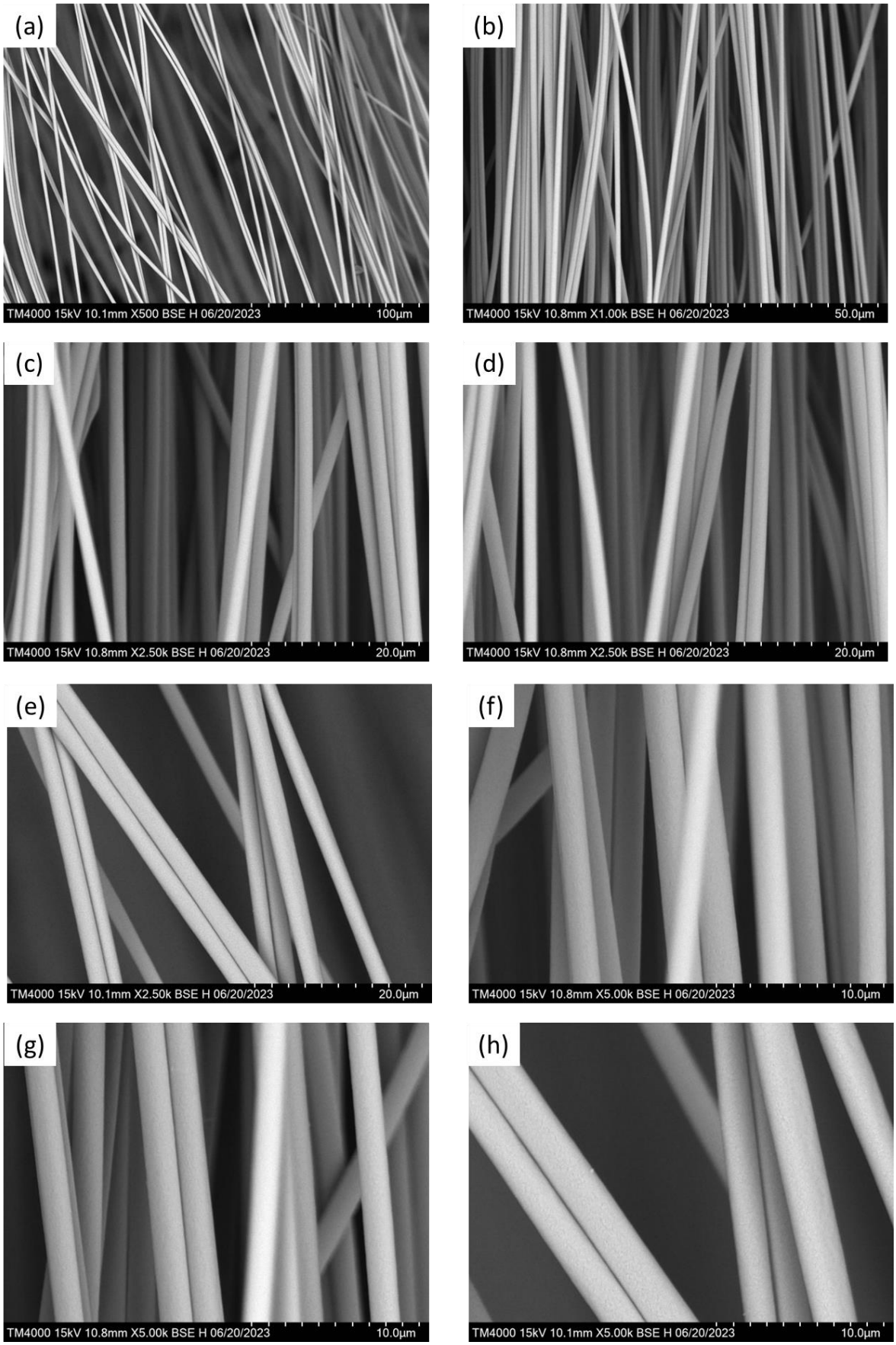

Figure 81. SEM micrographs for aligned Vee-shield 100% (w/v) lignin in DMSO electro-spun fibres from reflux temperature 140 °C; magnifications (a):x500, (b)x1000, (c), (d) and (e):x2500, (f), (g) and (h): 5000.

The fibre alignment distribution percentage for the 140 °C refluxed lignin/DMSO electro-spun fibres is shown in Table 21. The alignment data revealed that the majority of the fibres had excellent alignment, with 16% of fibres aligned at <1° and 16% at 1-2°. A further 22% of the fibres were aligned in the 2-3° range, and 18% in the 3-5° range, all of which indicate that the fibres were predominantly aligned in near-parallel directions. The 19% of fibres in the 5-10° range still showed good alignment but with slight misalignment. Only a small percentage of fibres were in the higher alignment ranges, with just 4% in the 10-20° category and 5% in the 20-45° range, indicating minimal misalignment. No fibres were found in the 45-90° range, showing that the aligned Vee-shield effectively minimised significant misalignment.

Table 21. Fibre alignment distribution percentage for 100% (w/v) electro-spun aligned fibres from 140 °C reflux temperature, using 1 cm Vee-shield

Fibre alignment (%)	**<1°**	**1°-2°**	**2°-3°**	**3°-5°**	**5°-10°**	**10°-20°**	**20°-45°**	**>45°**
140 °C reflux temperature	16	16	22	18	19	4	5	0

Comparing the fibre alignment data for the 120 °C and 140 °C refluxed lignin/DMSO solutions demonstrates a clear improvement in fibre alignment when using the 140 °C refluxed lignin DMSO solution compared to the one prepared at 120 °C, as shown in Figure 82.

At 120 °C, a large proportion of the fibres fell within poorly aligned ranges, with 38% in the 20°–45° range and 12% above 45°. Only 15% of fibres were within the tightly aligned ranges of <1° to 3°. In contrast, at 140 °C reflux temperature solution, the fibre distribution shifted significantly towards stronger alignment, with 54% of fibres in the <1° to 3° range, only 5% in the 20°–45° range, and 0% above 45°. This suggests that refluxing the lignin solution at 140 °C greatly improved fibre orientation during electro-spinning. The significant drop in misaligned fibres and the increase in those within <5° indicates a more uniform fibre alignment. There is no fibre alignment dataset for the 160 °C reflux solution, as the fibres could not be aligned using the Vee-shaped collector during electro-spinning.

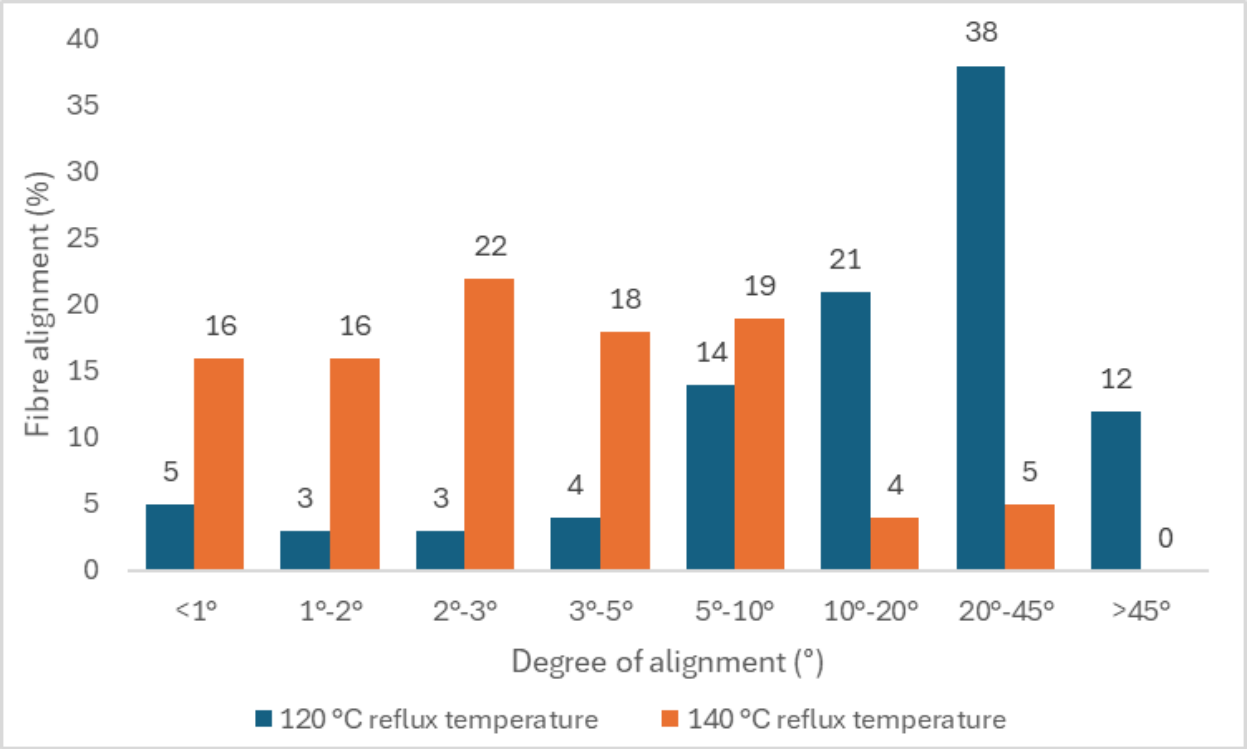

Figure 82. Comparison of electro-spun fibre alignment percentage for the 120 °C and 140 °C refluxed lignin/DMSO solutions.

In summary, at 140 °C, using the aligned Vee-shield, the electro-spinning process resulted in bead-free, uniform, and predominantly well-aligned fibres. While there were slight deviations in fibre alignment, the overall structure was highly aligned (72% of fibres aligned within 5° of mean average fibre direction), suggesting that this temperature and setup were optimal for producing high-quality, aligned neat lignin fibres, with a lignin polymer concentration of 100% (w/v) in DMSO.

4.4.7. Combined analysis of lignin solution properties and fibre morphology

To further understand the relationship between spinning solution properties and fibre morphology, an Ashby-style diagram was created, see Figure 83, to plot solution viscosity against electrical conductivity, with bubble size representing the average fibre diameter obtained under each condition. Solutions treated at 80–120 °C are shown as red bubbles and produced beaded fibres, whereas those treated at 140–160 °C are shown as blue bubbles and produced uniform, bead-free fibres.

A trend emerges; where solutions with low viscosity and intermediate conductivity (80–120 °C) produced unstable jets during electro-spinning, resulting in beads and irregular morphologies. As viscosity increased (≥ 3.5 Pa·s) and conductivity rose above approximately 110 µS cm^{-1}, a stable spinning window was achieved, yielding smooth, continuous fibres (140–160 °C).

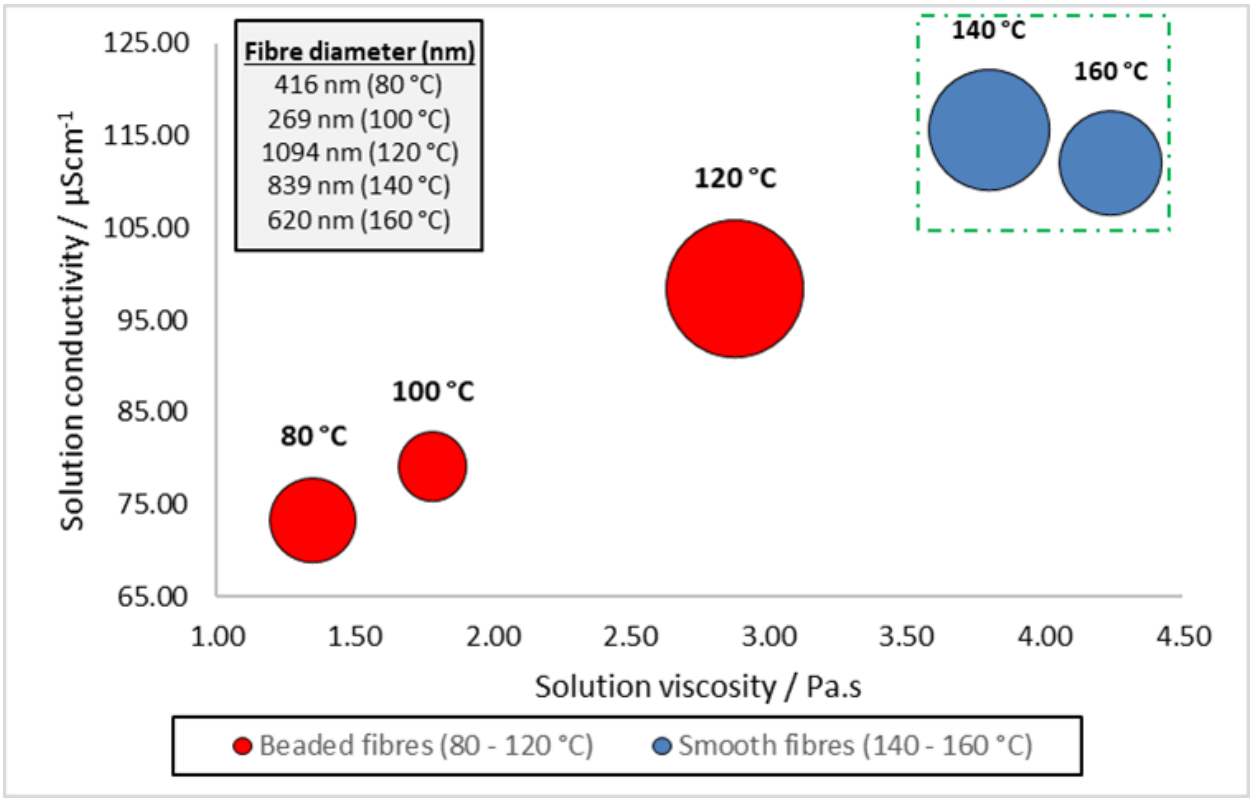

Figure 83. Ashby-style plot of viscosity and conductivity for neat lignin/DMSO solutions at 55 °C, with bubble size representing the diameter of the resulting electro-spun fibres. Red points (80–120 °C) produced beaded fibres, while blue points (140–160 °C) yielded smooth fibres. The green dashed box highlights the ideal range for bead-free fibre formation and reproducible fibre alignment, where consistent fibre morphology was achieved.

The highlighted region on the diagram represents this optimal processing zone, where the balance of charge transport (via solution conductivity) and polymer chain entanglement (via solution viscosity) supports uniform fibre formation (219,404). As viscosity decreased across the lignin solutions tested, fibre diameters were also reduced. This observation aligns with the mechanism described by Li et al., (511), who attributed the reduction in lignin fibre diameter to the combined effect of lower solution viscosity and increased electrical conductivity contributed by lignin. They noted that when viscosity decreases, polymer chain entanglement is reduced, lowering jet resistance during electro-spinning and allowing the charged jet to fragment into smaller droplets.

Bubble size further illustrates how solution properties influence fibre diameter. At higher viscosities and conductivities, thicker fibres were generally observed, reflecting reduced jet thinning but improved fibre integrity (18). Together, these results demonstrate that neither viscosity nor conductivity alone is sufficient to predict fibre quality; rather, it is the combined

effect of these two parameters that defines the transition from beaded to smooth fibre morphology.

To contextualise the properties of the lignin solutions and fibres produced in this study, values reported in the literature for different lignin types, solvents, and polymer blends were collated in Table 22. These data provide reference ranges for solution viscosity, electrical conductivity and resulting fibre diameters. Comparing these literature values to the present work enables assessment of whether the neat lignin/DMSO solutions developed here fall within, or extend beyond, the processing window typically reported for lignin-based electro-spinning systems.

Table 22. Reported literature values for lignin solution viscosity, conductivity (25 °C) and resulting fibre diameters across different lignin types, solvents and blends, for comparison with this study.

Lignin type	Solvent	Polymer blend	Blend ratio of lignin / polymer (w/w)	Total polymer concentration / % (w/v)	Solution viscosity / Pa.s	Solution conductivity / μScm^{-1}	Fibre diameter / nm	Reference
Lignosulfonate	DMSO	PAN	50/50	10	1.20 (25 °C)	470 (25 °C)	N/A	(512)
Softwood Kraft	DMSO	PVA	50/50	30	N/A	50 (25 °C)	750	(513)
Acetone soluble Softwood Kraft	Acetone/DMSO 2:1	N/A	N/A	58	0.62 (25 °C)	2.37 (25 °C)	1160	(404)
Acetone soluble and ethanol soluble Softwood Kraft	Acetone/DMSO 2:1	N/A	N/A	55	1.13 (25 °C)	3.31 (25 °C)	1600	(405)
Organosolv	DMSO	N/A	N/A	55	4.30 (25 °C)	0.95 (25 °C)	1140	(514)
Softwood Kraft	DMF	PEO	50/50	50	2.34 (25 °C)	N/A	1318	(177)
Kraft	DMF	PAN	50/50	50	0.44 (25 °C)	N/A	1200	(515)
Lignosulfonate Kraft	DMF	PAN	90/10	18	0.20 (25 °C)	N/A	228	(516)

This study (Softwood Kraft)	DMSO	N/A	N/A	100	1.35–4.24 (55 °C)	73–115 (55 °C)	416–1094	*This study*

The values reported in Table 22 largely reflect studies using lignin blended with co-polymers such as PAN or PVA, and often in mixed solvent systems (e.g. DMF or acetone/DMSO). In contrast, the present work utilises neat lignin in DMSO alone, without the rheological or electro-spinning support of a carrier polymer. Consequently, the measured viscosities of the neat lignin solutions (1.35–4.24 Pa·s) are generally higher than those reported for lignin/PAN and lignin/PVA blends (0.20–2.34 Pa·s), while electrical conductivities (73–115 μS cm^{-1}) fall within or slightly below the range typically reported. It is also important to note that most literature values are recorded at room temperature (25 °C), whereas the viscosity and conductivity measurements in this study were carried out at 55 °C to reflect the processing conditions used. Despite the absence of a co-polymer, the fibres produced here (416–1094 nm) are comparable in diameter to those reported for lignin blends (228–1600 nm), demonstrating that neat lignin solutions can achieve fibre formation within established size ranges while offering a clearer understanding of lignin's intrinsic solution behaviour.

4.4.8. Fourier-transform infrared spectroscopy of electro-spun lignin fibre

The FTIR spectra of the as-received, vacuum dried and vacuum dried electro-spun fibre from refluxed lignin/DMSO solution (displayed in spectra from 120 °C reflux temperature) is shown offset together for comparison in Figure 84.

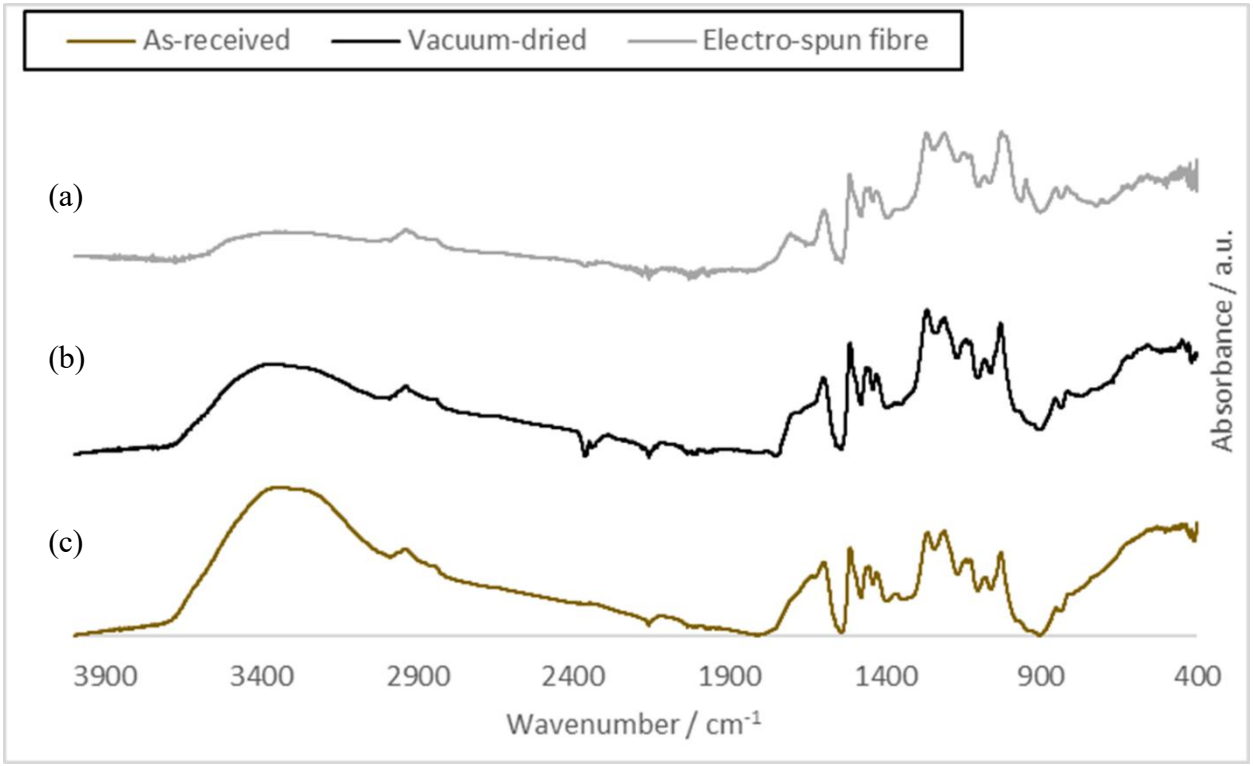

Figure 84. FTIR spectra for; (a): the vacuum dried electro-spun lignin fibre from the 120 °C refluxed lignin/DMSO solution, (b): the vacuum dried 80 °C for 6 hours lignin sample and (c): as-received lignin sample, offset by absorbance to enable comparison.

The FTIR spectra of the vacuum dried electro-spun fibres obtained from reflux heating lignin in DMSO were similar to those of the vacuum-dried lignin, indicating that the refluxing process does not induce significant structural changes in lignin. This suggests that both vacuum drying (80 °C, 6 hours) and refluxing in DMSO (120 °C, 6 hours) primarily remove moisture without altering the core lignin structure. The key spectral feature supporting this is the absence of significant differences between the vacuum-dried lignin and vacuum dried electro-spun fibre reflux-treated lignin samples, except for one notable peak in the fingerprint region and a reduction in absorbance of the O-H water peak at 3400 cm^{-1}.

The broad O-H stretching band at 3400 cm^{-1} is further reduced in the vacuum dried electro-spun fibre sample compared to the vacuum-dried lignin (absorbance decrease of ~0.04 a.u.). This is most likely due to the additional heating steps involved in the reflux process, which would further remove residual moisture (68,271). These combined thermal treatments help explain the

continued decrease in hydroxyl absorbance in the vacuum dried electro-spun fibre spectra relative to the vacuum-dried lignin spectra.

The FTIR spectrum of the electro-spun lignin fibres exhibited some changes compared to the as-received lignin powder and vacuum-dried samples, indicating chemical modifications during the electro-spinning and refluxing processes. Subtle changes in the aromatic skeletal vibrations at 1510–1600 cm^{-1} and the C–O–C stretching in aryl–alkyl ethers at 1210–1260 cm^{-1} further imply mild cleavage of ether linkages (442,517). A new shoulder peak emerged around 1720 cm^{-1}, which is attributed to unconjugated carbonyl stretching (C=O) vibrations from ester or carboxylic acid groups, suggesting partial oxidation or esterification of lignin during solution processing and subsequent fibre formation (114,308,442). While the broad O–H stretching band near 3400 cm^{-1} remained evident, it appeared slightly narrowed and shifted, indicating changes in hydrogen bonding and a possible reduction in free hydroxyl groups (518). Together, these spectral changes suggest that electro-spinning, combined with refluxing, induces slight oxidation and structural rearrangement of lignin, potentially influencing the fibre's crosslinking density and downstream thermal behaviour.

Given that refluxing involves prolonged heating in DMSO, potential explanations include minor condensation reactions between hydroxyl or carbonyl groups, slight rearrangements of ether linkages, or weak interactions between lignin and residual DMSO. However, the absence of changes in the key aromatic and ether regions suggests that no cross-linking or chemical degradation occurs at these temperatures. Although, studies have shown that heating lignin under such conditions can lead to the cleavage of β-O-4 ether linkages (as seen in Figure 6), resulting in the formation of free phenolic hydroxyl groups and carbonyl functionalities (447,519). Prolonged heat treatment can also encourage lignin fragment condensation processes. Carbon–carbon (C–C) bonds are frequently formed between aromatic rings in these reactions, which results in a more condensed lignin structure (123,361). All the vacuum dried electro-spun fibre samples from the refluxed lignin/DMSO solutions had similar FTIR spectra with no significant changes seen for any of the heating temperatures used (80, 100, 120, 140 °C respectively), shown in Figure 85. A decrease of the moisture peak at 3400 cm^{-1} is seen which is to be expected, which corresponds to the increase lignin heating temperature.

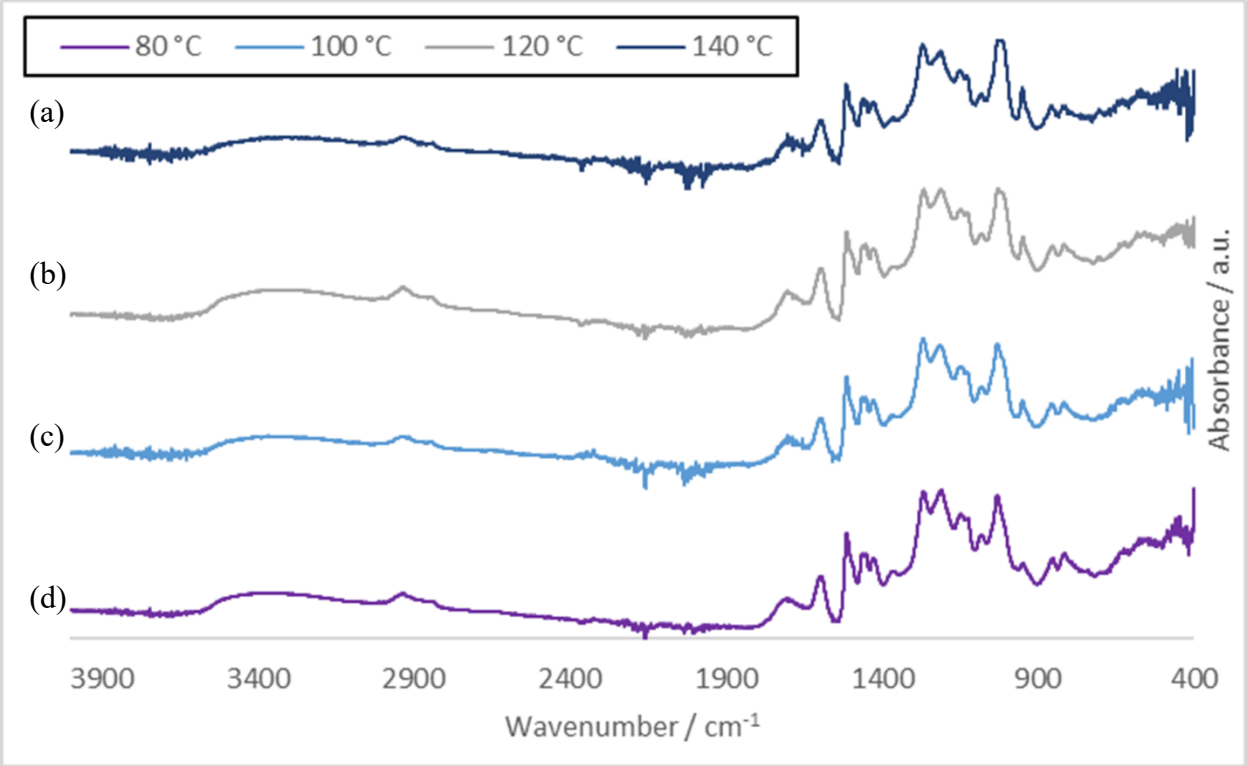

Figure 85. FTIR spectra of vacuum-dried electro-spun lignin fibres produced from lignin/DMSO solutions refluxed at; (a): 140 °C, (b): 120 °C, (c): 100 °C and (d): 80 °C, offset by absorbance to enable comparison .

The FTIR spectra presented in Figure 85 were obtained from single-run measurements for each fibre sample due to the limited material available. As such, minor noise and baseline fluctuations are present, particularly in lower absorbance regions, which may account for slight differences between the spectra. No spectrum is reported for the 160 °C refluxed sample as insufficient fibre was produced for analysis. Future work should repeat these measurements with replicate scans and ensure all reflux conditions, including 160 °C, are represented to strengthen reproducibility and completeness of the dataset.

In conclusion, the FTIR analysis of the lignin samples revealed key peaks corresponding to various functional groups as also reported in literature (324,444,445), providing valuable insights into the molecular structure of the sample. Notably, a significant peak at around 3400 cm^{-1} was observed, which is typically associated with the O-H stretching vibration, reflecting the presence of water. This peak diminished as the lignin sample was heated when vacuum dried and further diminished in comparison to the vacuum dried electro-spun fibre samples that were subjected to reflux temperatures (80, 100, 120, 140 & 160 °C, respectively) prior to electro-spinning and subsequent vacuum drying of the fibre samples, indicating water loss during the heating process.

The main difference observed in the lignin FTIR spectra was the reduction in intensity of the water-related peak, highlighting the impact of heat treatment on water content in lignin. Apart from this, no other discernible differences are observed between the lignin spectra, indicating heating the lignin to temperatures up to 160 °C does not disrupt lignin's ether linkages, aromatic rings, or other functional groups.

4.4.9. NMR of electro-spun lignin fibre

NMR spectroscopy was employed to characterise the structural features of vacuum dried electro-spun lignin fibres from the refluxed lignin/DMSO solutions. The ^{1}H NMR for the electro-spun lignin fibre (lignin/DMSO solution refluxed at 80 °C for 4 hours) is shown in Figure 86.

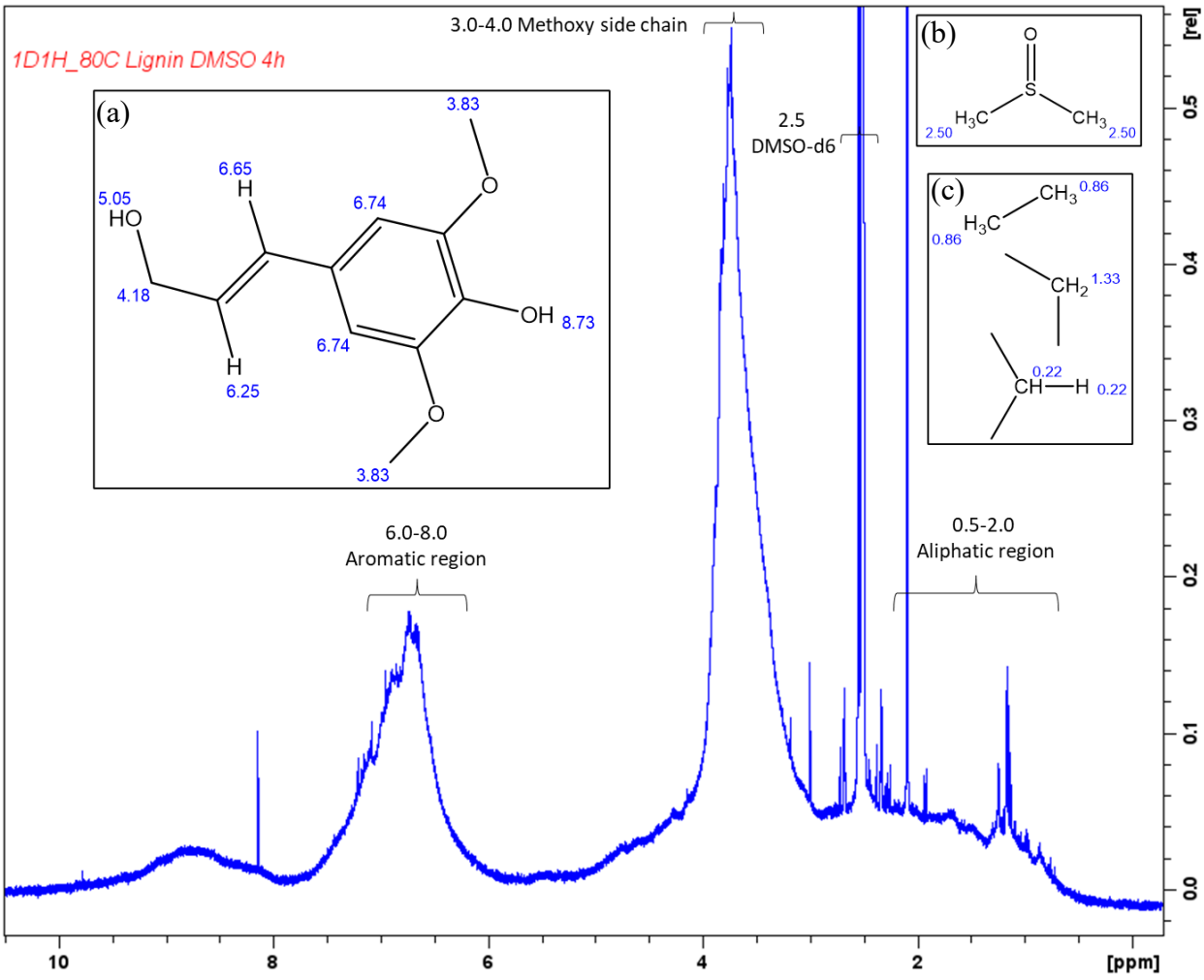

Figure 86. ^{1}H NMR spectra of electro-spun lignin fibre (lignin/DMSO solution refluxed at 80 °C for 4 hours), and assignments of the structural features with labelled literature ppm values: (a): sinapyl alcohol repeating lignin monomer including methoxy side chain, (b): DMSO solvent structure and (c): aliphatic region containing methyl (-CH_3), methylene (-CH_2 and methine group (-CH) (333,342,451).

The produced electro-spun fibres were vacuum dried and then dissolved in DMSO-d_6 solution for NMR analysis.

The ^{1}H NMR spectrum of the electro-spun lignin fibres was found to be similar to that of both the as-received lignin powder and the vacuum-dried lignin powder, indicating that the electro-spinning process and prior reflux heat treatment of lignin/DMSO solutions, did not significantly alter the chemical structure of the lignin.

The increased noise observed in the ^{1}H NMR spectrum of the electro-spun lignin fibres compared to the spectra of the as-received and vacuum-dried lignin powders is likely due to the lower sample mass and reduced concentration of analyte in the prepared NMR solution (351). The electro-spun fibres typically yielded a smaller quantity of material, which limited the amount of sample available for dissolution.

Peaks seen include; between 0.8-2.0 ppm (aldehyde, carboxylic acid and phenolic H peaks, 2.07 ppm methyl groups (CH_3), residual DMSO-d_6 solvent quintet at 2.50 ppm, hydrogen singlet at 2.54 ppm, methoxy side chain 3.2-3.9 ppm, broad-OH of coniferyl singlet 3.00 ppm, solvent H peak 3.17 ppm, aromatic region between 6.0-8.0 ppm, between 8.0 to 10.0 ppm is formyl/phenolic hydroxyl groups (9.4-11.0 ppm): aldehyde, benzaldehyde proton at 9.78 ppm, 8.5-9.4 ppm: unsubstituted phenolic, 7.9-8.5 ppm: substituted phenolic, aromatic hydroxyl 8.14 ppm (271,403).

The ^{13}C NMR for the electro-spun lignin fibre is shown in Figure 87 for the electro-spun fibre from the 80 °C refluxed lignin/DMSO solution. The ^{13}C NMR spectrum of the electro-spun lignin fibres was also consistent with previous observations, showing a dominant solvent peak from DMSO-d_6.

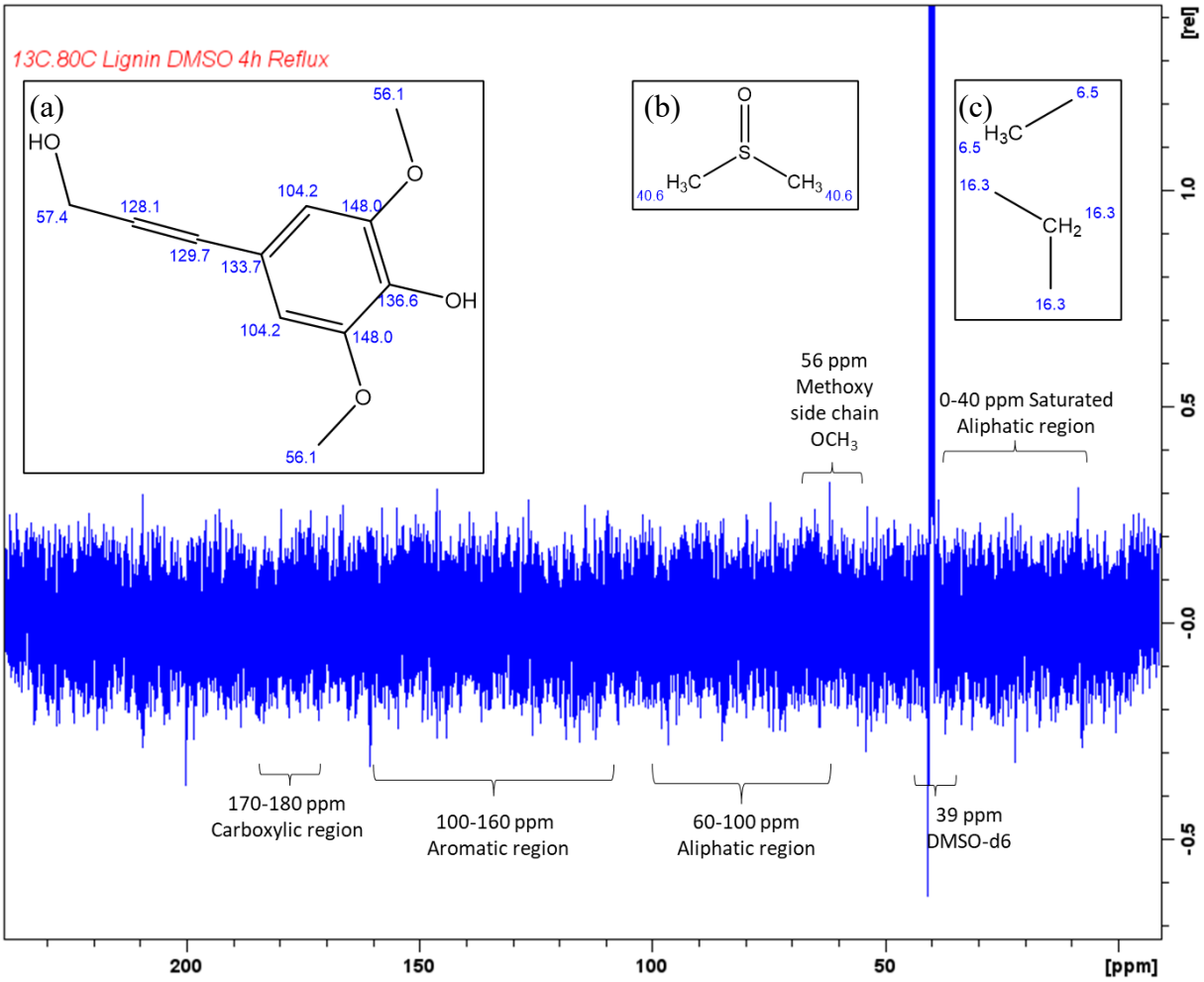

Figure 87.[13]C NMR spectra of electro-spun lignin fibre (lignin/DMSO solution refluxed at 80 °C for 4 hours), and assignments of the structural features with labelled literature ppm values: (a): sinapyl alcohol repeating lignin monomer including methoxy side chain, (b): DMSO solvent structure and (c): aliphatic region containing methyl (-CH_3), methylene (-CH_2 and methine group (-CH) (333,342,451).

However, due to significant noise, likely a result of the limited sensitivity of the university NMR instrumentation and the low sample concentration, quantitative analysis of other carbon signals was challenging. Nonetheless, key structural features could be confirmed through complementary HSQC NMR spectra and comparison with reported literature values.

Peaks seen are at 39 ppm = DMSO d_6, 56 ppm = OCH_3 methoxyl , 60-100 ppm = aliphatic (CHO, C-CH_2-O), 100-160 ppm = C-aromatic and 175 ppm = carboxylic carbon.

The ^{1}H-^{13}C HSQC for 80 °C lignin fibre is shown in Figure 88. The HSQC NMR spectra for the 80 °C refluxed lignin fibre is similar to the previous spectra with peak areas seen; δC/δH, δ31.1/2.09 ppm, methyl group CH_3, δ42.5/2.50 ppm, DMSO-d_6, δ40.8/2.54 ppm, H-solvent peak and δ58.9/3.75 ppm methoxy side chain OCH_3.

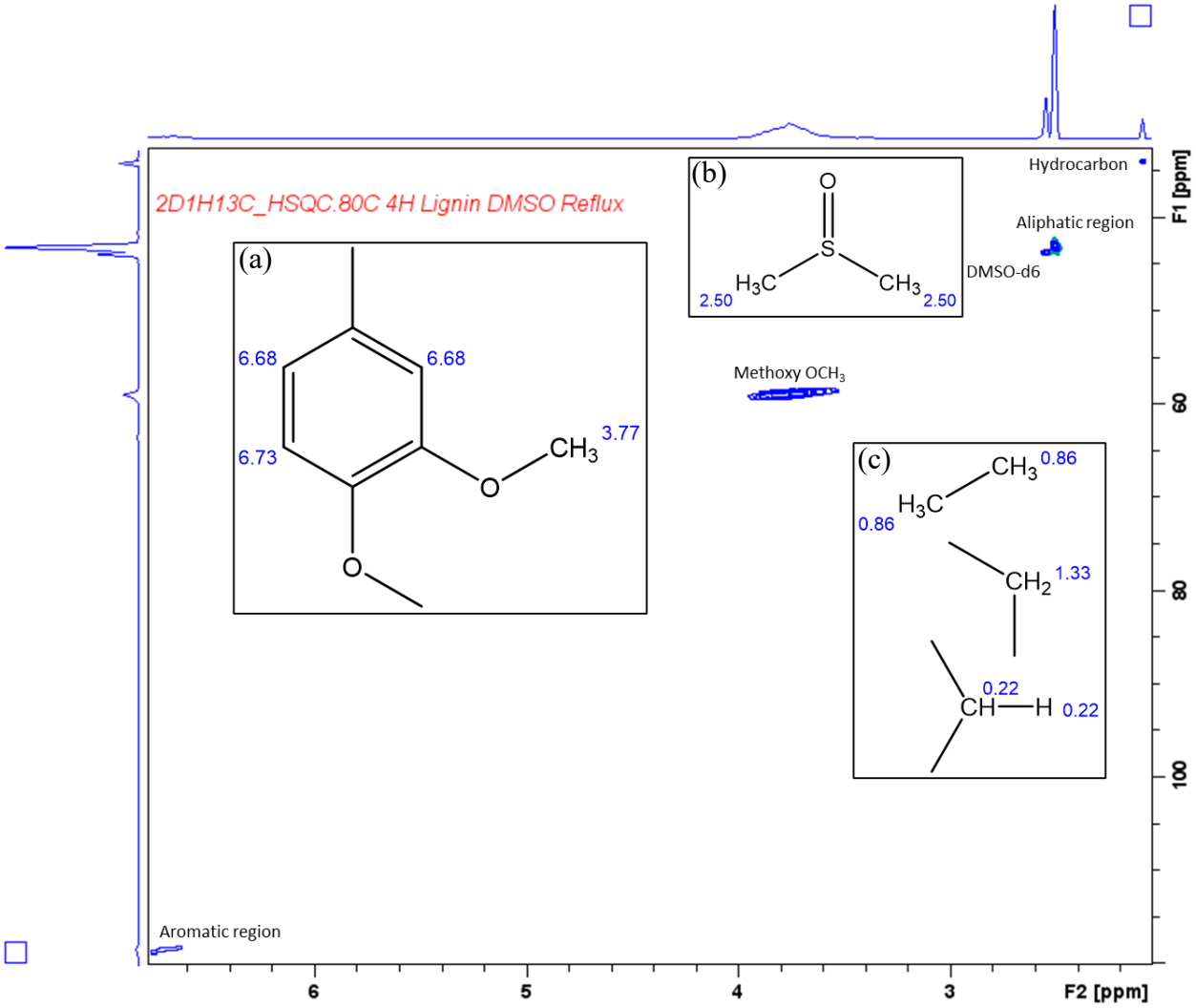

Figure 88. $^{1}H^{13}C$ – HSQC spectra for the electro-spun lignin fibre (lignin/DMSO solution refluxed at 80 °C for 4 hours), and assignments, and assignments of the structural features with labelled literature ^{1}H NMR ppm values: (a): guaiacyl lignin repeating unit including methoxy side chain, (b): DMSO solvent structure and (c): aliphatic region containing methyl (-CH_3), methylene (-CH_2 and methine group (-CH) (333,342,451).

The ^{1}H-^{1}H COSY spectra, see Figure 89, are also similar to the as-received and vacuum dried lignin powder spectra, confirming the peaks seen in the ^{1}H NMR for the electro-spun lignin fibre, shown in Figure 86. The peaks seen correspond as follows; 0.85 ppm carboxylic acid, 1.16 ppm substituted phenolic -H, 2.09 ppm methyl group -CH_3, 2.50 ppm DMSO-d_6, 3.45 methoxy side chain OCH_3, 3.74 ppm ethyl group CH_2, and 6.71 for the aromatic C-H (271,403).

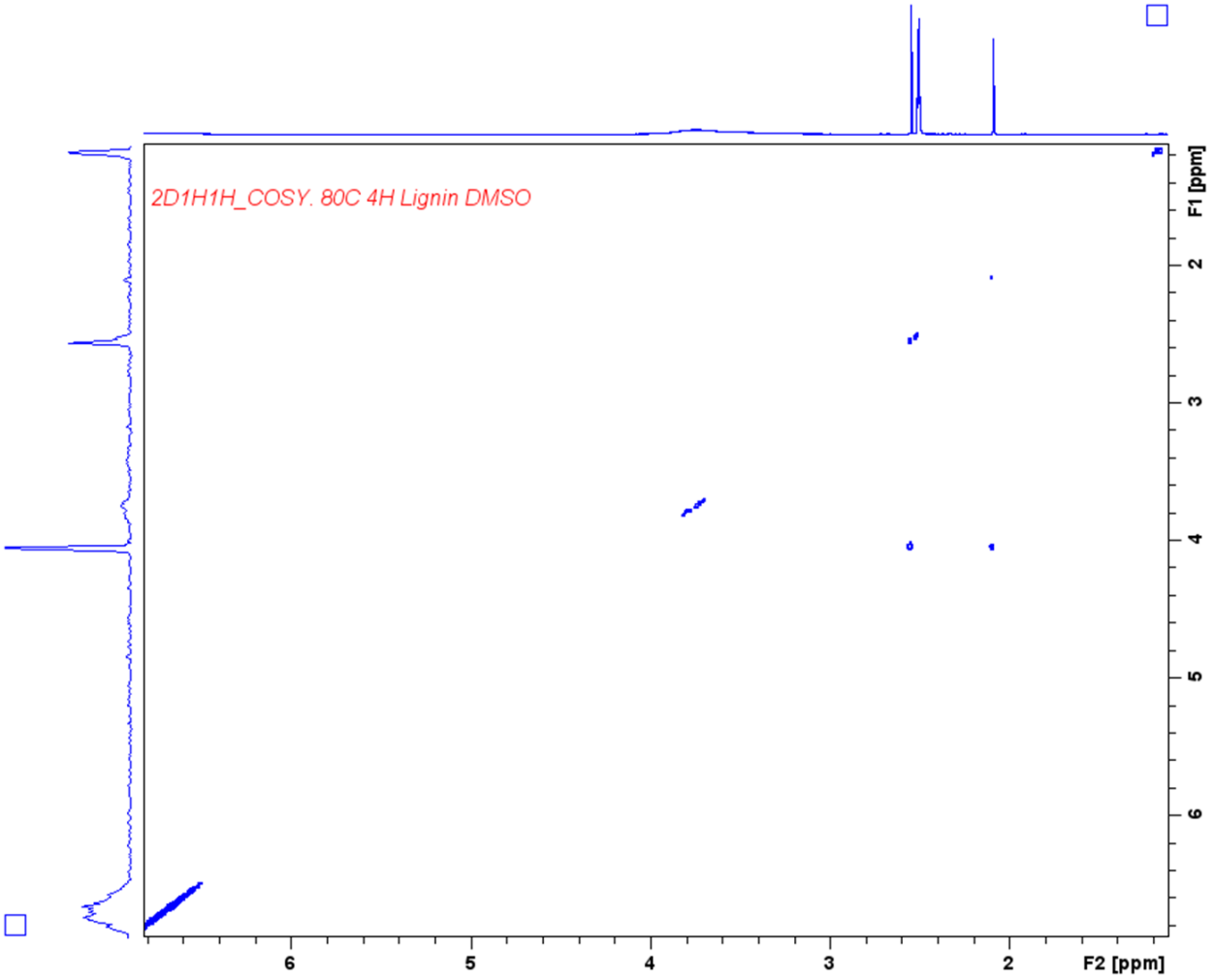

Figure 89. ^{1}H-^{1}H COSY of 80 °C 4 hour refluxed lignin/DMSO solution electro-spun lignin fibre.

The NMR spectra for the electro-spun lignin fibre prepared from the 100 °C refluxed lignin/DMSO solution is similar to that of the NMR spectra for the electro-spun fibre prepared from the 80 °C refluxed lignin/DMSO solution; for the ^{1}H, ^{13}C, ^{1}H-^{1}H COSY and ^{1}H-^{13}C HSQC NMR spectra respectively. The NMR spectra for the electro-spun lignin fibre prepared from the 120 °C refluxed lignin/DMSO solution is also identical to the previous electro-spun refluxed fibre NMR peaks except for the ^{1}H NMR, see Figure 90. The exception is a split of a broad peak between 3.2-4.0 ppm, into 2 separate peaks, at 3.33 ppm a singlet & at 3.74 a broad peak, corresponding to the methylene group ($-CH_2$) in the β-O-4 linkage and a methoxy side chain ($-OCH_3$) peak, respectively, see Figure 8 (271,403). The NMR spectra for the electro-spun lignin fibre prepared from the 140 °C refluxed lignin/DMSO solution is also similar to the previous electro-spun refluxed fibre NMR peaks except for the ^{1}H NMR. The exception, like the ^{1}H NMR for the electro-spun lignin fibre prepared from the 120 °C refluxed lignin/DMSO solution, is again a doublet broad peak between 3.0 ppm to 4.0 ppm.

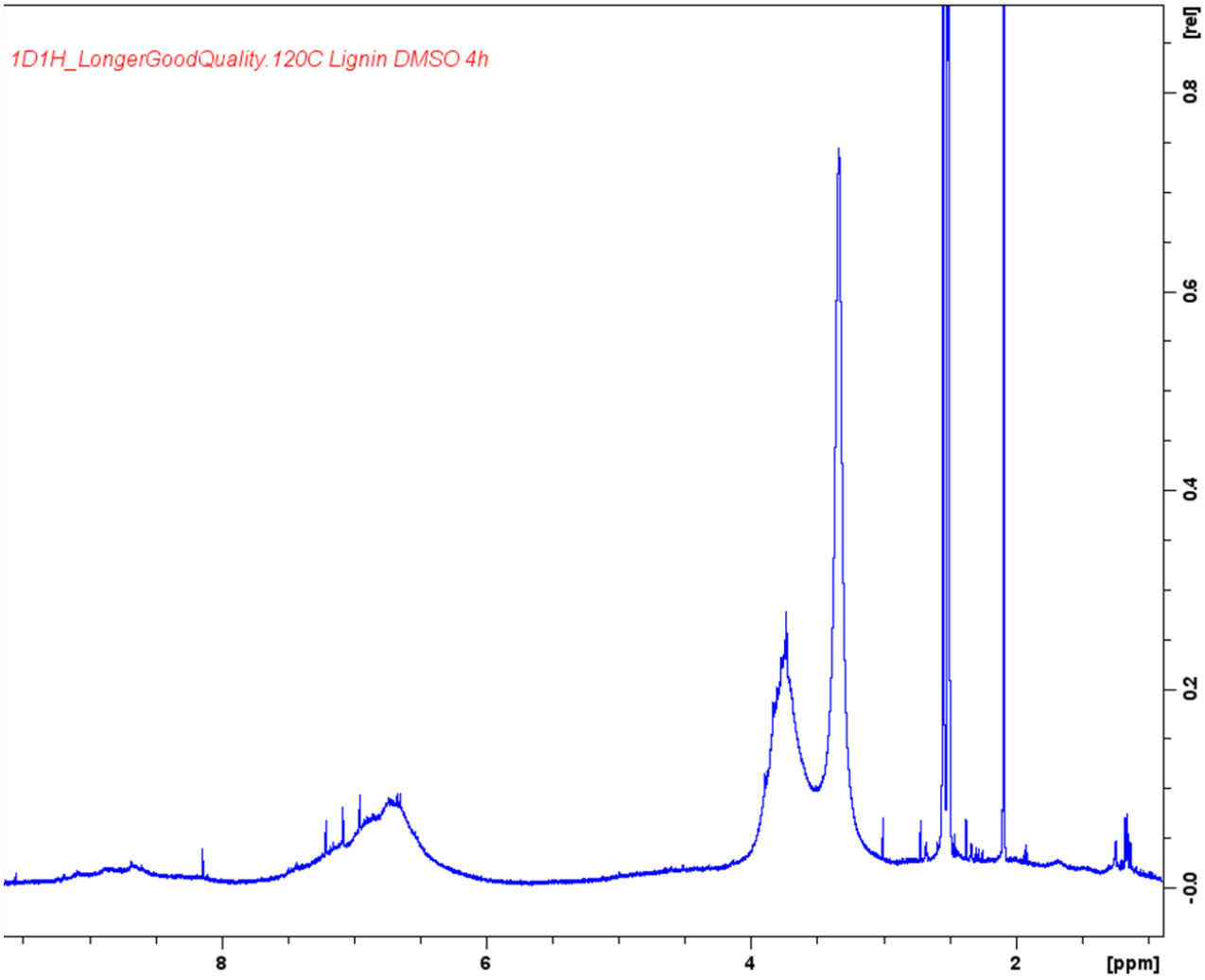

Figure 90. [1]H NMR spectra of electro-spun lignin fibre (lignin/DMSO solution refluxed at 120 °C for 4 hours),

The [1]H NMR for the electro-spun fibre prepared from the 140 °C refluxed lignin/DMSO solution, is shown in Figure 91. The [1]H NMR spectra of electro-spun lignin fibres prepared from DMSO solutions refluxed at 140 °C show a number of common features characteristic of lignin, with some notable differences in resolution and spectral clarity. In the spectra, the dominant solvent peak from DMSO-d_6 is visible around 2.50 ppm, as expected. Broad signals in the region between approximately 6.0 and 7.5 ppm are attributed to aromatic protons from guaiacyl (G) and syringyl (S) units, shown in Figure 3, which are common in lignin. Additionally, the broad signals observed between 8.5–9.5 ppm correspond to hydrogen-bonded phenolic protons. The peaks observed around 3.5 to 4.5 ppm correspond to methoxyl ($-OCH_3$) groups and protons from β-O-4 ether linkages, shown in Figure 6, a major structural feature of lignin (49,53). The peak seen at 2.09 ppm corresponds to methylene ($-CH_2$) peaks adjacent to carbonyl groups. The peaks in the 1.5 to 2.0 ppm region are associated with aliphatic side chains, such as benzylic protons,

while signals at approximately 0.8 to 1.2 ppm likely arise from terminal methyl groups in aliphatic chains (271,403). Despite the noise in the 140 °C spectrum, the presence of key lignin features including aromatic protons, methoxyl groups, and aliphatic side chains, confirms that the core lignin structure remains identifiable even after thermal reflux heat treatment.
No NMR data was obtained for the electro-spun fibre prepared from the 160 °C refluxed lignin/DMSO solution, due to time constraints, which was an oversight during the experimental phase; this would require further analysis in future work and is the reason it has not been included in this thesis.

The NMR analysis of lignin samples, including as-received lignin powder, vacuum-dried lignin powder, and vacuum-dried electro-spun lignin fibres, provided detailed insights into their structural features and any potential chemical changes. The ^{1}H NMR, ^{13}C NMR, ^{1}H-^{1}H COSY,

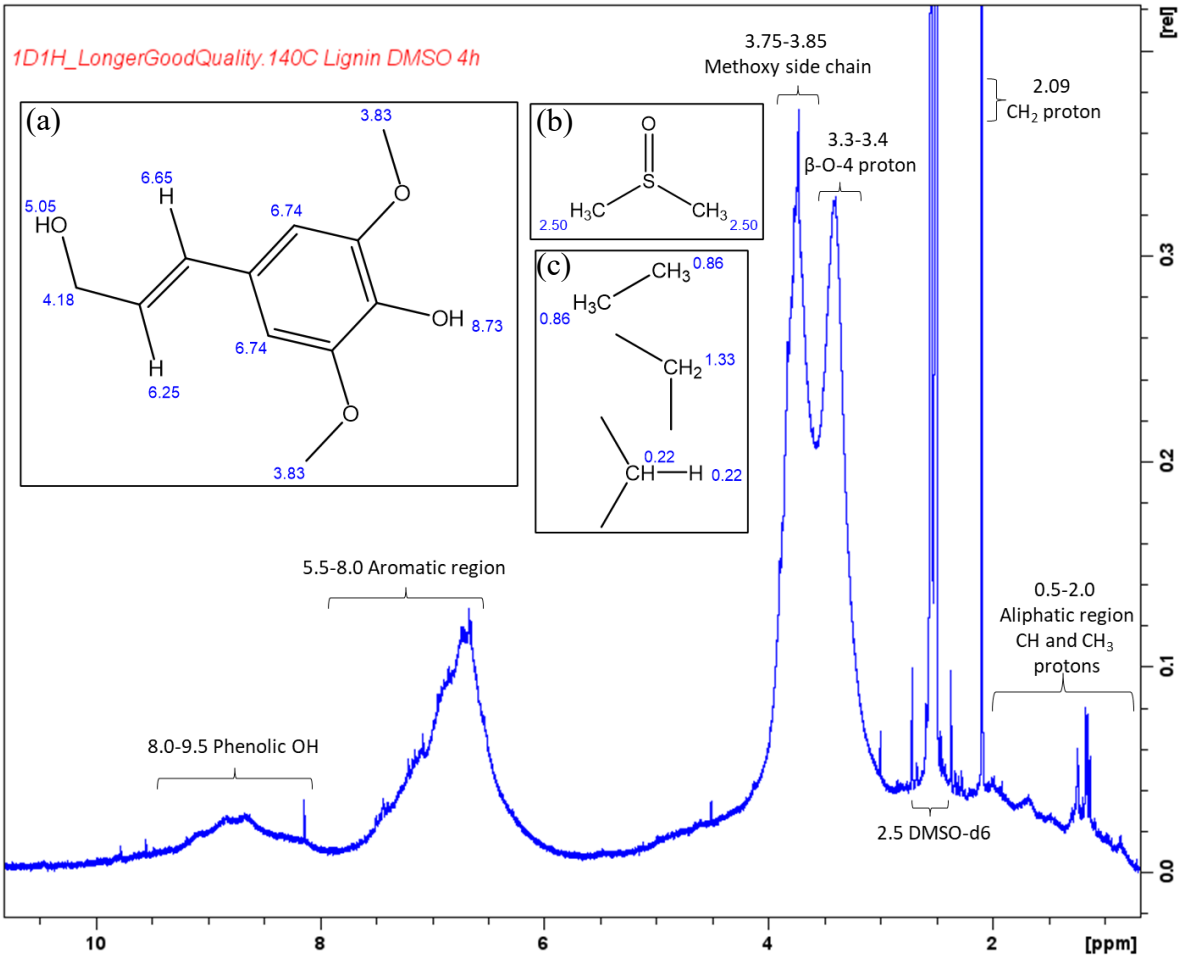

Figure 91. ^{1}H NMR spectra of electro-spun lignin fibre (lignin/DMSO solution refluxed at 140 °C for 4 hours), and assignments of the structural features with labelled literature ppm values: (a): sinapyl alcohol repeating lignin monomer including methoxy side chain, (b): DMSO solvent structure and (c): aliphatic region containing methyl (-CH_3), methylene (-CH_2 and methine group (-CH) (333,342,451).

and ^{1}H-^{13}C HSQC spectra demonstrated that the key structural components of lignin, such as aromatic rings, methoxy groups, and aliphatic side chains, remained consistent across all sample types (354). However, noticeable differences in the water peak intensity, particularly the significant reduction in the vacuum-dried and electro-spun samples, confirmed the successful removal of bound and free water during drying and sample processing (see Section 2.1.2).

Evidence of cross-linking or condensation reactions was not clearly observed from the NMR spectra as the aromatic structure was retained in all of the reflux heat treated electro-spun fibre samples (264,349). The characteristic inter-unit linkages, including β-O-4, β-β, and β-5, remained intact, indicating that the reflux thermal or vacuum drying treatments did not cause significant structural rearrangements or condensation reactions. The consistent appearance of methoxy, aromatic, and aliphatic signals across the spectra supports the conclusion that the fundamental lignin structure was preserved, structures shown in Figure 32 (271,403). The absence of new peaks or significant chemical shifts further suggest that processing conditions were mild enough to avoid extensive chemical modification or cross-linking.

Overall, the NMR analysis confirmed that the drying and electro-spinning processes primarily affected the water content and physical properties of lignin without altering its core chemical structure. The NMR analysis successfully quantified the lignin samples, with the identified peaks aligning well with those reported in literature, confirming the presence of characteristic lignin structural features such as aromatic rings, methoxy groups, and inter-unit linkages.

4.4.10. DSC of vacuum dried electro-spun lignin fibre

The T_g values for the electro-spun vacuum-dried lignin fibres produced from refluxed lignin/DMSO solutions at different temperatures (80, 100, 120, 140 and 160 °C), are shown in Figure 92. The data shown is the calculated T_g for the first heating scans for each of the lignin fibre samples. No endotherm was seen for the second and third heating scans for the fibre samples. These T_g values are from single DSC runs due to the limited fibre quantities available; future work should repeat these measurements to confirm reproducibility.

The data reveals a clear trend of increasing T_g with higher reflux temperatures, for each of the fibre samples. For the fibres produced from lignin solutions refluxed at 80 °C and 100 °C, the T_g values were 122.4 °C and 122.9 °C, respectively, showing minimal variation.

A noticeable increase in T_g for the first heating scans is observed at reflux temperatures of 120 °C and above. The T_g increased to 131.6 °C for the 120 °C reflux sample. This indicates that

higher reflux temperatures promote increased polymer chain alignment and network formation through condensation reactions, see Figure 92, resulting in an increased T_g (463). The most significant increases in T_g were seen for fibres produced from lignin refluxed at 140 °C and 160 °C, where T_g values rose to 160.6 °C and 166.0 °C, respectively. This sharp increase suggests that higher reflux temperatures cause greater structural reorganisation and increased cross-link density within the lignin matrix (9,464).

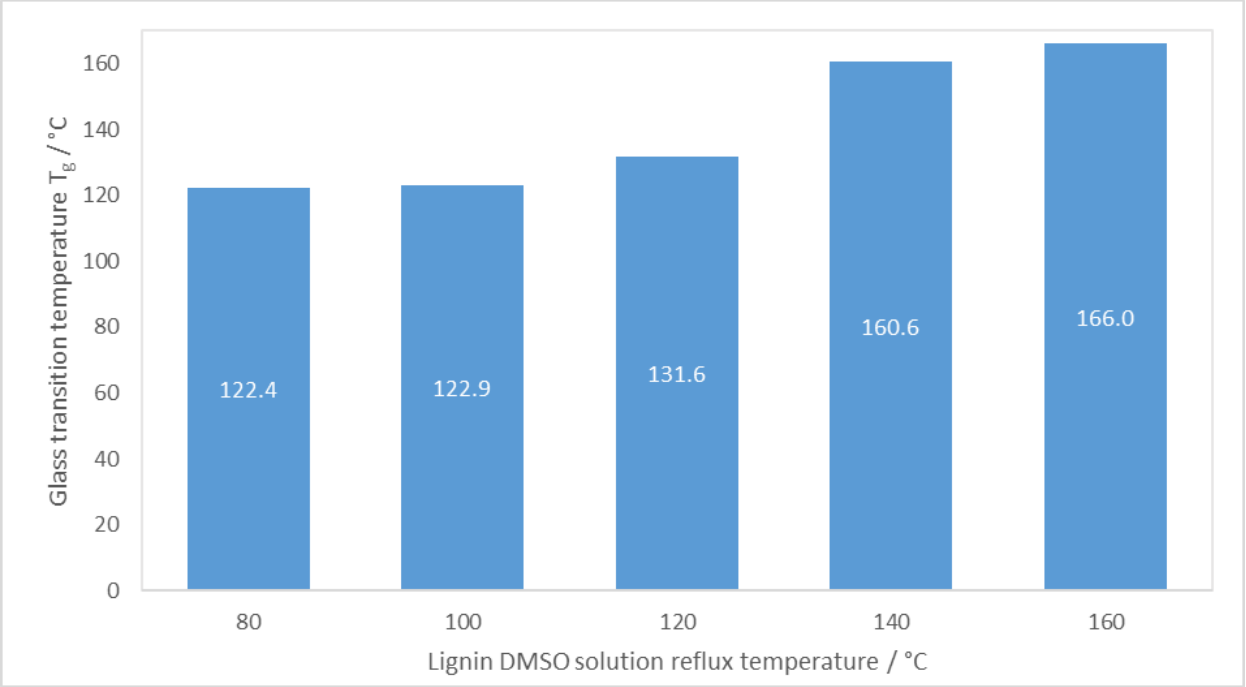

Figure 92. T_g for 1st heating scan for each of the vacuum dried electro-spun lignin fibres at separate reflux temperatures (80, 100, 120, 140 and 160 °C), with trendline of data.

The increase in T_g with reflux temperature highlights the effect of thermal treatment on lignins molecular structure. Higher reflux temperatures likely facilitate dehydration, condensation, and partial cross-linking (see Section 2.2.2), contributing to a more tightly bound polymer network (286,463).

The absence of a clear T_g in the second and third heating scans of the electro-spun lignin fibre samples can be attributed to the extensive thermal exposure the samples experienced prior to DSC analysis. Table 23 presents thermal response across multiple heating cycles for each reflux condition for the vacuum-dried electro-spun lignin fibres. The fibres were subjected to multiple thermal treatments, including reflux heat treatment, electro-spinning in a heated atmosphere, and vacuum drying both before and after spinning.

Table 23. Summary of DSC heating scans (first, second, and third) for vacuum-dried electro-spun lignin fibres refluxed at five different temperatures (80–160 °C).

Reflux temperature / °C	1st heating scan	2nd heating scan	3rd heating scan
80	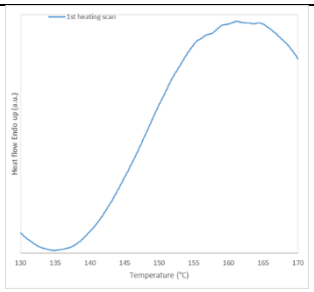	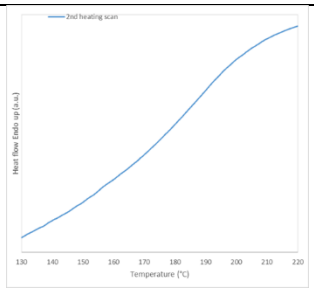	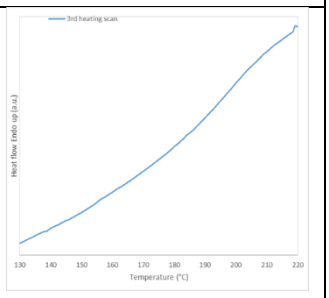
100	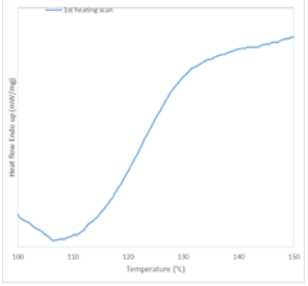	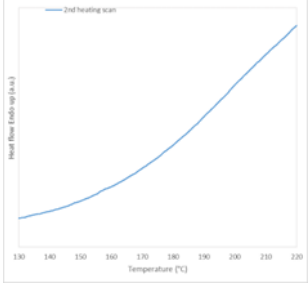	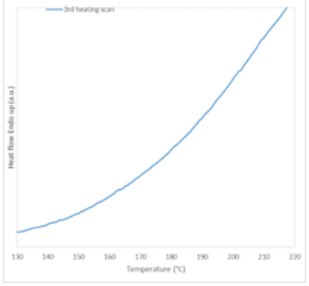
120	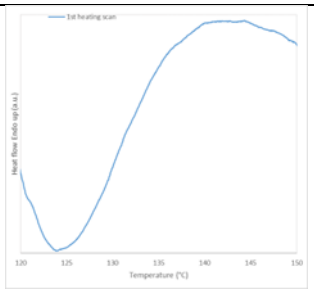	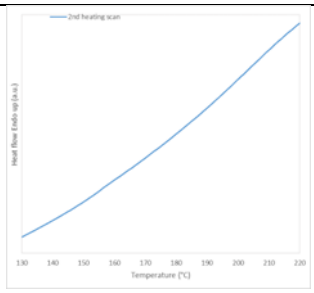	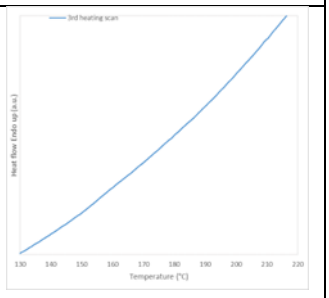
140	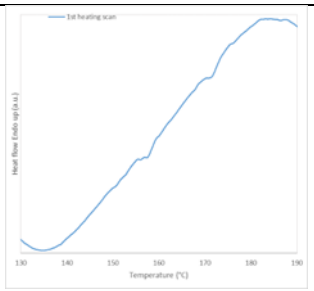	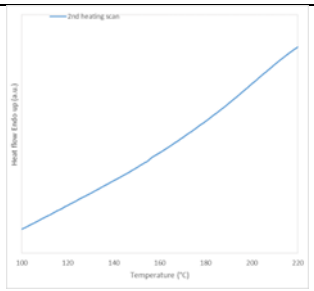	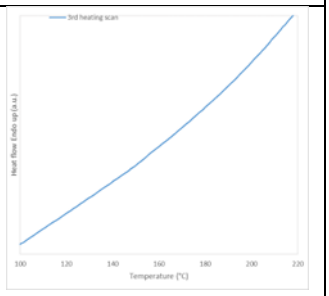
160	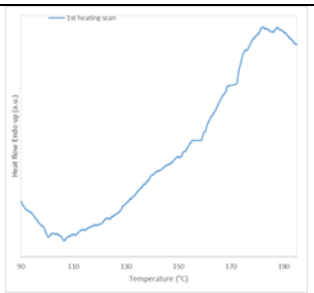	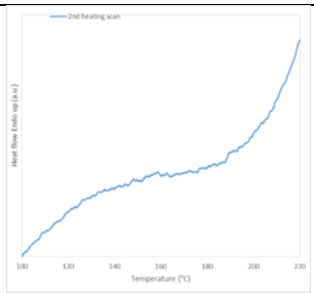	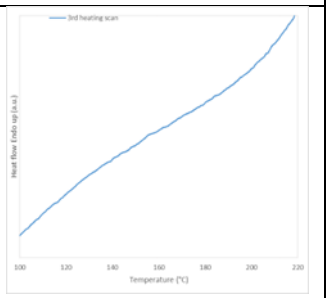

The initial reflux treatment likely promoted condensation, dehydration, and partial cross-linking in the lignin, reducing low-molecular-weight components and moisture while increasing molecular cohesion. Electro-spinning under heated conditions and subsequent vacuum drying of fibres would have removed remaining moisture and promoted additional network formation. By the time of DSC analysis, most thermal relaxation and structural changes had occurred (140,146,435). Shear viscosity of the lignin/DMSO solutions (see Section 4.3.1) increased with reflux temperature, mirroring the trend observed in the T_g of the resulting electro-spun fibres.

Comparing the T_g from DSC analysis for the 1st heating scans, the T_g of as-received lignin powder was 155.3 °C, while vacuum drying at 80 °C for 6 hours increased the T_g to 165.3 °C, suggesting that removal of moisture and volatiles reduced chain mobility (25). In contrast, electro-spun lignin fibres refluxed at lower temperatures (80 °C to 120 °C) exhibited significantly lower T_g values (122.4 °C to 131.6 °C). However, fibres refluxed at higher temperatures (140 °C and 160 °C) showed much higher T_g values (160.6 and 166.0 °C, respectively), comparable to vacuum-dried lignin powder.

Electro-spun lignin fibres refluxed at lower temperatures (80–120 °C) exhibited markedly lower Tg values than the as-received lignin powder, while fibres refluxed at higher temperatures (140–160 °C) showed T_g values approaching that of vacuum-dried lignin powder. This behaviour can be partly explained by the effect of fibre structure; electro-spun fibres generally possess lower packing density and greater free volume than bulk powders, which allows for increased chain mobility and thus a lower T_g (520–522). Supporting GPC analysis of lignin powders, see Section 4.1.7, showed that M_w and PDI increased with higher vacuum drying temperatures (up to 140 °C), suggesting that crosslinking and condensation reactions during heating reduce chain mobility, an effect likely mirrored in the high-temperature refluxed fibres. In contrast, fibres treated at lower reflux temperatures (80–120 °C) may not have undergone sufficient condensation, leaving a lower effective M_w, contributing to the T_g depression observed. This interpretation aligns with literature reporting that reduced M_w in lignin leads to a lower T_g (521,523). The brittle, fragile nature of these lower-temperature refluxed fibres may further indicate incomplete structural stabilisation. Future work should aim to repeat DSC experiments for these samples, as each reflux condition was measured only once due to limited fibre quantities, to confirm these preliminary observations.

The DSC analysis provided valuable insights into the thermal behaviour of both as-received and vacuum-dried lignin, as well as electro-spun lignin fibres. The T_g increased progressively with successive heating scans for both as-received and vacuum-dried lignin. For the electro-spun lignin fibres produced from refluxed lignin/DMSO solutions, the first heating scans revealed a clear trend of increasing T_g with higher reflux temperatures.

4.4.11. TGA of electro-spun lignin fibre

Similar thermal degradation behaviour is observed in the TGA thermograms for the vacuum dried, refluxed electro-spun fibre samples (reflux temperatures 80, 100, 120 and 140 °C), as shown in Figure 93. This mirrors the trend seen in the lignin powder samples, as discussed in Section 4.1.6. However, the onset of degradation in the fibres has shifted to a higher temperature (~400 °C), which is consistent with expectations due to the prior refluxing treatment. The refluxing process likely promoted dehydration, condensation, and partial cross-linking within the lignin structure, leading to the removal of thermally labile components and the formation of more thermally stable linkages (308,406). As a result, the fibres exhibit delayed thermal degradation, indicating increased resistance to thermal breakdown (408). The degradation of the refluxed electro-spun lignin fibres took place in a temperature range between 400-600 °C, with maxima at around 500 °C, as evidenced in the thermogram. Notably, fibres prepared at higher reflux temperatures exhibit less total weight loss, indicating enhanced resistance to thermal degradation.

The electro-spun fibres produced from lignin refluxed at 80 °C showed the highest mass loss at 98.1%, which decreased progressively with increasing reflux temperature to 85.4% at 100 °C, 72.8% at 120 °C, and 63.8% at 140 °C. This trend suggests that reflux heat treatment enhances the thermal stability of lignin fibres, by promoting condensation reactions, increasing the reflux temperature of the lignin solution leads to electro-spun fibres with a higher percentage of weight remaining after thermal degradation, indicating improved resistance to mass loss. Given that the mass loss for the fibre from the 80 °C reflux is substantially higher than the others, this result may be an outlier and warrants repetition in future work to confirm its accuracy.

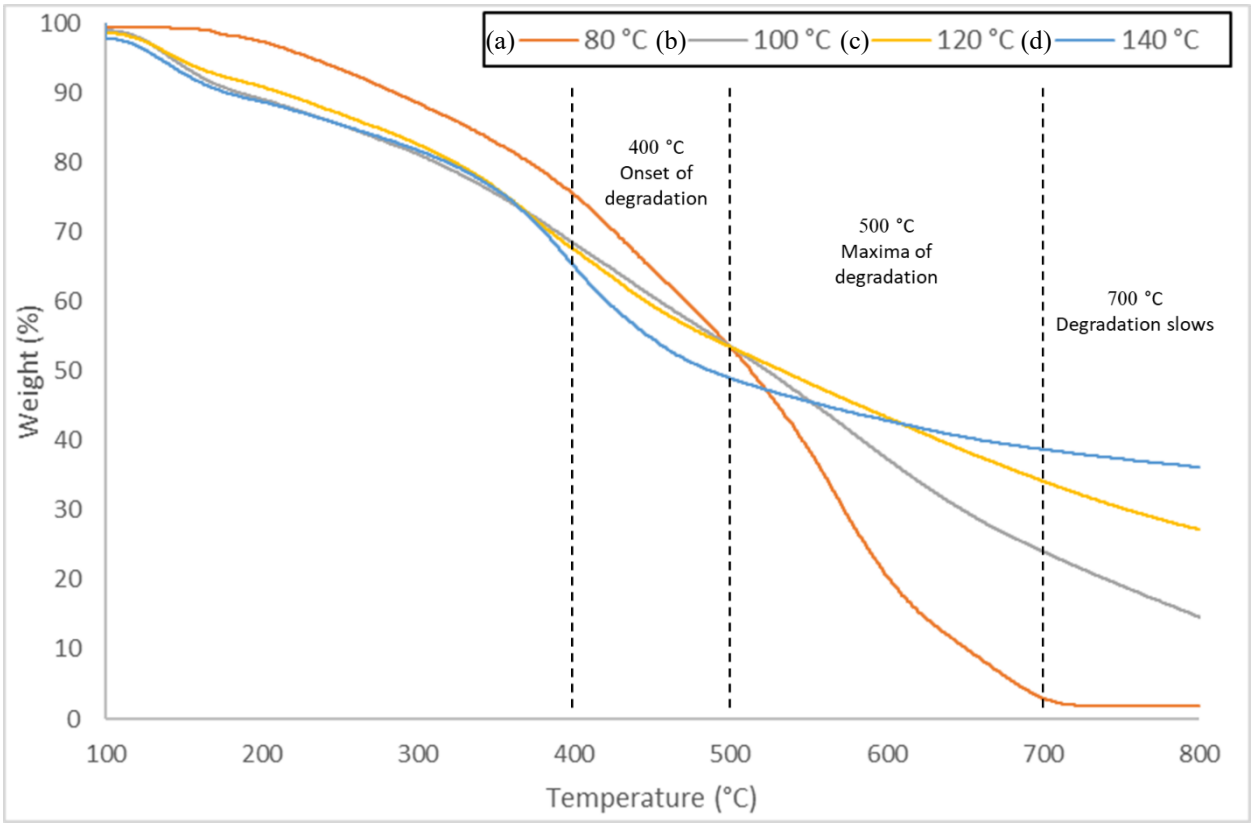

Figure 93. TGA thermogram for the electro-spun lignin fibre from reflux temperatures; (a): 80 °C, (b): 100 °C, (c): 120 °C and (d): 140 °C.

The weight loss data for the electro-spun refluxed lignin fibres shows a clear trend of increasing thermal stability with higher reflux temperatures, but the overall thermal stability of the fibres remains lower than that of the as-received and vacuum-dried lignin powder samples, see Table 24. The total weight loss for the as-received lignin was 61.0%, while the vacuum-dried sample exhibited a slightly lower total mass loss of 58.6%, reflecting improved thermal stability due to the removal of moisture and low-molecular-weight volatiles. In comparison, the electro-spun lignin fibres exhibited higher weight loss percentages, for example, the 120 °C reflux solution electro-spun lignin fibre had a 72.8% weight loss, greater thermal degradation during heating (286,524).

Table 24. Percentage weight loss for the lignin samples from TGA, including temperature at which 50% weight loss occurred.

Lignin sample	Weight loss at 800 °C (%)	Weight loss of 50% at temperature (°C)
As-received powder	61.0	558.0
Vacuum-dried powder (80 °C for 6 hours)	58.6	565.0
Refluxed solution (80 °C for 4 hours) electro-spun fibre	98.1	514.1
Refluxed solution (100 °C for 4 hours) electro-spun fibre	85.4	524.0
Refluxed solution (120 °C for 4 hours) electro-spun fibre	72.8	533.8
Refluxed solution (140 °C for 4 hours) electro-spun fibre	63.8	487.9

The higher weight loss for the electro-spun refluxed lignin fibres compared to the as-received and vacuum-dried lignin powder samples can be attributed to the structural characteristics of electro-spun fibres, which are more fragile and prone to thermal degradation. One factor is the high surface area and thin morphology of electro-spun fibres in comparison to the powder samples. The electro-spinning process produces fibres with a large surface-to-volume ratio, which increases their exposure to heat and oxidative degradation. This makes the fibres more susceptible to rapid thermal decomposition compared to bulk lignin powder, where the heat transfer and degradation occur more gradually due to lower surface exposure (3,525). Additionally, while refluxing typically promotes condensation and cross-linking reactions, the rapid solvent evaporation and jet stretching during electro-spinning can prevent the formation of a fully developed molecular network (245). This leaves behind low-molecular-weight fragments and loosely bound chains that are more prone to thermal breakdown, leading to higher mass loss under heating (135,285). Physical defects introduced during the electro-spinning process may also reduce thermal stability (see Section 4.4.5). Electro-spinning often results in structural imperfections such as bead formation, uneven fibre diameters, and breakage points (526–528). These defects can act as initiation sites for thermal degradation, making the fibres more vulnerable to thermal decomposition (411,492).

4.5. Characterisation of thermostabilised and carbonised electro-spun lignin fibre

Thermally stabilised and carbonised electro-spun lignin fibres were characterised using SEM and XRD. SEM was used to observe morphological changes during thermal treatment. XRD was employed to assess structural changes, during thermal treatment.

4.5.1. SEM of thermostabilised and carbonised electro-spun fibre

The morphological effects of thermostabilisation atmosphere on electro-spun lignin fibres were investigated using SEM, as shown in Figure 94. Both fibre mats were stabilised at 260 °C for 2 hours with a heating rate of 1 °C min^{-1}, under either nitrogen or air atmospheres.

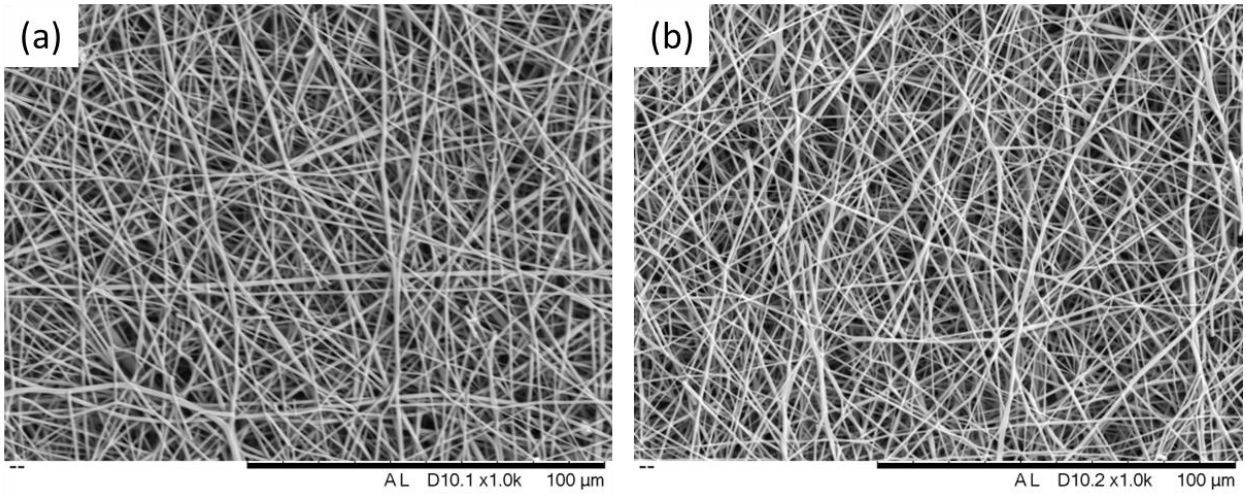

Figure 94. SEM micrographs of electro-spun lignin fibres after thermostabilisation at 260 °C in atmospheres of; (a): dry compressed air and (b): dry nitrogen.

The nitrogen-stabilised fibres exhibited a generally well-preserved, continuous fibrous structure with random orientation, with an average fibre diameter of 735 nm. The fibres remained smooth and uniform with minimal deformation, indicating effective stabilisation under inert conditions. However, some fibre fusion at contact points and occasional breakage were observed, likely due to localised thermal stress or softening during the prolonged heating period (35,262).

In contrast, the air-stabilised fibres showed more pronounced morphological disruption. While the fibrous network remained largely intact, broken fibres and areas of local fusion or flattening were more prevalent. The average fibre diameter increased to 806 nm, which may reflect oxidation-induced swelling, partial cross-linking, or thermal degradation in the oxidative environment (261,263). These features indicate that stabilisation in air introduces greater structural stress, leading to increased fragmentation and less uniform fibre morphology compared to nitrogen-treated fibres. The fibre diameter increased significantly after thermostabilisation in both air (806 nm) and nitrogen (735 nm) compared to the as-electro-spun

fibres (269 nm) produced from the same 100 °C reflux lignin–DMSO solution (see Section 4.4.5). Overall, the comparison highlights that nitrogen provides a more protective environment, allowing for better preservation of fibre morphology during thermostabilisation. In contrast, air induced more significant structural alterations, which may compromise the mechanical integrity of the fibres ahead of carbonisation.

The morphological evolution of electro-spun lignin fibres following carbonisation in a nitrogen atmosphere at 600 °C, 900 °C, and 1200 °C is shown in Figure 95.

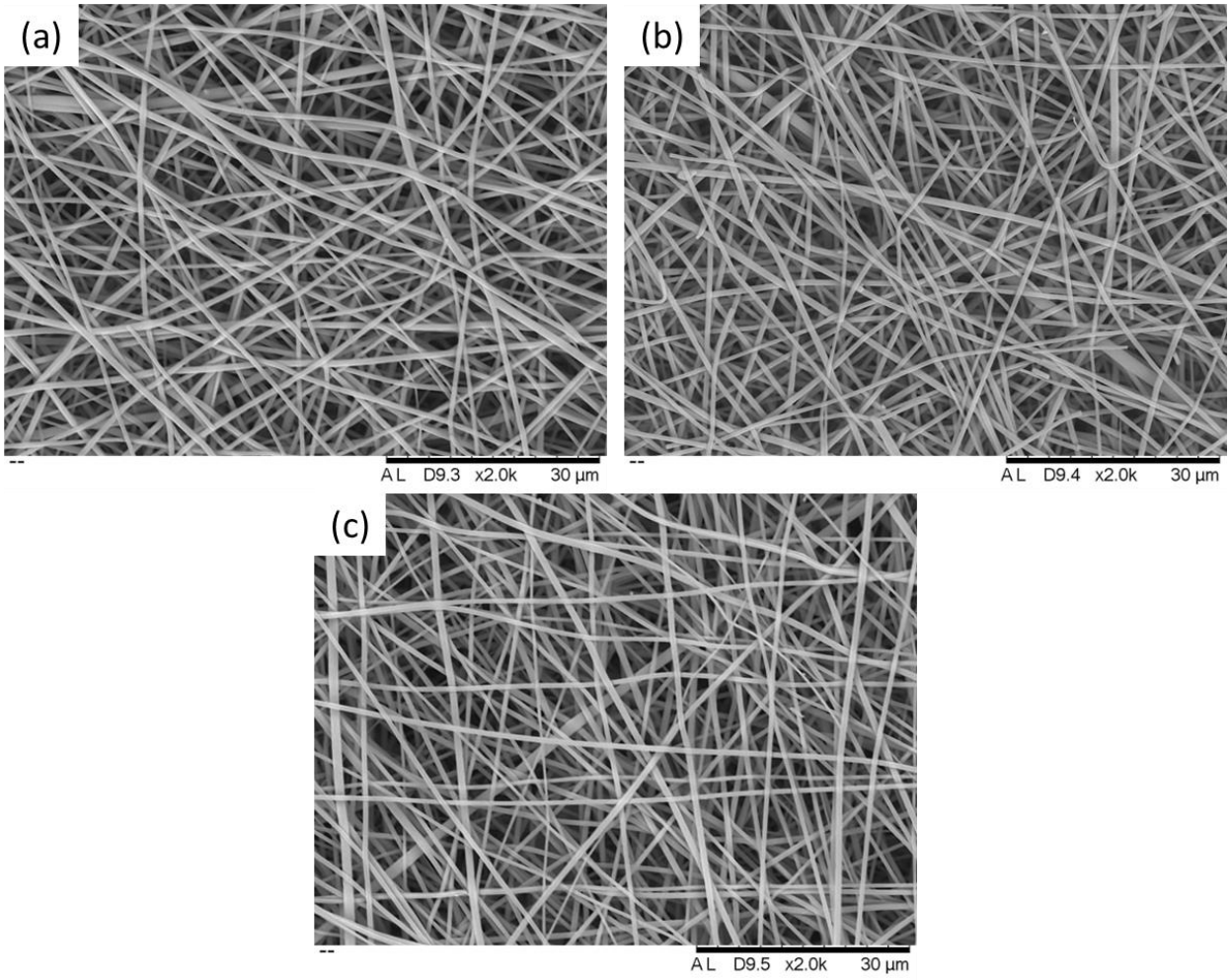

Figure 95. SEM micrographs of electro-spun lignin fibres after carbonisation at different temperatures; (a): 600 °C, (b): 900 °C, and (c): 1200 °C.

All carbonised fibres maintained a randomly oriented, nonwoven fibrous structure with smooth surfaces and no bead formation, indicating successful thermostabilisation prior to carbonisation. However, variations in fibre diameter, integrity, and fragmentation were observed with increasing temperature.

At 600 °C, the fibres exhibited a uniform morphology with an average diameter of 635 nm. The structure remained largely intact, though a small number of broken fibres were observed. This suggests that while carbonisation at this temperature preserves the general architecture, some thermal stress or brittleness may begin to develop.

At 900 °C, the fibres had an increased average diameter of 765 nm and showed more frequent signs of breakage and fragmentation compared to the 600 °C and 1200 °C fibres. In the 1200 °C micrograph, the average fibre diameter slightly decreased to 744 nm, consistent with densification and increased carbon ordering (252,529). While the overall fibre network remained intact and well-preserved, some broken fibres were still evident, suggesting that although high temperature carbonisation treatment promotes structural consolidation, thermal stress can still contribute to occasional fibre failure (160).

In summary, all samples retained their fibrous morphology after carbonisation, but fibre breakage was most pronounced at 900 °C, indicating this temperature may represent a critical threshold for structural transformation. Minor breakage at 600 °C and 1200 °C further highlights the sensitivity of lignin-based fibres to thermal stress across the carbonisation process.

4.5.2. XRD of carbonised lignin fibre

X-ray diffraction was also carried out on carbonised electro-spun lignin fibre samples, each of which was first oxidised in air at a heating rate of 1 °C min^{-1} to 260 °C for 2 hours, followed by carbonisation under nitrogen to final temperatures of 600 °C, 900 °C, and 1200 °C, each held respectively for 2 hours. The XRD patterns for the 600 °C and 900 °C carbonised fibre is displayed in Figure 96.

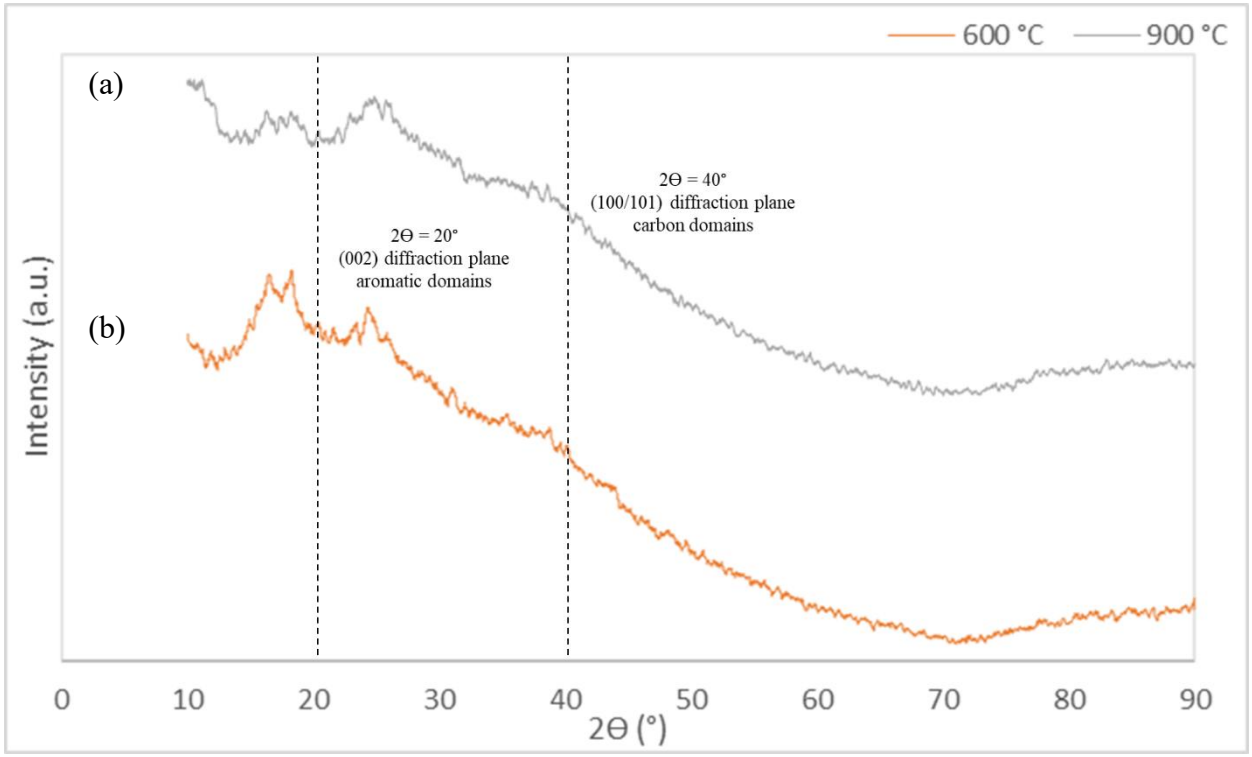

Figure 96. X-ray diffraction pattern for, (a): 900 °C carbonised fibre and (b) 600 °C carbonised fibre, offset by intensity to enable comparison.

All carbonised lignin fibre samples exhibited broad peaks characteristic of disordered carbon, with two key features becoming increasingly defined at higher temperatures. The first, a broad diffraction peak centred around 2Θ = 25.5°, corresponding to the (002) reflection, associated with the stacking of aromatic layers (457). At 600 °C, this peak is broad and diffuse, indicating a predominantly amorphous carbon structure. As the carbonisation temperature increases to 900 °C, the (002) peak becomes noticeably sharper and more intense, reflecting the onset of turbostratic carbon formation and partial alignment of aromatic domains (249,530).
This trend continues at 1200 °C, where the peak shows the greatest intensity and definition at 2Θ = 25.5°, shown in Figure 97, suggesting improved structural ordering and development of graphitic-like layers (283).

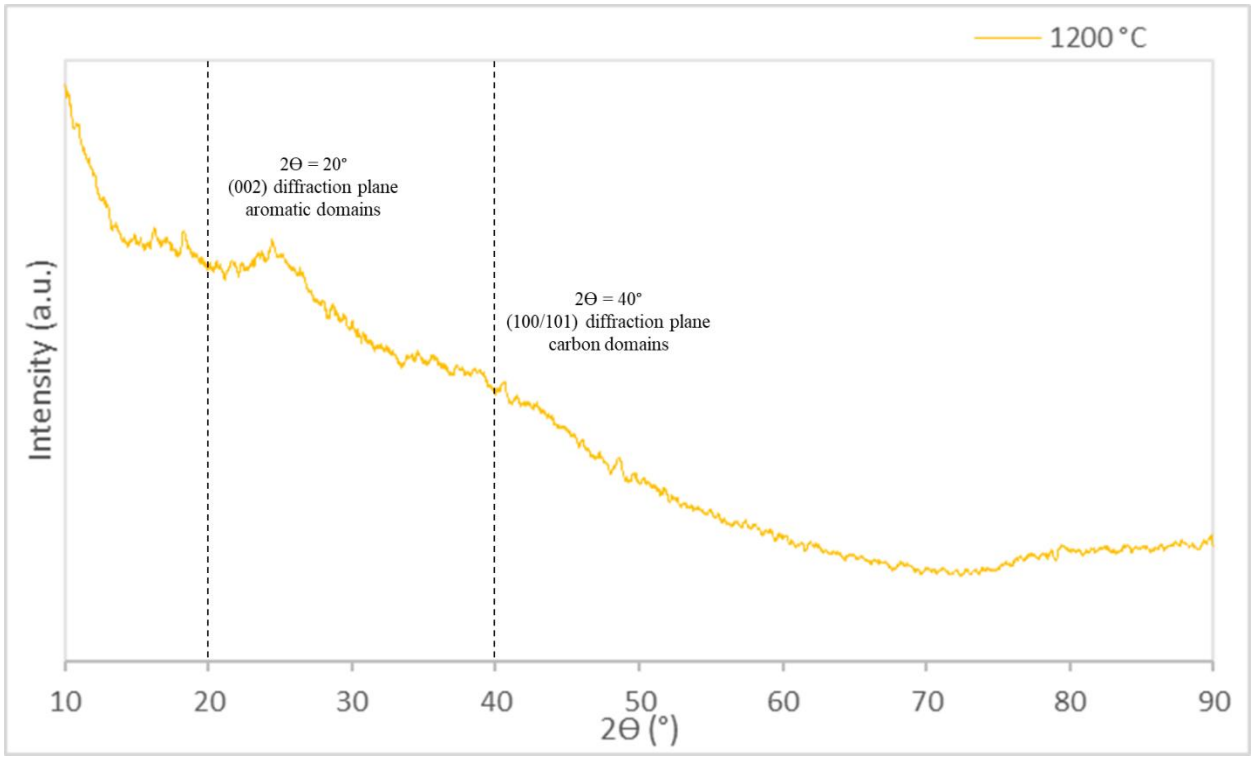

Figure 97. X-ray diffraction pattern for the 1200 °C carbonised lignin fibre.

A second feature, a weaker diffraction signal near 2Θ = 40°, corresponds to the (100/101) reflections, related to in-plane ordering within the carbon structure. A subtle rise in intensity around 2Θ = 80°, corresponding to the (110) reflection of graphitic carbon, was observed consistently in all three carbonised fibre samples (600 °C, 900 °C, and 1200 °C), but was notably absent in the as-received and vacuum-dried lignin powders, indicating that this feature emerges only after high-temperature carbonisation (267,278).

X-ray diffraction analysis confirmed that the as-received and vacuum-dried lignin powders exhibit typical amorphous scattering patterns, with no evidence of long-range structural order. Upon carbonisation, the electro-spun lignin fibres developed increasingly defined (002) and (100)/(101) diffraction features with rising temperature, consistent with the formation of turbostratic and partially graphitised carbon structures (283). The appearance of a weak (110) reflection near 2Θ = 80° in all carbonised samples further suggests the onset of higher-order graphitic stacking, particularly at 1200 °C. Overall, these results imply that thermal treatment promotes structural reorganisation, transitioning lignin from a disordered polymeric material into a more ordered carbon framework.

5. Conclusions

This thesis has successfully demonstrated the production of aligned neat lignin fibres using 100% (w/v) lignin dissolved in a single-solvent system of dimethyl sulfoxide (DMSO). The ability to electro-spin neat lignin fibres without the need for a co-polymer represents a significant advancement in lignin-based fibre production and sustainable material development. Through a systematic investigation of lignin solution properties and fibre characterisation, the influence of processing conditions and thermal treatment on fibre formation from electro-spinning was thoroughly explored.

Aligned neat lignin fibres were successfully produced from lignin/DMSO solutions using a novel Vee-shield method, which enabled the fabrication of highly aligned fibres (see Section 4.4.6). The electro-spinning process was optimised by adjusting solution viscosity and electro-spinning temperature to minimise bead formation and maximise fibre uniformity (see Section 4.4.4). The production of smooth, continuous fibres from 100% (w/v) neat lignin in DMSO underscores the importance of achieving an optimal balance between solution viscosity, chain entanglement, and conductivity for successful jet formation and fibre deposition.

Rheological analysis provided key insights into the flow behaviour of lignin/DMSO solutions, highlighting the impact of lignin concentration and reflux temperature on solution viscosity. Shear solution viscosity increased with lignin content, rising from 0.17 Pa·s at 50% (w/v) to 3.68 Pa·s at 90% (w/v), indicating increased molecular interactions and chain entanglement at higher lignin concentrations. Reflux temperature also influenced solution viscosity, with viscosity increasing from 1.35 Pa·s at 80 °C to 4.24 Pa·s at 160 °C, induced by higher reflux temperatures. The viscosity ramp data showed a decrease in viscosity with increasing temperature, explaining why electro-spinning at elevated temperatures (55 °C) facilitated smoother fibre formation (see Section 4.3.1).

Conductivity analysis showed that lignin/DMSO solution conductivity increased with both lignin concentration and reflux temperature, with higher reflux temperatures leading to increased ionic mobility and enhanced charge transport. This enhanced conductivity contributed to improved jet stability during electro-spinning, supporting the formation of smooth, aligned fibres. Conductivity measurements of DMSO alone demonstrated a clear increase with temperature, confirming the effect of enhanced molecular mobility on charge transport in the spinning solution (see Section 4.3.2).

FTIR and NMR analysis confirmed the retention of key functional groups and aromatic structures within the electro-spun lignin fibres. FTIR spectra showed the presence of hydroxyl, methoxy, and carbonyl groups characteristic of lignin, with shifts in peak intensity and position suggesting reduced free hydroxyl content following reflux and electro-spinning (see Section 4.4.8). NMR analysis further validated the retention of aromatic integrity and the formation of condensed structures at higher reflux temperatures, supporting increased thermal and structural stability (see Section 4.4.9).

XRD analysis revealed that carbonisation led to increasing structural order in electro-spun lignin fibres, with sharper (002) peaks and the emergence of (100)/(101) and (110) reflections at higher temperatures. These changes indicate a gradual transition from amorphous to partially graphitised carbon, particularly pronounced at 1200 °C (see Section 4.5.2). GPC analysis revealed that vacuum drying lignin at increasing temperatures led to a gradual rise in both the number-average and weight-average molecular weights of lignin, as well as the polydispersity (see Section 4.1.7). This behaviour is attributed to thermally induced condensation and possible cross-linking reactions, which result in a broader and more cohesive molecular structure. These findings help explain why lignin pre-treated at higher temperatures exhibited improved fibre formation and spinnability.

DSC analysis demonstrated that the glass transition temperature (T_g) of lignin increased with reflux temperature. T_g increased from 122.4 °C at 80 °C reflux to 166.0 °C at 160 °C reflux. For electro-spun fibres, a T_g was only observed during the first heating scan, with no transition in subsequent scans. This suggests that the combined effects of reflux treatment, electro-spinning, and vacuum drying resulted in extensive molecular stabilisation, eliminating further structural relaxation upon heating.

TGA analysis revealed that electro-spun lignin fibres exhibited lower overall thermal stability than as-received and vacuum-dried lignin, with mass loss decreasing from 98.1% at 80 °C reflux to 63.8% at 160 °C reflux. This reduction in thermal stability is likely due to the high surface area and reduced cross-link density within the fibres, which makes them more susceptible to thermal degradation compared to bulk lignin samples. However, the trend of increasing thermal stability with higher reflux temperatures confirms that thermal treatment enhances structural integrity and also reduced mass loss during thermal decomposition (see Section 4.4.11).

SEM imaging confirmed the successful production of smooth, aligned electro-spun lignin fibres at reflux temperatures of 140 °C, see Figure 81. At lower lignin concentrations (50–60% (w/v)), bead formation was observed due to insufficient chain entanglement. However, at higher lignin concentrations (75–100% (w/v)), increased viscosity and molecular cohesion facilitated the formation of continuous, bead-free fibres (see Section 4.4.2). Reflux-treated solutions produced finer, more uniform fibres, with increased alignment and reduced defects at higher reflux temperatures (see Section 4.4.6).

Electro-spun neat lignin fibres were successfully thermostabilised and carbonised, as confirmed by SEM analysis (see Section 4.5.1). The fibres retained a continuous, nonwoven structure throughout thermal treatment, with nitrogen providing better morphological preservation during stabilisation than air. Following carbonisation at 600 °C, 900 °C, and 1200 °C, all samples maintained fibrous integrity, demonstrating thermal stability and resilience under controlled treatment conditions.

6. Recommendations for future work

This work has demonstrated that neat lignin, dissolved in DMSO, can be electro-spun into continuous, aligned fibres without the need for co-polymers or additives. The successful optimisation of solution properties including viscosity and conductivity; and thermal stability through reflux treatment establishes a foundation for producing sustainable, bio-based lignin fibres with enhanced structural integrity and thermal performance.

Future research should focus on further refining the electro-spinning process to enhance fibre uniformity and mechanical strength. Investigating the effect of different lignin sources and refining post-spinning stabilisation techniques could further improve the performance and applicability of lignin-based fibres. Additionally, exploring alternative solvents and functionalisation strategies may enable the production of lignin fibres with tailored mechanical, thermal, and chemical properties, expanding their potential for high-performance bio-based applications. Further studies should also examine the impact of thermostabilisation conditions on fibre fusion. As observed, stabilisation under nitrogen can promote controlled fibre interconnection, which may significantly improve the morphology of resulting carbon fibres. Additional characterisation of the carbonised electro-spun neat lignin fibres, both pre- and post-carbonisation, particularly their mechanical strength, electrical conductivity, and surface area; would provide valuable insights into their potential applications as lignin-derived carbon materials.

This study marks a significant step forward in neat lignin-based fibre production, showcasing the potential of lignin as a sustainable, renewable resource for advanced materials and reinforcing its viability for use in high-performance applications.

7. List of References

1. Lu F, Ralph J. Lignin. In: Cereal Straw as a Resource for Sustainable Biomaterials and Biofuels: Chemistry, Extractives, Lignins, Hemicelluloses and Cellulose [Internet]. Elsevier; 2010 [cited 2024 Apr 11]. p. 169–207. Available from: https://doi.org/10.1016/B978-0-444-53234-3.00006-7

2. Cho MJ, Ji L, Liu LY, M. Johnson A, Potter S, Mansfield SD, et al. High performance electrospun carbon nanofiber mats derived from flax lignin. Ind Crops Prod [Internet]. 2020 Nov 1 [cited 2022 Mar 21];155. Available from: https://doi.org/10.1016/j.indcrop.2020.112833

3. Grothe T, Storck JL, Dotter M, Ehrmann A. Impact of solid content in the electrospinning solution on the physical and chemical properties of polyacrylonitrile (Pan) nanofibrous mats. Tekstilec [Internet]. 2020 [cited 2022 Feb 22];63(3):225–32. Available from: https://doi.org/10.14502/Tekstilec2020.63.225-232

4. Bhardwaj N, Kundu SC. Electrospinning: A fascinating fiber fabrication technique [Internet]. Vol. 28, Biotechnology Advances. Elsevier; 2010 [cited 2024 Mar 28]. p. 325–47. Available from: https://doi.org/10.1016/j.biotechadv.2010.01.004

5. Toriello M, Afsari M, Shon HK, Tijing LD. Progress on the fabrication and application of electrospun nanofiber composites [Internet]. Vol. 10, Membranes. MDPI AG; 2020 [cited 2024 Nov 22]. p. 1–35. Available from: https://pmc.ncbi.nlm.nih.gov/articles/PMC7559347/

6. Burger C, Hsiao BS, Chu B. Nanofibrous materials and their applications [Internet]. Vol. 36, Annual Review of Materials Research. Annual Reviews; 2006 [cited 2024 Mar 28]. p. 333–68. Available from: https://www.annualreviews.org/content/journals/10.1146/annurev.matsci.36.011205.123537

7. Guo Y, Wang X, Shen Y, Dong K, Shen L, Alzalab AAA. Research progress, models and simulation of electrospinning technology: a review [Internet]. Vol. 57, Journal of Materials Science. Springer; 2022 [cited 2024 Feb 20]. p. 58–104. Available from: https://link.springer.com/article/10.1007/s10853-021-06575-w

8. Huang X. Fabrication and properties of carbon fibers [Internet]. Vol. 2, Materials. Molecular Diversity Preservation International; 2009 [cited 2023 Apr 24]. p. 2369–403. Available from: http://www.mdpi.com/1996-1944/2/4/2369/

9. Braun JL, Holtman KM, Kadla JF. Lignin-based carbon fibers: Oxidative thermostabilization of kraft lignin. Carbon N Y [Internet]. 2005 Jan;43(2):385–94. Available from: https://doi.org/10.1016/j.carbon.2004.09.027

10. Maradur SP, Kim CH, Kim SY, Kim BH, Kim WC, Yang KS. Preparation of carbon fibers from a lignin copolymer with polyacrylonitrile. Synth Met [Internet]. 2012 [cited 2022 Mar 4];162(5–6):453–9. Available from: https://doi.org/10.1016/j.synthmet.2012.01.017

11. Melro E, Alves L, Antunes FE, Medronho B. A brief overview on lignin dissolution [Internet]. Vol. 265, Journal of Molecular Liquids. Elsevier; 2018 [cited 2023 Oct 19]. p. 578–84. Available from: https://doi.org/10.1016/j.molliq.2018.06.021

12. Li S, Lundquist K. A new method for the analysis of phenolic groups in lignins by ′H NMR spectrometry. Nord Pulp Pap Res J [Internet]. 1994 Aug 1 [cited 2022 Aug 12];9(3):191–5. Available from: https://www.degruyter.com/document/doi/10.3183/npprj-1994-09-03-p191-195/html?lang=en

13. Ramakrishna S, Fujihara K, Teo WE, Lim TC, Ma Z. An introduction to electrospinning and nanofibers. An Introduction to Electrospinning and Nanofibers. World Scientific Publishing Co.; 2005. 1–382 p.

14. Kadla JF, Kubo S. Lignin-based polymer blends: analysis of intermolecular interactions in lignin–synthetic polymer blends. Compos Part A Appl Sci Manuf. 2004 Mar 1;35(3):395–400.

15. Orfão JJM, Antunes FJA, Figueiredo JL. Pyrolysis kinetics of lignocellulosic materials - Three independent reactions model. Fuel. 1999 Feb 1;78(3):349–58.

16. Mazoochi T, Hamadanian M, Ahmadi M, Jabbari V. Investigation on the morphological characteristics of nanofiberous membrane as electrospun in the different processing parameters. Int J Ind Chem. 2012;3(1):1–8.

17. Deitzel JM, Kleinmeyer J, Harris D, Beck Tan NC. The effect of processing variables on

the morphology of electrospun nanofibers and textiles. Polymer (Guildf). 2001 Jan 1;42(1):261–72.

18. Wang S, Bai J, Innocent MT, Wang Q, Xiang H, Tang J, et al. Lignin-based carbon fibers: Formation, modification and potential applications. Vol. 7, Green Energy and Environment. Elsevier; 2021. p. 578–605.

19. Shao S, Ma T, Fernando GF. Electro-spinning of highly-aligned polyacrylonitrile nano-fibres with continuous spooling. Sci Rep [Internet]. 2021 Nov 5 [cited 2022 Feb 16];11(1):21713. Available from: https://www.nature.com/articles/s41598-021-99890-w

20. Zargham S, Bazgir S, Tavakoli A, Rashidi AS, Damerchely R. The Effect of Flow Rate on Morphology and Deposition Area of Electrospun Nylon 6 Nanofiber. 2012;7(4):42–9.

21. Singh N, Singhania RR, Nigam PS, Dong C Di, Patel AK, Puri M. Global status of lignocellulosic biorefinery: Challenges and perspectives [Internet]. Vol. 344, Bioresource Technology. Elsevier; 2022 [cited 2024 May 21]. p. 126415. Available from: https://doi.org/10.1016/j.biortech.2021.126415

22. Evans RJ, Milne TA, Soltys MN. Direct mass-spectrometric studies of the pyrolysis of carbonaceous fuels. III. Primary pyrolysis of lignin. J Anal Appl Pyrolysis [Internet]. 1986;9(3):207–36. Available from: https://doi.org/10.1016/0165-2370(86)80012-2

23. Rytioja J, Hildén K, Yuzon J, Hatakka A, de Vries RP, Mäkelä MR. Plant-Polysaccharide-Degrading Enzymes from Basidiomycetes. Microbiol Mol Biol Rev [Internet]. 2014 Dec [cited 2025 May 20];78(4):614–49. Available from: https://doi.org/10.1128/mmbr.00035-14

24. Chang H m., Li J. Isolation of Lignin from Wood. Bachelor's Thesis. 2011;1(1):57.

25. Watkins D, Nuruddin M, Hosur M, Tcherbi-Narteh A, Jeelani S. Extraction and characterization of lignin from different biomass resources. J Mater Res Technol [Internet]. 2015 Jan 1 [cited 2024 Apr 30];4(1):26–32. Available from: www.sciencedirect.com

26. Yoo CG, Meng X, Pu Y, Ragauskas AJ. The critical role of lignin in lignocellulosic biomass conversion and recent pretreatment strategies: A comprehensive review [Internet]. Vol. 301, Bioresource Technology. Elsevier; 2020 [cited 2023 May 15]. p.

122784. Available from: https://doi.org/10.1016/j.biortech.2020.122784

27. Yang H, Yan R, Chen H, Lee DH, Zheng C. Characteristics of hemicellulose, cellulose and lignin pyrolysis. Fuel [Internet]. 2007 Aug 1 [cited 2024 Nov 8];86(12–13):1781–8. Available from: https://www.researchgate.net/publication/229343954_Characteristics_of_Hemicellulose_Cellulose_and_Lignin_Pyrolysis

28. Carvajal JC, Gómez Á, Cardona CA. Comparison of lignin extraction processes: Economic and environmental assessment. Bioresour Technol [Internet]. 2016 Aug 1;214:468–76. Available from: https://doi.org/10.1016/j.biortech.2016.04.103

29. Sun RC. Lignin Source and Structural Characterization [Internet]. Vol. 13, ChemSusChem. John Wiley & Sons, Ltd; 2020 [cited 2024 Apr 10]. p. 4385–93. Available from: https://onlinelibrary.wiley.com/doi/full/10.1002/cssc.202001324

30. Liu WJ, Yu HQ. Thermochemical Conversion of Lignocellulosic Biomass into Mass-Producible Fuels: Emerging Technology Progress and Environmental Sustainability Evaluation. Vol. 2, ACS Environmental Au. American Chemical Society; 2022. p. 98–114.

31. Vanholme R, Demedts B, Morreel K, Ralph J, Boerjan W. Lignin Biosynthesis and Structure. Plant Physiol [Internet]. 2010 [cited 2017 Oct 24];153(3):895–905. Available from: https://doi.org/10.1104/pp.110.155119

32. Pettersen RC. The Chemical Composition of Wood. In 1984. p. 57–126. Available from: https://doi.org/10.1021/ba-1984-0207.ch002

33. Asmadi M, Kawamoto H, Saka S. Characteristics of softwood and hardwood pyrolysis in an ampoule reactor. J Anal Appl Pyrolysis [Internet]. 2017;124:523–35. Available from: https://doi.org/10.1016/j.jaap.2017.01.029

34. Obst JR, Ralph J. Characterization of hardwood lignin: Investigation of syringyl/guaiacyl composition by13C nuclear magnetic resonance spectroscopy. Holzforschung [Internet]. 1983 [cited 2022 Aug 18];37(6):297–302. Available from: https://doi.org/10.1515/hfsg.1983.37.6.297

35. Fang W, Yang S, Wang XL, Yuan TQ, Sun RC. Manufacture and application of lignin-

based carbon fibers (LCFs) and lignin-based carbon nanofibers (LCNFs). Green Chem [Internet]. 2017;19(8):1794–827. Available from: https://doi.org/10.1039/C6GC03206K

36. Sette M, Wechselberger R, Crestini C. Elucidation of lignin structure by quantitative 2D NMR. Chem - A Eur J [Internet]. 2011 Aug 16 [cited 2022 Aug 1];17(34):9529–35. Available from: https://doi.org/10.1002/chem.201003045

37. Lourenço A, Pereira H. Compositional Variability of Lignin in Biomass. In: Lignin - Trends and Applications [Internet]. IntechOpen; 2018 [cited 2022 May 30]. Available from: https://doi.org/10.5772/intechopen.71208

38. Nimz HH, Nemr M, Robert D, Faix O. Carbon-13 NMR spectra of lignins. Structural differences between lignins of hardwoods, softwoods, grasses and compression wood. Holzforschung [Internet]. 1981 [cited 2022 Aug 15];35(1):16–26. Available from: https://doi.org/10.1515/hfsg.1981.35.1.16

39. Lancefield CS, Westwood NJ. The synthesis and analysis of advanced lignin model polymers. Green Chem [Internet]. 2015 Aug 3 [cited 2023 May 10];17(11):4980–90. Available from: https://doi.org/10.1039/c5gc01334h

40. Silva TCF, Santos RB, Jameel H, Colodette JL, Lucia LA. Quantitative molecular structure-pyrolytic energy correlation for hardwood lignins. Energy and Fuels [Internet]. 2012 Feb 16 [cited 2022 Aug 18];26(2):1315–22. Available from: https://pubs.acs.org/doi/full/10.1021/ef2014869

41. Naron DR, Collard FX, Tyhoda L, Görgens JF. Characterisation of lignins from different sources by appropriate analytical methods: Introducing thermogravimetric analysis-thermal desorption-gas chromatography–mass spectroscopy. Ind Crops Prod [Internet]. 2017 Jul 1;101:61–74. Available from: https://doi.org/10.1016/j.indcrop.2017.02.041

42. Schutyser W, Renders T, Van den Bossche G, Van den Bosch S, Koelewijn S, Ennaert T, et al. Catalysis in Lignocellulosic Biorefineries: The Case of Lignin Conversion. In: Nanotechnology in Catalysis [Internet]. Wiley; 2017 [cited 2024 Jul 22]. p. 537–84. Available from: https://www.researchgate.net/publication/318158851_Catalysis_in_Lignocellulosic_Biorefineries_The_Case_of_Lignin_Conversion_Applications_in_the_Chemical_Industry_Energy_Development_and_Environment_Protection

43. Du B, Zhu H, Chai L, Cheng J, Wang X, Chen X, et al. Effect of lignin structure in different biomass resources on the performance of lignin-based carbon nanofibers as supercapacitor electrode. Ind Crops Prod [Internet]. 2021 [cited 2022 Mar 30];170. Available from: https://doi.org/10.1016/j.indcrop.2021.113745

44. K. M. Holtman. An Investigation of The Milled Wood Lignin Isolation Procedure by Solution and Solid State NMR Spectroscopy. Wood Pap Sci [Internet]. 2003 Feb 22;Cap. 2. Available from: http://www.lib.ncsu.edu/resolver/1840.16/5436

45. Lochab B, Shukla S, Varma IK. Naturally occurring phenolic sources: Monomers and polymers. RSC Adv [Internet]. 2014 [cited 2023 Apr 24];4(42):21712–52. Available from: www.rsc.org/advances

46. Stewart JJ, Akiyama T, Chapple C, Ralph J, Mansfield SD. The effects on lignin structure of overexpression of ferulate 5-hydroxylase in hybrid poplar1[W]. Plant Physiol [Internet]. 2009 [cited 2023 Apr 24];150(2):621–35. Available from: www.plantphysiol.org/cgi/doi/10.1104/pp.109.137059

47. Liu CJ. Deciphering the enigma of lignification: Precursor transport, oxidation, and the topochemistry of lignin assembly. In: Molecular Plant [Internet]. Oxford University Press; 2012 [cited 2023 Apr 24]. p. 304–17. Available from: https://doi.org/10.1093/mp/ssr121

48. Beste A. ReaxFF study of the oxidation of lignin model compounds for the most common linkages in softwood in view of carbon fiber production. J Phys Chem A [Internet]. 2014 [cited 2023 Apr 24];118(5):803–14. Available from: https://doi.org/10.1021/jp410454q

49. Varila T, Romar H, Luukkonen T, Hilli T, Lassi U. Characterization of lignin enforced tannin/furanic foams. Heliyon [Internet]. 2020 Jan 1 [cited 2023 May 10];6(1). Available from: https://doi.org/10.1016/j.heliyon.2020.e03228

50. Mccarthy JL, Islam A. Lignin Chemistry, Technology, and Utilization: A Brief History. 2000 [cited 2023 May 11]; Available from: https://doi.org/10.1021/bk-2000-0742.ch001

51. Evstigneev EI. Factors affecting lignin solubility. Russ J Appl Chem [Internet]. 2011 Jun 16;84(6):1040–5. Available from: https://doi.org/10.1134/S1070427211060243

52. Evstigneyev EI, Shevchenko SM. Structure, chemical reactivity and solubility of lignin: a fresh look. Wood Sci Technol [Internet]. 2019 Jan 24 [cited 2023 May 10];53(1):7–47.

Available from: https://link.springer.com/article/10.1007/s00226-018-1059-1

53. Li Y, Shuai L, Kim H, Motagamwala AH, Mobley JK, Yue F, et al. An ideal lignin facilitates full biomass utilization. Sci Adv [Internet]. 2018 [cited 2023 May 10];4(9). Available from: https://doi.org/10.1126/sciadv.aau2968

54. Meng LY, Kang SUM, Zhang XM, Yu-Ying WU, Sun RC. Isolation and physico-chemical characterization of lignin from hybrid poplar in dmso/licl system induced by microwave-assisted irradiation. Cellul Chem Technol [Internet]. 2012 [cited 2023 Jan 23];46(5–6):409–18. Available from: https://bioresources.cnr.ncsu.edu/resources/isolation-and-physico-chemical-characterization-of-lignins-from-ultrasound-irradiated-fast-growing-poplar-wood/

55. Mottweiler J, Rinesch T, Besson C, Buendia J, Bolm C. Iron-catalysed oxidative cleavage of lignin and β-O-4 lignin model compounds with peroxides in DMSO. Green Chem [Internet]. 2015 [cited 2023 Jan 17];17(11):5001–8. Available from: https://doi.org/10.1039/c5gc01306b

56. van Parijs FRD, Morreel K, Ralph J, Boerjan W, Merks RMH. Modeling Lignin Polymerization. I. Simulation Model of Dehydrogenation Polymers. Plant Physiol [Internet]. 2010;153(3):1332–44. Available from: https://doi.org/10.1104/pp.110.154468

57. Chatel G, Rogers RD. Review: Oxidation of lignin using ionic liquids-an innovative strategy to produce renewable chemicals [Internet]. Vol. 2, ACS Sustainable Chemistry and Engineering. 2014 [cited 2023 Apr 26]. p. 322–39. Available from: https://doi.org/10.1021/sc4004086

58. Zhang Y, Huo F, Wang Y, Xia Y, Tan X, Zhang S, et al. Theoretical elucidation of β-O-4 bond cleavage of lignin model compound promoted by sulfonic acid-functionalized ionic liquid. Front Chem [Internet]. 2019 Feb 15 [cited 2023 Apr 26];7(FEB):78. Available from: https://doi.org/10.3389/fchem.2019.00078

59. Zemek J, Košíková B, Augustín J, Joniak D. Antibiotic properties of lignin components. Folia Microbiol (Praha) [Internet]. 1979 Dec [cited 2023 Nov 9];24(6):483–6. Available from: https://pubmed.ncbi.nlm.nih.gov/389763/

60. Jung HG, Fahey GC. Nutritional Implications of Phenolic Monomers and Lignin: a

Review. J Anim Sci [Internet]. 1983 Jul 1 [cited 2023 Nov 9];57(1):206–19. Available from: https://dx.doi.org/10.2527/jas1983.571206x

61. Grima-Pettenati J, Goffner D. Lignin genetic engineering revisited [Internet]. Vol. 145, Plant Science. 1999 [cited 2023 Nov 9]. p. 51–65. Available from: https://www.academia.edu/10027642/Lignin_genetic_engineering

62. Baurhoo B, Ruiz-Feria CA, Zhao X. Purified lignin: Nutritional and health impacts on farm animals-A review [Internet]. Vol. 144, Animal Feed Science and Technology. 2008 [cited 2023 Nov 9]. p. 175–84. Available from: https://doi.org/10.1016/j.anifeedsci.2007.10.016

63. Ding L, Gruber JN, Ray AE, Donohoe BS, Li C. Distribution of Bound and Free Water in Anatomical Fractions of Pine Residues and Corn Stover as a Function of Biological Degradation. ACS Sustain Chem Eng [Internet]. 2021 Nov 29 [cited 2023 Aug 14];9(47):15884–96. Available from: https://doi.org/10.1021/acssuschemeng.1c05606

64. Davies GC, Bruce DM. Effect of Environmental Relative Humidity and Damage on the Tensile Properties of Flax and Nettle Fibers. Text Res J [Internet]. 1998 Sep 1 [cited 2023 Aug 30];68(9):623–9. Available from: https://journals.sagepub.com/doi/10.1177/004051759806800901

65. Pejic BM, Kostic MM, Skundric PD, Praskalo JZ. The effects of hemicelluloses and lignin removal on water uptake behavior of hemp fibers. Bioresour Technol [Internet]. 2008 Oct 1 [cited 2023 Aug 30];99(15):7152–9. Available from: https://doi.org/10.1016/j.biortech.2007.12.073

66. Machmudah S, Wicaksono DT, Happy M, Winardi S, Wahyudiono, Kanda H, et al. Water removal from wood biomass by liquefied dimethyl ether for enhancing heating value. Energy Reports [Internet]. 2020 [cited 2023 Aug 14];6:824–31. Available from: https://doi.org/10.1016/j.egyr.2020.04.006

67. Rowell R. Taylor & Francis Group. 2005 [cited 2023 Aug 14]. Handbook of Wood Chemistry and Wood Composites, Second Edition - Google Books. Available from: https://books.google.co.uk/books?hl=en&lr=&id=QMn6rsl_PPgC&oi=fnd&pg=PP1&ots=oF_RQQMLG-&sig=7uySTnvbgL2kxqKuqtTV25RQxTc&redir_esc=y#v=onepage&q&f=false

68. Cousins WJ. Elastic modulus of lignin as related to moisture content. Wood Sci Technol [Internet]. 1976 Mar [cited 2023 Aug 30];10(1):9–17. Available from: https://link.springer.com/article/10.1007/BF00376380

69. Mujumdar AS. Handbook of Industrial Drying [Internet]. Handbook of Industrial Drying. 2020 [cited 2023 Aug 14]. Available from: https://books.google.co.uk/books?hl=en&lr=&id=82_OBQAAQBAJ&oi=fnd&pg=PP1&ots=Mfy5s4uOdg&sig=9Wd79eA2To5SKyhcddjyfHC9qXo&redir_esc=y#v=onepage&q&f=false

70. Chen CL, Chang JS, Lee DJ. Dewatering and Drying Methods for Microalgae. Dry Technol [Internet]. 2015 Mar 12 [cited 2023 Aug 14];33(4):443–54. Available from: https://www.tandfonline.com/action/journalInformation?journalCode=ldrt20

71. Stenström S. Drying of paper: A review 2000–2018. Dry Technol [Internet]. 2020 May 4 [cited 2023 Aug 14];38(7):825–45. Available from: https://www.tandfonline.com/doi/abs/10.1080/07373937.2019.1596949

72. Neagu RC, Gamstedt EK. Modelling of effects of ultrastructural morphology on the hygroelastic properties of wood fibres. J Mater Sci [Internet]. 2007 Dec 1 [cited 2023 Aug 30];42(24):10254–74. Available from: https://link.springer.com/article/10.1007/s10853-006-1199-9

73. Marklund E, Varna J. Modeling the hygroexpansion of aligned wood fiber composites. Compos Sci Technol [Internet]. 2009 Jun 1 [cited 2023 Aug 30];69(7–8):1108–14. Available from: https://doi.org/10.1016/j.compscitech.2009.02.006

74. Célino A, Fréour S, Jacquemin F, Casari P, Mensitieri G. The hygroscopic behavior of plant fibres: a review The hygroscopic behavior of plant fibers: a review. Chemistry (Easton) [Internet]. 2014 [cited 2023 Jul 25];1:43. Available from: https://doi.org/10.3389/fchem.2013.00043ï

75. Berthold J, Olsson RJO, Salmén L. Water sorption to hydroxyl and carboxylic acid groups in Carboxymethylcellulose (CMC) studied with NIR-spectroscopy. Cellulose [Internet]. 1998 [cited 2023 Aug 30];5(4):281–98. Available from: https://link.springer.com/article/10.1023/A:1009298907734

76. Pouteau C, Cathala B, Dole P, Kurek B, Monties B. Structural modification of Kraft lignin after acid treatment: characterisation of the apolar extracts and influence on the antioxidant properties in polypropylene. Ind Crops Prod [Internet]. 2005 Jan 1 [cited 2018 Mar 20];21(1):101–8. Available from: https://www.sciencedirect.com/science/article/pii/S0926669004000287

77. Giummarella N, Pylypchuk I V., Sevastyanova O, Lawoko M. New Structures in Eucalyptus Kraft Lignin with Complex Mechanistic Implications. ACS Sustain Chem Eng [Internet]. 2020 Jul 27 [cited 2022 Aug 18];8(29):10983–94. Available from: https://pubs.acs.org/doi/full/10.1021/acssuschemeng.0c03776

78. Zhao X, Cheng K, Liu D. Organosolv pretreatment of lignocellulosic biomass for enzymatic hydrolysis [Internet]. Vol. 82, Applied Microbiology and Biotechnology. 2009. p. 815–27. Available from: https://doi.org/10.1007/s00253-009-1883-1

79. Uraki Y, Kubo S, Nigo N, Sano Y, Sasaya T. Preparation of Carbon Fibers from Organosolv Lignin Obtained by Aqueous Acetic Acid Pulping. Holzforschung [Internet]. 1995 Jan 1 [cited 2022 Aug 18];49(4):343–50. Available from: https://www.degruyter.com/document/doi/10.1515/hfsg.1995.49.4.343/html

80. Liao JJ, Latif NHA, Trache D, Brosse N, Hussin MH. Current advancement on the isolation, characterization and application of lignin [Internet]. Vol. 162, International Journal of Biological Macromolecules. Elsevier; 2020 [cited 2023 May 16]. p. 985–1024. Available from: https://doi.org/10.1016/j.ijbiomac.2020.06.168

81. Bajpai P. Pulping Fundamentals. In: Biermann's Handbook of Pulp and Paper [Internet]. Elsevier; 2018 [cited 2023 Apr 26]. p. 295–351. Available from: https://doi.org/10.1016/b978-0-12-814240-0.00012-4

82. Meyer JR, Waghmode SB, He J, Gao Y, Hoole D, da Costa Sousa L, et al. Isolation of lignin from Ammonia Fiber Expansion (AFEX) pretreated biorefinery waste. Biomass and Bioenergy [Internet]. 2018 Dec 1 [cited 2023 May 16];119:446–55. Available from: https://doi.org/10.1016/j.biombioe.2018.09.017

83. Smink D, Kersten SRA, Schuur B. Recovery of lignin from deep eutectic solvents by liquid-liquid extraction. Sep Purif Technol [Internet]. 2020 Mar 18 [cited 2023 May 16];235:116127. Available from: https://doi.org/10.1016/j.seppur.2019.116127

84. Ovejero-Pérez A, Rigual V, Domínguez JC, Alonso MV, Oliet M, Rodriguez F. Acidic depolymerization vs ionic liquid solubilization in lignin extraction from eucalyptus wood using the protic ionic liquid 1-methylimidazolium chloride. Int J Biol Macromol [Internet]. 2020;157:461–9. Available from: https://doi.org/10.1016/j.ijbiomac.2020.04.194

85. Lobato-Peralta DR, Duque-Brito E, Villafán-Vidales HI, Longoria A, Sebastian PJ, Cuentas-Gallegos AK, et al. A review on trends in lignin extraction and valorization of lignocellulosic biomass for energy applications [Internet]. Vol. 293, Journal of Cleaner Production. Elsevier Ltd; 2021 [cited 2023 Apr 26]. Available from: https://doi.org/10.1016/j.jclepro.2021.126123

86. Prado R, Erdocia X, Serrano L, Labidi J. Lignin purification with green solvents. Cellul Chem Technol [Internet]. 2012;46:1–5. Available from: https://cellulosechemtechnol.ro/pdf/CCT3-4(2012)/p.221-225.pdf

87. Zhang R, Sun S, Wang L, Guo L, Shi Q, Jia J, et al. Lignin structure defines the properties of asphalt binder as a modifier. Constr Build Mater [Internet]. 2021 Dec 6 [cited 2022 Aug 18];310:125156. Available from: https://doi.org/10.1016/j.conbuildmat.2021.125156

88. Poursorkhabi V, Mohanty A, Misra M. Characterization of electrospun lignin based carbon fibers. In: AIP Conference Proceedings [Internet]. 2015 [cited 2018 Jan 11]. Available from: https://doi.org/10.1063/1.4918499

89. Nadif A, Hunkeler D, Käuper P. Sulfur-free lignins from alkaline pulping tested in mortar for use as mortar additives. Bioresour Technol [Internet]. 2002 Mar 1 [cited 2023 May 16];84(1):49–55. Available from: https://doi.org/10.1016/S0960-8524(02)00020-2

90. Saake B, Lehnen R. Lignin. Ullmann's Encycl Ind Chem [Internet]. 2007 Jul 15 [cited 2023 May 16]; Available from: https://onlinelibrary.wiley.com/doi/10.1002/14356007.a15_305.pub3

91. Gierer J. Chemical aspects of kraft pulping. Wood Sci Technol [Internet]. 1980 Dec [cited 2024 Mar 15];14(4):241–66. Available from: https://link.springer.com/article/10.1007/BF00383453

92. Loutfi H, Blackwell B, Uloth V. Lignin recovery from kraft black liquor : preliminary

process design. Tappi J [Internet]. 1991 [cited 2023 Apr 24];74(1):203–10. Available from: file:///M:/LigninRecovery-PreliminaryProcessDesignbyLoutfi.pdf

93. Olsson MR, Axelsson E, Berntsson T. Exporting lignin or power from heat-integrated kraft pulp mills: A techno-economic comparison using model mills. Nord Pulp Pap Res J [Internet]. 2006 Nov 1 [cited 2023 Apr 24];21(4):476–84. Available from: https://www.degruyter.com/document/doi/10.3183/npprj-2006-21-04-p476-484/html?lang=en

94. Kaur H, Dutt D, Tyagi CH. Optimization of soda pulping process of ligno-cellulosic residues of lemon and sofia grasses produced after steam distillation. Vol. 6, BioResources. 2010.

95. Vishtal A, Kraslawski A. Challenges of lignins. BioResources [Internet]. 2011 [cited 2023 Apr 24];6(3):3547–68. Available from: https://bioresources.cnr.ncsu.edu/resources/challenges-in-industrial-applications-of-technical-lignins/

96. Mohamad Aini NA, Othman N, Hussin MH, Sahakaro K, Hayeemasae N. Effect of extraction methods on the molecular structure and thermal stability of kenaf (Hibiscus cannabinus core) biomass as an alternative bio-filler for rubber composites. Int J Biol Macromol [Internet]. 2020 Jul 1 [cited 2023 Apr 26];154:1255–64. Available from: https://doi.org/10.1016/J.IJBIOMAC.2019.10.280

97. Sánchez R, Espinosa E, Domínguez-Robles J, Loaiza JM, Rodríguez A. Isolation and characterization of lignocellulose nanofibers from different wheat straw pulps. Int J Biol Macromol. 2016 Nov 1;92:1025–33.

98. Pabby AK. Handbook of Membrane Separations [Internet]. Handbook of Membrane Separations. CRC Press; 2008 [cited 2023 Apr 24]. Available from: https://www.taylorfrancis.com/books/mono/10.1201/9781420009484/handbook-membrane-separations-anil-kumar-pabby-syed-rizvi-ana-maria-sastre-requena

99. Bisgard-Frantzen H, Svendsen A. Method for preparing alkaline solutions containing aromatic polymers [Internet]. Vol. 339. 2000 [cited 2023 Apr 24]. Available from: www.rcsb.org

100. Ghatak HR. Spectroscopic comparison of lignin separated by electrolysis and acid precipitation of wheat straw soda black liquor. Ind Crops Prod. 2008 Sep 1;28(2):206–12.

101. Doherty WOS, Mousavioun P, Fellows CM. Value-adding to cellulosic ethanol: Lignin polymers [Internet]. Industrial Crops and Products Elsevier; Mar 1, 2011 p. 259–76. Available from: https://www.sciencedirect.com/science/article/pii/S0926669010002670

102. Toledano A, García A, Mondragon I, Labidi J. Lignin separation and fractionation by ultrafiltration. Sep Purif Technol. 2010 Jan 29;71(1):38–43.

103. Santos JI, Fillat Ú, Martín-Sampedro R, Eugenio ME, Negro MJ, Ballesteros I, et al. Evaluation of lignins from side-streams generated in an olive tree pruning-based biorefinery: Bioethanol production and alkaline pulping. Int J Biol Macromol. 2017 Dec 1;105:238–51.

104. Toledano A, Serrano L, Garcia A, Mondragon I, Labidi J. Comparative study of lignin fractionation by ultrafiltration and selective precipitation. Chem Eng J. 2010 Feb 15;157(1):93–9.

105. Restolho JA, Prates A, de Pinho MN, Afonso MD. Sugars and lignosulphonates recovery from eucalyptus spent sulphite liquor by membrane processes. Biomass and Bioenergy. 2009 Nov 1;33(11):1558–66.

106. Rabinovich ML. Wood hydrolysis industry in the soviet union and Russia: A mini-review. Vol. 44, Cellulose Chemistry and Technology. 2010. p. 173–86.

107. Dalimova GN. Modification of hydrolyzed lignin in acidic and basic media. Chem Nat Compd [Internet]. 2006 [cited 2023 Apr 24];42(1):88–91. Available from: https://link.springer.com/article/10.1007/s10600-006-0042-5

108. Ma X, Chen J, Zhu J, Yan N. Lignin-Based Polyurethane: Recent Advances and Future Perspectives. Macromol Rapid Commun. 2021 Feb 1;42(3).

109. Ahmed F, Ayoub Arbab A, Jatoi AW, Khatri M, Memon N, Khatri Z, et al. Ultrasonic-assisted deacetylation of cellulose acetate nanofibers: A rapid method to produce cellulose nanofibers. Ultrason Sonochem [Internet]. 2017 May 1 [cited 2019 Apr 11];36:319–25. Available from: https://www.sciencedirect.com/science/article/pii/S1350417716304527

110. Macfarlane AL, Prestidge R, Farid MM, Chen JJJ. Dissolved air flotation: A novel approach to recovery of organosolv lignin. Chem Eng J. 2009 May 1;148(1):15–9.

111. Kim GH, Um BH. Fractionation and characterization of lignins from Miscanthus via organosolv and soda pulping for biorefinery applications. Int J Biol Macromol [Internet]. 2020 Sep 1 [cited 2023 Apr 26];158:443–51. Available from: https://doi.org/10.1016/j.ijbiomac.2020.04.229

112. Cook P, Hess S. Organosolv lignin-modified phenolic resins and method for their preparation. 1990 [cited 2023 Apr 24]; Available from: https://patents.google.com/patent/US5010156

113. Sun RC, Lawther JM, Banks WB. Isolation and Characterization of Organosolv Lignins From Wheat Straw. Wood Fiber Sci [Internet]. 1998 [cited 2023 Apr 24];56–63. Available from: https://wfs.swst.org/index.php/wfs/article/view/177

114. Martín-Sampedro R, Santos JI, Fillat Ú, Wicklein B, Eugenio ME, Ibarra D. Characterization of lignins from Populus alba L. generated as by-products in different transformation processes: Kraft pulping, organosolv and acid hydrolysis. Int J Biol Macromol. 2019 Apr 1;126:18–29.

115. van Spronsen J, Cardoso MAT, Witkamp GJ, de Jong W, Kroon MC. Separation and recovery of the constituents from lignocellulosic biomass by using ionic liquids and acetic acid as co-solvents for mild hydrolysis. Chem Eng Process Process Intensif [Internet]. 2011 Feb 1 [cited 2023 Apr 24];50(2):196–9. Available from: https://faculty.kaust.edu.sa/en/publications/separation-and-recovery-of-the-constituents-from-lignocellulosic-

116. Rashid T, Gnanasundaram N, Appusamy A, Kait CF, Thanabalan M. Enhanced lignin extraction from different species of oil palm biomass: Kinetics and optimization of extraction conditions. Ind Crops Prod. 2018 Jun 1;116:122–36.

117. Chakar FS, Ragauskas AJ. Review of current and future softwood kraft lignin process chemistry. In: Industrial Crops and Products. Elsevier; 2004. p. 131–41.

118. Gosselink RJA, De Jong E, Guran B, Abächerli A. Co-ordination network for lignin - Standardisation, production and applications adapted to market requirements (Eurolignin).

In: Industrial Crops and Products [Internet]. Elsevier; 2004 [cited 2024 Aug 6]. p. 121–9. Available from: https://doi.org/10.1016/j.indcrop.2004.04.015

119. Mansouri NE El, Salvadó J. Structural characterization of technical lignins for the production of adhesives: Application to lignosulfonate, kraft, soda-anthraquinone, organosolv and ethanol process lignins. Ind Crops Prod. 2006 Jul 1;24(1):8–16.

120. Argyropoulos DS. Quantitative phosphorus-31 nmr analysis of lignins, a new tool for the lignin chemist. J Wood Chem Technol. 1994 Feb 1;14(1):45–63.

121. Yuan TQ, Sun SN, Xu F, Sun RC. Structural characterization of lignin from triploid of populus tomentosa carr. J Agric Food Chem. 2011 Jun 22;59(12):6605–15.

122. Norgren M, Edlund H. Lignin: Recent advances and emerging applications [Internet]. Vol. 19, Current Opinion in Colloid and Interface Science. 2014 [cited 2023 Oct 19]. p. 409–16. Available from: http://dx.doi.org/10.1016/j.cocis.2014.08.004

123. Funaoka M, Kako T, Abe I. Condensation of lignin during heating of wood. Wood Sci Technol [Internet]. 1990 Jul [cited 2024 Aug 6];24(3):277–88. Available from: https://link.springer.com/article/10.1007/BF01153560

124. Zhang J, Chevali VS, Wang H, Wang CH. Current status of carbon fibre and carbon fibre composites recycling. Vol. 193, Composites Part B: Engineering. Elsevier; 2020. p. 108053.

125. Kadla JF, Kubo S, Venditti RA, Gilbert RD, Compere AL, Griffith W. Lignin-based carbon fibers for composite fiber applications. Carbon N Y. 2002;40(15):2913–20.

126. Kai D, Tan MJ, Chee PL, Chua YK, Yap YL, Loh XJ. Towards lignin-based functional materials in a sustainable world [Internet]. Vol. 18, Green Chemistry. The Royal Society of Chemistry; 2016 [cited 2024 Aug 6]. p. 1175–200. Available from: https://pubs.rsc.org/en/content/articlehtml/2016/gc/c5gc02616d

127. Passoni V, Scarica C, Levi M, Turri S, Griffini G. Fractionation of Industrial Softwood Kraft Lignin: Solvent Selection as a Tool for Tailored Material Properties. ACS Sustain Chem Eng [Internet]. 2016 Apr 4 [cited 2023 Nov 16];4(4):2232–42. Available from: https://pubs.acs.org/doi/abs/10.1021/acssuschemeng.5b01722

128. Ponnuchamy V, Gordobil O, Diaz RH, Sandak A, Sandak J. Fractionation of lignin using organic solvents: A combined experimental and theoretical study. Int J Biol Macromol [Internet]. 2021 [cited 2023 Nov 16];168:792–805. Available from: https://doi.org/10.1016/j.ijbiomac.2020.11.139

129. Zhang Y, He H, Dong K, Fan M, Zhang S. A DFT study on lignin dissolution in imidazolium-based ionic liquids. RSC Adv [Internet]. 2017 Feb 21 [cited 2023 Nov 16];7(21):12670–81. Available from: https://pubs.rsc.org/en/content/articlehtml/2017/ra/c6ra27059j

130. Duval A, Vilaplana F, Crestini C, Lawoko M. Solvent screening for the fractionation of industrial kraft lignin. Holzforschung [Internet]. 2016 Jan 1 [cited 2023 Nov 17];70(1):11–20. Available from: https://www.degruyter.com/document/doi/10.1515/hf-2014-0346/html

131. Sadeghifar H, Argyropoulos DS. Macroscopic Behavior of Kraft Lignin Fractions: Melt Stability Considerations for Lignin-Polyethylene Blends. ACS Sustain Chem Eng [Internet]. 2016 Oct 3 [cited 2023 Nov 17];4(10):5160–6. Available from: https://pubs.acs.org/doi/full/10.1021/acssuschemeng.6b00636

132. Ji H, Lv P. Mechanistic insights into the lignin dissolution behaviors of a recyclable acid hydrotrope, deep eutectic solvent (DES), and ionic liquid (IL). Green Chem [Internet]. 2020 Feb 24 [cited 2024 Mar 15];22(4):1378–87. Available from: https://pubs.rsc.org/en/content/articlehtml/2020/gc/c9gc02760b

133. Jia G, Innocent MT, Yu Y, Hu Z, Wang X, Xiang H, et al. Lignin-based carbon fibers: Insight into structural evolution from lignin pretreatment, fiber forming, to pre-oxidation and carbonization. Vol. 226, International Journal of Biological Macromolecules. Elsevier; 2023. p. 646–59.

134. Li Z. Fractionation of Lignin for Valorization. In: Lignin - Chemistry, Structure, and Application [Internet]. IntechOpen; 2023 [cited 2023 Nov 16]. Available from: https://www.intechopen.com/chapters/84728

135. Maitra J, Shukla VK. Cross-linking in Hydrogels - A Review. Am J Polym Sci [Internet]. 2014 [cited 2024 Jun 3];4(2):25–31. Available from: Hydrogels represent a class of high water content polymers with physical or chemical crosslinks. Their physical properties are

similar to soft tissues. Cross linking is a stabilization process in polymer chemistry which leads to multidimensional extension

136. Li S, Han G, Zhang W. Cross-linking approaches for block copolymer nano-assemblies: Via RAFT-mediated polymerization-induced self-assembly. Polym Chem [Internet]. 2020 Jul 28 [cited 2024 Jun 3];11(29):4681–92. Available from: https://pubs.rsc.org/en/content/articlehtml/2020/py/d0py00627k

137. Mateescu A, Wang Y, Dostalek J, Jonas U. Thin hydrogel films for optical biosensor applications [Internet]. Vol. 2, Membranes. Multidisciplinary Digital Publishing Institute (MDPI); 2012 [cited 2024 Jun 3]. p. 49–69. Available from: /pmc/articles/PMC4021880/

138. Kim S, Chung H. Convenient Cross-Linking Control of Lignin-Based Polymers Influencing Structure-Property Relationships. ACS Sustain Chem Eng [Internet]. 2023 Feb 6 [cited 2024 Jun 3];11(5):1709–19. Available from: https://pubs.acs.org/doi/full/10.1021/acssuschemeng.2c05651

139. Nielsen LE. Cross-Linking–Effect on Physical Properties of Polymers. J Macromol Sci Part C [Internet]. 1969 Jan 1 [cited 2024 Jun 3];3(1):69–103. Available from: https://www.tandfonline.com/doi/abs/10.1080/15583726908545897

140. Mane S, Ponrathnam S, Chavan N. Effect of Chemical Crosslinking on Properties of Polymer Microbeads: A Review. Can Chem Trans. 2016 Jan 11;473–85.

141. Duval A, Lawoko M. A review on lignin-based polymeric, micro- and nano-structured materials. React Funct Polym. 2014 Dec 1;85:78–96.

142. Gadhave R V., Mahanwar PA, Gadekar PT. Lignin-Polyurethane Based Biodegradable Foam. Open J Polym Chem [Internet]. 2018 Jan 25 [cited 2024 Jun 3];08(01):1–10. Available from: http://www.scirp.org/journal/PaperInformation.aspx?PaperID=81972

143. Buono P, Duval A, Verge P, Averous L, Habibi Y. New Insights on the Chemical Modification of Lignin: Acetylation versus Silylation. ACS Sustain Chem Eng [Internet]. 2016 Oct 3 [cited 2024 Mar 15];4(10):5212–22. Available from: https://pubs.acs.org/doi/full/10.1021/acssuschemeng.6b00903

144. Saraf VP, Glasser WG, Wilkes GL. Engineering plastics from lignin. VII. Structure property relationships of poly(butadiene glycol)-containing polyurethane networks. J Appl

Polym Sci [Internet]. 1985 Sep 1 [cited 2024 Jun 3];30(9):3809–23. Available from: https://onlinelibrary.wiley.com/doi/full/10.1002/app.1985.070300921

145. Cateto CA, Barreiro MF, Rodrigues AE, Belgacem MN. Kinetic study of the formation of lignin-based polyurethanes in bulk. React Funct Polym. 2011 Aug 1;71(8):863–9.

146. Vanderlaan MN, Thring RW. Polyurethanes from Alcell® lignin fractions obtained by sequential solvent extraction. Biomass and Bioenergy. 1998 May 1;14(5–6):525–31.

147. Chen X, Li L, Torkelson JM. Recyclable polymer networks containing hydroxyurethane dynamic cross-links: Tuning morphology, cross-link density, and associated properties with chain extenders. Polymer (Guildf). 2019 Sep 12;178:121604.

148. Chung H, Washburn NR. Improved lignin polyurethane properties with lewis acid treatment. ACS Appl Mater Interfaces [Internet]. 2012 Jun 27 [cited 2024 Jun 3];4(6):2840–6. Available from: https://pubs.acs.org/doi/full/10.1021/am300425x

149. Barman SR, Nain A, Jain S, Punjabi N, Mukherji S, Satija J. Dendrimer as a multifunctional capping agent for metal nanoparticles for use in bioimaging, drug delivery and sensor applications [Internet]. Vol. 6, Journal of Materials Chemistry B. The Royal Society of Chemistry; 2018 [cited 2024 Jun 3]. p. 2368–84. Available from: https://pubs.rsc.org/en/content/articlehtml/2018/tb/c7tb03344c

150. Niu Z, Li Y. Removal and utilization of capping agents in nanocatalysis [Internet]. Vol. 26, Chemistry of Materials. American Chemical Society; 2014 [cited 2024 Jun 3]. p. 72–83. Available from: https://pubs.acs.org/doi/full/10.1021/cm4022479

151. de Paula DM, Lomonaco D, Parente da Ponte AM, Cordeiro KE, Magalhães Moreira M, Giovarruscio M, et al. Collagen Cross-Linking Lignin Improves the Bonding Performance of Etch-and-Rinse Adhesives to Dentin. Materials (Basel) [Internet]. 2022 Apr 29 [cited 2024 Jun 5];15(9):3218. Available from: https://www.mdpi.com/1996-1944/15/9/3218/htm

152. Hatfield RD, Ralph J, Grabber JH. Cell wall cross-linking by ferulates and diferulates in grasses. J Sci Food Agric J Sci Food Agric [Internet]. 1999 [cited 2024 Jun 5];79(October 1998):403–7. Available from: https://onlinelibrary.wiley.com/doi/10.1002/

153. Fry SC, Miller JG. Toward a Working Model of the Growing Plant Cell Wall. In 1989

[cited 2024 Jun 5]. p. 33–46. Available from: https://pubs.acs.org/doi/abs/10.1021/bk-1989-0399.ch003

154. Fry SC. Feruloylated pectins from the primary cell wall: their structure and possible functions. Planta [Internet]. 1983 Mar [cited 2024 Jun 5];157(2):111–23. Available from: https://link.springer.com/article/10.1007/BF00393644

155. Parr AJ, Waldron KW, Ng A, Parker ML. The wall-bound phenolics of Chinese water chestnut (Eleocharis dulcis). J Sci Food Agric [Internet]. 1996 [cited 2024 Jun 5];71(4):501–7. Available from: https://onlinelibrary.wiley.com/doi/10.1002/

156. Ishii T, Hiroi T. Isolation and characterization of feruloylated arabinoxylan oligosaccharides from bamboo shoot cell-walls. Carbohydr Res. 1990 Feb 25;196(C):175–83.

157. Ishii T. Structure and functions of feruloylated polysaccharides. Plant Sci. 1997 Sep 12;127(2):111–27.

158. Mainka H, Hilfert L, Busse S, Edelmann F, Haak E, Herrmann AS. Characterization of the major reactions during conversion of lignin to carbon fiber. J Mater Res Technol. 2015 Oct 1;4(4):377–91.

159. Yiamsawas D, Watcharin K, Pongprayoon T. Enhanced Performance of Lignin Recovery with a Carbon Dioxide Acidification Method. ACS Omega [Internet]. 2023 Feb 28 [cited 2023 Nov 7];8(8):7438–47. Available from: https://pubs.acs.org/doi/full/10.1021/acsomega.2c06153

160. Norberg I. Carbon fibres from Kraft lignin. 2012. 69 p.

161. Miller-Chou BA, Koenig JL. A review of polymer dissolution. Vol. 28, Progress in Polymer Science (Oxford). Pergamon; 2003. p. 1223–70.

162. Rashid T, Kait CF, Regupathi I, Murugesan T. Dissolution of kraft lignin using Protic Ionic Liquids and characterization. Ind Crops Prod [Internet]. 2016 [cited 2023 Oct 19];84:284–93. Available from: http://dx.doi.org/10.1016/j.indcrop.2016.02.017

163. Hart WES, Harper JB, Aldous L. The effect of changing the components of an ionic liquid upon the solubility of lignin†. Green Chem. 2015 Jan 1;17(1):214–8.

164. Horváth IT. Solvents from nature. Green Chem [Internet]. 2008 Oct 1 [cited 2023 Oct 19];10(10):1024–8. Available from: https://pubs.rsc.org/en/content/articlehtml/2008/gc/b812804a

165. Lee SH, Doherty T V., Linhardt RJ, Dordick JS. Ionic liquid-mediated selective extraction of lignin from wood leading to enhanced enzymatic cellulose hydrolysis. Biotechnol Bioeng. 2009 Apr 1;102(5):1368–76.

166. Vitz J, Erdmenger T, Haensch C, Schubert US. Extended dissolution studies of cellulose in imidazolium based ionic liquids. Green Chem. 2009;11(3):417–24.

167. Sameni J, Krigstin S, Sain M. Solubility of Lignin and Acetylated Lignin in Organic Solvents. BioResources [Internet]. 2017 Jan 1 [cited 2023 Jan 17];12(1):1548–65. Available from: https://jtatm.textiles.ncsu.edu/index.php/BioRes/article/view/BioRes_12_1_1548_Sameni_Solubility_Lignin_Acetylated_Lignin_Organic_Solvents

168. Shukry N, Fadel SM, Agblevor FA, El-Kalyoubi SF. Some physical properties of acetosolv lignins from bagasse. J Appl Polym Sci [Internet]. 2008 Jul 5 [cited 2023 Oct 10];109(1):434–44. Available from: https://onlinelibrary.wiley.com/doi/full/10.1002/app.28059

169. Olarte MV. Base-catalyzed depolymerization of lignin and hydrodeoxygenation of lignin model compounds for alternative fuel production. 2011.

170. Zhang M, Ogale AA. Carbon fibers from dry-spinning of acetylated softwood kraft lignin. Vol. 69, Carbon. Pergamon; 2014. p. 626–9.

171. Jeong H, Park J, Kim S, Lee J, Ahn N, Roh H gyoo. Preparation and characterization of thermoplastic polyurethanes using partially acetylated kraft lignin. Fibers Polym [Internet]. 2013 Jul 31 [cited 2023 Oct 10];14(7):1082–93. Available from: https://link.springer.com/article/10.1007/s12221-013-1082-7

172. Jeong H, Park J, Kim S, Lee J, Cho JW. Use of acetylated softwood kraft lignin as filler in synthetic polymers. Fibers Polym [Internet]. 2012 Dec 1 [cited 2023 Oct 10];13(10):1310–8. Available from: https://link.springer.com/article/10.1007/s12221-012-1310-6

173. Ding Y, Asrar J. Lignin-based microparticles for the controlled release of agricultural actives. Vol. 1, System and Method for Programming a Weighing Scale Usinga Key Signal To Enter a Programming Mode. 2010. p. 14.

174. Quesada-Medina J, López-Cremades FJ, Olivares-Carrillo P. Organosolv extraction of lignin from hydrolyzed almond shells and application of the δ-value theory. Bioresour Technol. 2010 Nov 1;101(21):8252–60.

175. Hansen CM. Methods of characterization - surfaces. In: Hansen Solubility Parameters: A Users Handbook, Second Edition [Internet]. CRC Press; 2007 [cited 2023 Oct 10]. p. 113–23. Available from: https://www.taylorfrancis.com/books/mono/10.1201/9781420006834/hansen-solubility-parameters-charles-hansen

176. Majumder S, Matin A, Sharif A, Arafat MT. Understanding solubility, spinnability and electrospinning behaviour of cellulose acetate using different solvent systems. Bull Mater Sci [Internet]. 2034 [cited 2020 Jan 6];42:171. Available from: https://doi.org/10.1007/s12034-019-1857-6

177. Dallmeyer I, Ko F, Kadla JF. Electrospinning of technical lignins for the production of fibrous networks. J Wood Chem Technol. 2010;30(4):315–29.

178. Pan XJ, Sano Y. Atmospheric acetic acid pulping of rice straw IV: physico-chemical characterization of acetic acid lignins from rice straw and woods. Part 2. Chemical structures. Holzforschung [Internet]. 1999 Sep 10 [cited 2023 Oct 10];53(6):590–6. Available from: https://www.degruyter.com/document/doi/10.1515/HF.1999.084/html?lang=en

179. Mohan M, Huang K, Pidatala VR, Simmons BA, Singh S, Sale KL, et al. Prediction of solubility parameters of lignin and ionic liquids using multi-resolution simulation approaches. Green Chem [Internet]. 2022 Feb 7 [cited 2024 Mar 15];24(3):1165–76. Available from: https://pubs.rsc.org/en/content/articlehtml/2022/gc/d1gc03798f

180. Tungprapa S, Puangparn T, Weerasombut M, Jangchud I, Fakum P, Semongkhol S, et al. Electrospun cellulose acetate fibers: Effect of solvent system on morphology and fiber diameter. Cellulose. 2007;14(6):563–75.

181. Brown W. Solution properties of lignin. Thermodynamic properties and molecular weight determinations. J Appl Polym Sci [Internet]. 1967 Nov 1 [cited 2023 Jan 12];11(11):2381–96. Available from: https://onlinelibrary.wiley.com/doi/full/10.1002/app.1967.070111125

182. Huggins ML. The Solubility of Nonelectrolytes. By Joel H. Hildebrand and Robert S. Scott. J Phys Chem [Internet]. 1951 Apr [cited 2023 Oct 10];55(4):619–20. Available from: https://pubs.acs.org/doi/abs/10.1021/j150487a027

183. Ni Y, Hu Q. Alcell® lignin solubility in ethanol–water mixtures. J Appl Polym Sci [Internet]. 1995 Sep 19 [cited 2023 Oct 11];57(12):1441–6. Available from: https://onlinelibrary.wiley.com/doi/full/10.1002/app.1995.070571203

184. Coccia A, Indovina PL, Podo F, Viti V. PMR studies on the structures of water-ethyl alcohol mixtures. Chem Phys. 1975 Jan 1;7(1):30–40.

185. Schuerch C. The Solvent Properties of Liquids and Their Relation to the Solubility, Swelling, Isolation and Fractionation of Lignin. J Am Chem Soc [Internet]. 1952 Oct 1 [cited 2023 Oct 11];74(20):5061–7. Available from: https://pubs.acs.org/doi/abs/10.1021/ja01140a020

186. Vázquez-Torres H, Canché-Escamilla G, Cruz-Ramos CA. Coconut husk lignin. II. Characterization by infrared and nuclear magnetic resonance spectroscopy. J Appl Polym Sci [Internet]. 1992 Jun 5 [cited 2023 Oct 11];45(4):645–53. Available from: https://onlinelibrary.wiley.com/doi/full/10.1002/app.1992.070450411

187. Wang Q, Chen K, Li J, Yang G, Liu S, Xu J. The solubility of lignin from bagasse in a 1,4-butanediol/water system. BioResources. 2011 Aug;6(3):3034–43.

188. Balogh DT, Curvelo AAS, De Groote RAMC. Solvent Effects on Organosolv Lignin from Pinus Caribaeahondurensis. Holzforschung [Internet]. 1992 Jan 1 [cited 2023 Oct 11];46(4):343–8. Available from: https://www.degruyter.com/document/doi/10.1515/hfsg.1992.46.4.343/html

189. Xue Z, Zhao X, Sun RC, Mu T. Biomass-derived γ-valerolactone-based solvent systems for highly efficient dissolution of various lignins: Dissolution behavior and mechanism study. ACS Sustain Chem Eng [Internet]. 2016 [cited 2023 Oct 19];4(7):3864–70.

Available from: https://pubs.acs.org/sharingguidelines

190. Fegyverneki D, Orha L, Láng G, Horváth IT. Gamma-valerolactone-based solvents. Tetrahedron. 2010;66(5):1078–81.

191. Ismalaj E, Strappaveccia G, Ballerini E, Elisei F, Piermatti O, Gelman D, et al. γ-valerolactone as a renewable dipolar aprotic solvent deriving from biomass degradation for the Hiyama reaction. ACS Sustain Chem Eng [Internet]. 2014 [cited 2023 Oct 19];2(10):2461–4. Available from: http://pubs.acs.org.

192. Lynam JG, Kumar N, Wong MJ. Deep eutectic solvents' ability to solubilize lignin, cellulose, and hemicellulose; thermal stability; and density. Bioresour Technol [Internet]. 2017 [cited 2023 Oct 19];238:684–9. Available from: http://dx.doi.org/10.1016/j.biortech.2017.04.079

193. Sun J, Dutta T, Parthasarathi R, Kim KH, Tolic N, Chu RK, et al. Rapid room temperature solubilization and depolymerization of polymeric lignin at high loadings. Green Chem [Internet]. 2016 Nov 7 [cited 2023 Jul 13];18(22):6012–20. Available from: https://pubs.rsc.org/en/content/articlehtml/2016/gc/c6gc02258h

194. Erdtman H. Lignins: Occurrence, formation, structure and reactions, K. V. Sarkanen and C. H. Ludwig, Eds., John Wiley & Sons, Inc., New York, 1971. 916 pp. $35.00. J Polym Sci Part B Polym Lett [Internet]. 1972 Mar 1 [cited 2022 Aug 4];10(3):228–30. Available from: https://onlinelibrary.wiley.com/doi/full/10.1002/pol.1972.110100315

195. Wen JL, Yuan TQ, Sun SL, Xu F, Sun RC. Understanding the chemical transformations of lignin during ionic liquid pretreatment. Green Chem [Internet]. 2014 Dec 17 [cited 2023 Oct 19];16(1):181–90. Available from: https://pubs.rsc.org/en/content/articlehtml/2014/gc/c3gc41752b

196. Sun N, Rodríguez H, Rahman M, Rogers RD. Where are ionic liquid strategies most suited in the pursuit of chemicals and energy from lignocellulosic biomass? Chem Commun [Internet]. 2011 Feb 7 [cited 2023 Oct 19];47(5):1405–21. Available from: https://pubs.rsc.org/en/content/articlehtml/2011/cc/c0cc03990j

197. Swatloski RP, Spear SK, Holbrey JD, Rogers RD. Dissolution of Cellose with Ionic Liquids. J AM CHEM SOC. 2002;124:4974–5.

198. Fedors RF. A method for estimating both the solubility parameters and molar volumes of liquids. Polym Eng Sci [Internet]. 1974 [cited 2023 Oct 10];14(2):147–54. Available from: https://4spepublications.onlinelibrary.wiley.com/doi/10.1002/pen.760140211

199. Barton AFM. CRC handbook of solubility parameters and other cohesion parameters, second edition [Internet]. CRC Handbook of Solubility Parameters and Other Cohesion Parameters, Second Edition. CRC Press; 2017 [cited 2023 Oct 26]. 1–739 p. Available from: https://www.taylorfrancis.com/books/mono/10.1201/9781315140575/crc-handbook-solubility-parameters-cohesion-parameters-allan-barton

200. Martin D, Weise A, Niclas H -J. The Solvent Dimethyl Sulfoxide. Angew Chemie Int Ed English. 1967;6(4):318–34.

201. Soroko I, Bhole Y, Livingston AG. Environmentally friendly route for the preparation of solvent resistant polyimide nanofiltration membranes. Green Chem [Internet]. 2011 Jan 10 [cited 2023 Jan 12];13(1):162–8. Available from: https://pubs.rsc.org/en/content/articlehtml/2011/gc/c0gc00155d

202. Wu XF, Natte K. The Applications of Dimethyl Sulfoxide as Reagent in Organic Synthesis [Internet]. Vol. 358, Advanced Synthesis and Catalysis. 2016 [cited 2023 Jan 12]. p. 336–52. Available from: https://onlinelibrary.wiley.com/doi/10.1002/adsc.201501007

203. Wang Z, Richter SM, Bellettini JR, Pu YM, Hill DR. Safe scale-up of pharmaceutical manufacturing processes with dimethyl sulfoxide as the solvent and a reactant or a byproduct. Org Process Res Dev [Internet]. 2014 Dec 19 [cited 2023 Jan 19];18(12):1836–42. Available from: https://pubs.acs.org/doi/full/10.1021/op500260n

204. Khan I, Hararak B, Fernando GF. Improved procedure for electro-spinning and carbonisation of neat solvent-fractionated softwood Kraft lignin. Sci Rep [Internet]. 2021 [cited 2022 Feb 16];11(1):16237. Available from: www.nature.com/scientificreports

205. Yang M, Zhao W, Singh S, Simmons B, Cheng G. On the solution structure of kraft lignin in ethylene glycol and its implication for nanoparticle preparation. Nanoscale Adv [Internet]. 2019 Jan 15 [cited 2023 Jan 17];1(1):299–304. Available from: https://pubs.rsc.org/en/content/articlehtml/2019/na/c8na00042e

206. Li S, Lundquist K. Analysis of hydroxyl groups in lignins by 1H NMR spectrometry. Nord Pulp Pap Res J [Internet]. 2001 Jan 1 [cited 2022 Aug 12];16(1):63–7. Available from: https://www.degruyter.com/document/doi/10.3183/npprj-2001-16-01-p063-067/html?lang=en

207. Mobley JK, Yao SG, Crocker M, Meier M. Oxidation of lignin and lignin β-O-4 model compounds via activated dimethyl sulfoxide. RSC Adv [Internet]. 2015 Dec 10 [cited 2023 Jun 22];5(127):105136–48. Available from: https://pubs.rsc.org/en/content/articlehtml/2015/ra/c5ra33240k

208. Balakshin M, Capanema E, Gracz H, Chang H min, Jameel H. Quantification of lignin-carbohydrate linkages with high-resolution NMR spectroscopy. Planta [Internet]. 2011 Jun [cited 2024 Jun 11];233(6):1097–110. Available from: https://pubmed.ncbi.nlm.nih.gov/21298285/

209. Crestini C, Crucianelli M, Orlandi M, Saladino R. Oxidative strategies in lignin chemistry: A new environmental friendly approach for the functionalisation of lignin and lignocellulosic fibers. Catal Today. 2010 Oct 25;156(1–2):8–22.

210. Pan H, Shupe TF, Hse CY. Characterization of liquefied wood residues from different liquefaction conditions. J Appl Polym Sci. 2007 Sep 15;105(6):3740–6.

211. Huang X, Korányi TI, Boot MD, Hensen EJM. Catalytic depolymerization of lignin in supercritical ethanol. ChemSusChem [Internet]. 2014 [cited 2024 Jun 11];7(8):2276–88. Available from: https://pubmed.ncbi.nlm.nih.gov/24867490/

212. Laurichesse S, Avérous L. Chemical modification of lignins: Towards biobased polymers. Vol. 39, Progress in Polymer Science. Pergamon; 2014. p. 1266–90.

213. Chowdhury M, Stylios G. Effect of experimental parameters on the morphology of electrospun Nylon 6 fibres. Int J Basic Appl Sci. 2010;10(06):116–31.

214. Park J. Electric spinning apparatus for mass-production of nano-fiber. Korea; 2011. p. US 7980838.

215. Yuan H, Zhou Q, Zhang Y. Improving fiber alignment during electrospinning. In: Electrospun Nanofibers. Elsevier Inc.; 2017. p. 125–47.

216. Nayak R. Review of Literature: Melt Electrospinning. In 2017. p. 9–39.

217. Liu WJ, Jiang H, Yu HQ. Thermochemical conversion of lignin to functional materials: a review and future directions. Green Chem [Internet]. 2015;17(11):4888–907. Available from: www.rsc.org/greenchem

218. Luo CJ, Nangrejo M, Edirisinghe M. A novel method of selecting solvents for polymer electrospinning. Polymer (Guildf). 2010 Mar 24;51(7):1654–62.

219. Fernández de la Mora J. The fluid dynamics of Taylor Cones [Internet]. Vol. 39, Annual Review of Fluid Mechanics. 2007 [cited 2022 Feb 25]. p. 217–43. Available from: www.annualreviews.org

220. Qin XH, Yang EL, Li N, Wang SY. Effect of different salts on electrospinning of polyacrylonitrile (PAN) polymer solution. J Appl Polym Sci. 2007 Mar 15;103(6):3865–70.

221. Greiner A, Wendorff JH. Electrospinning: A fascinating method for the preparation of ultrathin fibers. Vol. 46, Angewandte Chemie - International Edition. 2007. p. 5670–703.

222. Worarutariyachai T, Chuangchote S. Carbon fibers derived from pure alkali lignin fibers through electrospinning with carbonization. BioResources. 2020;15(2):2412–27.

223. Rodoplu D, Mutlu M. Effects of Electrospinning Setup and Process Parameters on Nanofiber Morphology Intended for the Modification of Quartz Crystal Microbalance Surfaces. J Eng Fiber Fabr. 2012;7(2):155892501200700.

224. Quan SL, Kang SG, Chin IJ. Characterization of cellulose fibers electrospun using ionic liquid. Cellulose. 2010;17(2):223–30.

225. Ou Y, Wu QY, Wan LS, Yang HC, Xu ZK. Preparation of porous polyacrylonitrile ultrathin fibers by electrospinning with nonsolvent induced phase separation. Acta Polym Sin. 2013 Feb 20;(2):248–54.

226. Bosworth LA, Downes S. Acetone, a Sustainable Solvent for Electrospinning Poly(ε-Caprolactone) Fibres: Effect of Varying Parameters and Solution Concentrations on Fibre Diameter. J Polym Environ. 2012 Sep 22;20(3):879–86.

227. Sun Z, Deitzel JM, Knopf J, Chen X, Gillespie JW. The effect of solvent dielectric

properties on the collection of oriented electrospun fibers. J Appl Polym Sci. 2012 Aug 15;125(4):2585–94.

228. Joshua Avossa, Gordon Herwig, Claudio Toncelli, Fabian Itel, Michel Rossi R, Avossa J, et al. Electrospinning based on benign solvents: current definitions, implications and strategies. Green Chem [Internet]. 2022 Mar 21 [cited 2022 Apr 27];24(6):2347–75. Available from: https://pubs.rsc.org/en/content/articlehtml/2022/gc/d1gc04252a

229. Lv D, Zhu M, Jiang Z, Jiang S, Zhang Q, Xiong R, et al. Green Electrospun Nanofibers and Their Application in Air Filtration. Vol. 303, Macromolecular Materials and Engineering. Wiley-VCH Verlag; 2018.

230. Abbas Adam A, Ojur Dennis J, Al-Hadeethi Y, Mkawi EM, Abubakar Abdulkadir B, Usman F, et al. State of the art and new directions on electrospun lignin/cellulose nanofibers for supercapacitor application: A systematic literature review [Internet]. Polymers 2020 p. 1–36. Available from: www.mdpi.com/journal/polymers

231. Sun D, Chang C, Li S, Lin L. Near-field electrospinning. Nano Lett. 2006;6(4):839–42.

232. Nazemi MM, Khodabandeh A, Hadjizadeh A. Near-Field Electrospinning: Crucial Parameters, Challenges, and Applications [Internet]. Vol. 5, ACS Applied Bio Materials. American Chemical Society; 2022 [cited 2024 Oct 7]. p. 394–412. Available from: https://pubs.acs.org/doi/full/10.1021/acsabm.1c00944

233. He XX, Zheng J, Yu GF, You MH, Yu M, Ning X, et al. Near-Field Electrospinning: Progress and Applications. J Phys Chem C [Internet]. 2017 Apr 27 [cited 2024 Oct 7];121(16):8663–78. Available from: https://pubs.acs.org/doi/full/10.1021/acs.jpcc.6b12783

234. Härdelin L, Perzon E, Hagström B, Walkenström P, Gatenholm P. Influence of molecular weight and rheological behavior on electrospinning cellulose nanofibers from ionic liquids. J Appl Polym Sci. 2013 Nov 15;130(4):2303–10.

235. Casasola R, Thomas NL, Trybala A, Georgiadou S. Electrospun poly lactic acid (PLA) fibres: Effect of different solvent systems on fibre morphology and diameter. Polym (United Kingdom). 2014 Sep 2;55(18):4728–37.

236. Poursorkhabi V, Abdelwahab MA, Misra M, Khalil H, Gharabaghi B, Mohanty AK.

Processing, Carbonization, and Characterization of Lignin Based Electrospun Carbon Fibers: A Review. Front Energy Res. 2020 Sep 9;8:208.

237. Wang C, Chien HS, Yan KW, Hung CL, Hung KL, Tsai SJ, et al. Correlation between processing parameters and microstructure of electrospun poly(D,l-lactic acid) nanofibers. Polymer (Guildf). 2009 Nov 27;50(25):6100–10.

238. Scheideler WJ, Chen CH. The minimum flow rate scaling of Taylor cone-jets issued from a nozzle. Appl Phys Lett [Internet]. 2014 Jan 15 [cited 2022 Mar 4];104(2):024103. Available from: https://aip.scitation.org/doi/abs/10.1063/1.4862263

239. Al-Abduljabbar A, Farooq I. Electrospun Polymer Nanofibers: Processing, Properties, and Applications [Internet]. Vol. 15, Polymers. Multidisciplinary Digital Publishing Institute; 2023 [cited 2024 Jun 11]. p. 65. Available from: https://www.mdpi.com/2073-4360/15/1/65/htm

240. Huang ZM, Zhang YZ, Kotaki M, Ramakrishna S. A review on polymer nanofibers by electrospinning and their applications in nanocomposites. Compos Sci Technol. 2003 Nov 1;63(15):2223–53.

241. Li D, Wang Y, Xia Y. Electrospinning of polymeric and ceramic nanofibers as uniaxially aligned arrays. Nano Lett [Internet]. 2003 Aug 1 [cited 2025 Apr 4];3(8):1167–71. Available from: https://pubs.acs.org/doi/full/10.1021/nl0344256

242. Theron SA, Zussman E, Yarin AL. Experimental investigation of the governing parameters in the electrospinning of polymer solutions. Polymer (Guildf) [Internet]. 2004 [cited 2022 Feb 21];45(6):2017–30. Available from: https://koreauniv.pure.elsevier.com/en/publications/experimental-investigation-of-the-governing-parameters-in-the-ele

243. Fong H, Chun I, Reneker DH. Beaded nanofibers formed during electrospinning. In: Polymer. Elsevier; 1999. p. 4585–92.

244. Shenoy SL, Bates WD, Frisch HL, Wnek GE. Role of chain entanglements on fiber formation during electrospinning of polymer solutions: Good solvent, non-specific polymer-polymer interaction limit. Polymer (Guildf). 2005 Apr 25;46(10):3372–84.

245. Doshi J, Reneker DH. Electrospinning process and applications of electrospun fibers. J

Electrostat. 1995 Aug 1;35(2–3):151–60.

246. Thenmozhi S, Dharmaraj N, Kadirvelu K, Kim HY. Electrospun nanofibers: New generation materials for advanced applications. Vol. 217, Materials Science and Engineering: B. Elsevier; 2017. p. 36–48.

247. Haider A, Haider S, Kang IK. A comprehensive review summarizing the effect of electrospinning parameters and potential applications of nanofibers in biomedical and biotechnology. Arabian Journal of Chemistry. 2015 Dec 12;

248. Chang FC, Chan KK, Chang CY. The effect of processing parameters on formation of lignosulfonate fibers produced using electrospinning technology. BioResources. 2016 Apr 13;11(2):4705–17.

249. Li Q, Xie S, Serem WK, Naik MT, Liu L, Yuan JS. Quality carbon fibers from fractionated lignin. Green Chem. 2017;19(7):1628–34.

250. Latham J, Roxburgh I. Disintegration of pairs of water drops in an electric field. Proc R Soc London Ser A Math Phys Sci [Internet]. 1966 Nov 8 [cited 2024 Aug 7];295(1440):84–97. Available from: https://royalsocietypublishing.org/doi/10.1098/rspa.1966.0227

251. Megelski S, Stephens JS, Bruce Chase D, Rabolt JF. Micro- and nanostructured surface morphology on electrospun polymer fibers. Macromolecules [Internet]. 2002 Oct 22 [cited 2024 Mar 28];35(22):8456–66. Available from: https://pubs.acs.org/doi/full/10.1021/ma020444a

252. Roman J, Neri W, Derré A, Poulin P. Electrospun lignin-based twisted carbon nanofibers for potential microelectrodes applications. Carbon N Y. 2019 Apr 1;145:556–64.

253. Yao M, Bi X, Wang Z, Yu P, Dufresne A, Jiang C. Recent advances in lignin-based carbon materials and their applications: A review. Vol. 223, International Journal of Biological Macromolecules. Elsevier; 2022. p. 980–1014.

254. Brandt A, Gräsvik J, Hallett JP, Welton T. Deconstruction of lignocellulosic biomass with ionic liquids [Internet]. Vol. 15, Green Chemistry. The Royal Society of Chemistry; 2013 [cited 2024 Aug 8]. p. 550–83. Available from: https://pubs.rsc.org/en/content/articlehtml/2013/gc/c2gc36364j

255. Liu H, Hsieh YL Lo. Ultrafine fibrous cellulose membranes from electrospinning of cellulose acetate. J Polym Sci Part B Polym Phys [Internet]. 2002 Sep 15 [cited 2019 Jul 19];40(18):2119–29. Available from: http://doi.wiley.com/10.1002/polb.10261

256. Ludmila H, Michal J, Andrea Š, Aleš H. Lignin, potential products and their market value. Wood Res. 2015;60(6):973–86.

257. Janssen M, Gustafsson E, Echardt L, Wallinder J, Wolf J, Skogsägarna ekonomisk förening S. Life cycle assessment of lignin-based carbon fibres. 2019;(October):1–10.

258. Parot M, Rodrigue D, Stevanovic T. Electrospinning of Softwood Organosolv Lignin without Polymer Addition. ACS Sustain Chem Eng [Internet]. 2023 Jan 16 [cited 2024 Aug 7];11(2):607–16. Available from: https://pubs.acs.org/doi/full/10.1021/acssuschemeng.2c05233

259. Mikeš P, Baker DA, Uhlin A, Lukáš D, Kuželová-Košťáková E, Vidrich A, et al. The Mass Production of Lignin Fibres by Means of Needleless Electrospinning. J Polym Environ [Internet]. 2021 [cited 2022 Mar 4];29(7):2164–73. Available from: https://doi.org/10.1007/s10924-020-02029-7

260. Hararak B, Khan I, Fernando GF. Single-Solvent Fractionation and Electro-Spinning Neat Softwood Kraft Lignin. ACS Appl Bio Mater [Internet]. 2023 [cited 2024 Aug 6];6(8):3153–65. Available from: https://doi.org/10.1021/acsabm.3c00278

261. Hosseinaei O, Harper DP, Bozell JJ, Rials TG. Role of Physicochemical Structure of Organosolv Hardwood and Herbaceous Lignins on Carbon Fiber Performance. ACS Sustain Chem Eng. 2016;4(10):5785–98.

262. Poursorkhabi V, Mohanty AK, Misra M. Statistical analysis of the effects of carbonization parameters on the structure of carbonized electrospun organosolv lignin fibers. J Appl Polym Sci. 2016 Dec 5;133(45).

263. Misra M, Poursorkhabi V, Schreiber M, Vivekanandhan S, Mohanty AK, Discovery B, et al. Carbonized Electrospun Lignin Fibers : Processing and Characterization. 2015;(July):19–24.

264. Foston M, Nunnery GA, Meng X, Sun Q, Baker FS, Ragauskas A. NMR a critical tool to study the production of carbon fiber from lignin. Carbon N Y [Internet]. 2013 [cited 2022

Aug 3];52:65–73. Available from: http://dx.doi.org/10.1016/j.carbon.2012.09.006

265. Kleinhans H, Salmén L. Development of lignin carbon fibers: Evaluation of the carbonization process. J Appl Polym Sci. 2016 Oct 10;133(38).

266. Frank E, Hermanutz F, Buchmeiser MR. Carbon fibers: Precursors, manufacturing, and properties. Vol. 297, Macromolecular Materials and Engineering. 2012. p. 493–501.

267. Kawamoto H. Lignin pyrolysis reactions. Vol. 63, Journal of Wood Science. 2017. p. 117–32.

268. Custodis VBF, Bährle C, Vogel F, Van Bokhoven JA. Phenols and aromatics from fast pyrolysis of variously prepared lignins from hard- and softwoods. J Anal Appl Pyrolysis. 2015 Sep 1;115:214–23.

269. Wei L, Agarwal UP, Matuana L, Sabo RC, Stark NM. Performance of high lignin content cellulose nanocrystals in poly(lactic acid). Polymer (Guildf). 2018 Jan 17;135:305–13.

270. Dong Z, Dufour A, Laine R, Leclerc S, Jia L, Chen Y, et al. Impacts of the hydroxyls crosslinking on lignin softening and pyrolysis via in situ 1H NMR, rheology, DRIFT and SPI-MS. Fuel Process Technol. 2022 Nov 1;236.

271. Suota MJ, da Silva TA, Zawadzki SF, Sassaki GL, Hansel FA, Paleologou M, et al. Chemical and structural characterization of hardwood and softwood LignoForce^{TM} lignins. Ind Crops Prod. 2021 Dec 1;173:114138.

272. Tang M., Bacon R. Carbonization of cellulose fibers—I. Low temperature pyrolysis. Carbon N Y [Internet]. 1964 Dec [cited 2019 Jul 8];2(3):211–20. Available from: https://linkinghub.elsevier.com/retrieve/pii/0008622364900351

273. Shrestha B, Le Brech Y, Ghislain T, Leclerc S, Carré V, Aubriet F, et al. A Multitechnique Characterization of Lignin Softening and Pyrolysis. ACS Sustain Chem Eng [Internet]. 2017 Aug 7 [cited 2023 May 11];5(8):6940–9. Available from: https://pubs.acs.org/doi/full/10.1021/acssuschemeng.7b01130

274. Shen D, Xiao R, Gu S, Luo K. The pyrolytic behavior of cellulose in lignocellulosic biomass: A review. Vol. 1, RSC Advances. 2011. p. 1641–60.

275. Constant S, Wienk HLJ, Frissen AE, Peinder P De, Boelens R, Van Es DS, et al. New

insights into the structure and composition of technical lignins: A comparative characterisation study. Green Chem [Internet]. 2016 May 3 [cited 2022 Aug 18];18(9):2651–65. Available from: https://pubs.rsc.org/en/content/articlehtml/2016/gc/c5gc03043a

276. Sharma RK, Wooten JB, Baliga VL, Lin X, Chan WG, Hajaligol MR. Characterization of chars from pyrolysis of lignin. In: Fuel. 2004. p. 1469–82.

277. Yang J, Wang X, Shen B, Hu Z, Xu L, Yang S. Lignin from energy plant (Arundo donax): Pyrolysis kinetics, mechanism and pathway evaluation. Renew Energy [Internet]. 2020 Dec 1 [cited 2025 Aug 6];161:963–71. Available from: https://www.sciencedirect.com/science/article/pii/S0960148120312611?via%3Dihub#fig7

278. Li R, Greenchem /, Liu SL, Yuan JS, Li Q, Xie S, et al. Cutting-edge research for a greener sustainable future As featured in: Quality carbon fibers from fractionated lignin. Green Chem. 2017;19(7):1589–784.

279. Meek N, Penumadu D, Hosseinaei O, Harper D, Young S, Rials T. Synthesis and characterization of lignin carbon fiber and composites. Compos Sci Technol. 2016 Dec 12;137:60–8.

280. König S, Bauch V, Herbert C, Wego A, Steinmann M, Frank E, et al. High-Performance Carbon Fibers Prepared by Continuous Stabilization and Carbonization of Electron Beam-Irradiated Textile Grade Polyacrylonitrile Fibers. Macromol Mater Eng. 2021 Dec 1;306(12).

281. Imarc. imarc. 2023 [cited 2024 Oct 7]. p. 1 Acrylonitrile Prices, News, Chart, Index, Analysis & Demand. Available from: https://www.imarcgroup.com/acrylonitrile-pricing-report

282. Mainka H, Täger O, Körner E, Hilfert L, Busse S, Edelmann FT, et al. Lignin - An alternative precursor for sustainable and cost-effective automotive carbon fiber. J Mater Res Technol. 2015;4(3):283–96.

283. Goudarzi A, Lin LT, Ko FK. X-Ray Diffraction Analysis of Kraft Lignins and Lignin-Derived Carbon Nanofibers. J Nanotechnol Eng Med. 2014 Sep 4;5(2):021006.

284. Kubo S, Kadla JF. Lignin-based carbon fibers: Effect of synthetic polymer blending on

fiber properties. J Polym Environ [Internet]. 2005 Apr [cited 2024 Oct 3];13(2):97–105. Available from: https://link.springer.com/article/10.1007/s10924-005-2941-0

285. Baker DA, Rials TG. Recent advances in low-cost carbon fiber manufacture from lignin. Vol. 130, Journal of Applied Polymer Science. 2013. p. 713–28.

286. Norberg I, Nordström Y, Drougge R, Gellerstedt G, Sjöholm E. A new method for stabilizing softwood kraft lignin fibers for carbon fiber production. J Appl Polym Sci. 2013;128(6):3824–30.

287. Ragauskas AJ, Beckham GT, Biddy MJ, Chandra R, Chen F, Davis MF, et al. Lignin valorization: Improving lignin processing in the biorefinery [Internet]. Vol. 344, Science. American Association for the Advancement of Science; 2014 [cited 2025 Jul 23]. Available from: https://pubmed.ncbi.nlm.nih.gov/24833396/

288. Frank E, Steudle LM, Ingildeev D, Spörl JM, Buchmeiser MR. Carbon fibers: Precursor systems, processing, structure, and properties. Vol. 53, Angewandte Chemie - International Edition. Wiley-VCH Verlag; 2014. p. 5262–98.

289. Baker FS. Low Cost Carbon Fiber from Renewable Resources. 2010 [cited 2017 Nov 23]; Available from: https://www1.eere.energy.gov/vehiclesandfuels/pdfs/merit_review_2010/lightweight_materials/lm005_baker_2010_o.pdf

290. Park SJ, Heo GY. Precursors and Manufacturing of Carbon Fibers. [cited 2019 Jul 8]; Available from: https://pdfs.semanticscholar.org/783c/c5143885e3a460a78c0a35890f0a25fea096.pdf

291. Gliścińska E, Babeł K. Preparation of activated carbon fibres from electrospun polyacrylonitrile fibre mat and characterisation of their chemical and structural properties. Fibres Text East Eur. 2013;99(3):42–7.

292. Ma A, Zhou L, Chang J. Conversion of lignin-nanofibers to CNFs. Nano. 2015 Aug 31;10(6).

293. Hu P, Jin H, Wang K, Zhao Z, Qu W. Lignin-based carbon nanofibers: Morphologies, properties, and features as substrates for pseudocapacitor electrodes. Int J Biol Macromol [Internet]. 2021 Dec 15 [cited 2022 Apr 8];193:519–27. Available from:

https://doi.org/10.1016/j.ijbiomac.2021.10.108

294. Saha D, Payzant EA, Kumbhar AS, Naskar AK. Sustainable mesoporous carbons as storage and controlled-delivery media for functional molecules. ACS Appl Mater Interfaces [Internet]. 2013 Jun 26 [cited 2025 Jul 23];5(12):5868–74. Available from: /doi/pdf/10.1021/am401661f?ref=article_openPDF

295. Zhou L, Budarin V, Fan J, Sloan R, Macquarrie D. Efficient Method of Lignin Isolation Using Microwave-Assisted Acidolysis and Characterization of the Residual Lignin. ACS Sustain Chem Eng [Internet]. 2017 May 10 [cited 2017 Oct 10];5(5):3768–74. Available from: http://pubs.acs.org/doi/abs/10.1021/acssuschemeng.6b02545

296. Wang S, Li WX, Yang YQ, Chen X, Ma J, Chen C, et al. Unlocking Structure–Reactivity Relationships for Catalytic Hydrogenolysis of Lignin into Phenolic Monomers. ChemSusChem [Internet]. 2020 Sep 7 [cited 2024 Apr 11];13(17):4548–56. Available from: https://onlinelibrary.wiley.com/doi/full/10.1002/cssc.202000785

297. Sun JX, Sun XF, Sun RC, Fowler P, Baird MS. Inhomogeneities in the Chemical Structure of Sugarcane Bagasse Lignin. J Agric Food Chem [Internet]. 2003 Nov 6 [cited 2024 Mar 14];51(23):6719–25. Available from: https://www.degruyter.com/document/doi/10.1515/HF.2003.025/html

298. Sun RC. Cereal straw as a resource for sustainable biomaterials and biofuels: Chemistry, extractives, lignins, hemicelluloses and cellulose. Cereal Straw as a Resource for Sustainable Biomaterials and Biofuels: Chemistry, Extractives, Lignins, Hemicelluloses and Cellulose. Elsevier; 2010. 1–292 p.

299. Galkin S, Ämmälahti E, Kilpeläinen I, Brunow G, Hatakka A. Characterisation of milled wood lignin from reed canary grass (Phalaris arundinacea). Holzforschung. 1997;51(2):130–4.

300. Santos RB, Capanema EA, Balakshin MY, Chang HM, Jameel H. Lignin structural variation in hardwood species. J Agric Food Chem [Internet]. 2012 May 16 [cited 2023 Dec 18];60(19):4923–30. Available from: https://pubs.acs.org/doi/full/10.1021/jf301276a

301. Rolando C, Monties B, Lapierre C. Thioacidolysis. In: Methods In Lignin Chemistry [Internet]. Springer, Berlin, Heidelberg; 1992 [cited 2024 Mar 7]. p. 334–49. Available

from: https://link.springer.com/chapter/10.1007/978-3-642-74065-7_23

302. Yuan TQ, Xu F, Sun RC. Role of lignin in a biorefinery: Separation characterization and valorization [Internet]. Vol. 88, Journal of Chemical Technology and Biotechnology. John Wiley & Sons, Ltd; 2013 [cited 2024 Apr 11]. p. 346–52. Available from: https://onlinelibrary.wiley.com/doi/full/10.1002/jctb.3996

303. Mechanism study of wood lignin pyrolysis by using TG–FTIR analysis. J Anal Appl Pyrolysis [Internet]. 2008 May 1 [cited 2017 Oct 18];82(1):170–7. Available from: http://www.sciencedirect.com/science/article/pii/S0165237008000351?via%3Dihub

304. J Am HJ, Haw JF, Maciel GE, Schroeder HA. Carbon-13 Nuclear Magnetic Resonance Spectrometric Study of Wood and Wood Pulping with Cross Polarization and Magic-Angle Spinning [Internet]. Vol. 56, Pattern Recognition Principles. Addison-Wesley; 1984 [cited 2024 Apr 30]. Available from: https://pubs.acs.org/sharingguidelines

305. Pu Y, Cao S, Ragauskas AJ. Application of quantitative 31P NMR in biomass lignin and biofuel precursors characterization [Internet]. Vol. 4, Energy and Environmental Science. The Royal Society of Chemistry; 2011 [cited 2022 Aug 18]. p. 3154–66. Available from: https://pubs.rsc.org/en/content/articlehtml/2011/ee/c1ee01201k

306. Lundquist K, Sjöholm R, Teien G, Pakkanen T, Servin R, Sternerup H, et al. NMR Studies of Lignins. 2. Interpretation of the 1H NMR Spectrum of Acetylated Birch Lignin. Acta Chem Scand. 1979;33b:27–30.

307. Seo DK, Jeun JP, Kim H Bin, Kang PH. Preparation and Characterization of the Carbon Nanofiber Mat Produced From Electrospun Pan / Lignin Precursors By Electron Beam Irradiation. Rev Adv Mater Sci. 2011;28(3):31–4.

308. Tejado A, Peña C, Labidi J, Echeverria JM, Mondragon I. Physico-chemical characterization of lignins from different sources for use in phenol-formaldehyde resin synthesis. Bioresour Technol [Internet]. 2007 May [cited 2023 Oct 26];98(8):1655–63. Available from: https://pubmed.ncbi.nlm.nih.gov/16843657/

309. Chen Y, Zou C, Mastalerz M, Hu S, Gasaway C, Tao X. Applications of micro-fourier transform infrared spectroscopy (FTIR) in the geological sciences—A Review [Internet]. Vol. 16, International Journal of Molecular Sciences. Multidisciplinary Digital Publishing

Institute; 2015 [cited 2024 May 15]. p. 30223–50. Available from: https://www.mdpi.com/1422-0067/16/12/26227/htm

310. von Aulock FW, Kennedy BM, Schipper CI, Castro JM, E. Martin D, Oze C, et al. Advances in Fourier transform infrared spectroscopy of natural glasses: From sample preparation to data analysis. Vols. 206–207, Lithos. Elsevier; 2014. p. 52–64.

311. Rossman GR. Analytical methods for measuring water in nominally anhydrous minerals. In: Water in Nominally Anhydrous Minerals. GeoScienceWorld; 2018. p. 1–28.

312. Gao J, Liang Z, Liang J, Wang W, Lü J, Qin Y. Spectrum Reconstruction of a Spatially Modulated Fourier Transform Spectrometer Based on Stepped Mirrors. Appl Spectrosc [Internet]. 2017 Jun 1 [cited 2024 May 15];71(6):1348–56. Available from: https://journals.sagepub.com/doi/full/10.1177/0003702816669729

313. Sa'don NA, Rahim AA, Hussin MH. The effect of p-nitrophenol toward the structural characteristics and antioxidant activity of oil palm fronds (OPF) lignin polymers. Int J Biol Macromol [Internet]. 2017 [cited 2024 Apr 30];98:701–8. Available from: http://dx.doi.org/10.1016/j.ijbiomac.2017.01.137

314. Lisperguer J, Perez P, Urizar S. Structure and thermal properties of lignins: Characterization by infrared spectroscopy and differential scanning calorimetry. J Chil Chem Soc [Internet]. 2009 [cited 2024 Apr 30];54(4):460–3. Available from: http://www.scielo.cl/scielo.php?script=sci_arttext&pid=S0717-97072009000400030&lng=es&nrm=iso&tlng=en

315. Wiercigroch E, Szafraniec E, Czamara K, Pacia MZ, Majzner K, Kochan K, et al. Raman and infrared spectroscopy of carbohydrates: A review [Internet]. Vol. 185, Spectrochimica Acta - Part A: Molecular and Biomolecular Spectroscopy. 2017 [cited 2024 Apr 30]. p. 317–35. Available from: http://dx.doi.org/10.1016/j.saa.2017.05.045

316. Law KN, Daud WRW, Ghazali A. Morphological and chemical nature of fiber strands of oil palm empty-fruit-bunch (OPEFB). BioResources. 2007;2(3):351–62.

317. Li J, Gellerstedt G. Improved lignin properties and reactivity by modifications in the autohydrolysis process of aspen wood. Ind Crops Prod. 2008;27(2):175–81.

318. Moubarik A, Grimi N, Boussetta N, Pizzi A. Isolation and characterization of lignin from

Moroccan sugar cane bagasse: Production of lignin-phenol-formaldehyde wood adhesive. Ind Crops Prod [Internet]. 2013 [cited 2024 Apr 30];45:296–302. Available from: http://dx.doi.org/10.1016/j.indcrop.2012.12.040

319. Nadji H, Diouf PN, Benaboura A, Bedard Y, Riedl B, Stevanovic T. Comparative study of lignins isolated from Alfa grass (Stipa tenacissima L.). Bioresour Technol. 2009;100(14):3585–92.

320. Day A, Ruel K, Neutelings G, Crônier D, David H, Hawkins S, et al. Lignification in the flax stem: Evidence for an unusual lignin in bast fibers. Planta [Internet]. 2005 Oct 21 [cited 2024 Apr 30];222(2):234–45. Available from: https://link.springer.com/article/10.1007/s00425-005-1537-1

321. Hussin MH, Rahim AA, Mohamad Ibrahim MN, Brosse N. Physicochemical characterization of alkaline and ethanol organosolv lignins from oil palm (Elaeis guineensis) fronds as phenol substitutes for green material applications. Ind Crops Prod [Internet]. 2013 [cited 2024 Apr 30];49:23–32. Available from: http://dx.doi.org/10.1016/j.indcrop.2013.04.030

322. Latif NHA, Rahim AA, Brosse N, Hussin MH. The structural characterization and antioxidant properties of oil palm fronds lignin incorporated with p-hydroxyacetophenone. Int J Biol Macromol [Internet]. 2019 [cited 2024 Apr 30];130:947–57. Available from: https://doi.org/10.1016/j.ijbiomac.2019.03.032

323. Hazwan Hussin M, Aziz AA, Iqbal A, Ibrahim MNM, Latif NHA. Development and characterization novel bio-adhesive for wood using kenaf core (Hibiscus cannabinus) lignin and glyoxal. Int J Biol Macromol. 2019 Feb 1;122:713–22.

324. Akbari S, Bahi A, Farahani A, Milani AS, Ko F. Fabrication and characterization of lignin/dendrimer electrospun blended fiber mats. Molecules [Internet]. 2021 [cited 2024 May 13];26(3). Available from: https://doi.org/10.3390/molecules26030518

325. Fengel D, Wegener G. Wood: Chemistry, Ultrastructure, Reactions. 1983;

326. López Pasquali CE, Herrera H. Pyrolysis of lignin and IR analysis of residues. Thermochim Acta. 1997 Jun 1;293(1–2):39–46.

327. Mohseni M, Akbari S, Pajootan E, Mazaheri F. Amine-terminated dendritic polymers as a

multifunctional chelating agent for heavy metal ion removals. Environ Sci Pollut Res [Internet]. 2019 May 1 [cited 2024 May 15];26(13):12689–97. Available from: https://link.springer.com/article/10.1007/s11356-019-04765-3

328. Shen DK, Gu S, Luo KH, Wang SR, Fang MX. The pyrolytic degradation of wood-derived lignin from pulping process. Bioresour Technol. 2010 Aug 1;101(15):6136–46.

329. Liu Q, Wang S, Zheng Y, Luo Z, Cen K. Mechanism study of wood lignin pyrolysis by using TG-FTIR analysis. J Anal Appl Pyrolysis. 2008 May 1;82(1):170–7.

330. Fenner RA, Lephardt JO. Examination of the Thermal Decomposition of Kraft Pine Lignin by Fourier Transform Infrared Evolved Gas Analysis. J Agric Food Chem [Internet]. 1981 [cited 2024 May 15];29(4):846–9. Available from: https://pubs.acs.org/doi/abs/10.1021/jf00106a042

331. Kanani-Jazi MH, Akbari S, Haghighat Kish M. Efficient removal of Cr (VI) from aqueous solution by halloysite/poly(amidoamine) dendritic nano-hybrid materials: kinetic, isotherm and thermodynamic studies. Adv Powder Technol. 2020 Sep 1;31(9):4018–30.

332. Liu J, Dai Y, Li L. Progress in the development of a 25 T all superconducting NMR magnet. Cryogenics (Guildf). 2016 Oct 1;79:79–84.

333. Ralph S, Landucci L, Service UF, Ralph J. NMR Database of Lignin and Cell Wall Model Compounds. 2004 [cited 2022 Aug 15]; Available from: http://www.dfrc.ars.usda.gov

334. Carreras H. Technology Networks. 2021 [cited 2024 Mar 6]. p. 1 NMR Spectroscopy Principles, Interpreting an NMR Spectrum and Common Problems. Available from: https://www.technologynetworks.com/analysis/articles/nmr-spectroscopy-principles-interpreting-an-nmr-spectrum-and-common-problems-355891

335. Wen JL, Sun SL, Xue BL, Sun RC. Recent advances in characterization of lignin polymer by solution-state nuclear magnetic resonance (NMR) methodology [Internet]. Vol. 6, Materials. Materials (Basel); 2013 [cited 2022 Jul 13]. p. 359–91. Available from: https://pubmed.ncbi.nlm.nih.gov/28809313/

336. PJ H. Nuclear magnetic resonance. Oxford Univ Press [Internet]. 2015 [cited 2024 Mar 6];2:23. Available from: https://global.oup.com/academic/product/nuclear-magnetic-resonance-9780198703419

337. Schnell I. Basic One- and Two-Dimensional NMR Spectroscopy. Fourth, Completely Revised and Updated Edition. By Horst Friebolin. ChemPhysChem [Internet]. 2005 Jun 13 [cited 2024 Mar 6];6(6):1187–8. Available from: https://onlinelibrary.wiley.com/doi/full/10.1002/cphc.200500002

338. Barbucci R, Leone G, Chiumiento A, Di Cocco ME, D'Orazio G, Gianferri R, et al. Low- and high-resolution nuclear magnetic resonance (NMR) characterisation of hyaluronan-based native and sulfated hydrogels. Carbohydr Res [Internet]. 2006 Aug 14 [cited 2022 Nov 21];341(11):1848–58. Available from: https://pubmed.ncbi.nlm.nih.gov/16716277/

339. Lee JH, Okuno Y, Cavagnero S. Sensitivity enhancement in solution NMR: Emerging ideas and new frontiers. J Magn Reson [Internet]. 2014 Apr 1 [cited 2022 Nov 21];241(1):18–31. Available from: /pmc/articles/PMC3967054/

340. Spyros A, Dais P. Theoretical Aspects. In: NMR Spectroscopy in Food Analysis [Internet]. The Royal Society of Chemistry; 2012 [cited 2024 Mar 6]. p. 5–66. Available from: https://books.rsc.org/books/monograph/973/chapter/773330/Theoretical-Aspects

341. Griesinger C, Bennati M, Vieth HM, Luchinat C, Parigi G, Höfer P, et al. Dynamic nuclear polarization at high magnetic fields in liquids. Vol. 64, Progress in Nuclear Magnetic Resonance Spectroscopy. Pergamon; 2012. p. 4–28.

342. Ralph J, Landucci L. NMR of Lignins. In: Lignin and Lignans. 2010. p. 137–243.

343. Ralph J, Marita JM, Ralph SA, Hatfield RD, Lu F, Ede RM, et al. Solution-State NMR of Lignins Chapter 3. Adv Lignocellul Charact Chapter 3. 1999;3(5):55–108.

344. Meng X, Crestini C, Ben H, Hao N, Pu Y, Ragauskas AJ, et al. Determination of hydroxyl groups in biorefinery resources via quantitative 31P NMR spectroscopy. Nat Protoc [Internet]. 2019 Aug 7 [cited 2023 Nov 27];14(9):2627–47. Available from: https://www.nature.com/articles/s41596-019-0191-1

345. Crestini C, Lange H, Sette M, Argyropoulos DS. On the structure of softwood kraft lignin. Green Chem [Internet]. 2017 Aug 29 [cited 2023 Dec 18];19(17):4104–21. Available from: https://pubs.rsc.org/en/content/articlehtml/2017/gc/c7gc01812f

346. Chen CL, Robert D. Characterization of lignin by 1H and 13C NMR spectroscopy. Methods Enzymol. 1988 Jan 1;161(C):137–74.

347. Robert D, Ämmälahti E, Bardet M, Brunow G, Kilpeläinen I, Lundquist K, et al. Improvement in NMR Structural Studies of Lignin Through Two- and Three-Dimensional NMR Detection and Isotopic Enrichment. ACS Symp Ser. 1998;697:237–54.

348. Gil AM, Lopes MH, Pascoal Neto C, Rocha J. Very high-resolution 1H MAS NMR of a natural polymeric material. Solid State Nucl Magn Reson. 1999 Oct 1;15(1):59–67.

349. Rönnols J, Danieli E, Freichels H, Aldaeus F. Lignin analysis with benchtop NMR spectroscopy. Holzforschung [Internet]. 2020 Feb 1 [cited 2022 Aug 1];74(2):226–31. Available from: https://www.degruyter.com/document/doi/10.1515/hf-2018-0282/html

350. Ludwig CH, Nist BJ, McCarthy JL. Lignin. XII.1 The High Resolution Nuclear Magnetic Resonance Spectroscopy of Protons in Compounds Related to Lignin. J Am Chem Soc [Internet]. 1964 Mar 1 [cited 2022 Aug 4];86(6):1186–96. Available from: https://pubs.acs.org/doi/abs/10.1021/ja01060a046

351. Lundquist K. Proton (1H) NMR Spectroscopy. In: Methods In Lignin Chemistry [Internet]. Springer, Berlin, Heidelberg; 1992 [cited 2022 Aug 4]. p. 242–9. Available from: https://link.springer.com/chapter/10.1007/978-3-642-74065-7_17

352. Kelly TJ, O'Connor C, Kilcawley KN. Sources of Volatile Aromatic Congeners in Whiskey. Beverages [Internet]. 2023 Sep 1 [cited 2024 Aug 8];9(3). Available from: https://www.researchgate.net/publication/372872754_Sources_of_Volatile_Aromatic_Congeners_in_Whiskey

353. Pylypchuk I V., Lindén PA, Lindström ME, Sevastyanova O. New Insight into the Surface Structure of Lignin Nanoparticles Revealed by 1H Liquid-State NMR Spectroscopy. ACS Sustain Chem Eng [Internet]. 2020 Sep 14 [cited 2022 Aug 3];8(36):13805–12. Available from: https://pubs.acs.org/doi/full/10.1021/acssuschemeng.0c05119

354. Sette M, Lange H, Crestini C. Quantitative HSQC analyses of lignin: A practical comparison. Comput Struct Biotechnol J [Internet]. 2013 [cited 2022 Jul 13];6(7):e201303016. Available from: https://pubmed.ncbi.nlm.nih.gov/24688724/

355. Lundquist K. 1H NMR spectral studies of lignins. Nord Pulp Pap Res J [Internet]. 1991 Aug 1 [cited 2024 Apr 30];6(3):140–6. Available from:

https://www.degruyter.com/document/doi/10.3183/npprj-1991-06-03-p140-146/html

356. Hu J, Xiao R, Shen D, Zhang H. Structural analysis of lignin residue from black liquor and its thermal performance in thermogravimetric-Fourier transform infrared spectroscopy. Bioresour Technol [Internet]. 2013 [cited 2024 Apr 30];128:633–9. Available from: http://dx.doi.org/10.1016/j.biortech.2012.10.148

357. Zeng J, Helms GL, Gao X, Chen S. Quantification of wheat straw lignin structure by comprehensive NMR analysis. J Agric Food Chem [Internet]. 2013 [cited 2022 Aug 1];61(46):10848–57. Available from: https://doi.org/10.1021/jf4030486

358. Buranov AU, Mazza G. Lignin in straw of herbaceous crops. Vol. 28, Industrial Crops and Products. 2008. p. 237–59.

359. Capanema EA, Balakshin MY, Kadla JF. A Comprehensive Approach for Quantitative Lignin Characterization by NMR Spectroscopy. J Agric Food Chem [Internet]. 2004 Apr 7 [cited 2022 Aug 1];52(7):1850–60. Available from: https://pubs.acs.org/doi/full/10.1021/jf035282b

360. Capanema EA, Balakshin MY, Kadla JF. Quantitative characterization of a hardwood milled wood lignin by nuclear magnetic resonance spectroscopy. J Agric Food Chem [Internet]. 2005 Dec 14 [cited 2022 Aug 18];53(25):9639–49. Available from: https://pubs.acs.org/doi/full/10.1021/jf0515330

361. Xu F, Sun JX, Sun R, Fowler P, Baird MS. Comparative study of organosolv lignins from wheat straw. Ind Crops Prod. 2006;23(2):180–93.

362. Pang B, Yang S, Fang W, Yuan TQ, Argyropoulos DS, Sun RC. Structure-property relationships for technical lignins for the production of lignin-phenol-formaldehyde resins. Ind Crops Prod [Internet]. 2017 [cited 2024 Apr 30];108:316–26. Available from: http://dx.doi.org/10.1016/j.indcrop.2017.07.009

363. Faix O, Argyropoulos DS, Robert D, Neirinck V. Determination of hydroxyl groups in lignins evaluation of 1H- 13C-, 31P-NMR, FTIR and wet chemical methods. Holzforschung [Internet]. 1994 Jan 1 [cited 2024 Apr 30];48(5):387–94. Available from: https://www.degruyter.com/document/doi/10.1515/hfsg.1994.48.5.387/html

364. Pan X, Arato C, Gilkes N, Gregg D, Mabee W, Pye K, et al. Biorefining of softwoods

using ethanol organosolv pulping: Preliminary evaluation of process streams for manufacture of fuel-grade ethanol and co-products. Biotechnol Bioeng [Internet]. 2005 May 20 [cited 2024 Apr 30];90(4):473–81. Available from: https://onlinelibrary.wiley.com/doi/full/10.1002/bit.20453

365. Bonawitz ND, Chapple C. The genetics of lignin biosynthesis: Connecting genotype to phenotype [Internet]. Vol. 44, Annual Review of Genetics. Annual Reviews; 2010 [cited 2022 Aug 18]. p. 337–63. Available from: https://www.annualreviews.org/doi/abs/10.1146/annurev-genet-102209-163508

366. Giummarella N, Gioia C, Lawoko M. A one-pot biomimetic synthesis of selectively functionalized lignins from monomers: A green functionalization platform. Green Chem. 2018;20(11):2651–62.

367. Obst BJR, Landucci LL. Quantitative 13-C NMR of Lignins – Methoxyl : Aryl Ratio. Holzforschung. 1986;40:87–92.

368. Landucci LL, Ralph SA. Assessment of lignin model quality in lignin chemical shift assignments - Substituent and solvent effects. J Wood Chem Technol [Internet]. 1997 [cited 2022 Aug 15];17(4):361–82. Available from: https://www.tandfonline.com/doi/abs/10.1080/02773819708003138

369. Watkins CL. Introduction to NMR spectroscopy. J Magn Reson [Internet]. 1989 [cited 2022 Aug 18];84(1):220. Available from: https://www.wiley.com/en-gb/Introduction+to+Solid+State+NMR+Spectroscopy-p-9781405109147

370. Bardet M, Foray MF, Guillermo A. High-Resolution Solid-State NMR as an Analytical Tool to Study Plant Seeds. In: Modern Magnetic Resonance [Internet]. Springer, Dordrecht; 2008 [cited 2022 Aug 18]. p. 1777–81. Available from: https://link.springer.com/chapter/10.1007/1-4020-3910-7_201

371. Hatcher PG. Chemical structural studies of natural lignin by dipolar dephasing solid-state 13C nuclear magnetic resonance. Org Geochem. 1987 Jan 1;11(1):31–9.

372. Ibrahim MNM, Wan Rosli WD, Chuah SB. Monitoring Quality of Soda Black Liquor of Oil Palm Empty Fruit Bunch Fibers in Terms of Storage Time and Temperature. J Teknol. 2012 Feb 25;42(C):21–8.

373. Kim H, Ralph J, Akiyama T. Solution-state 2D NMR of Ball-milled Plant Cell Wall Gels in DMSO-d 6. Org Biomol Chem [Internet]. 2010 Mar 4 [cited 2023 Dec 18];8(3):56–66. Available from: https://pubs.rsc.org/en/content/articlehtml/2010/ob/b916070a

374. She D, Nie XN, Xu F, Geng ZC, Jia HT, Jones GL, et al. Physico-chemical characterization of different alcoholsoluble lignins from rice straw. In: Cellulose Chemistry and Technology. 2012. p. 207–19.

375. Du X, Gellerstedt G, Li J. Universal fractionation of lignin-carbohydrate complexes (LCCs) from lignocellulosic biomass: An example using spruce wood. Plant J [Internet]. 2013 Apr 1 [cited 2023 Dec 18];74(2):328–38. Available from: https://onlinelibrary.wiley.com/doi/full/10.1111/tpj.12124

376. Zhang L, Gellerstedt G. Quantitative 2D HSQC NMR determination of polymer structures by selecting suitable internal standard references. Magn Reson Chem [Internet]. 2007 Jan 1 [cited 2022 Aug 18];45(1):37–45. Available from: https://onlinelibrary.wiley.com/doi/full/10.1002/mrc.1914

377. Mansfield SD, Kim H, Lu F, Ralph J. Whole plant cell wall characterization using solution-state 2D NMR. Nat Protoc [Internet]. 2012 Aug 2 [cited 2023 Dec 18];7(9):1579–89. Available from: https://www.nature.com/articles/nprot.2012.064

378. Yoo CG, Pu Y, Li M, Ragauskas AJ. Elucidating Structural Characteristics of Biomass using Solution-State 2 D NMR with a Mixture of Deuterated Dimethylsulfoxide and Hexamethylphosphoramide. ChemSusChem [Internet]. 2016 May 23 [cited 2023 Dec 18];9(10):1090–5. Available from: https://onlinelibrary.wiley.com/doi/full/10.1002/cssc.201600135

379. Shi Z, Xu G, Deng J, Dong M, Murugadoss V, Liu C, et al. Structural characterization of lignin from D. sinicus by FTIR and NMR techniques. Green Chem Lett Rev [Internet]. 2019 Jul 3 [cited 2023 Nov 27];12(3):235–43. Available from: https://www.tandfonline.com/doi/abs/10.1080/17518253.2019.1627428

380. Amiri MT, Bertella S, Questell-Santiago YM, Luterbacher JS. Establishing lignin structure-upgradeability relationships using quantitative 1H-13C heteronuclear single quantum coherence nuclear magnetic resonance (HSQC-NMR) spectroscopy. Chem Sci. 2019;10(35):8135–42.

381. Holombo B. Extractives. In: Sjöström E., Alén R. (eds) Analytical Methods in Wood Chemistry, Pulping, and Papermaking. Analytical methods in wood chemistry, pulping, and papermaking. Springer, Berlin, Heidelberg; 1999. 125–148 p.

382. Lange H, Rulli F, Crestini C. Gel Permeation Chromatography in Determining Molecular Weights of Lignins: Critical Aspects Revisited for Improved Utility in the Development of Novel Materials. ACS Sustain Chem Eng [Internet]. 2016 Oct 3 [cited 2024 May 16];4(10):5167–80. Available from: https://pubs.acs.org/doi/full/10.1021/acssuschemeng.6b00929

383. Trache D, Hussin MH, Hui Chuin CT, Sabar S, Fazita MRN, Taiwo OFA, et al. Microcrystalline cellulose: Isolation, characterization and bio-composites application—A review [Internet]. Vol. 93, International Journal of Biological Macromolecules. 2016 [cited 2024 May 1]. p. 789–804. Available from: http://dx.doi.org/10.1016/j.ijbiomac.2016.09.056

384. Faris AH, Ibrahim MNM, Rahim AA, Hussin MH, Brosse N. Preparation and characterization of lignin polyols from the residues of oil palm empty fruit bunch. BioResources. 2015;10(4):7339–52.

385. Melro E, Filipe A, Sousa D, Medronho B, Romano A. Revisiting lignin: A tour through its structural features, characterization methods and applications. Vol. 45, New Journal of Chemistry. 2021. p. 6986–7013.

386. Chen F, Li J. Aqueous gel permeation chromatographic methods for technical lignins. J Wood Chem Technol [Internet]. 2000 [cited 2024 May 16];20(3):265–76. Available from: https://www.tandfonline.com/doi/abs/10.1080/02773810009349636

387. Alvarez-Vasco C, Ma R, Quintero M, Guo M, Geleynse S, Ramasamy KK, et al. Unique low-molecular-weight lignin with high purity extracted from wood by deep eutectic solvents (DES): A source of lignin for valorization. Green Chem [Internet]. 2016 Sep 26 [cited 2024 May 16];18(19):5133–41. Available from: https://pubs.rsc.org/en/content/articlehtml/2016/gc/c6gc01007e

388. Gordobil O, Moriana R, Zhang L, Labidi J, Sevastyanova O. Assesment of technical lignins for uses in biofuels and biomaterials: Structure-related properties, proximate analysis and chemical modification. Ind Crops Prod. 2016 May 1;83:155–65.

389. Brosse N, Sannigrahi P, Ragauskas A. Pretreatment of miscanthus x giganteus using the ethanol organosolv process for ethanol production. Ind Eng Chem Res [Internet]. 2009 Sep 16 [cited 2024 May 1];48(18):8328–34. Available from: https://pubs.acs.org/doi/full/10.1021/ie9006672

390. El Hage R, Brosse N, Sannigrahi P, Ragauskas A. Effects of process severity on the chemical structure of Miscanthus ethanol organosolv lignin. Polym Degrad Stab. 2010;95(6):997–1003.

391. Himmel ME, Tatsumoto K, Oh KK, Grohmann K, Johnson DK, Chum HL. Molecular Weight Distribution of Aspen Lignins Estimated by Universal Calibration. In 1989 [cited 2024 May 2]. p. 82–99. Available from: https://pubs.acs.org/doi/abs/10.1021/bk-1989-0397.ch006

392. Chum HL, Johnson DK, Tucker MP, Himmel ME. Some aspects of lignin characterization by high performance size exclusion chromatography using styrene divinylbenzene copolymer gels. Holzforschung [Internet]. 1987 Jan 1 [cited 2024 May 2];41(2):97–108. Available from: https://www.degruyter.com/document/doi/10.1515/hfsg.1987.41.2.97/html

393. Cathala B, Saake B, Faix O, Monties B. Association behaviour of lignins and lignin model compounds studied by multidetector size-exclusion chromatography. J Chromatogr A. 2003;1020(2):229–39.

394. Norgren M, Edlund H, Wågberg L. Aggregation of lignin derivatives under alkaline conditions. Kinetics and aggregate structure. Langmuir [Internet]. 2002 Apr 2 [cited 2024 May 2];18(7):2859–65. Available from: https://pubs.acs.org/doi/full/10.1021/la011627d

395. Tolbert A, Akinosho H, Khunsupat R, Naskar AK, Ragauskas AJ. Characterization and analysis of the molecular weight of lignin for biorefining studies [Internet]. Vol. 8, Biofuels, Bioproducts and Biorefining. John Wiley & Sons, Ltd; 2014 [cited 2024 May 2]. p. 836–56. Available from: https://onlinelibrary.wiley.com/doi/full/10.1002/bbb.1500

396. Hussin MH, Rahim AA, Mohamad Ibrahim MN, Brosse N. Improved corrosion inhibition of mild steel by chemically modified lignin polymers from Elaeis guineensis agricultural waste. Mater Chem Phys [Internet]. 2015 [cited 2024 May 2];163:201–12. Available from: http://dx.doi.org/10.1016/j.matchemphys.2015.07.030

397. Carraher CE. Introduction to polymer chemistry fourth edition [Internet]. Introduction to Polymer Chemistry Fourth Edition. CRC Press; 2017 [cited 2024 Oct 2]. 1–560 p. Available from: https://www.taylorfrancis.com/books/mono/10.1201/9781315369488/introduction-polymer-chemistry-charles-carraher-jr

398. Sperling LH. Introduction to Physical Polymer Science: Fourth Edition [Internet]. Introduction to Physical Polymer Science: Fourth Edition. John Wiley and Sons; 2005 [cited 2024 Oct 2]. 1–845 p. Available from: https://onlinelibrary.wiley.com/doi/book/10.1002/0471757128

399. Billmeyer F. Textbook of polymer science. Vol. 13, Polymer. 1972. 597 p.

400. Sa'don NA, Rahim AA, Ibrahim MNM, Brosse N, Hussin MH. Modification of oil palm fronds lignin by incorporation of m-cresol for improving structural and antioxidant properties. Int J Biol Macromol [Internet]. 2017 [cited 2024 May 2];104:251–60. Available from: http://dx.doi.org/10.1016/j.ijbiomac.2017.06.038

401. Hussin MH, Han Zhang H, Aziz NA, Samad NA, Faris AH, Mohamad Ibrahim MN, et al. Preparation of environmental friendly phenol-formaldehyde wood adhesive modified with kenaf lignin. Beni-Suef Univ J Basic Appl Sci [Internet]. 2017 [cited 2024 May 2];6(4):409–18. Available from: http://dx.doi.org/10.1016/j.bjbas.2017.06.004

402. Del Río JC, Rencoret J, Gutiérrez A, Nieto L, Jiménez-Barbero J, Martínez ÁT. Structural characterization of guaiacyl-rich lignins in flax (Linum usitatissimum) fibers and shives. J Agric Food Chem [Internet]. 2011 Oct 26 [cited 2024 May 2];59(20):11088–99. Available from: https://pubs.acs.org/doi/full/10.1021/jf201222r

403. Hu Z, Du X, Liu J, Chang HM, Jameel H. Structural Characterization of Pine Kraft Lignin: BioChoice Lignin vs Indulin AT. J Wood Chem Technol [Internet]. 2016 Nov 1 [cited 2023 May 18];36(6):432–46. Available from: https://www.tandfonline.com/action/journalInformation?journalCode=lwct20

404. Hararak B. Fibre formation, characterisation and carbonisation of bio-based precursors. Thesis. 2020;(March):331.

405. Khan I. The fractionation, carbonisation and characterisation of electro-spun lignin fibres.

Thesis. 2020;(March):330.

406. Morandim-Giannetti AA, Agnelli JAM, Lanças BZ, Magnabosco R, Casarin SA, Bettini SHP. Lignin as additive in polypropylene/coir composites: Thermal, mechanical and morphological properties. Carbohydr Polym. 2012;87(4):2563–8.

407. Garcia-Maraver A, Salvachúa D, Martínez MJ, Diaz LF, Zamorano M. Analysis of the relation between the cellulose, hemicellulose and lignin content and the thermal behavior of residual biomass from olive trees. Waste Manag [Internet]. 2013 [cited 2024 May 2];33(11):2245–9. Available from: http://dx.doi.org/10.1016/j.wasman.2013.07.010

408. Sun RC, Lu Q, Sun XF. Physico-chemical and thermal characterization of lignins from Caligonum monogoliacum and Tamarix spp. Polym Degrad Stab [Internet]. 2001 [cited 2024 May 2];72(2):229–38. Available from: www.elsevier.nl/locate/polydegstab

409. Hazwan Hussin M, Samad NA, Latif NHA, Rozuli NA, Yusoff SB, Gambier F, et al. Production of oil palm (Elaeis guineensis) fronds lignin-derived non-toxic aldehyde for eco-friendly wood adhesive. Int J Biol Macromol. 2018 Jul 1;113:1266–72.

410. Pouteau C, Dole P, Cathala B, Averous L, Boquillon N. Antioxidant properties of lignin in polypropylene. Polym Degrad Stab [Internet]. 2003 [cited 2024 May 2];81(1):9–18. Available from: https://doi.org/10.1016/S0141-3910(03)00057-0

411. Cho M, Karaaslan MA, Renneckar S, Ko F. Enhancement of the mechanical properties of electrospun lignin-based nanofibers by heat treatment. J Mater Sci [Internet]. 2017 Aug 1 [cited 2024 May 15];52(16):9602–14. Available from: https://link.springer.com/article/10.1007/s10853-017-1160-0

412. Giummarella N, Lindgren C, Lindström ME, Henriksson G. Lignin prepared by ultrafiltration of black liquor: Investigation of solubility, viscosity, and ash content. BioResources. 2016 May 1;11(2):3494–510.

413. Motyka AL. An Introduction to Rheology with an Emphasis on Application to Dispersions. J Chem Educ [Internet]. 1996 Apr [cited 2024 Jun 14];73(4):374. Available from: https://pubs.acs.org/doi/abs/10.1021/ed073p374

414. Funk JE, Dinger DR. Viscosity and Rheology. In: Predictive Process Control of Crowded Particulate Suspensions [Internet]. Springer, Boston, MA; 1994 [cited 2024 Jun 14]. p.

235–52. Available from: https://link.springer.com/chapter/10.1007/978-1-4615-3118-0_20

415. Menard KP. Dynamic Mechanical Analysis: A Practical Introduction: Second Edition [Internet]. Dynamic Mechanical Analysis: A Practical Introduction: Second Edition. CRC Press; 2008 [cited 2024 Jun 14]. 1–203 p. Available from: https://www.taylorfrancis.com/books/mono/10.1201/9781420053135/dynamic-mechanical-analysis-kevin-menard

416. Malkin AY, Isayev AI. Rheology: Concepts, methods, and applications: Second edition [Internet]. Rheology: Concepts, Methods, and Applications: Second Edition. Chemtec; 2011 [cited 2024 Jun 14]. 1–473 p. Available from: http://www.sciencedirect.com:5070/book/9781895198492/rheology-concepts-methods-and-applications

417. Macosko CW. Viscous Liquid. In: Rheology - Principles, Measurements and Applications [Internet]. John Wiley & Sons; 1994 [cited 2024 Jun 14]. p. 65–108. Available from: https://www.wiley.com/en-us/Rheology%3A+Principles%2C+Measurements%2C+and+Applications-p-9780471185758

418. Gedde UW. Polymer Physics. Polymer Physics. Springer Netherlands; 1999.

419. Dong D, Fricke AL. Intrinsic viscosity and the molecular weight of kraft lignin. Polymer (Guildf). 1995 May 1;36(10):2075–8.

420. Siochi EJ, Ward TC, Haney MA, Mahn B. The Absolute Molecular Weight Distribution of Hydroxypropylated Lignins. Macromolecules [Internet]. 1990 [cited 2024 May 15];23(5):1420–9. Available from: https://doi.org/10.1021/ma00207a029

421. Tiwari SK, Venkatraman SS. Importance of viscosity parameters in electrospinning: Of monolithic and core-shell fibers. Mater Sci Eng C. 2012 Jul 1;32(5):1037–42.

422. Thompson CJ, Chase GG, Yarin AL, Reneker DH. Effects of parameters on nanofiber diameter determined from electrospinning model. Polymer (Guildf). 2007 Nov 2;48(23):6913–22.

423. Srinivasan R. SUMMARY TABLE OF ELECTROSPUN POLYMER NANOFIBERS [Internet]. Kulpinski; 2006 [cited 2018 Aug 14]. Available from:

https://onlinelibrary.wiley.com/doi/pdf/10.1002/9780470229842.app2

424. Cintra ILR, Rezende MC, Guerrini LM, Nahra LR, Lucas RR, Montagna LS, et al. Electrospinning of PAN/lignin blends aiming the production of carbon nanofibers. MRS Commun [Internet]. 2024 Feb 1 [cited 2024 Oct 9];14(1):82–9. Available from: https://link.springer.com/article/10.1557/s43579-023-00504-5

425. Pu Y, Jiang N, Ragauskas AJ. Ionic liquid as a green solvent for lignin. J Wood Chem Technol. 2007;27(1):23–33.

426. Attia AAM, Abas KM, Ahmed Nada AA, Shouman MAH, Šišková AO, Mosnáček J. Fabrication, Modification, and Characterization of Lignin-Based Electrospun Fibers Derived from Distinctive Biomass Sources. Polymers (Basel). 2021 Jul 2;13(14).

427. Schreiber M, Vivekanandhan S, Mohanty AK, Misra M. Iodine treatment of lignin-cellulose acetate electrospun fibers: Enhancement of green fiber carbonization. ACS Sustain Chem Eng [Internet]. 2015 Jan 5 [cited 2022 Feb 9];3(1):33–41. Available from: https://pubs.acs.org/doi/full/10.1021/sc500481k

428. Heindl RA, Mong LE. Young's modulus of elasticity, strength, and extensibility of refractories in tension. J Res Natl Bur Stand (1934). 1936 Sep;17(3):463.

429. Gotoh K, Yoshitaka S. Improvement of soil release from polyester fabric with atmospheric pressure plasma jet. Text Res J. 2013;83(15):1606–14.

430. Frigerio P, Zoia L, Orlandi M, Hanel T, Castellani L. Application of sulphur-free lignins as a filler for elastomers: Effect of hexamethylenetetramine treatment. Vol. 9, BioResources. 2014.

431. Mandlekar NK. Integration of wood waste to develop multifunctional fully biobased textile structure. 2019.

432. Malaeke H, Housaindokht MR, Monhemi H, Izadyar M. Deep eutectic solvent as an efficient molecular liquid for lignin solubilization and wood delignification. J Mol Liq. 2018 Aug 1;263:193–9.

433. Ali Mohammadpoor S, Akbari S, Sadrjahani M, Nourpanah P. Fabrication of electrospun ibuprofen-loaded poly(vinyl alcohol)/hyper-branched poly(ethylenimine) fibers and their

release behaviors. J Biomater Sci Polym Ed [Internet]. 2020 Jan 22 [cited 2024 May 16];31(2):261–75. Available from: https://www.tandfonline.com/doi/abs/10.1080/09205063.2019.1685759

434. Kim JY, Hwang H, Oh S, Kim YS, Kim UJ, Choi JW. Investigation of structural modification and thermal characteristics of lignin after heat treatment. Int J Biol Macromol. 2014 May 1;66:57–65.

435. Schlee P, Hosseinaei O, O'Keefe CA, Mostazo-López MJ, Cazorla-Amorós D, Herou S, et al. Hardwood: versus softwood Kraft lignin-precursor-product relationships in the manufacture of porous carbon nanofibers for supercapacitors. J Mater Chem A [Internet]. 2020 Nov 17 [cited 2024 Oct 10];8(44):23543–54. Available from: https://pubs.rsc.org/en/content/articlehtml/2020/ta/d0ta09093j

436. Zhou Y, Han Y, Li G, Chu F. Effects of lignin-based hollow nanoparticle structure on the loading and release behavior of doxorubicin. Materials (Basel) [Internet]. 2019 May 24 [cited 2024 May 16];12(10):1694. Available from: https://www.mdpi.com/1996-1944/12/10/1694/htm

437. Zhang Z, Terrasson V, Guénin E. Lignin nanoparticles and their nanocomposites [Internet]. Vol. 11, Nanomaterials. Multidisciplinary Digital Publishing Institute; 2021 [cited 2024 Oct 10]. p. 1336. Available from: https://www.mdpi.com/2079-4991/11/5/1336/htm

438. Hekmati AH, Rashidi A, Ghazisaeidi R, Drean JY. Effect of needle length, electrospinning distance, and solution concentration on morphological properties of polyamide-6 electrospun nanowebs. Text Res J. 2013;83(14):1452–66.

439. Patterson RK. Automated Pregl-Dumas Technique for Determining Total Carbon, Hydrogen, and Nitrogen in Atmospheric Aerosols. Anal Chem [Internet]. 1973 Mar 1 [cited 2023 Oct 4];45(3):605–9. Available from: https://pubs.acs.org/doi/abs/10.1021/ac60325a050

440. Madhu R, Periasamy AP, Schlee P, Hérou S, Titirici MM. Lignin: A sustainable precursor for nanostructured carbon materials for supercapacitors. Vol. 207, Carbon. Pergamon; 2023. p. 172–97.

441. Gordobil O, Herrera R, Poohphajai F, Sandak J, Sandak A. Impact of drying process on kraft lignin: Lignin-water interaction mechanism study by 2D NIR correlation spectroscopy. J Mater Res Technol. 2021 May 1;12:159–69.

442. Faix O. Classification of Lignins from Different Botanical Origins by FT-IR Spectroscopy. Holzforschung [Internet]. 1991 Jan 1 [cited 2024 Nov 4];45(s1):21–8. Available from: https://www.degruyter.com/document/doi/10.1515/hfsg.1991.45.s1.21/html

443. Ponomarenko J, Dizhbite T, Lauberts M, Viksna A, Dobele G, Bikovens O, et al. Characterization of softwood and hardwood lignoboost kraft lignins with emphasis on their antioxidant activity. BioResources. 2014 Feb 20;9(2):2051–68.

444. Özgenç Ö, Durmaz S, Kuştaş S. Tree bark analyses. Vol. 12, BioResources. 2017.

445. Prchal J. Infrared Spectroscopy-Analytical chemistry laboratory, ICT Prague. 2018 [cited 2025 Mar 6];1–27. Available from: https://uanlch.vscht.cz

446. Zhou G, Taylor G, Polle A. FTIR-ATR-based prediction and modelling of lignin and energy contents reveals independent intra-specific variation of these traits in bioenergy poplars. Plant Methods [Internet]. 2011 Apr 10 [cited 2023 Dec 18];7(1):1–10. Available from: https://plantmethods.biomedcentral.com/articles/10.1186/1746-4811-7-9

447. Gu X, Ma X, Li L, Liu C, Cheng K, Li Z. Pyrolysis of poplar wood sawdust by TG-FTIR and Py-GC/MS. J Anal Appl Pyrolysis. 2013 Jul 1;102:16–23.

448. Guo G, Li S, Wang L, Ren S, Fang G. Separation and characterization of lignin from bio-ethanol production residue. Bioresour Technol [Internet]. 2013 [cited 2024 May 29];135:738–41. Available from: https://pubmed.ncbi.nlm.nih.gov/23186676/

449. Abolore RS, Jaiswal S, Jaiswal AK. Green and sustainable pretreatment methods for cellulose extraction from lignocellulosic biomass and its applications: A review. Vol. 7, Carbohydrate Polymer Technologies and Applications. Elsevier; 2024. p. 100396.

450. Kubo S, Kadla JF. Hydrogen bonding in lignin: A fourier transform infrared model compound study. Biomacromolecules [Internet]. 2005 [cited 2023 May 11];6(5):2815–21. Available from: https://pubs.acs.org/sharingguidelines

451. Lupoi JS, Singh S, Parthasarathi R, Simmons BA, Henry RJ. Recent innovations in analytical methods for the qualitative and quantitative assessment of lignin. Renew Sustain Energy Rev. 2015 Sep 1;49:871–906.

452. Balakshin MY, Capanema EA, Chen CL, Gracz HS. Elucidation of the structures of residual and dissolved pine kraft lignins using an HMQC NMR technique. J Agric Food Chem [Internet]. 2003 Oct 8 [cited 2023 May 18];51(21):6116–27. Available from: https://pubmed.ncbi.nlm.nih.gov/14518932/

453. Altarabeen R, Rusakov D, Manke E, Gibowsky L, Schroeter B, Liebner F, et al. Lignin Polyurethane Aerogels: Influence of Solvent on Textural Properties. Gels [Internet]. 2024 Dec 1 [cited 2025 Mar 11];10(12):827. Available from: https://www.mdpi.com/2310-2861/10/12/827/htm

454. Emsley J. Very strong hydrogen bonding. Chem Soc Rev [Internet]. 1980 Jan 1 [cited 2023 Dec 5];9(1):91–124. Available from: https://pubs.rsc.org/en/content/articlehtml/1980/cs/cs9800900091

455. Cotugno S, Larobina D, Mensitieri G, Musto P, Ragosta G. A novel spectroscopic approach to investigate transport processes in polymers: The case of water-epoxy system. Polymer (Guildf). 2001 Jul 1;42(15):6431–8.

456. Brebu M, Tamminen T, Spiridon I. Thermal degradation of various lignins by TG-MS/FTIR and Py-GC-MS. J Anal Appl Pyrolysis. 2013 Nov 1;104:531–9.

457. Sameni J, Krigstin S, Rosa D dos S, Leao A, Sain M. Thermal characteristics of lignin residue from industrial processes. Vol. 9, BioResources. 2014. p. 725–37.

458. Ding R, Wu H, Thunga M, Bowler N, Kessler MR. Processing and characterization of low-cost electrospun carbon fibers from organosolv lignin/polyacrylonitrile blends. Carbon N Y. 2016 Apr 1;100:126–36.

459. Nunes KSD, Pardini LC. Purification and characterization methods for lignin biomass as a potential precursor for carbon materials. Cellul Chem Technol. 2019;53(3–4):227–42.

460. Gulati T, Datta AK. Mechanistic understanding of case-hardening and texture development during drying of food materials. J Food Eng. 2015 Dec 1;166:119–38.

461. Cui W, Li X, Zhou S, Weng J. Investigation on process parameters of electrospinning system through orthogonal experimental design. J Appl Polym Sci. 2007 Mar 5;103(5):3105–12.

462. Newman A, Zografi G. Commentary: Considerations in the Measurement of Glass Transition Temperatures of Pharmaceutical Amorphous Solids [Internet]. Vol. 21, AAPS PharmSciTech. Springer; 2020 [cited 2025 Mar 14]. p. 26. Available from: https://pmc.ncbi.nlm.nih.gov/articles/PMC6917632/

463. Bonjour O, Nederstedt H, Arcos-Hernandez M V., Laanesoo S, Vares L, Jannasch P. Lignin-Inspired Polymers with High Glass Transition Temperature and Solvent Resistance from 4-Hydroxybenzonitrile, Vanillonitrile, and Syringonitrile Methacrylates. ACS Sustain Chem Eng [Internet]. 2021 Dec 20 [cited 2025 Mar 14];9(50):16874–80. Available from: https://pmc.ncbi.nlm.nih.gov/articles/PMC8693774/

464. Mariana M, Alfatah T, Abdul Khalil HPS, Yahya EB, Olaiya NG, Nuryawan A, et al. A current advancement on the role of lignin as sustainable reinforcement material in biopolymeric blends. Vol. 15, Journal of Materials Research and Technology. Elsevier; 2021. p. 2287–316.

465. Liu R, Smeds A, Willför S, Xu C. Structural properties of softwood lignin fractions: Revealed by NMR and Py-GC/MS. Ind Crops Prod. 2024 Mar 1;209:118055.

466. Hosseinaei O, Harper DP, Bozell JJ, Rials TG. Improving processing and performance of pure lignin carbon fibers through hardwood and herbaceous lignin blends. Int J Mol Sci. 2017;18(7).

467. Fisher T, Hajaligol M, Waymack B, Kellogg D. Pyrolysis behavior and kinetics of biomass derived materials. J Anal Appl Pyrolysis. 2002 Feb 1;62(2):331–49.

468. Boateng AA, Hicks KB, Vogel KP. Pyrolysis of switchgrass (Panicum virgatum) harvested at several stages of maturity. J Anal Appl Pyrolysis. 2006 Mar 1;75(2):55–64.

469. Dallmeyer I, Chowdhury S, Kadla JF. Preparation and characterization of kraft lignin-based moisture-responsive films with reversible shape-change capability. Biomacromolecules. 2013;14(7):2354–63.

470. Poursorkhabi V, Mohanty AK, Misra M. Electrospinning of aqueous lignin/poly(ethylene

oxide) complexes. J Appl Polym Sci. 2015 Jan 10;132(2).

471. Tam N, Oguz S, Aydogdu A, Sumnu G, Sahin S. Influence of solution properties and pH on the fabrication of electrospun lentil flour/HPMC blend nanofibers. Food Res Int. 2017 Dec 1;102:616–24.

472. Ahn Y, Hu DH, Hong JH, Lee SH, Kim HJ, Kim H. Effect of co-solvent on the spinnability and properties of electrospun cellulose nanofiber. Carbohydr Polym. 2012 Jun 20;89(2):340–5.

473. Yang GZ, Li HP, Yang JH, Wan J, Yu DG. Influence of Working Temperature on The Formation of Electrospun Polymer Nanofibers. Nanoscale Res Lett [Internet]. 2017 Dec 1 [cited 2024 Mar 28];12(1):1–10. Available from: https://link.springer.com/article/10.1186/s11671-016-1824-8

474. Dallmeyer I, Lin LT, Li Y, Ko F, Kadla JF. Preparation and characterization of interconnected, Kraft lignin-based carbon fibrous materials by electrospinning. Macromol Mater Eng. 2014 May;299(5):540–51.

475. Yang LJ, Yang XQ, Huang KM, Jia GZ, Shang H. Dielectric properties of binary solvent mixtures of dimethyl sulfoxide with water. Int J Mol Sci [Internet]. 2009 [cited 2024 Nov 25];10(3):1261–70. Available from: https://pmc.ncbi.nlm.nih.gov/articles/PMC2672028/

476. De Schoenmaker B, Van Der Schueren L, Ceylan Ö, De Clerck K. Electrospun polyamide 4.6 nanofibrous nonwovens: Parameter study and characterization. J Nanomater. 2012 May 7;2012:1–9.

477. Wu H, Liu C, Jiang Z, Yang Z, Mao X, Wei L, et al. Electrospun flexible lignin/polyacrylonitrile-based carbon nanofiber and its application in electrode materials for supercapacitors. Text Res J. 2021;

478. García-Mateos FJ, Ruiz-Rosas R, Rosas JM, Rodríguez-Mirasol J, Cordero T. Controlling the composition, morphology, porosity, and surface chemistry of lignin-based electrospun carbon materials. Vol. 6, Frontiers in Materials. Frontiers Media S.A.; 2019. p. 114.

479. Du B, Chen C, Sun Y, Yu M, Liu B, Wang X, et al. Lignin bio-oil-based electrospun nanofibers with high substitution ratio property for potential carbon nanofibers applications. Polym Test. 2020 Sep 1;89:106591.

480. Kumar M, Hietala M, Oksman K. Lignin-based electrospun carbon nanofibers. Vol. 6, Frontiers in Materials. Frontiers Media S.A.; 2019. p. 62.

481. Ahn Y, Kang Y, Park B, Ku MK, Lee SH, Kim H. Influence of lignin on rheological behaviors and electrospinning of polysaccharide solution. J Appl Polym Sci [Internet]. 2014 Apr 5 [cited 2022 Feb 9];131(7):40031. Available from: https://onlinelibrary.wiley.com/doi/full/10.1002/app.40031

482. Jin Y, Lin J, Cheng Y, Lu C. Lignin-based high-performance fibers by textile spinning techniques. Materials (Basel) [Internet]. 2021 Jun 18 [cited 2022 Mar 1];14(12):3378. Available from: https://www.mdpi.com/1996-1944/14/12/3378/htm

483. Hayati I, Bailey AI, Tadros TF. Investigations into the mechanisms of electrohydrodynamic spraying of liquids. I. Effect of electric field and the environment on pendant drops and factors affecting the formation of stable jets and atomization. J Colloid Interface Sci. 1987 May 1;117(1):205–21.

484. Areskogh D, Li J, Gellerstedt G, Henriksson G. Structural modification of commercial lignosulphonates through laccase catalysis and ozonolysis. Ind Crops Prod. 2010 Nov 1;32(3):458–66.

485. Adler E. Lignin chemistry-past, present and future. Wood Sci Technol [Internet]. 1977 Sep [cited 2025 Feb 6];11(3):169–218. Available from: https://link.springer.com/article/10.1007/BF00365615

486. Mirtič J, Balažic H, Zupančič Š, Kristl J. Effect of solution composition variables on electrospun alginate nanofibers: Response surface analysis. Polymers (Basel) [Internet]. 2019 Apr 16 [cited 2024 Mar 27];11(4):692. Available from: https://www.mdpi.com/2073-4360/11/4/692/htm

487. Dong X, Lu C, Zhou P, Zhang S, Wang L, Li D. Polyacrylonitrile/lignin sulfonate blend fiber for low-cost carbon fiber. RSC Adv [Internet]. 2015 [cited 2022 Mar 1];5(53):42259–65. Available from: www.rsc.org/advances

488. Wei XF, Nilsson F, Yin H, Hedenqvist MS. Microplastics Originating from Polymer Blends: An Emerging Threat? Environ Sci Technol [Internet]. 2021 Apr 20 [cited 2025 Feb 10];55(8):4190–3. Available from: https://pubmed.ncbi.nlm.nih.gov/33733742/

489. Kun D, Pukánszky B. Polymer/lignin blends: Interactions, properties, applications [Internet]. Vol. 93, European Polymer Journal. Elsevier Ltd; 2017 [cited 2022 Mar 3]. p. 618–41. Available from: http://dx.doi.org/10.1016/j.eurpolymj.2017.04.035

490. Ding B, Li C, Miyauchi Y, Kuwaki O, Shiratori S. Formation of novel 2D polymer nanowebs via electrospinning. Nanotechnology [Internet]. 2006 Jun 27 [cited 2024 Mar 28];17(15):3685–91. Available from: https://iopscience.iop.org/article/10.1088/0957-4484/17/15/011

491. He Q, Zhou P, Hao J, Lu C, Liu Y. Incorporation of alkali lignin in polyacrylonitrile: Phase separation, coagulation, and cyclization kinetics. ACS Omega [Internet]. 2019 [cited 2022 Mar 11];4(7):11346–53. Available from: https://pubs.acs.org/sharingguidelines

492. Nezarati RM, Eifert MB, Cosgriff-Hernandez E. Effects of humidity and solution viscosity on electrospun fiber morphology. Tissue Eng - Part C Methods [Internet]. 2013 Oct 1 [cited 2024 Mar 28];19(10):810–9. Available from: https://www.liebertpub.com/doi/10.1089/ten.tec.2012.0671

493. Topuz F, Satilmis B, Uyar T. Electrospinning of uniform nanofibers of Polymers of Intrinsic Microporosity (PIM-1): The influence of solution conductivity and relative humidity. Polymer (Guildf). 2019 Sep 12;178:121610.

494. Williams GR, Raimi-Abraham BT, Luo CJ. Electrospinning fundamentals. In: Nanofibres in Drug Delivery. UCL Press; 2018. p. 24–59.

495. Hossain MF, Gong RH, Rigout M. Optimization of the process variables for electrospinning of poly(ethylene oxide)-loaded hydroxypropyl-β-cyclodextrin nanofibres. J Text Inst [Internet]. 2016 Jan 2 [cited 2024 Mar 28];107(1):1–11. Available from: https://www.tandfonline.com/doi/abs/10.1080/00405000.2014.999478

496. Yao E, Yu G, Li B, Zhao L, Li Y, Bai H, et al. High-Temperature-Resistant, Low-Concentration Water-Controlling Composite Cross-Linked Polyacrylamide Weak Gel System Prepared from Oilfield Sewage. ACS Omega [Internet]. 2022 Apr 19 [cited 2025 Mar 11];7(15):12570–9. Available from: https://pubs.acs.org/doi/full/10.1021/acsomega.1c05675

497. Ksapabutr B, Chalermkiti T, Panapoy M. Effect of Nozzle Shapes on the Formation of Taylor Cone and the Oscillation of Fibers During Electrospinning Process. C J Spec Issue Nanotechnol. 2005;4(1).

498. Zhang M, Ogale AA. Effect of temperature and concentration of acetylated-lignin solutions on dry-spinning of carbon fiber precursors. J Appl Polym Sci [Internet]. 2016 Dec 5 [cited 2024 Mar 14];133(45). Available from: https://onlinelibrary.wiley.com/doi/full/10.1002/app.43663

499. Li X, Bian F, Lin J, Zeng Y. Effect of electric field on the morphology and mechanical properties of electrospun fibers. RSC Adv. 2016;6(56):50666–72.

500. Chupka EI, Rykova TM. Electrical properties of lignin. Chem Nat Compd [Internet]. 1983 Jan [cited 2024 Nov 8];19(1):78–80. Available from: https://link.springer.com/article/10.1007/BF00579968

501. Liitiä TM, Maunu SL, Hortling B, Toikka M, Kilpeläinen I. Analysis of technical lignins by two- and three-dimensional NMR spectroscopy. J Agric Food Chem [Internet]. 2003 [cited 2022 Aug 1];51(8):2136–43. Available from: https://pubs.acs.org/sharingguidelines

502. Köhnke J, Gierlinger N, Mateu BP, Unterweger C, Solt P, Mahler AK, et al. Comparison of four technical lignins as a resource for electrically conductive carbon particles. BioResources. 2019 Feb 1;14(1):1091–109.

503. Grothe T, Wehlage D, Böhm T, Remche A, Ehrmann A. Needleless Electrospinning of PAN Nanofibre Mats. Tekstilec. 2017;60(4):290–5.

504. Jalili R, Morshed M, Ravandi SAH. Fundamental parameters affecting electrospinning of PAN nanofibers as uniaxially aligned fibers. J Appl Polym Sci. 2006 Sep 15;101(6):4350–7.

505. Pillay V, Dott C, Choonara YE, Tyagi C, Tomar L, Kumar P, et al. A review of the effect of processing variables on the fabrication of electrospun nanofibers for drug delivery applications. Vol. 2013, Journal of Nanomaterials. 2013.

506. Zahra FT, Zhang Y, Ajayi AO, Quick Q, Mu R. Optimization of Electrospinning Parameters for Lower Molecular Weight Polymers: A Case Study on Polyvinylpyrrolidone. Polymers (Basel) [Internet]. 2024 May 1 [cited 2025 Feb

20];16(9):1217. Available from: https://pmc.ncbi.nlm.nih.gov/articles/PMC11085657/

507. Amariei N, Manea LR, Bertea AP, Bertea A, Popa A. The Influence of Polymer Solution on the Properties of Electrospun 3D Nanostructures. In: IOP Conference Series: Materials Science and Engineering [Internet]. IOP Publishing; 2017 [cited 2024 Mar 27]. p. 012092. Available from: https://iopscience.iop.org/article/10.1088/1757-899X/209/1/012092

508. Korntner P, Sumerskii I, Bacher M, Rosenau T, Potthast A. Characterization of technical lignins by NMR spectroscopy: Optimization of functional group analysis by 31P NMR spectroscopy. Holzforschung [Internet]. 2015 Aug 1 [cited 2022 Aug 3];69(6):807–14. Available from: https://www.degruyter.com/document/doi/10.1515/hf-2014-0281/html?lang=en

509. Wildy M, Wei W, Xu K, Schossig J, Hu X, Hyun DC, et al. Heat's Role in Solution Electrospinning: A Novel Approach to Nanofiber Structure Optimization. Langmuir [Internet]. 2024 Apr 16 [cited 2025 Apr 8];40(15):7982–91. Available from: https://pubs.acs.org/doi/full/10.1021/acs.langmuir.3c03919

510. Haider S, Al-Zeghayer Y, Ahmed Ali FA, Haider A, Mahmood A, Al-Masry WA, et al. Highly aligned narrow diameter chitosan electrospun nanofibers. J Polym Res [Internet]. 2013 Apr 1 [cited 2019 Apr 9];20(4):1–11. Available from: https://link.springer.com/article/10.1007/s10965-013-0105-9

511. Li X, Chen W, Qian Q, Huang H, Chen Y, Wang Z, et al. Electrospinning-Based Strategies for Battery Materials [Internet]. Vol. 11, Advanced Energy Materials. Wiley-VCH Verlag; 2021 [cited 2025 Jul 30]. p. 2000845. Available from: /doi/pdf/10.1002/aenm.202000845

512. Zhang X, Dong S, Wu W, Yang J, Li J, Shi K, et al. Influence of Lignin units on the properties of Lignin/PAN-derived carbon fibers. J Appl Polym Sci [Internet]. 2020 Nov 10 [cited 2025 Jul 30];137(42). Available from: https://www.researchgate.net/publication/340085511_Influence_of_Lignin_units_on_the_properties_of_LigninPAN-derived_carbon_fibers

513. Roman J, Neri W, Derré A, Poulin P. Electrospun lignin-based twisted carbon nanofibers for potential microelectrodes applications. Carbon N Y [Internet]. 2019 Apr 1 [cited 2025 Jul 30];145:556–64. Available from:

https://www.sciencedirect.com/science/article/pii/S0008622319300351?via%3Dihub#fig2

514. Ekila RJ, Stevanovic T, Rodrigue D. Electrospinning of Miscanthus x giganteus Organosolv Lignin in Dimethyl Sulfoxide (DMSO). Polymers (Basel) [Internet]. 2025 Jun 1 [cited 2025 Jul 30];17(12):1695. Available from: https://pmc.ncbi.nlm.nih.gov/articles/PMC12197072/

515. Cintra ILR, Rezende MC, Guerrini LM, Nahra LR, Lucas RR, Montagna LS, et al. Electrospinning of PAN/lignin blends aiming the production of carbon nanofibers. MRS Commun [Internet]. 2024 [cited 2025 Jul 30];14(1):82–9. Available from: https://doi.org/10.1557/s43579-023-00504-5

516. de Gonzaga LAC, Martins MCF, Correa AC, Facchinatto WM, da Silva CMP, Colnago LA, et al. Production of carbon nanofibers from PAN and lignin by solution blow spinning. J Polym Res [Internet]. 2021 Jul 1 [cited 2025 Jul 30];28(7). Available from: https://www.researchgate.net/publication/352157713_Production_of_carbon_nanofibers_from_PAN_and_lignin_by_solution_blow_spinning

517. Zhao J, Xiuwen W, Hu J, Liu Q, Shen D, Xiao R. Thermal degradation of softwood lignin and hardwood lignin by TG-FTIR and Py-GC/MS. Polym Degrad Stab. 2014 Oct 1;108:133–8.

518. Stewart D. Fourier transform infrared microspectroscopy of plant tissues. Appl Spectrosc [Internet]. 1996 Mar 1 [cited 2025 Jul 25];50(3):357–65. Available from: https://opg.optica.org/abstract.cfm?uri=as-50-3-357

519. Hill C, Altgen M, Rautkari L. Thermal modification of wood—a review: chemical changes and hygroscopicity [Internet]. Vol. 56, Journal of Materials Science. 2021 [cited 2025 Apr 9]. p. 6581–614. Available from: https://doi.org/10.1007/s10853-020-05722-z

520. Sadeghifar H, Cui C, Argyropoulos DS. Toward thermoplastic lignin polymers. Part 1. Selective masking of phenolic hydroxyl groups in kraft lignins via methylation and oxypropylation chemistries. Ind Eng Chem Res [Internet]. 2012 Dec 26 [cited 2025 Jul 25];51(51):16713–20. Available from: https://bioresources.cnr.ncsu.edu/

521. Henrik-Klemens Å, Caputo F, Ghaffari R, Westman G, Edlund U, Olsson L, et al. The glass transition temperature of isolated native, residual, and technical lignin.

Holzforschung [Internet]. 2024 Apr 1 [cited 2025 Jul 25];78(4):216–30. Available from: https://www.degruyterbrill.com/document/doi/10.1515/hf-2023-0111/html

522. Kanhere S V., Tindall GW, Ogale AA, Thies MC. Carbon fibers derived from liquefied and fractionated poplar lignins: The effect of molecular weight. iScience [Internet]. 2022 Dec 22 [cited 2025 Jul 25];25(12):105449. Available from: https://pmc.ncbi.nlm.nih.gov/articles/PMC9663315/

523. Ma Q, Zhang X. An integral method for determining the molecular composition of lignin and its application. Sci Rep [Internet]. 2022 Dec 1 [cited 2025 Jul 25];12(1):19136. Available from: https://pmc.ncbi.nlm.nih.gov/articles/PMC9646882/

524. Horie K, Hiura H, Sawada M, Mita I, Kambe H. Calorimetric investigation of polymerization reactions. III. Curing reaction of epoxides with amines. J Polym Sci Part A-1 Polym Chem [Internet]. 1970 Jun 1 [cited 2023 Dec 5];8(6):1357–72. Available from: https://onlinelibrary.wiley.com/doi/full/10.1002/pol.1970.150080605

525. Ghorani B, Russell SJ, Goswami P. Controlled morphology and mechanical characterisation of electrospun cellulose acetate fibre webs. Int J Polym Sci. 2013 Apr 4;2013:1–12.

526. Abdel-Hady F, Alzahrany A, Hamed M. Experimental Validation of Upward Electrospinning Process. ISRN Nanotechnol. 2011;2011:1–14.

527. Zhang C, Yuan X, Wu L, Han Y, Sheng J. Study on morphology of electrospun poly(vinyl alcohol) mats. Eur Polym J. 2005;41(3):423–32.

528. Youe WJ, Lee SM, Lee SS, Lee SH, Kim YS. Characterization of carbon nanofiber mats produced from electrospun lignin-g-polyacrylonitrile copolymer. Int J Biol Macromol. 2016 Jan 1;82:497–504.

529. Souto F, Calado V, Pereira N. Lignin-based carbon fiber: a current overview. Mater Res Express. 2018;5:72001.

530. Kurban Z, Lovell A, Jenkins D, Bennington S, Loader I, Schober A, et al. Turbostratic graphite nanofibres from electrospun solutions of PAN in dimethylsulphoxide. Eur Polym J. 2010;46(6):1194–202.

531. Carbon R. Lignin Development at Domtar Takes Next Step with Prisma - DOMTAR Newsroom [Internet]. 2018 [cited 2025 Jun 26]. Available from: https://renewable-carbon.eu/news/domtar-takes-next-step-in-lignin-development-with-prisma/